ALFRED-WEGENER-INSTITUT
HELMHOLTZ-ZENTRUM FÜR POLAR- UND MEERESFORSCHUNG

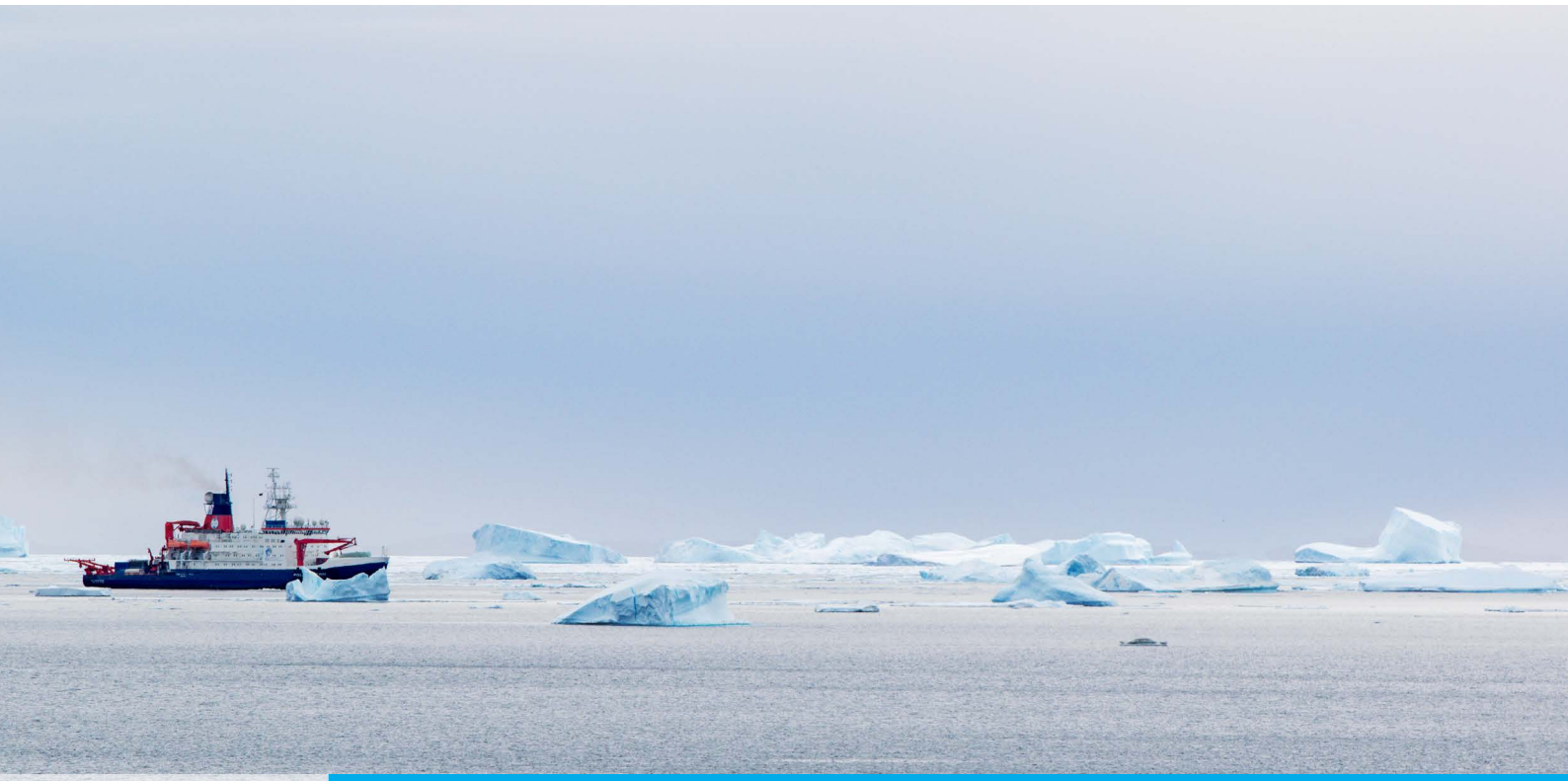

790
2024

Berichte
zur Polar- und Meeresforschung

Reports on Polar and Marine Research

The Expedition PS140 of the Research Vessel POLARSTERN to the Cooperation Sea and Davis Sea in 2023/2024

Edited by

Marcus Gutjahr and Oliver Esper
with contributions of the participants

HELMHOLTZ

Die Berichte zur Polar- und Meeresforschung werden vom Alfred-Wegener-Institut, Helmholtz-Zentrum für Polar- und Meeresforschung (AWI) in Bremerhaven, Deutschland, in Fortsetzung der vormaligen Berichte zur Polarforschung herausgegeben. Sie erscheinen in unregelmäßiger Abfolge.

Die Berichte zur Polar- und Meeresforschung enthalten Darstellungen und Ergebnisse der vom AWI selbst oder mit seiner Unterstützung durchgeführten Forschungsarbeiten in den Polargebieten und in den Meeren.

Die Publikationen umfassen Expeditionsberichte der vom AWI betriebenen Schiffe, Flugzeuge und Stationen, Forschungsergebnisse (inkl. Dissertationen) des Instituts und des Archivs für deutsche Polarforschung, sowie Abstracts und Proceedings von nationalen und internationalen Tagungen und Workshops des AWI.

Die Beiträge geben nicht notwendigerweise die Auffassung des AWI wider.

Herausgeber
Dr. Horst Bornemann

Redaktionelle Bearbeitung und Layout
Susan Amir Sawadkuhi

Alfred-Wegener-Institut
Helmholtz-Zentrum für Polar- und Meeresforschung
Am Handelshafen 12
27570 Bremerhaven
Germany

www.awi.de
www.awi.de/reports

The Reports on Polar and Marine Research are issued by the Alfred Wegener Institute, Helmholtz Centre for Polar and Marine Research (AWI) in Bremerhaven, Germany, succeeding the former Reports on Polar Research. They are published at irregular intervals.

The Reports on Polar and Marine Research contain presentations and results of research activities in polar regions and in the seas either carried out by the AWI or with its support.

Publications comprise expedition reports of the ships, aircrafts, and stations operated by the AWI, research results (incl. dissertations) of the Institute and the Archiv für deutsche Polarforschung, as well as abstracts and proceedings of national and international conferences and workshops of the AWI.

The papers contained in the Reports do not necessarily reflect the opinion of the AWI.

Editor
Dr. Horst Bornemann

Editorial editing and layout
Susan Amir Sawadkuhi

Alfred-Wegener-Institut
Helmholtz-Zentrum für Polar- und Meeresforschung
Am Handelshafen 12
27570 Bremerhaven
Germany

www.awi.de
www.awi.de/en/reports

Titel: Polarstern vor der Davis Station in der östlichen Prydz-Bucht
(Foto: Marcus Gutjahr, GEOMAR)

Cover: Polarstern close to Davis Station in eastern Prydz Bay
(Photo: Marcus Gutjahr, GEOMAR)

The Expedition PS140 of the Research Vessel POLARSTERN to the Cooperation Sea and Davis Sea in 2023 / 2024

Edited by

Marcus Gutjahr and Oliver Esper
with contributions of the participants

Please cite or link this publication using the identifiers

https://epic.awi.de/id/eprint/59815
https://doi.org/10.57738/BzPM_0790_2024

ISSN 1866-3192

PS140

25 November 2023 – 01 February 2024

Cape Town – Hobart

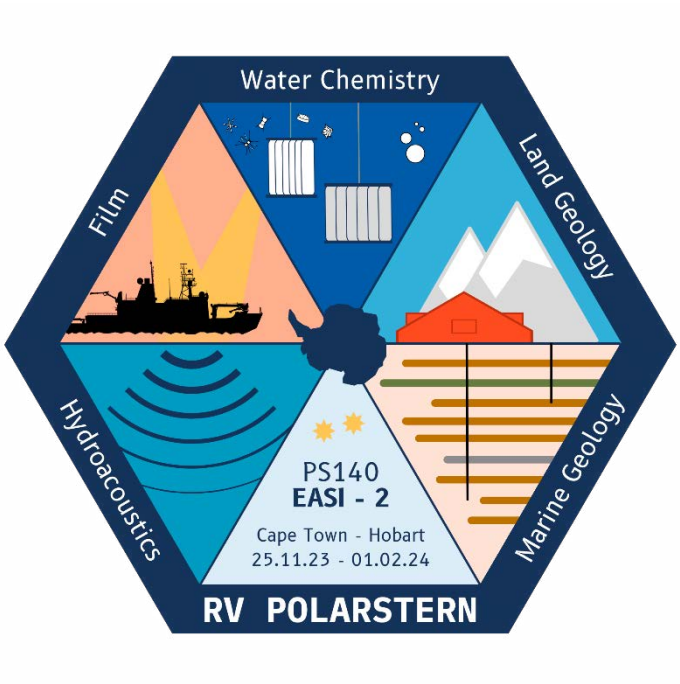

Chief scientist
Marcus Gutjahr

Co-chief scientist
Oliver Esper

Coordinator
Ingo Schewe

Contents

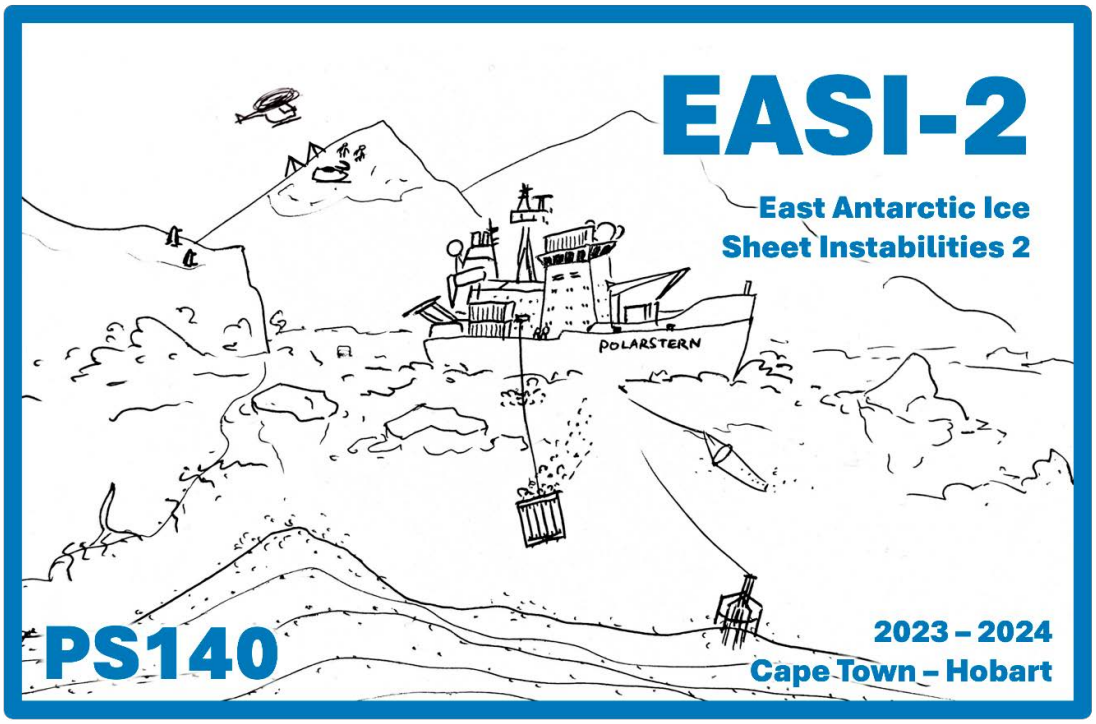

Runner-up logo designed by Florine Kooij for EASI-2.
The winner logo shown on the front page
was designed by Manuel Ehnis, Johanna Brehmer-Moltmann,
Anni Lemire, and Pascal Andreas.

1. ÜBERBLICK UND EXPEDITIONSVERLAUF

Marcus Gutjahr[1], Oliver Esper[2], Martin Melles[3]

[1]DE.GEOMAR
[2]DE.AWI
[3]DE.UNI-Köln

Die Expedition EASI-2 (Instabilität des Ostantarktischen Eisschildes) ist die zweite von drei gemeinsam konzipierten *Polarstern*-Expeditionen, in welchen die Geschichte der Instabilität des Ostantarktischen Eisschildes (EAIS) und ihre Wechselwirkung mit Veränderungen in der Zirkulation des Südozeans (SO) untersucht werden. Während die erste der drei Expeditionen (EASI-1) bereits vom 6. Januar bis 28. Februar 2022 stattfand, folgte die dritte (EASI-3) unmittelbar nach EASI-2 (6. Februar bis 16. April 2024) (Abb. 1.1). Jede der drei koordinierten Expeditionen hat einen eigenen Forschungsschwerpunkt im Zusammenhang mit der potenziellen Instabilität des EAIS während aktueller und vergangener Klimaveränderungen. Im Vergleich zu den beiden anderen Expeditionen konzentriert sich EASI-2 am stärksten auf aktuelle Prozesse in der Wassersäule des Südpolarmeeres, die beobachtbare moderne Nährstoffverfügbarkeit mit besonderem Augenmerk auf die Lieferung essenzieller Mikronährstoffe vom Meeresboden und der Ostantarktis. Zwei Transekte der Wassersäule im offenen Ozean wurden realisiert, um die Struktur, die chemische Zusammensetzung sowie den aktuellen Zirkulationszustand im Untersuchungsgebiet zu ermitteln. Analoge Arbeiten auf dem ostantarktischen Schelf liefern die proximale antarktische Perspektive auf sowohl physikalische als auch chemische ozeanografische Trends, die heute in Zeiten allgemein steigender Meerestemperaturen, abnehmender Meereisausdehnung und einer Abnahme des Salzgehalts verschiedener Wassermassen im SO wie dem Antarktischen Bodenwasser (AABW) zu beobachten sind. An der Mehrzahl der Tiefenwasserstationen der beiden Transekte ermöglicht die komplementäre Beprobung tiefmariner Sedimente von bis zu 25 Metern Tiefe unter dem Meeresboden die Rückverfolgung von Veränderungen in den Eigenschaften der Wassersäule über mehr als die letzten 800 Tausend Jahre. Im Fokus der sedimentären Arbeiten stehen die pleistozäne Dynamik ozeanischer Fronten des Antarktischen Zirkumpolarstroms, Veränderungen der Meeresoberflächenwasser-temperaturen, das vergangene Kohlenstoffbudget der Wassersäule und die vergangene Meereisausdehnung. Auf dem ostantarktischen Schelf erlauben uns kombinierte Parasound-Profile und Sedimentprobennahme die Beantwortung von Fragen zur Geschichte des quartären Eisschildes und zur vergangenen Tiefenwasserbildung. Vor allem im südöstlichen Teil der Prydz-Bucht konnten auch ausgedehnte Sedimentkerne gewonnen werden, die zeitlich hochaufgelöste Rekonstruktionen des holozänen Klimaverlaufs in der Region ermöglichen. Diese Kerne sind auch deshalb sehr wertvoll, da parallel zu den marinen Arbeiten das Team der Landgeologen in der Nähe der australischen *Davis-Station* während einer knapp dreiwöchigen Landkampagne limnische und marine Kerne in einem Fjord gewinnen konnten. Wir können somit die Brücke schlagen von terrestrischen zu marinen Klimarekonstruktionen, ein wesentliches übergeordnetes Ziel der EASI-Ausfahrten.

Das wohl herausragendste Merkmal dieser Expedition ist das Bestreben, moderne Beobachtungen aus der Wassersäulenarbeit eng mit früheren Zuständen der SO-Zirkulationsmodi zu verknüpfen, indem eine Vielzahl modernster Methoden und/oder Proxies sowie Probenahmestrategien verwendet werden. Beispielsweise können wir sedimentäre diagenetische Prozesse an vielen realisierten Probenahmestellen quantifizieren, parallel

zur Anwendung paläozeanographischer Proxies, wie z. B. der Gewinnung authigener (aus dem Meerwasser ausgefallener) Spurenmetalle (z.B. Nd und Pb). An gewonnenem Material (Wasser, Eis und Sedimente) werden in den Heimatlaboren verschiedene geochemische Methoden angewendet, um die Verlässlichkeit mariner sedimentärer Archive zu evaluieren. In einem weiteren Schritt werden dann paläozeanographische Rekonstruktionen erfolgen. Unser Fahrtabschnitt umfasst eine Reihe von Klimazonen, von den gemäßigten Breiten nördlich der subtropischen Front, durch sämtliche Frontensysteme des Südozeans, bis hin zum Ostantarktischen Eisschild. Die Beschaffenheit der Sedimente ist dementsprechend vielfältig und umfasst rein biogene bis hin zu rein terrestrischen Sedimenten, mit entsprechend variabel ausgebildeter diagenetischer Redox-Zonierung in beprobtem Sediment.

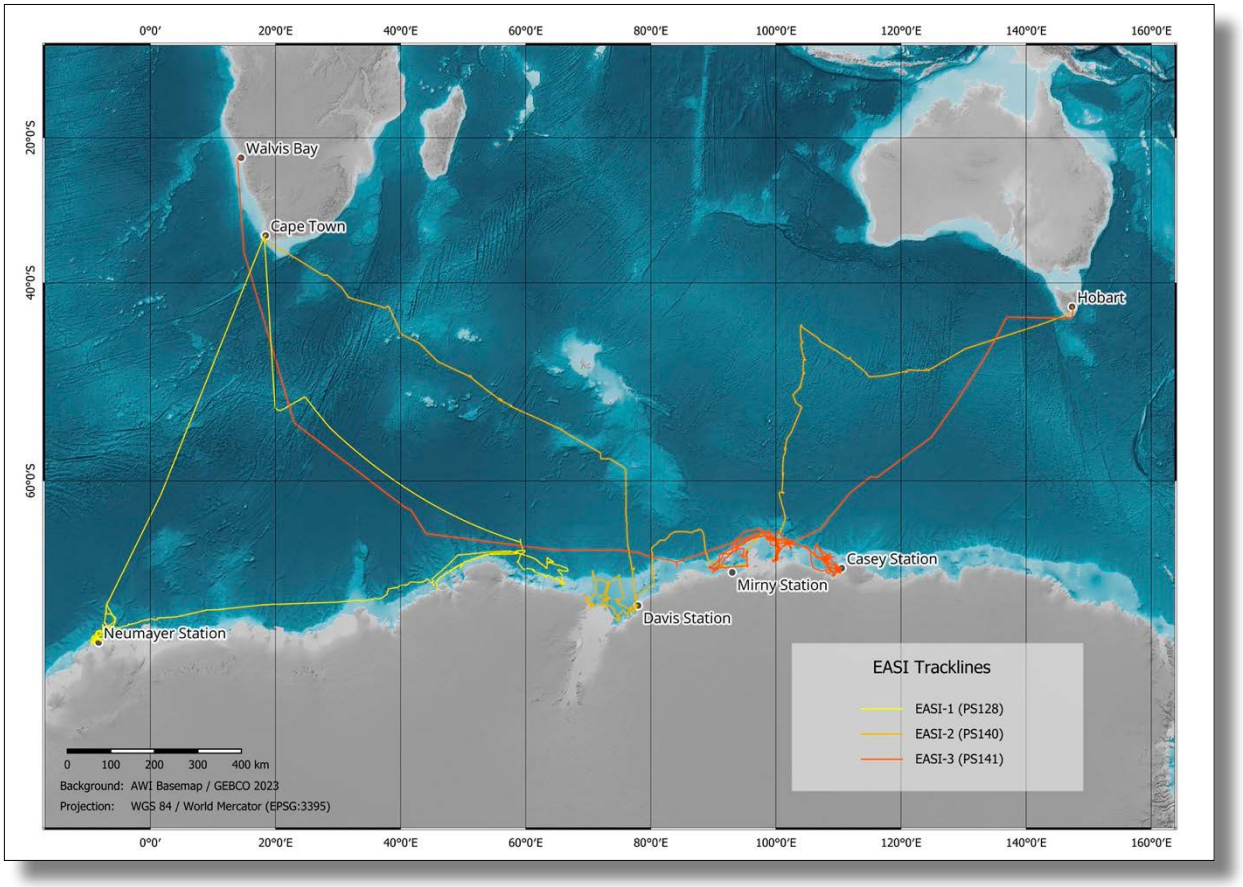

Abb. 1.1: Fahrtverlauf der drei koordiniert geplanten Ausfahrten EASI-1, -2 und -3. Siehe https://doi.pangaea.de/10.1594/PANGAEA.967415 für eine Darstellung des Master tracks in Verbindung mit der Stationsliste für PS140. EASI-1 fand Anfang 2022 statt, während EASI-2 von 28. November 2023 bis 1. Februar 2024 und EASI-3 vom 6. Februar bis 16. April durchgeführt wurden.

Fig. 1.1: Cruise tracks of the three coordinated expeditions EASI-1, -2 and -3. EASI-1: https://doi.pangaea.de/10.1594/PANGAEA.967415 to display the master track in conjunction with the station list for PS140. EASI-1 took place in early 2022, while EASI-2 was realised from 28 November 2023 to 1 February 2024 and EASI-3 from 6 February to 16 April 2024.

Temperatur (z. B. Mg/Ca, $\delta^{18}O$, Transferfunktionen) und Karbonatsystem-bezogene Proxies (B/Ca, $\delta^{11}B$), die an Planktonproben und Mikrofossilien im Sediment gemessen werden, können direkt mit den Parametern des Karbonatsystems ($\delta^{13}C$, TA, DIC) der heutigen Wassersäule verglichen werden, die wir gleichermaßen erhalten haben. Darüber hinaus werden Proxies für

die Meereisausdehnung in der Vergangenheit (z.B. PIPSO25, Diatomeen-Transferfunktionen) Fragen zur Meereisdynamik im Pleistozän beantworten. Dank der Verwendung eines spurenmetallsauberem Wasserschöpfers sind wir in der einmaligen Lage, qualitativ hochwertige Daten zu heutigen Austauschprozessen verschiedenster Spurenmetalle zwischen (i) dem Meeresboden und dem Bodenwasser, sowie (ii) verschiedenen Wassermassen in der offenen Wassersäule des Südlichen Ozeans zu messen. Nicht zuletzt werden wir (iii) den anthropogenen Eintrag ausgewählter Spurenmetalle wie zum Beispiel Blei in die Wassersäule des Südozeans, und als Folge auch in antarktische Gewässer, bestimmen. Unsere Analysen erstrecken sich auch auf die Quantifizierung des subglazialen Eintrags von Übergangsmetallen und anderen analytisch anspruchsvollen Spurenmetallen, für die bislang kaum Daten aus der Antarktis vorliegen. Ebenso gewonnen wurden Wasserproben, um den Radiokohlenstoffgehalt der heutigen Wassersäule sowie die Methankonzentrationen in den antarktischen Gewässern und der Atmosphäre zu ermitteln. An der Mehrzahl der durchgeführten Stationen während EASI-2 wurde ein erweitertes Spektrum an Probenahmestrategien verfolgt:

1. Durch den Einsatz eines normalen Wasserschöpfers wurde zuerst die Struktur der Wassersäule ermittelt und Wasserproben für verschiedene Anwendungen genommen.
2. Die Verwendung eines spurenmetallsauberen Wasserschöpfers erlaubte die Probennahme von Wasserproben für die zuverlässige Bestimmung verschiedener kontaminationsanfälliger Spurenmetalle.
3. Die obersten Zentimeter des Meeresbodens wurden mithilfe eines Multi-Corers an einer Vielzahl von Stationen beprobt.
4. Je nach Standort wurden Sedimentkerne mit einer Länge von fünf bis zu 25 Metern entweder mit einem Kolben-, Schwere- oder Kastenlot beprobt.
5. Die obersten 500 Meter der Wassersäule wurden mithilfe eines Multinetzes und/oder eines Einzelplanktonnetzes auf Plankton beprobt.
6. In einzelnen Schwerpunktgebieten (Prydz-Bucht und vor dem Denman-Gletscher) wurde ein ausgedehntes Wasserprogramm durchgeführt, um die Wassermassen-verteilung und deren physikalisch-chemischen Eigenschaften im Hinblick auf das Einströmen modifizierten Zirkumpolaren Tiefenwassers zu charakterisieren.
7. Viele biologische Hälterungsstudien wurden an Bord während der Ausfahrt durchgeführt. Diese setzen die chemisch-ozeanographischen Beobachtungen der Ausfahrt in Kontext mit der Primärproduktivität im Arbeitsgebiet.
8. Ausgiebige landgeologische Arbeiten rundeten das wissenschaftliche Programm ab.

Fahrtverlauf

Die Strecke unseres Fahrtabschnitts war mit 10.379 Seemeilen sehr transitintensiv (Abb. 1.2), weshalb beim Einreichen des Fahrtantrags auch die maximal möglichen 70 Tage Fahrtdauer beantragt wurden. In Kapstadt wurde die Abfahrt jedoch zunächst durch Reparaturen des Bugstrahlers und dem Austausch eines defekten X-Band Radars um mehrere Tage verzögert. Dank des sehr engagierten Einsatzes der Schiffsleitung konnten beide Reparaturen trotz erheblicher Lieferprobleme erfolgreich abgeschlossen werden, sodass wir am 28.11.23 Kapstadt mit drei Tagen Verspätung am frühen Abend verlassen konnten.

Die erste wissenschaftliche Station erreichten wir nach nicht einmal zwei Tagen, und dort konnten die meisten Geräte schon erfolgreich eingesetzt werden. Die Struktur der offenmarinen

Stationen beinhaltete immer den Einsatz einer Reihe von Instrumenten: CTD, Clean-CTD, Multinetz, manchmal Planktonnetz, Multi Corer, Schwere- oder Kolbenlot. Zwei unterschiedliche Wasserschöpfer mussten wir einsetzen, da der spurenmetallsaubere Wasserschöpfer (Clean-CTD) durch das Fahren über das 11 mm Dyneemaseil nicht elektronisch mit dem Schiff verbunden werden konnte und deshalb einen ersten Durchgang mit dem schiffseigenen Wasserschöpfer erforderte. Durch die Vielzahl an Instrumenten erstreckten sich die Stationszeiten im offenen Südozean oft auf 14 bis 20 Stunden. Wegen der erwarteten teils ungünstigen Wetterlage konnten deshalb die schweren Geräte manchmal nicht gefahren werden, oder es wurde ein Schwerelot anstelle eines Kolbenlots eingesetzt. Hierbei funktionierte auch die Koordination mit den Meteorologen an Bord sehr gut. Die Clean-CTD hatte zu Beginn technische Probleme, die durch den geräteverantwortlichen Wissenschaftler aber nach wenigen verpassten Stationen gelöst werden konnten. Die Zusammenarbeit von Wissenschaftlern und Mannschaft an Deck hat sich auf dem ersten Fahrtabschnitt von Kapstadt in Richtung Prydz-Bucht schnell eingespielt und hat die gesamte Reise über sehr gut funktioniert. Da das Wetter im Verlauf des Transits von Kapstadt in die Prydz-Bucht meist zu erheblichem Wellengang führte, konnten auf diesem Fahrtabschnitt leider nicht an allen Stationen Kolben- bzw Schwerelote gewonnen werden. Die Probenausbeute mit dem regulären Wasserschöpfer, die MUC-Beprobungen, und nach anfänglichen Schierigkeiten auch Probennahmen mit dem spurenmetallsauberem Wasserschöpfer verliefen wie erwartet gut. An einer Vielzahl von Stationen wurden zudem Multi- oder Planktonnetz eingesetzt.

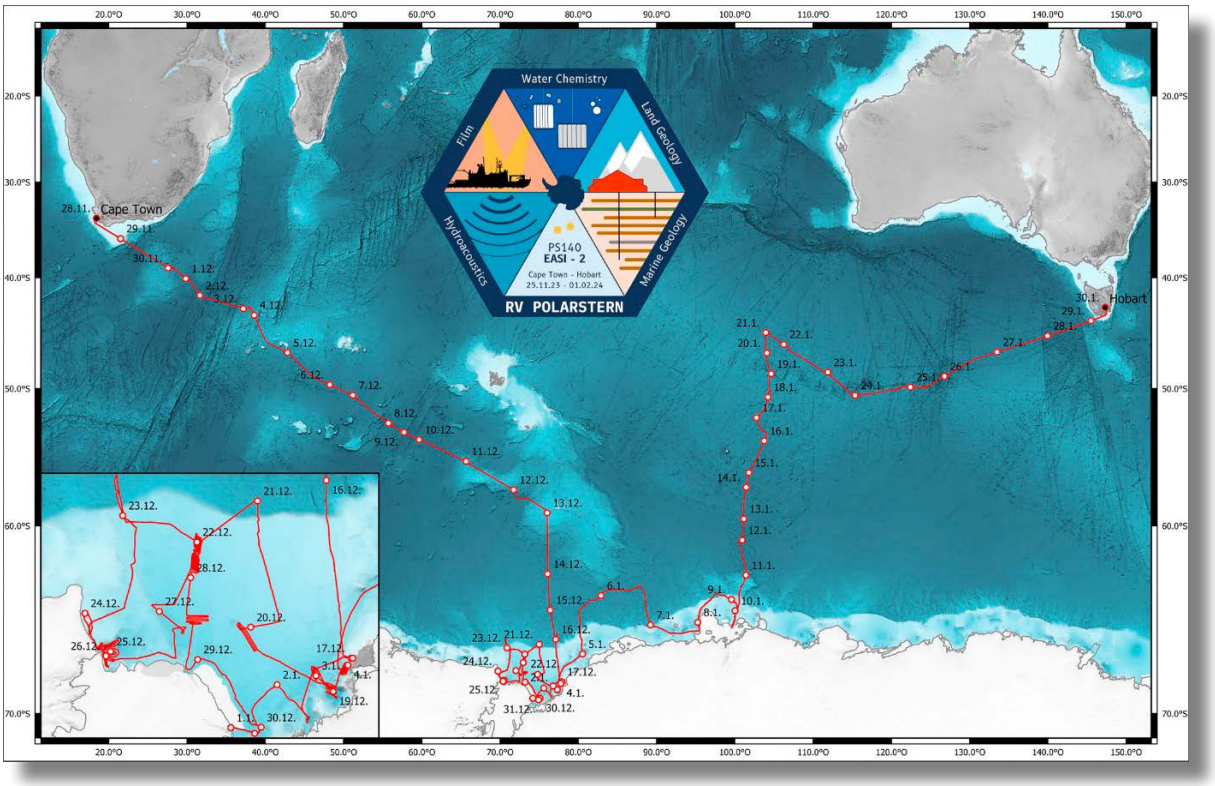

Abb. 1.2: Detaillierter Verlauf von EASI-2. Polarstern konnte Kapstadt erst mit drei Tagen Verspätung verlassen, und musste Hobart zwei Tage früher als geplant wegen Bunkerproblemen vor Ort anlaufen. Die detaillierte Karte unten links zeigt den Fahrtverlauf während der Stationsarbeit in der Prydz-Bucht.

Fig. 1.2: Detailed cruise track of EASI-2. Polarstern was only able to leave Cape Town with a delay of three days and had to call at Hobart two days earlier than planned due to bunker problems. The detailed map at the bottom left shows the course of the journey during station work in Prydz Bay.

Nach 18 Tagen Reisezeit erreichten wir den ersten größeren Wegpunkt, die australische Forschungsstation „*Davis Station*“ in der östlichen Prydz-Bucht. Hier erfolgte das Ausfliegen der Landgeologen in das Vestfold Hills Arbeitsgebiet. Der Helikoptertransfer vom Schiff ins Feld hat außerordentlich gut funktioniert. Das Wetter passte, der Einsatz des Helikopterteams war effizient und professionell, australische Kollegen der *Davis-Station* halfen uns bei logistischen Details, und das Landgeologenteam durfte sogar eine Schutzhütte der Australier (Watts Hut) als Unterkunft für ihr Camp nutzen (siehe Kapitel 6). Wir nutzten die Zwangspause während des Ausfliegens der Landgeologen für einen Besuch der *Davis-Station* durch die übrigen Wissenschaftler und die *Polarstern*-Mannschaft der *Davis-Station*. Auch wurde eine kleinere Gruppe Australier, die Mannschaftsmitglieder der *Polarstern* mit den Zodiacs zum Schiff brachten, über unser Schiff geführt. Dieser beiderseitige Austausch war ein voller Erfolg.

Nach dem Aussetzen der Landgeologen hatten wir knapp drei Wochen Arbeitszeit in der Prydz-Bucht. Durch die weitestgehend eisfreien Bedingungen konnten wir ein unerwartet ausgiebiges Stationsprogramm realisieren. Wir fuhren sämtliche klimatologisch-ozeanographisch wichtigen Gebiete an und studierten die Begebenheiten vor Ort. So ermittelten wir (i) im NE der Prydz-Bucht das Einströmverhalten modifizierten Zirkumpolaren Tiefenwassers, (ii) untersuchten im NW das Ausfließverhalten neu gebildeten dichten Schelfwassers, (iii) fuhren einen Schnitt entlang eisnaher Gebiete entlang der gesamten westlichen und südlichen Prydz-Bucht, um die Hydrographie eisnaher Wassermassen zu quantifizieren und (iv) beprobten an verschiedenen Stationen in der zentralen Prydz-Bucht die Wassersäule, um die Interaktion zwischen einfließendem Wasser aus dem offenen Südozean und lokaler Schelfwassermassen zu bestimmen. An mehreren Stationen der Prydz-Bucht führten wir ausgedehnte bathymetrische Kartierungen durch, um einerseits die besten Kernstationen zu ermitteln, andererseits um glazial-morphologische Strukturen des Meeresbodens aufzulösen. So konnten die Positionen vergangener Auflagezonen des Antarktischen Eisschildes am Meeresboden kartiert werden, die der Entschlüsselung der postglazialen Eisrückzugsgeschichte dienen werden. Schwerelotsedimentproben entlang der Auflagezonenkeile werden dabei zur exakten Datierung der Rückzugsdynamik dienen. Analysen von Kolbenlotsedimentkerne mit bis zu 22 Meter Länge aus tiefen Rinnen und Senken mit erhöhter Sedimentationsrate entlang der Schelfeisfront werden Details der postglazialen Geschichte der Prydz-Bucht in bisher nicht erreichter zeitlicher Auflösung ermöglichen. Auch mussten wir des öftren feststellen, dass existierende satellitenbasierte Tiefenangaben in Schelfeisnahen Gebieten unzuverlässig waren.

Nur kurze Zeit mussten wir in der südöstlichen Prydz-Bucht durch Festeis brechen, um auf die Rückseite eines neu geöffneten Spalts des östlichen Amery-Eisschilds zu gelangen (Abb. 1.3). Dieses Ziel konnten wir nach anderthalb Tagen Eisfahrt auch erreichen. Ziel dieser Station ist die Evaluation, inwieweit die lokalen Wassermassen der südlichen Amery Eisschelffront schon Anzeichen menschlicher Aktivitäten aufweisen. Im Großen und Ganzen war das Wasser- und Geologie-Programm in der Prydz-Bucht sehr ergiebig, und eine derart ausführliche Bestandsaufnahme der aktuellen Wassermassenverteilung wurde seit langem nicht mehr durchgeführt; durch *Polarstern*-Wissenschaftler noch nie.

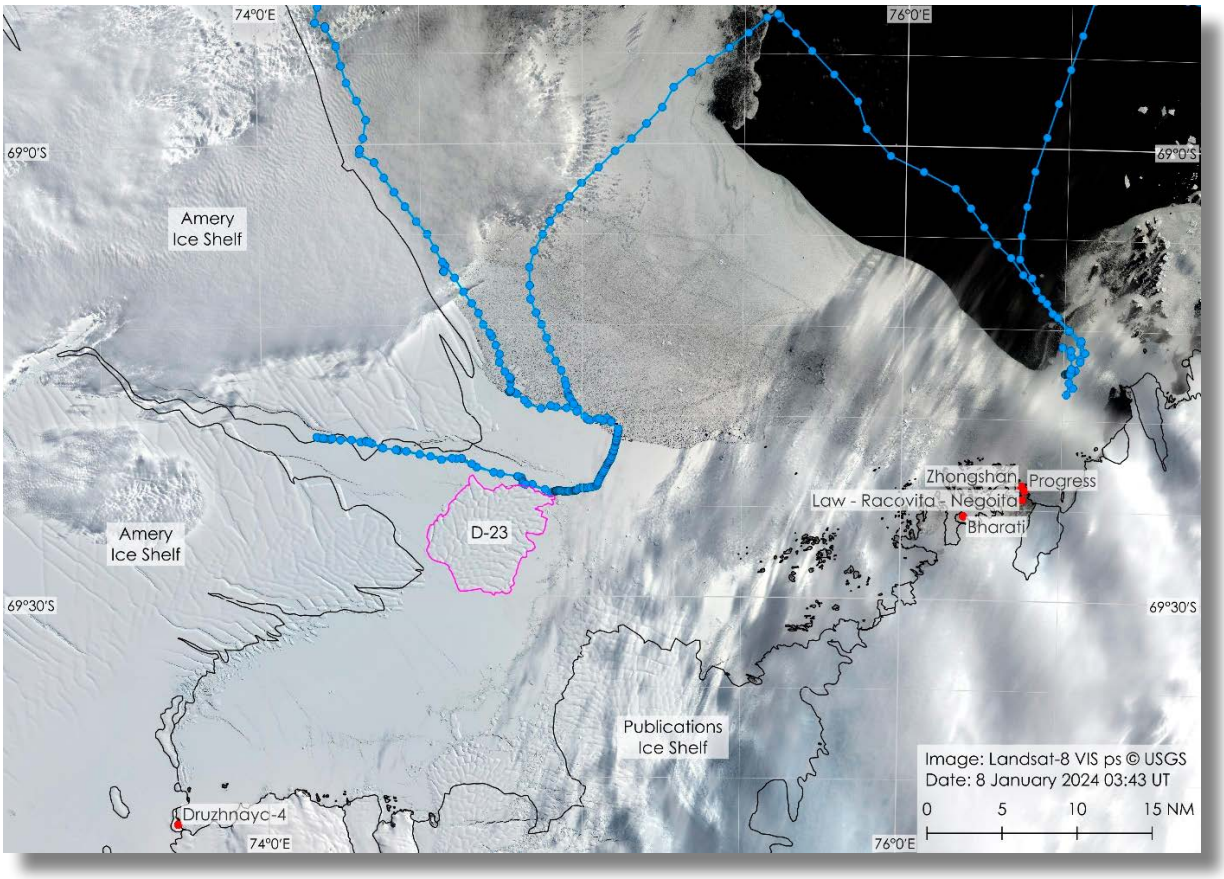

Abb. 1.3 Satellitenaufnahme des östlichen Bereichs Amery Eisschelfs Ende Dezember 2023 während unserer Ausfahrt. Wir nutzten die Schelfeisbegebenheiten, um einen neu geöffneten Spalt zu befahren. Treibeis- und Festeisgebiete sind gut zu erkennen. Der weitere Fahrtverlauf in Richtung Davis-Station ist auch dargestellt.Sowohl die chinesische wie die russische und die indische Forschungsstation sind am östlichen Bildrand gezeigt. Quelle der Landsat-Aufnahme: U.S. Geological Survey. Abbildung bereitgestellt durch Jan Lieser (ACECRC Hobart).

Fig. 1.3: Satellite image of the southeastern area of the Amery ice shelf at the end of December 2023 during our expedition. We took advantage of the ice shelf conditions to stear Polarstern through a newly opened gap in the ice shelf. Drift ice and fast ice areas are clearly recognisable. The further course of the journey towards Davis Station is also shown, with the Chinese, Russian and Indian research stations at the eastern edge of the picture. Source of Landsat data: U.S. Geological Survey. Image provided by Jan Lieser (ACECRC Hobart).

Wegen angekündigten schlechten Flugwetters holten wir die Landgeologen zwei Tage früher als ursprünglich geplant bereits am 4. Januar 2024 aus dem Feld. Diese Entscheidung erwies sich als sehr weise, da wir östlich der Prydz-Bucht vor dem West Eisschelf in ein großes Treibeisgebiet gerieten, welches wir großräumig umfahren mussten. Wegen der Eisverhältnisse konnte auch ein Zielgebiet der geplanten Landgeologie nicht angeflogen werden, da es außerhalb der Flugreichweite lag. Westlich, nördlich und östlich des Shackleton Eisschelfs und vor dem Denman-Gletscher führten wir erneut ein intensives Wasserprogramm durch, wobei wir auch dort ein großes Treibeisfeld umfahren mussten. In diesem Bereich des ostantarktischen Schelfs strömt modifiziertes Zirkumpolares Tiefenwasser auf den Schelf, was zu erheblichen basalen Schmelzraten des lokalen Schelfeises führt. Innerhalb von zwei Tagen konnten wir alle erreichbaren ozeanographisch relevanten Punkte anfahren und untersuchen.

Den Antarktischen Schelf verließen wir am 10.1.24. In den folgenden 12 Tagen realisierten wir einen einzigartigen Schnitt entlang ~100-105°E, der sich vom Antarktischen Schelf bis

hin zu 45°S erstreckt, mit insgesamt zwölf gekoppelten Wasser- und Sedimentstationen. Wissenschaft und Mannschaft waren perfekt eingespielt und wir hatten sehr viel Glück mit dem Wetter. Die Ergebnisse dieses Arbeitsabschnitts sind ein weiteres wissenschaftliches Highlight dieser Ausfahrt. Während das Wasserprogramm nach Abschluss des Süd-Nord-Schnitts weitestgehend abgeschlossen war, wurden danach noch mehrere marine Geologie-Stationen angefahren. Auch dort konnten erfolgreich mehrere lange Sedimentkerne gewonnen werden, wenn auch wetterbedingt am Ende die letzten Kernlokationen ausfallen mussten. Sedimentkerne aus Schwereloten und Kolbenloten mit bis zu 24 Metern Länge werden Rekonstruktionen der Frontendynamik, der Paläoproduktivität und der Meereisausdehnung im indischen Sektor des Südozeans bis zu geologischen Altern von 800.000 Jahren ermöglichen und als Grundlage für mikropaläontologische, geochemische und geophysikalische Analysemethoden in den heimischen Laboren dienen.

Der TV-MUC kam auf PS140 nur selten zum Einsatz, da es Probleme mit den Telemetrie-Komponenten, oder aber dem Lichtwellenleiterkabel (LWL) gab. Während das LWL noch um 600 Meter während der Ausfahrt eingekürzt wurde, konnten dennoch kaum Videoaufnahmen bei MUC-Einsätzen mehr gemacht werden.

Leider erreichten uns knapp zwei Wochen vor Fahrtende zwei unerfreuliche Nachrichten: Erstens war die Bunker-Pier in Hobart defekt, zweitens ein Lotsenstreik in Hobart während der Zeit unseres Aufenthaltes angekündigt. In Anbetracht der Tatsache, dass während des Aufenthaltes von *Polarstern* in Hobart ein reges wissenschaftliches Austauschprogramm geplant war inklusive Botschaftsempfang am 5. Februar 2024 an Bord von *Polarstern* und der Hafeneinlauf nicht verschoben werden sollte, mussten wir deshalb schon am Vormittag des 30. Januars 2024 in Hobart sein und fuhren dort als erstes zur Bunker-Pier. Das Bunkern erfolgte am 31. Januar. Wegen zu starken Windes war die Durchfahrt der Tasman-Brücke im Hafen von Hobart am 1. Februar gesperrt, weshalb die Wissenschaftlerinnen und Wissenschaftler von EASI-2 an der Bunkerpier von Bord gehen mussten. Dass wir trotz des Wegfalls von fünf Expeditionstagen alle gesteckten wissenschaftlichen Ziele erreichen konnten verdanken wir in erster Linie dem Kapitän Felix Lauber, der die verlorene Zeit durch erhöhte Transitgeschwindigkeiten aufholte. Die Atmosphäre zwischen Mannschaft und Wissenschaft war ausgesprochen angenehm und produktiv während der gesamten Ausfahrt.

Verlauf der Landkampagne

Die geologischen und geodätischen Untersuchungen in den Vestfold Hills, einem eisfreien Küstengebiet am Ostrand der Prydz-Bucht, konzentrierten sich auf den südlichen Teil dieser sogenannten „Oase“. Die Landgruppe bestand aus sechs Personen sowie umfangreicher Feldtechnik und Verbrauchsmaterial mit einem Gesamtgewicht von ca. 3600 kg.

Am 17. Dezember 2023 wurden die Teilnehmer und die Ausrüstung mit insgesamt 11 Flügen eines Hubschraubers vom „*Polarstern*“ zur Watts Hut, einer Schutzhütte der Australian Antarctic Division (AAD), ausgeflogen. Dort wurde unter Nutzung der Infrastruktur der Hütte ein Feldlager mit Schlafzelten aufgebaut und betrieben, unterbrochen lediglich für die Nacht vom 25. auf den 26. Dezember, die auf Einladung der AAD an der australischen Forschungsstation Davis verbracht wurde. Die Landkampagne hatte täglich zwei Mal Kontakt zur *Polarstern* (über Satellitentelefon) und einmal zur *Davis-Station* (über UKW-Funk), jeweils mit Lage- und Wetterbericht. Die Evakuierung der Feldkampagne zurück zum Polarstern erfolgte am 4. Januar 2024 mit insgesamt 12 Hubschrauber-Flügen.

In der Zeit vom 18. bis zum 22. Dezember 2023 wurde aus dem Watts Lake, einem 35 m tiefen See direkt südlich der Watts Hut, ein ca. 13,2 m langer Sedimentkern von der Seeeisdecke aus gewonnen, der aus 14 überlappenden Schwerelot- und Kolbenlotkernen besteht. Anschließend wurde die Kerntechnik an der Watts Hut vorbei zum etwa 250 m entfernten

Ufer des Ellis Fjords nördlich der Hütte getragen. Von dort erfolgte der Transport überwiegend per Schneemobil und Schlitten auf dem Meereis des Ellis Fjords. Aus dem Fjord wurden zwischen dem 23. Dezember 2023 und dem 2. Januar 2024 überlappende Schwerelot- und Kolbenlotkernen an vier Lokationen gewonnen. Drei der Lokationen liegen in Becken zwischen 110 und 85 m Wassertiefe und bilden einen ca. 7,5 km langen Ost-West Transekt über den südlichen Teil der Oase. An diesen Stationen wurden Sedimenttiefen zwischen 12,6 und 8,0 m erreicht. An einer vierten Station in einer Lagune am Nordufer des Ellis Fjords wurden am 2. Januar 2024 zwei Schwerelotkerne und zwei Kolbenlotkerne erbohrt, die eine Sedimenttiefe von ca. 6,0 m erreichen, jedoch ohne Überlappung im unteren Teil.

Parallel zu den Bohrungen wurden während des gesamten Aufenthaltszeitraums mit Unterbrechungen eine Reihe von Messungen und Probennahmen an Land durchgeführt. Diese Untersuchungen konzentrierten sich auf gehobene Strandwälle, die bezüglich Morphologie per Lidar und geodätischen Methoden vermessen, bezüglich ihres internen Aufbaus per Bodenradar und Schürfen untersucht und für Lumineszenz- und Radiokohlenstoff-Datierungen beprobt wurden. Daneben wurden marine und lakustrine Sedimente im Einzugsgebiet des Watts Lake beprobt. Die Probenpunkte wurden z.T. mit geodätischen Methoden eingemessen, ebenso wie die aktuellen Wasserstände von Watts Lake und Ellis Fjord sowie die Morphologie von potentiellen Überflutungsflächen zwischen den Wasserkörpern. Darüber hinaus wurden an drei Lokationen Bodenkrusten für Biodiversitäts-Studien gewonnen.

Parallel und im Anschluss an die Arbeiten in den Vestfold Hills wurden weitere Landgebiete für wenige Stunden per Hubschrauber aufgesucht. Am 7. Januar 2024 wurden auf dem Gaußberg (ca. 89° E) eine geodätische Referenzstation aufgebaut, glazial transportierte Gerölle für Expositionsdatierungen genommen und die Möglichkeiten für ein Feldlager auf der Expedition PS141 erkundet. Auf der Gillis-Insel (ca. 66° E) wurde am 8. Jan. 2024 eine australische geodätische Referenzstation gewartet. Sedimentführendes Inlandeis wurde während insgesamt fünf Helikopter-basierten Feldkampagnen zwischen dem 1. und 10. Januar 2024 durchgeführt. Die ersten drei Flüge konzentrierten sich auf südlich an die Prydz-Bucht angrenzende Felsaufschlüsse. Während des dritten Fluges wurde eine Schermoräne in den östlichen Vestfold Hills, und am 10. Januar 2024 wurde am Ostrand der Bunger Hills (ca.101° E) sedimentführendes Inlandeis beprobt. Während der letzten Eisbeprobung in der Nähe des Denman-Gletschers übergaben wir außerdem noch ein wissenschaftliches Gerät an australische Kollegen, die in der Bunger-Oase ein Sommer-Feldlager aufgebaut hatten.

Die EASI-2-Expedition unterstützt die Ziele der Programmorientierten Förderung (PoF) der Helmholtz-Gemeinschaft, des Forschungsprogramms „Changing Earth – Sustaining our Future“. Die behandelten Themen fallen vor allem in Thema 2 (Ozean und Kryosphäre im Klima) und decken alle vier Unterbereiche ab. Innerhalb von Thema 6 (Meeres- und Polarleben) erstrecken sich die durchzuführenden Forschungsarbeiten auf die Unterthemen 6.1 bis 6.3. Die Forschung dieser beiden PoFs der Helmholtz-Gemeinschaft wird sowohl am AWI Bremerhaven als auch am GEOMAR Kiel durchgeführt.

SUMMARY AND ITINERARY

Expedition EASI-2 (East Antarctic Ice Sheet Instability) is the second of three jointly designed *Polarstern* expeditions aiming to investigate the history of East Antarctic Ice Sheet (EAIS) instability and its interaction with changes in Southern Ocean (SO) circulation. While the first of the three expeditions (EASI-1) already took place from 6 January to 28 February 2022, the third (EASI-3) followed immediately after EASI-2 (6 February to 16 April 2024) (Fig. 1.1). Each of the three coordinated expeditions has its own research focus related to the potential instability of the EAIS during current and past climatic changes. Compared with the other two expeditions, EASI-2 focuses most strongly on current processes in the Southern Ocean water column, observable modern nutrient availability with a particular emphasis on the delivery of essential micronutrients from the seafloor and East Antarctica. Two transects of the water column in the open ocean were realised to determine the structure, chemical composition and current circulation status in the study area. Analogous work on the East Antarctic shelf provides the proximal Antarctic perspective on both physical and chemical oceanographic trends that can be observed today in times of generally rising seawater temperatures, decreasing sea ice extent and a decline in the salinity of various water masses in the SO such as the Antarctic Bottom Water (AABW). At the majority of deep-water stations of the two transects, complementary sampling of deep marine sediments of up to 25 metres below the sea floor allows changes in the properties of the water column to be traced back over more than the last 800 thousand years. The sedimentary work focusses on the Pleistocene dynamics of oceanic fronts within the Antarctic Circumpolar Current, changes in sea surface water temperatures, the past carbon budget of the water column and past sea ice extent. On the East Antarctic shelf, combined parasound profiles and sediment sampling allow us to answer questions about the history of the Quaternary ice sheet and past deep-water formation. Particularly in the south-eastern part of Prydz Bay, extensive sediment cores have also been obtained, which allow us to reconstruct the Holocene climate in the region at high temporal resolution. These cores are also very valuable because, in parallel to the marine work, the team of land geologists was able to obtain limnic and marine cores in a fjord near the Australian *Davis Station* during a land campaign lasting almost three weeks. We are thus able to bridge the gap between terrestrial and marine climate reconstructions, a major overarching goal of the EASI expeditions.

Probably the most outstanding feature of this expedition is the endeavour to closely link modern observations from water column work with past states of SO circulation modes by using a variety of state-of-the-art methods and/or proxies and sampling strategies. For example, we can quantify sedimentary diagenetic processes at many realised sampling sites, in parallel with the application of palaeoceanographic proxies, such as the recovery of authigenic (i.e. seawater-derived) trace metals (e.g. Nd and Pb). Various geochemical methods are applied to extracted material (water, ice and sediments) in the home laboratories in order to evaluate the reliability of marine sedimentary archives. In a further step, palaeoceanographic reconstructions will be carried out. Our cruise section covers a range of climate zones, from the temperate latitudes north of the subtropical front, through all frontal systems of the Southern Ocean, to the East Antarctic Ice Sheet. The composition of the sediments is correspondingly diverse and ranges from purely biogenic to purely terrestrial sediments, with correspondingly variable diagenetic redox zonation in sampled sediment.

Temperature (e.g. Mg/Ca, $\delta^{18}O$, transfer functions) and carbonate system-related proxies (B/Ca, $\delta^{11}B$) measured on plankton samples and microfossils in the sediment can be directly compared with the carbonate system parameters ($\delta^{13}C$, TA, DIC) of the present-day water column, which we have also obtained. In addition, proxies for sea ice extent in the past (e.g. PIPSO25, diatom transfer functions) will answer questions about sea ice dynamics in the Pleistocene. Thanks to the use of a trace metal clean water sampler, we are in the unique position to measure high quality data on present-day exchange processes of various trace metals between (i) the seafloor and bottom water, and (ii) different water masses in the open water column of the Southern Ocean. Last but not least, we will (iii) determine the anthropogenic input of selected trace metals such as lead into the Southern Ocean water column, and subsequently also into Antarctic waters. Our analyses also extend to the quantification of the subglacial input of transition metals and other analytically challenging trace metals, for which hardly any data are available from the Antarctic to date. Water samples were also taken to determine the radiocarbon content of the present-day water column and the methane concentrations in Antarctic waters and the atmosphere. At the majority of the stations visited during EASI-2, an extended spectrum of sampling strategies was pursued:

1. By using the regular water sampler, the structure of the water column was first determined and water samples were taken for various applications.
2. The use of a trace metal clean water sampler allowed water samples to be taken for the reliable determination of various trace metals susceptible to contamination.
3. The uppermost centimetres of the seafloor were sampled at a number of stations using a multi-corer.
4. Depending on location, sediment cores ranging from five to 25 metres in length were sampled using either a piston, gravity or box corer.
5. The uppermost 500 metres of the water column were sampled for plankton using a multi-net and/or a single plankton net.
6. In individual focus areas (Prydz Bay and off Denman Glacier), an extensive water programme was carried out to characterise the water mass distribution and its physico-chemical properties with regard to the inflow of modified Circumpolar Deep Water.
7. Various biological culturing studies were conducted on board during the cruise. These put the chemical-oceanographic observations of the cruise in context with the primary productivity in the working area.
8. Extensive land geological work rounded off the scientific programme.

Itinerary

With a total covered distance of 10,379 nmi, the route of our cruise leg was very transit-intensive (Fig. 1.2), which is why the maximum possible duration for a *Polarstern* cruise of 70 days was requested when submitting the cruise proposal. In Cape Town, however, the departure was initially delayed by several days due to repairs to the bow thruster and the replacement of a defective X-band radar. Thanks to the very dedicated efforts of the ship's management, both repairs were successfully completed despite considerable delivery problems, so that we were able to leave Cape Town in the early evening of 28 November 2013, three days late.

We reached the first scientific station after less than two days of transit, and most of the equipment there was already successfully deployed. The structure of the open-marine stations always included the use of a range of instruments: CTD, clean CTD, multi-net, sometimes

plankton net, multi corer, gravity or piston corer. We had to use two different water samplers, as the clean CTD could not be electronically connected to the ship given that the 11 mm Dyneema cable had to be used for trace metal clean water sampling, and therefore required a first descent with the ship's own water sampler. Due to the large number of instruments, the station times in the open Southern Ocean often extended to 14 to 20 hours at deep water locations. Due to the unfavourable weather conditions sometimes expected, the heavy equipment could not be used in places, or a gravity corer bob was used instead of a piston corer. Coordination with the meteorologists on board also worked very well. The Clean CTD had technical problems at the beginning, but the scientist in charge for the Clean CTD was able to solve these after a few missed stations. The close cooperation between the scientists and crew on deck was quickly established during the first leg of the journey from Cape Town towards Prydz Bay and worked very well throughout the entire cruise. As the weather during the transit from Cape Town to Prydz Bay mostly led to considerable swell, it was unfortunately not possible to obtain piston or gravity cores at every station on this leg of the journey. The sample yield with the regular water sampler, the MUC sampling and, after initial difficulties, sampling with the trace metal-clean water sampler went well, as expected. Multi- or plankton nets were also used at many stations.

After 18 days of travelling, we reached the first major waypoint, the Australian research station "*Davis Station*" in eastern Prydz Bay. This is where the land geologists were flown out to the Vestfold Hills working area. The helicopter transfer from the ship to the field worked exceptionally well. The weather was fine, the helicopter team was efficient and professional, Australian colleagues from *Davis Station* helped us with logistical details, and the land geology team was even allowed to use an Australian shelter (Watts Hut) as accommodation for their camp (see Chapter 6). The remaining scientists as well as the *Polarstern* crew used the forced break during the land geologists' departure to visit *Davis Station*. A small group of Australians, brought towards *Polarstern* by our crew members in the Zodiacs, were also given a tour of our ship. This mutual exchange was a complete success.

After deploying the land geologists at their field camp, we had just under three weeks of working time in Prydz Bay. Thanks to the largely ice-free conditions, we were able to carry out an unexpectedly extensive station programme. We covered all climatologically and oceanographically important areas within Prydz Bay and studied the conditions on site. For example, we (i) determined the inflow behaviour of modified Circumpolar Deep Water in the NE of Prydz Bay, (ii) investigated the outflow behaviour of newly formed Dense Shelf Water in the NW, and (iii) sampled a water column section along the ice shelf edge along the entire western and southern Prydz Bay, to quantify the hydrography of water masses close to the ice shelf edge, and (iv) sampled the water column at various stations in central Prydz Bay to determine the interaction between inflowing water from the open Southern Ocean and local shelf water masses. We carried out extensive bathymetric mapping at several stations in Prydz Bay to identify the best sediment coring stations and to resolve glacial-morphological structures of the seafloor. This allowed us to map the positions of past Antarctic Ice Sheet grounding zones on the seafloor, which will help to decipher the post-glacial ice retreat history. Sediments sampled via gravity coring in proximity to identified grounding zone wedges will be used to precisely date the regional ice sheet retreat dynamics. Analyses of piston sediment cores up to 22 metres in length from deep channels and depressions with increased sedimentation rates along the ice shelf front will provide details of the post-glacial history of Prydz Bay at unprecedented temporal resolution. We also had to realise at several locations that existing satellite-based bathymetric data in areas close to the ice shelf were highly unreliable.

We only had to break through fast ice in south-eastern Prydz Bay for a short time in order to reach the back of a newly opened rift in the eastern Amery Ice Sheet (Fig. 1.3). We were able to reach this destination after one and a half days of ice breaking. The aim of this most remote station is to evaluate the extent to which the local water masses of the southern Amery ice shelf front already show signs of human activity. On the whole, the water and geology

programme in Prydz Bay was very productive, and such a detailed survey of the current water mass distribution has not been carried out for a long time; never before during a *Polarstern* expedition.

Due to predicted poor flying weather conditions, we brought the land geologists back from the field on 4 January 2024 two days earlier than originally planned. This decision proved to be very wise, as we subsequently had to transit through a large area of drift ice east of Prydz Bay off the West Ice Shelf, which we had to bypass in a substantial detour. Due to the ice conditions, it was also not possible to fly to one target area of the planned land geology, as it was outside the flight range. To the west, north and east of the Shackleton Ice Shelf and in front of the Denman Glacier, we again carried out an intensive water programme, whereby we also had to circumnavigate a large drift ice field. In this area of the East Antarctic shelf, modified Circumpolar Deep Water flows onto the Antarctic shelf, which leads to considerable basal melting rates of the local ice shelf. Within two days, we were able to visit and investigate all the oceanographically relevant points in reach.

We left the Antarctic shelf on 10 January 2024. In the following 12 days we realised a unique transect along ~100-105°E, extending from the Antarctic shelf to 45°S, with a total of twelve coupled water and sediment stations. Science and crew were perfectly synchronised and we got very lucky with the weather. The results of this work section are another scientific highlight of this EASI-2 cruise. While the water programme was largely completed once the south-north section was finished, several marine geology stations were still visited afterwards. Several long sediment cores were also successfully obtained there, even though the last core locations had to be cancelled due to poor weather conditions. Sediments from gravity cores and piston cores up to 24 metres in length will enable reconstructions of frontal dynamics, palaeoproductivity and sea ice extent in the Indian sector of the Southern Ocean up to geological ages of 800,000 years and serve as a basis for micropalaeontological, geochemical and geophysical analysis methods in the laboratories at home.

The TV-MUC was rarely used on PS140 due to problems with the telemetry components or the fibre optic cable. While the fibre optic cable was shortened by 600 metres during the trip, hardly any video recordings could be made during MUC missions.

Unfortunately, we received unpleasant news just two weeks before the end of the journey: Firstly, the bunker pier in Hobart was defective, and secondly, a pilot strike had been announced in Hobart during the time of our stay. In view of the fact that a lively scientific exchange programme was planned during *Polarstern*'s stay in Hobart, including an embassy reception on board *Polarstern* on 5 February 2024, and the port entry was not to be postponed, we therefore had to be in Hobart on the morning of 30 January 2024, hence two days earlier than planned, and went to the bunker pier first. Bunkering took place on 31 January. Due to strong winds, the passage of the Tasman Bridge in Hobart harbour was closed on 1 February, which is why the EASI-2 scientists had to disembark at the bunker pier. Yet despite the loss of five expedition days in total, we were able to achieve all our scientific goals thanks primarily to Captain Felix Lauber, who made up for lost time by increasing transit speeds. The atmosphere between the crew and scientists was extremely pleasant and productive throughout the entire expedition.

Itinerary of the land campaign

The geological and geodetic investigations in the Vestfold Hills, an ice-free coastal area on the eastern edge of Prydz Bay, focused on the southern part of this so-called “oasis”. The land group consisted of six people as well as extensive field technology and consumables with a total weight of approx. 3,600 kg.

On 17 December 2023, the participants and equipment were flown from *Polarstern* to Watts Hut, a refuge of the Australian Antarctic Division (AAD), in a total of 11 helicopter flights. A field camp with sleeping tents was set up and operated there using the hut’s infrastructure, interrupted only for the night of 25 and 26 December, which was spent at the Australian

research station Davis at the invitation of the AAD. The land campaign had daily contact with *Polarstern* twice (via satellite phone) and once with *Davis Station* (via VHF radio), each with a situation and weather report. The evacuation of the field campaign back to *Polarstern* took place on 4 January 2024 with a total of 12 helicopter flights.

Between 18 and 22 December 2023, a sediment core approximately 13.2 m long was recovered from the lake ice cover from Watts Lake, a lake of 35 m depth directly south of Watts Hut, consisting of 14 overlapping gravity and piston cores. The coring equipment was then carried past Watts Hut to the shore of Ellis Fjord, approximately 250 m away, north of the hut. From there the transport was mainly by snowmobile and sleigh on the sea ice of Ellis Fjord. Overlapping gravity and piston cores were obtained from the fjord at four locations between 23 December 2023 and 2 January 2024. Three of the locations lie in basins between 110 and 85 m water depth and form an approximately 7.5 km long east-west transect across the southern part of the oasis. At these stations, sediment depths of between 12.6 and 8.0 m were reached. At a fourth station in a lagoon on the north bank of Ellis Fjord, two gravity cores and two piston cores were drilled on 2 January 2024, reaching a sediment depth of approximately 6.0 m, but without overlap in the lower part.

In parallel with the drilling, a series of onshore measurements and sampling were carried out intermittently throughout the duration of the field campaign. These studies focused on uplifted beach ridges, which were surveyed for morphology using lidar and geodetic methods, examined for internal structure using ground penetrating radar and prospecting, and sampled for luminescence and radiocarbon dating. In addition, marine and lacustrine sediments were sampled in the Watts Lake catchment area. The sample points were partly measured using geodetic methods, as were the current water levels of Watts Lake and Ellis Fjord as well as the morphology of potential flood areas between the water bodies. In addition, soil crusts were obtained for biodiversity studies at three locations.

In parallel and following the work in the Vestfold Hills, other areas of the country were visited by helicopter for a few hours. On 7 January 2024, a geodetic reference station was set up at Gaußberg (approx. 89° E), glacially transported gravel was taken for exposure dating and the possibilities for a field camp on the PS141 expedition were explored. An Australian geodetic reference station was maintained on Gillis Island (approximately 66° E) on 8 January 2024. Sediment-bearing continental ice was collected during a total of five helicopter-based field campaigns between 1 and 10 January 2024. The first three flights focused on rock outcrops bordering Prydz Bay to the south. During the third flight, a shear moraine was sampled in the eastern Vestfold Hills, and on 10 January 2024, sediment-bearing inland ice was sampled on the eastern edge of the Bunger Hills (ca. 101° E). During the last ice sampling near the Denman Glacier, we also handed over a piece of scientific equipment to Australian colleagues who had set up a summer field camp in the Bunger Oasis.

The EASI-2 expedition supports the goals of the Helmholtz Association’s program-oriented funding (PoF), the research programme “Changing Earth – Sustaining our Future”. The topics covered fall primarily into Topic 2 (Ocean and Cryosphere in Climate) and cover all four sub-areas. Within Topic 6 (Marine and Polar Life), the research work to be carried out covers subtopics 6.1 to 6.3. The research of these two POFs of the Helmholtz Association is carried out at both AWI Bremerhaven and GEOMAR Kiel.

WEATHER CONDITIONS DURING PS140

Sonja Stöckle DE.DWD

Week 1: 27.11. – 03.12.2023 Cape Town-Prince Edward Islands

On Tuesday evening, 28.11.2023, *Polarstern* was able to leave the port of Cape Town after a three-day delay due to essential repair work. At the time of departure, it was partly cloudy with an air temperature of 19.0°C and a south-westerly wind of 6 to 7 Bft. At sea, a high-pressure zone had formed behind a cold front, which moved south-eastwards into the southern Indian Ocean. The weather was correspondingly calm at sea around the Cape of Good Hope during the first few days with weak winds from easterly, later north-easterly directions and significant seas of less than 3 meters. On Friday, 01.12.2023, the northeast current became stormy with wind peaks of up to 9 Bft. In addition, an interesting wave pattern developed with a wind sea from the Northeast, a first swell from the Southwest and a second swell from the South. Overall, the significant wave height was around 4 meters. This wave pattern accompanied *Polarstern* into the night of Saturday, 02.12.2023. During the night, a significant cold front with heavy rain crossed *Polarstern*. High pressure built up behind it, so that few to scattered clouds with weak winds prevailed during the second research station. At times the wind strength dropped to 2 Bft. The significant swell was 2 to 3 meters with a swell from North-Westerly directions.

Week 2: 04.12. – 10.12.2023 Prince Edward Islands - Prydz Bay

After a weak high pressure system, a severe storm depression dominated the weather at the beginning of the second week of the expedition. The storm developed south of the cruising area and moved further eastwards. On Monday, 04.12.2023, the warm front of the low pressure system crossed *Polarstern*, followed by the cold front in the evening. This caused the air temperature to drop from 13 degrees to 5 degrees. The water temperature also dropped significantly from 11.1°C to 6.1°C as we travelled southeast. Behind the cold front, *Polarstern* sailed southeast through the storm field towards the low center. The wind gradually increased and peaked at just 10 Bft (24.5 m/s, 48 KT) on Wednesday, 06.12.2023, which was also the highest mean wind measured during the voyage. At the same time, the significant sea increased to around 6 meters. On Thursday, 07.122023, *Polarstern* then reached the sixth research station just north of the oceanic polar front. The wind quickly dropped to 7 Bft and the sea also calmed down to 4 meters. The weekend was then calm thanks to a high pressure ridge that extended from the North to the edge of the ice shelf. South-westerly winds between 4 and 6 Bft and significant seas of 2 to 3 meters prevailed. Temperatures varied already only between 0 and 2°C.

Week 3: 11.12. – 17.12.2023 Prince Edward Islands – Prydz Bay

Several small-scale secondary lows developed on the eastern edge of an extremely extensive hurricane forced low between South Africa and the Antarctic mainland. These moved in the direction of the research area. As a result, *Polarstern* experienced several changes between the influence of secondary lows and high-pressure ridges. The wind directions changed frequently, starting on Monday, 11.12.2023, with winds from the West at 5 Bft, which turned to

the Northeast during the course of the day and temporarily decreased to 3 to 4 Bft. On Tuesday, 12.12.2023, the wind then shifted back to the West and increased to 7 to 8 Bft. Air of polar origin was brought in, causing temperatures to drop below 0 degrees for the first time on the expedition. The rapid changes in wind direction and speed prevented the sea from maturing, so that the significant swell remained at 2 to 3 meters. The most striking event of the week was a rapid cyclogenesis. The stormy low was initiated on Tuesday, 12.12.2023, just east of South Africa. As it progressed, the pressure in the center deepened by over 60 hPa within about 40 hours. At the same time, the storm moved southeastwards at 50 knots, so that *Polarstern* came under its influence on Thursday, 14.12.2023. About 400 nautical miles south of the low-pressure center, only moderate winds of around 5 Bft prevailed in the research area, initially from an easterly direction, later turning to the Southwest. The significant wave height remained calm at less than 2 meters. However, the low pressure caused a lot of snowfall, so that a 5 to 10 cm high layer of snow accumulated on the ship. With the passage of the depression, the wind turned completely clockwise once within 24 hours. A high pressure ridge extended southwards again behind the low pressure system, which resulted in light winds and partly sunny weather conditions in the sailing area. By the time *Polarstern* arrived at *Davis Station* on Sunday, 17.12.2023, a low-pressure trough had extended from the extensive hurricane low West of the research area to the West Ice Shelf. As a result, easterly winds prevailed over the weekend. Along the highly indented coastline with different ground conditions, between sea ice, icebergs, rocky coast, rocks and open water, in combination with very dry air (dew point dropping to -12.9°C) and strong winds in 950 hPa to 800 hPa, strong thermal and thus gusty winds with wind forces between 3 and 7 Bft developed. Since *Polarstern* was already in the area of sea ice, the significant wave height remained insignificant.

Week 4: 18.12. – 24.12.2023 Prydz Bay

At the beginning of the week, an area of low pressure was located far to the North of *Polarstern*. Easterly winds prevailed at the southern edge of the depression, so that dry continental air with wind speeds between 3 and 5 Bft prevailed in the research area. It was often sunny because only few clouds could develop in the dry air. On Wednesday, 20.12.2023, the low North of the bay shifted somewhat towards the South. This brought frontal clouds and some snow into the research area. Due to the snowfall and the increasing humidity, visibility was significantly reduced at times. The wind initially blew from easterly directions with 5 to 6 Bft in the frontal influence and shifted to southerly directions with 3 to 4 Bft on Thursday, 21.12.2023. It was not until the night of Saturday, 23.12.2023, that for a short while a high could spread its influence. The frontal clouds dissipated and it became sunny. In the evening, the high-pressure influence weakened again. During the night of Sunday, 24.12.2023, a low pressure system crossed *Polarstern* from West to East and brought many clouds and some snow. On the western edge of the bay, the wind was able to strengthen to South 6 to 7 Bft due to the channeling effect along the coastline. By midday, the wind had already shifted to the Southwest and therefore weakened considerably as a result. At the same time, very dry air was advected by the south-westerly flow, causing the clouds to clear quickly. So we were able to celebrate Christmas Eve with sunny -3°C and south-westerly winds of 3 to 4 Bft.

Week 5: 25.12. – 31.12.2023 Prydz Bay

The weather was initially characterized by weak pressure differences. Any pressure systems were far away from the research area, so the wind and weather pattern was mainly dominated by local and thermal effects. The weather on Monday, 25.12.2023, was characterized by an influx of dry, Antarctic air and was almost cloudless throughout the day. In the evening in particular, katabatic winds blowing off the shelf ice prevailed. Southerly winds of up to 6 Bft were observed with a simultaneous drop in temperature to -10.2°C, which was the lowest

measured temperature of the entire expedition. The dew point also reached its lowest value of the trip at -16.2°C. Over the course of the week, thermal lows repeatedly formed over the relatively warm waters of the bay. As a result, the supply of very dry Antarctic air alternated with the advection of moistened air masses, so that lighter cloud fields kept passing through. The wind came from the South to Southwest, mostly around 4 Bft. There were only significant seas out of sea ice, mostly below 0.5 meters. On Saturday, 30.12.2023, an extensive storm approached from far Northwest of Prydz Bay. This ensured an inflow of warm sea air from the Northeast at the weekend. In lower levels, Easterlies with 3 to 4 Bft dominated, with overcast sky and heavy snowfall at times. On Sunday, 31.12.2023, as *Polarstern* fought its way through dense perennial ice with a 30 cm thick layer of snow, the low pressure system North of Prydz Bay weakened. The air pressure rose continuously and a dry, Antarctic air mass was able to reassert itself. Apart from thin cirrus fields, the clouds dissipated. Temperatures dropped to around -5 °C.

Week 6: 01.01. – 07.01.2024 Prydz Bay – Davis Sea

An extensive and complex low-pressure system with several centers was located far North of Prydz Bay. The research area was located on the southern edge of the system in an easterly flow that continued to bring in very dry Antarctic continental air. The year began on the Amery Ice Shelf with bright sunshine and easterly winds around 3 Bft. The air pressure contrasts were so small and stable that the global periodicity of the air pressure could be observed. The air pressure showed a double maximum on both Monday, 01/01/2024, and Tuesday, 02/01/2024, with the highest maximum at around 09 UTC and a second 12 hours later. The amplitude of the air pressure fluctuation was about 1 hPa, which corresponds to the expected value. The temperature also showed a clear diurnal variation on the pure radiation days without any advection. The temperature rose with the position of the sun from -5 °C to around 0 °C. Due to katabatic or thermal effects at the boundary between water and ice, the wind reached wind speeds of up to 6 Bft at times. On Thursday, 04.01.2024, the complex low pressure system moved eastwards along the Antarctic coastline over the Davis Sea. A convergence line developed from this low pressure system, which moved to the eastern edge of Prydz Bay. On this day, *Polarstern* was in the vicinity of the *Davis Station* to bring the land geologists and their equipment back to the ship. The day began with clear skies. In the evening, the convergence line reached the ship with dense clouds and it began to snow lightly. The wind turned 360° from East to North to South and later back to East. With the convergence line, the humidity increased significantly; the dew point rose from -15.3°C to -0.1°C. At the same time, the pressure dropped to 968.4 hPa (lowest air pressure of the voyage). *Polarstern* spent the next few days in the area of the convergence line with almost overcast skies and repeated light snowfall. The wind fluctuated several times from easterly to westerly directions with a wind force between 3 and 5 Bft. It was only on Sunday, 07.01.2024, that *Polarstern* left the convergence area and entered a southeasterly airflow with dry air advection.

Week 7: 08.01. – 14.01.2024 Davis Sea including Denman Glacier

At the beginning of the week, *Polarstern* was in an area of weak pressure differences. A south-easterly breeze brought dry continental air into the research area. During the night of Tuesday, 09.01.2024, the cruise area passed through a shallow low-pressure trough that spread out from the East. Loose but multi-layered clouds prevailed. Occasionally, some snow fell out of cumulus congestus clouds. The wind blew from easterly directions around 3 Bft. On Wednesday, 10.01.2024, *Polarstern* sailed South at the exit of the Denman Glacier to the shelf ice edge. Very dry air was advected with weak southerly winds of 2 to 3 Bft, which dried out the clouds from the South. Apart from a few thin cirrus fields, there were no clouds during the day. The air temperature was between -4 and -1 °C. *Polarstern* continued northwards and reached

the Southern hemispheric Westerly wind zone on Thursday, 11.01.2024. The wind came from the West to Northwest at 6 to 7 Bft and ensured an influx of relatively mild and humid air. The dew point rose continuously from -7°C to +1°C by Saturday evening, 13.01.2024. Some snow or sleet fell from time to time. On Friday, 12.01.2024, there was also temporary fog. On the night of Saturday, 13.01.2024, *Polarstern* left the ice and entered the open sea again. A significant wave height of 3 meters and a swell from the West-Northwest awaited us there. On Saturday evening, a depression crossed *Polarstern* from Northwest to Southeast. With the passage of the low, the air pressure dropped from 1003.5 hPa to 988.5 hPa and the wind temporarily shifted to the North. At the same time, the cloud bases of the overcast stratus cloud layer dropped. This also resulted in partly limited visibility due to mist, later also in combination with drizzle. On Sunday, 14.01.2024, drier air then pushed in behind the low pressure system with a southwesterly to westerly flow.

Week 8: 15.01. – 21.01.2024 Davis Sea-Hobart

At the beginning of the week, the research area was located between a high in the Northeast and a low Southwest of *Polarstern* in a strong westerly airflow. Initially, North-westerly winds of 6 to 7 Bft prevailed. This intensified on Tuesday, 16 January 2024, to 8 Bft at times. The persistent north-westerly wind allowed a fully mature sea to develop with significant wave heights of 4 to 5 meters. *Polarstern* was sailing in a frontal line with an inflow of mild and humid air. As a result, the weather was rather cloudy with closed stratus clouds and very low cloud bases, as well as occasional drizzle. On the night of Wednesday, 17.01.2024, *Polarstern* reached the rear of the front. There, the wind shifted to the West and dropped to around 5 Bft. *Polarstern* then found itself in the middle of a high-pressure bridge. The significant swell flattened to about 2 meters by Thursday, 18.01.2024. At the weekend, *Polarstern* approached a central low that was in its final stages. The wind shifted to easterly directions and, after weakening temporarily, blew mostly at 6 Bft. The significant wave height hardly changed during this period.

Week 9: 22.01. – 28.01.2024 Davis Sea – Hobart

The week was characterized by a very extensive storm, which moved from West to East between the 50th and 60th latitude into the South Pacific. Initially, the research area was located East of the low pressure center in a northwesterly to northerly airflow that strengthened from 5 Bft to 6 Bft. Several lines of showers and fronts were embedded in the airflow, making the weather very unsetteled. Rain or rain showers occurred again and again. As bands of precipitation passed through, the wind increased to 7 Bft. On Tuesday evening, 23.01.2023, the cold front of the storm finally passed through. Behind the cold front, the wind quickly turned to the West at 6 to 7 Bft. *Polarstern* continued to move Southeast through an occlusion towards the low center. As a result, *Polarstern* was not affected by the storm field on the back of the depression until the night of Thursday, 25.01.2024. The wind blew from a south-westerly direction around 8 Bft. The significant wave height increased to 4 to 5 meters and reached its peak at midday on Thursday. A high pressure ridge swung through behind the storm, extending southwards from the subtropical high pressure belt. This temporarily calmed the significant wave height somewhat. On Friday afternoon, 26.01.2024, the cold front of another storm crossed the research area. As a result, the wind picked up again on Friday evening and blew from the West at 8 to 9 Bft. As the wind picked up, the wind sea in particular increased, while the swell remained at 2 to 3 meters. Overall, there was another significant wave height of around 4 meters. The weekend was also unsetteled in the westerly wind drift. High pressure ridges and low pressure troughs were repeatedly embedded in the strong westerly current. As a result, the wind fluctuated both in direction and speed between Southwest and Northwest, and between 6 Bft and 8 Bft. Only a few gaps in the cloud cover were visible. It also rained lightly to moderately from time to time and the significant wave height was at 3 to 4 meters.

Week 10: 29.01. – 01.02.2024 Davis Sea – Hobart

Polarstern also spent the last few days at sea in the westerly wind zone. On Monday, 29.01.2024, a severe storm was located South of Tasmania at around 58° South latitude. At the same time, the subtropical high pressure belt along the Australian South coast intensified, resulting in a strong to stormy westerly to worthwesterly wind of 7 to 8 Bft in the sailing area. The significant wave height was 3 to 4 meters. *Polarstern* reached the Hobart bunker pier on Tuesday evening, 30.01.2024. Due to the strengthening area of high pressure over Tasmania, we were greeted by an almost cloudless sky with weak winds from the West. The weather remained calm in the following days with scattered clouds and temperatures between 13 and 24 °C. *Polarstern* then moved to the final pier in Hobart harbour on Thursday morning, 01.02.2024, where the expedition came to an end.

2. BATHYMETRY OF THE EAST ANTARCTIC SEA

Yvonne Schulze Tenberge[1], Pascal Andreas[2], Annie Lemire[3]

[1]DE.AWI
[2]DE.UNI-Bremen
[3]DE.TUM

Not on board: Boris Dorschel[1], Simon Dreutter[1]

Grant-No. AWI_PS140_05

Objectives

Accurate knowledge of the seafloor topography, hence high-resolution bathymetry data, is key basic information necessary to understand many marine processes. It is of particular importance for the interpretation of scientific data in a spatial context. Bathymetry, hence geomorphology, is furthermore a basic parameter for the understanding of the general geological setting of an area and geological processes such as erosion, sediment transport and deposition. Even information on tectonic processes can be inferred from bathymetry.

While world bathymetric maps give the impression of a detailed knowledge of worldwide seafloor topography, most of the world's ocean floor remains unmapped by hydroacoustic systems. In these areas, bathymetry is modelled from satellite altimetry with a correspondingly low resolution. Satellite-altimetry derived bathymetry therefore lack the resolution necessary to resolve small- to meso-scale geomorphological features (e.g. sediment waves, glaciogenic features and small seamounts). Ship-borne multibeam data provide bathymetry information in a resolution sufficient to resolve those features and for site selection for the other scientific working groups on board.

Glacigenic landforms preserved on the seafloor can form the basis for the reconstruction of the dynamic history of Antarctic Ice Sheets. In particular, these landforms can shed light on its retreat since its maximum extent during the Last Glacial Maximum. Understanding the processes that led to this ice sheet retreat in the past can provide important information for predicting future responses of Antarctic Ice Sheets to changing climate conditions and oceanographic settings. Glacigenic landforms can only be determined in high-resolution bathymetric data sets. These data are however sparse for the study areas of the EASI-2 expedition. Therefore, it was planned to use the ships hydroacoustic instruments to acquire detailed bathymetric data of these areas.

Furthermore, the collection of underway data during PS140 will contribute to the bathymetry data archive at the AWI and thus to bathymetric world datasets such as IBCSO (International Bathymetric Chart of the Southern Ocean) and GEBCO (General Bathymetric Chart of the Ocean).

Work at sea

The main task of the bathymetry group was to plan and run bathymetric surveys in the study areas and during the transit. The raw bathymetric data was corrected for sound velocity changes in the water column, processed and cleaned for erroneous soundings and artefacts. Detailed seabed maps derived from the data were made available to other working groups

for station planning. During the survey, the acoustic measurements were conducted by three operators working 24/7-hour shifts (except for periods of stationary work).

Technical description

During expedition PS140, bathymetric surveys were conducted with the hull-mounted multibeam echosounder (MBES) Teledyne Reson HYDROSWEEP DS3 (HSDS3). The HYDROSWEEP is a deep water system for continuous mapping with the full swath potential. It operates on a frequency of ~14 kHz with chirped pulses. On *Polarstern*, the MBES transducer arrays are arranged in a Mills cross configuration of 3 m (transmit unit) by 3 m (receive unit). Combined motion, position (Trimble GNSS), and time information is provided by an iXBlue Hydrins motion reference unit (MRU). MRU data is directly transferred into the Processing Unit (PU) of the MBES for real-time motion compensation (Pitch, Roll and Yaw). With a combination of phase and amplitude detection algorithms the PU computes the water depth from the returning backscatter signal. The system can cover a sector of up to 140° with 70° per side. In the deep sea, an angle of ~50° to both sides could be achieved. In shallower shelf areas, the angle could be opened up to ~60° from nadir on both sides to get an overall swath width of approximately 3.5 times the water depth.

Data acquisition and processing

Bathymetric data acquisition was carried out throughout the entire expedition, as long as the ship was sailing in international waters or the Southern Ocean (south of 60°S). There the surveying was conducted in accordance to the Antarctic Treaty regulation set by the German Environmental Agency (Umweltbundesamt).

The HYDROSWEEP was operated with the software Sonar UI and for online data visualization, Teledyne PDS was used. Data was stored in S7K raw files in the shipboard file system for later transfer into the long-term data archive PANGAEA. Subsequent data processing was done with Caris HIPS and SIPS. For generating maps onboard, the data were exported to QGIS in the GeoTIFF raster format.

Tab. 2.1: List of bathymetric stations during PS140.

Station	Device	Action	Event time [UTC]	lat	lon
PS140_0_Underway-28	HSDS3	station start	30.11.2023 00:05:42	-37.561296	24.57822
PS140_0_Underway-28	HSDS3	profile start	30.11.2023 00:05:43	-37.561331	24.57829
PS140_0_Underway-28	HSDS3	profile end	04.12.2023 09:59:41	-43.207805	38.344852
PS140_0_Underway-28	HSDS3	profile start	05.12.2023 12:13:27	-46.965141	42.897372
PS140_0_Underway-28	HSDS3	profile end	28.01.2024 20:39:11	-45.037840	141.813398
PS140_0_Underway-28	HSDS3	station end	28.01.2024 20:40:15	-45.036907	141.817114
PS140_52-3	MIDAS_SVP	attached MUC_PS	28.12.2023 06:12:22	-67.424307	73.117660

Station	Device	Action	Event time [UTC]	lat	lon
PS140_65-2	MIDAS_SVP	attached to GC_PS	30.12.2023 13:23:02	-69.316765	75.112609
PS140_124-2	MIDAS_SVP	attached to MUC_PS	12.01.2024 07:31:35	-60.896268	100.973061
PS140_127-2	MIDAS_SVP	attached to MUC_PS	15.01.2024 11:15:20	-56.421205	101.779743
PS140_138-1	MIDAS_SVP	attached MUC_PS	25.01.2024 04:30:18	-50.039946	120.755997

Sound velocity profiles

For best survey results and to correct HYDROSWEEP depths for changes of the sound velocity (SV) in the water column, SV profiles were generated from CTD data that were collected and provided by the oceanographic group. SV correlates with the density of a water mass and is thus depending on pressure, temperature and salinity of the seawater at a given location at a given depth. Wrong or outdated SV profiles lead to refraction errors, reduced data quality and faulty depth measurements.

When the CTD rosette was not operated, SV profiles were obtained by the bathymetry group using a Valeport MIDAS Sound Velocity Profiler (MIDAS_SVP). The Valeport was attached to the winch cable of sampling instruments such as the Multi Corer (MUC_PS) or the Piston Corer (PC_PS). Table 2.1 lists all stations were the Valeport was used and the devices it was attached to.

During PS140, a total of 99 SV profiles were applied to the MBES. They include 85 SV profiles from the CTD data and 4 SV profiles recorded with the Valeport. The remaining 10 profiles were generated using the World Ocean Atlas 2018 (WOA18). A fifth Valeport profile (station PS140_124-2) was obtained in order to calibrate POSIDONIA, which was attached to the Titan trace metal clean seawater sampling system, when no CTD profile was available (see Chapter 3).

Stations

Data collection with the HYDROSWEEP received the number PS140_0_Underway-28 throughout the expedition. All bathymetry related stations are listed in Table 2.1. For MIDAS SVP only station starts are listed. For a complete station list see Appendix A.4.

Preliminary results

During 60 days of survey, a track length of 9,361 nmi (17,337 km) was surveyed with the HYDROSWEEP. The raw data volume of bathymetric data (S7K) was 155 GB broken up in 914 separated survey track lines. Figure 2.1 shows the coverage of the bathymetric data collected during transit and dedicated surveys in the research areas.

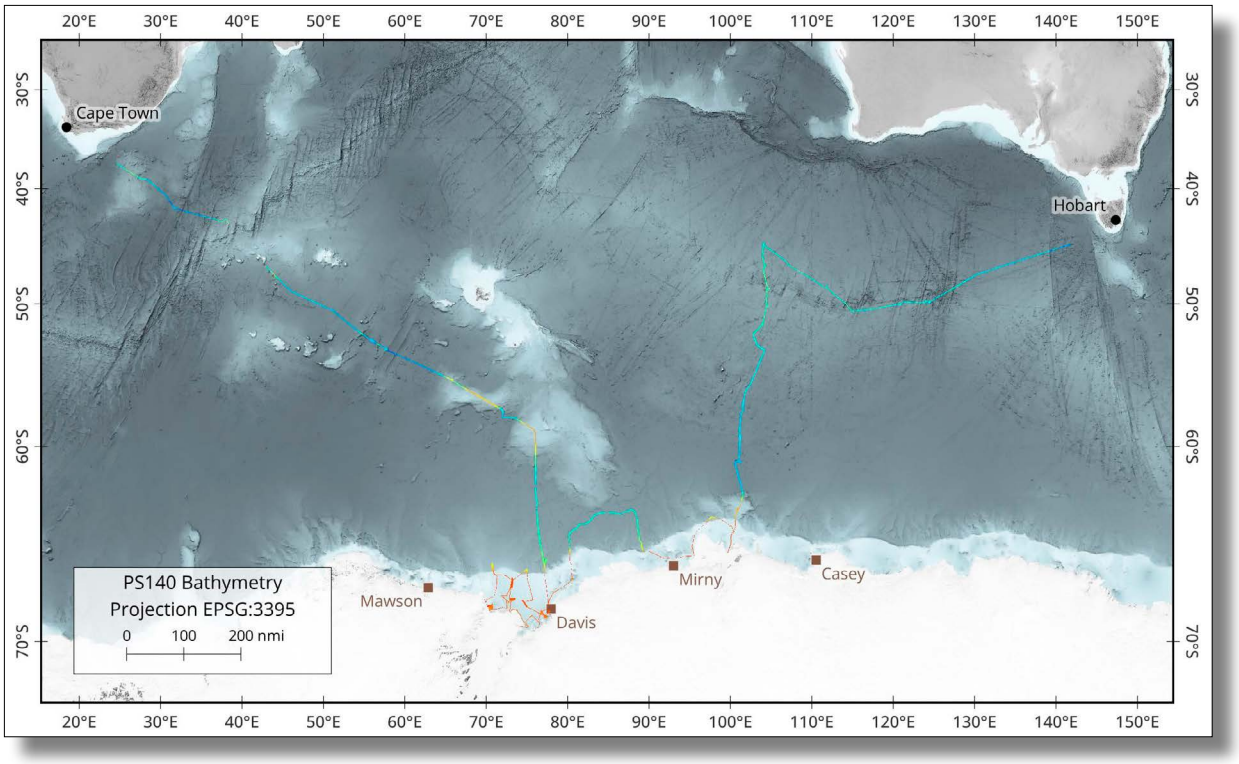

Fig. 2.1: Overview on the bathymetric data acquired during PS140 (background data used are IBCSO (Dorschel et al. 2022), GEBCO (GEBCO Bathymetric Compilation Group 2023 2023) and COMNAP Antarctic Facilities (The Council of Managers of National Antarctic Programs (COMNAP) 2023)). Colour coding of cruise track delineates observed water depth.

Amery Ice Shelf

For geological and oceanographic site selection and to get comprehensive information on the seabed topography for palaeo-glaciological interpretation (see Chapter 5), a systematic bathymetric survey has been conducted in the MacKenzie Bay in front off the Amery Ice Shelf (see red box 'A' in Fig. 2.2). An area of ~576 km² was mapped by following the slope direction and sailing parallel survey lines with a total length of ~178 nmi (330 km). Due to unknown seabed topography and a vast amount of ice bergs the course had to be adjusted multiple times. The depth in the survey area ranges from ~1,200 m in the middle on the western edge towards the Amery Ice Shelf up to ~250 m in the north.

Rauer Deep and Davis Station

Further surveys were conducted at the Rauer Deep and north east of it near the *Davis Station* (see red box 'B' in Fig. 2.2), again for geological and oceanographic site selections and for palaeo-glaciological interpretation of the information obtained on seabed topography. The Rauer Deep area was visited twice over a time span of 16 days. Parallel survey lines with a total track length of ~175 nmi (323 km) have been traversed to cover an area of ~408 km². The direction of the survey track was adjusted in order to follow the slope direction and the extent was limited by ice coverages. The depth in the survey area ranges from ~1,400 m in the Rauer Deep up to ~100 m to the north towards *Davis Station*.

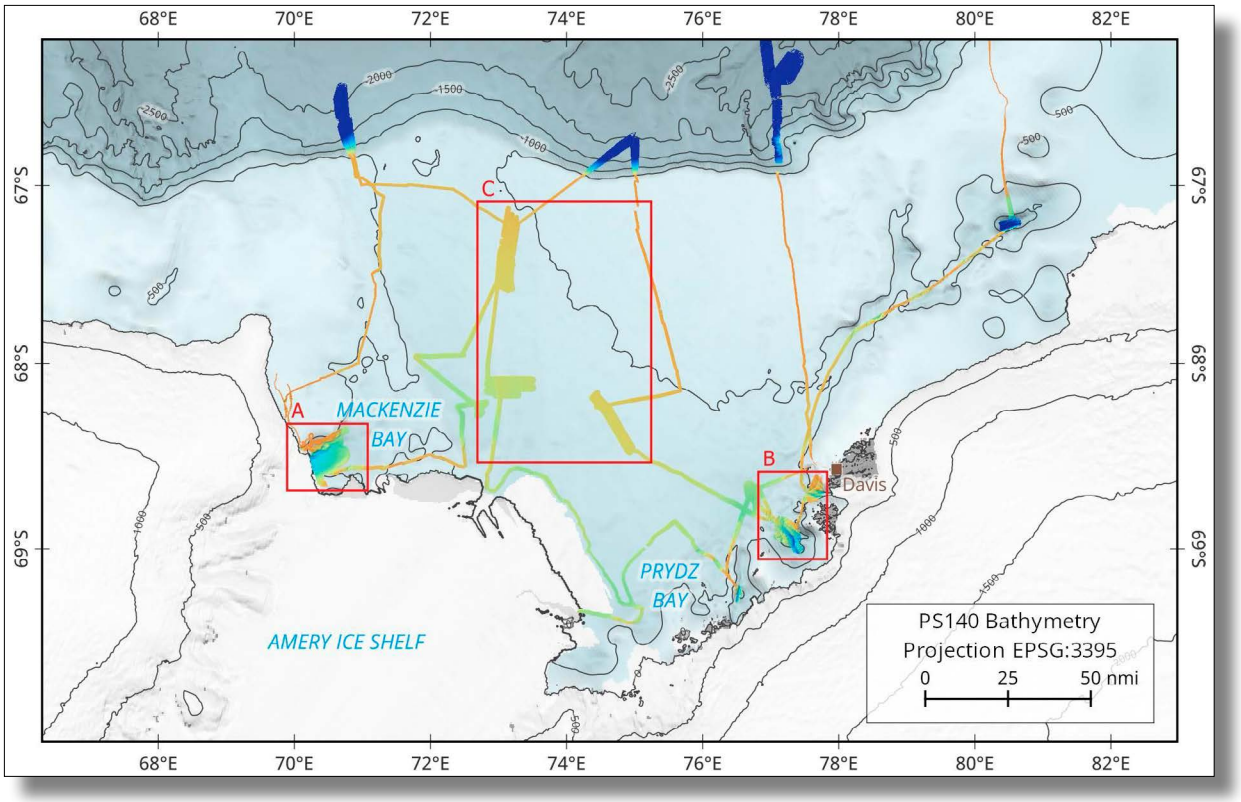

Fig. 2.2: Bathymetric data around Prydz Bay and MacKenzie Bay (background data used are IBCSO (Dorschel et al., 2022), GEBCO (GEBCO Bathymetric Compilation Group 2023, 2023), COMNAP Antarctic Facilities (The Council of Managers of National Antarctic Programs (COMNAP) 2023) and SCAR Composite Gazetteer of Antarctica (Secretariat SCAR 1992))

ANT-XXIII/9 (PS69) related sites

Systematic surveys were conducted in areas that were previously visited during expedition ANT-XXIII/9 (Hubberten, 2008) for geological site selection (see red box 'C' in Fig. 2.2). Parallel survey lines with a total track length of ~385 nm (712 km) have been sailed efficiently covering an area of ~1,272 km². The depth in the survey area ranges from ~770 m in the south west up to ~510 m in the north.

Data management

Environmental data will be archived, published and disseminated according to international standards by the World Data Center PANGAEA Data Publisher for Earth & Environmental Science (https://www.pangaea.de) within two years after the end of the expedition at the latest. By default, the CC-BY license will be applied. Furthermore, bathymetric data will be provided to the Nippon Foundation – GEBCO Seabed 2030 Project.

This expedition was supported by the Helmholtz Research Programme "Changing Earth – Sustaining our Future" Topic 2, Subtopic 3 Sea Level Change.

In all publications based on this expedition, the **Grant No. AWI_PS140_05** will be quoted and the following publication will be cited:

Alfred-Wegener-Institut Helmholtz-Zentrum für Polar- und Meeresforschung (2017) Polar Research and Supply Vessel POLARSTERN Operated by the Alfred-Wegener-Institute. Journal of large-scale research facilities, 3, A119. http://dx.doi.org/10.17815/jlsrf-3-163.

References

Dorschel B, Hehemann L, Viquerat S, et al (2022) The International Bathymetric Chart of the Southern Ocean Version 2. Scientific Data 9:275. https://doi.org/10.1038/s41597-022-01366-7

GEBCO Bathymetric Compilation Group 2023 (2023) The GEBCO_2023 Grid - a continuous terrain model of the global oceans and land. https://doi.org/10.5285/F98B053B-0CBC-6C23-E053-6C86ABC0AF7B

Hubberten H-W (2008) The Expedition of the Research Vessel Polarstern to the Antarctic in 2007 (ANT-XXIII/9). Alfred-Wegener-Institut für Polar- und Meeresforschung. https://doi.org/ 10.2312/BzPM_0583_2008

Secretariat SCAR (1992) SCAR Composite Gazetteer of Antarctica

The Council of Managers of National Antarctic Programs (COMNAP) (2023) COMNAP Antarctic Facilities

3. PHYSICAL OCEANOGRAPHY OF THE STUDY REGION

Ole Rieke[1], Annika Oetjens[1], Kathrin Groß[2], Marcus Gutjahr[2]

Not on board: Laura Herraiz-Borreguero[3], Markus Janout[4], Sandra Tippenhauer[4]

[1]AU.IMAS
[2]DE.GEOMAR
[3]AU.CSIRO-ENVIRONMENT
[4]DE.AWI

Grant-No. AWI_PS140_01, AWI_PS140_12

Objectives

The Indian sector of the Southern Ocean is characterised by the eastward Antarctic Circumpolar Current (ACC) that plays an important role in the global circulation system, for primary production and carbon uptake. The meridional extent of the ACC is crossed by several fronts which are highly important for the circulation and ecosystems. The water masses present include Antarctic Bottom Water (AABW) at the bottom, overlying Circumpolar Deep Water (CDW), Antarctic Intermediate Water (AAIW) and surface waters (Orsi et al., 1995; Meijers et al., 2010).

South of the ACC in the area of the continental shelf break, the westward flowing Antarctic Slope Current (ASC) prevents warm CDW from entering the continental shelf in most areas of East Antarctica, resulting in rather low melt rates of the East Antarctic Ice Sheet (EAIS; Williams et al., 2010).

AABW is known to be formed in four major formation sites around Antarctica, the Ross Sea, Weddell Sea, Adelie Land and Cape Darnley / Prydz Bay (Ohshima et al., 2013). Recent studies have indicated a decline in volume and density of AABW in the Southern Ocean (Purkey et al., 2018), coinciding with warming and a southward shift of CDW in East Antarctica that could threaten the EAIS (Herraiz-Borreguero & Naveira Garabato, 2022).

Prydz Bay is characterised by the formation of Dense Shelf Water (DSW), a key ingredient of AABW, in the Mackenzie and Davis polynyas (Williams et al., 2016). Previous observations have also identified an inflow pathway of CDW along the eastern side of Prydz Bay that leads to basal melting underneath the Amery Ice Shelf (Herraiz-Borreguero et al., 2015).

Hydrographic profiles during the transit to (western Indian Ocean transect) and from the Antarctic continental shelf (eastern Indian Ocean transect) contribute to an improved monitoring of the ACC, its fronts and the present water masses in the to date poorly sampled Indian sector of the Southern Ocean. Comparison with historical observations will detect movements of the fronts, its current circulation state and changes in water mass properties.

Oceanographic observations in Prydz Bay obtained during this cruise will be used to assess changes in the local formation of Dense Shelf Water (DSW) and the incursion of modified CDW on the continental shelf. Hydrographic profiles near the shelf break give insights into the dynamics of the ASC, and exchange processes between the shelf and the open ocean for both, DSW and CDW. Observations along the ice shelf front are designed to investigate the outflow of Ice Shelf Water (ISW), supercooled water that is the result of ice-ocean-interaction in the ice shelf cavity and is a potential source of iron, thereby very important for primary production.

Further work consisted of hydrographic observations near the West and Shackleton ice shelves where presence of warm modified CDW (mCDW) near the ice shelf front has been shown by Argo floats (van Wijk et al., 2022).

Work at sea

Hydrographic measurements during PS140 were conducted using the *Polarstern* CTD system CTD-PS (Tab. 3.1). An overview over all CTD stations is given in Figures 3.1 to 3.4. The working areas are subdivided into (i) the western Indian Ocean transect, (ii) Prydz Bay area, (iii) the Shackleton Ice Shelf / Denman Glacier area and (iv) the eastern Indian Ocean transect. Meta-data of all PS140 CTD stations are listed in Table 3.2.

The sensors and rosette of CTD-PS were provided by *Polarstern* and DE.AWI, with the addition of an LADCP system provided by the physical oceanography group from DE.AWI. In the following, we describe the technical setup of the CTD rosette, followed by a description of the general procedure of performing CTD casts during the cruise. We then present further information on the actual deployments and an overview of technical issues throughout the cruise. To obtain a higher resolution of temperature profiles we complemented the CTD transects on the shelf with the deployment of 36 Expandable Thermobathymeters (XBTs) provided by AU.CSIRO. In addition to the CTD casts eight Argo floats were deployed in cooperation with DE.AWI and BSH. Finally, a description of the technical setup of the Vessel mounted ADCP (SADCP) is provided.

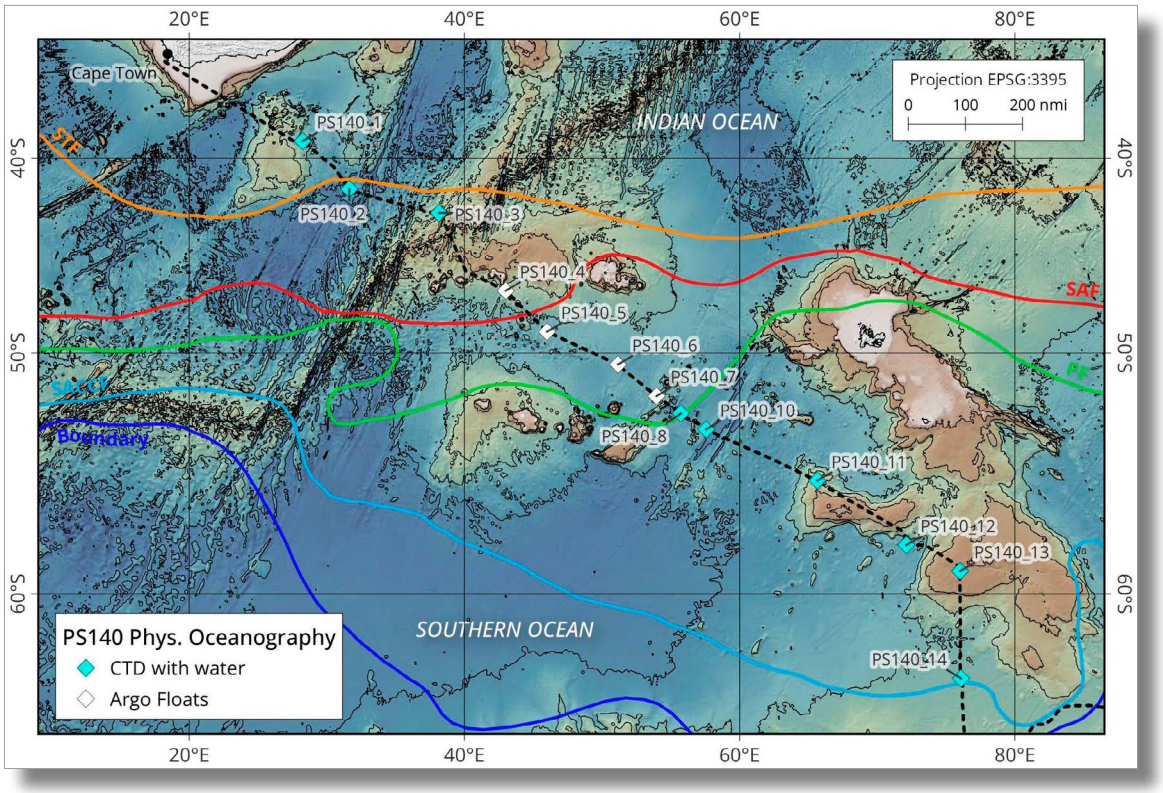

Fig. 3.1: Physical oceanography stations along the western Indian Ocean transect going south towards Prydz Bay. CTD stations were also used for water sampling (see Chapter 4). Four stations were dedicated to Argo deployment during transit south. Also shown are the major Southern Ocean fronts (STF: Subtropical Front; SAF: Subantarctic Front; PF: Polar Front; SACCF: Southern Front of the ACC; Boundary: Southern boundary of the ACC).

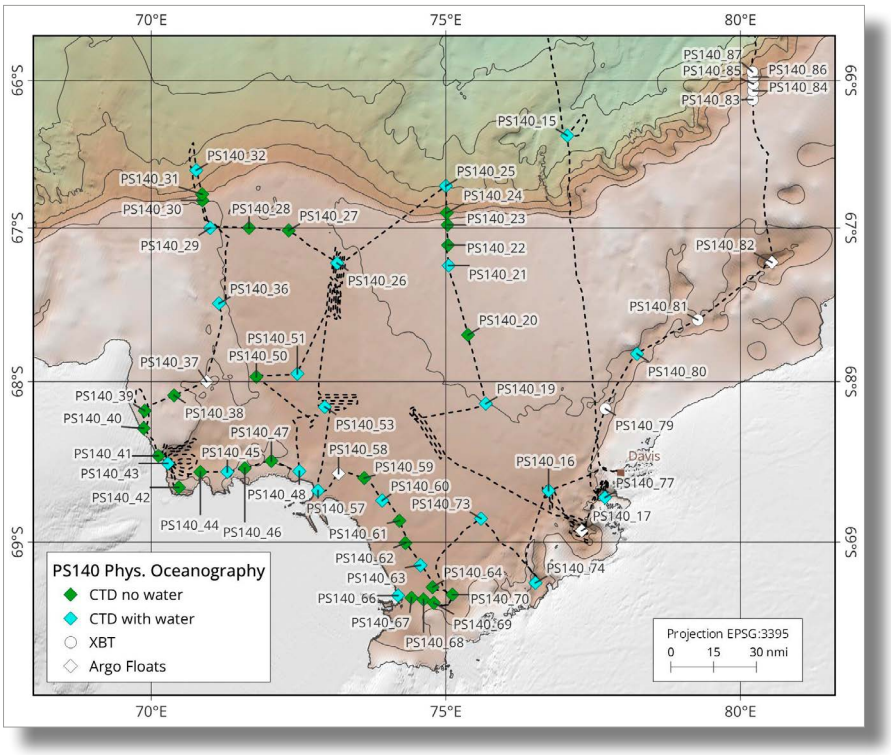

Fig. 3.2: Physical oceanography stations in the Prydz Bay working area. In order to obtain a higher spatial resolution of water mass properties some CTD stations were realised without additional water sampling (CTD no water). At various locations within Prydz Bay Argo floats were deployed. At few stations in the eastern part of the working area XBT probes were deployed.

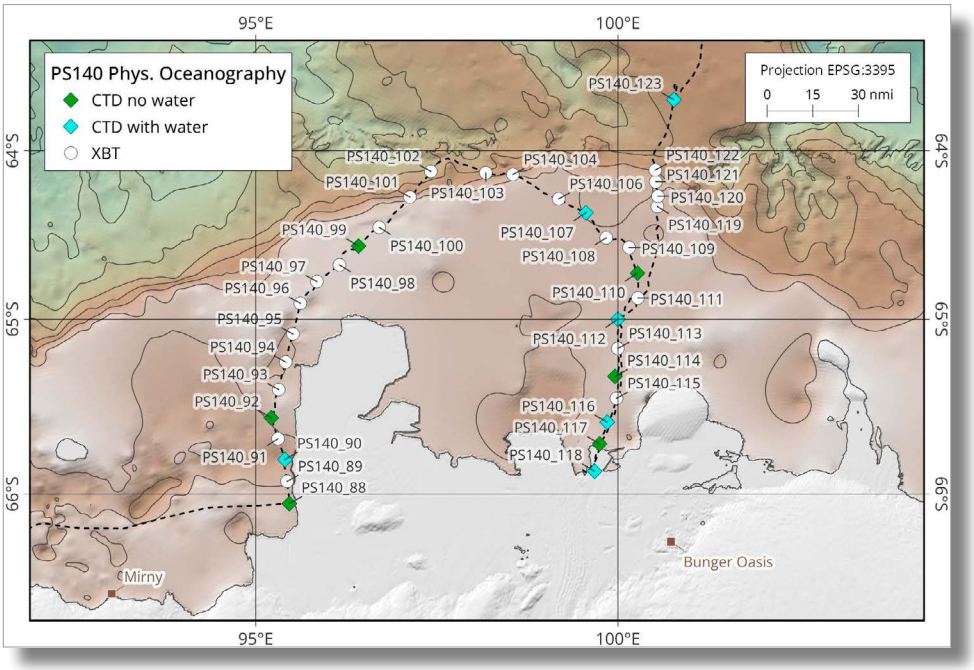

Fig. 3.3: Physical oceanography stations in the Shackleton Ice Shelf area and in front of the Denman Glacier. The western side of the Shackleton Ice Shelf was also targeted aiming to identify whether modified Circumpolar Deep Water may also be detected on the western side of this ice shelf.

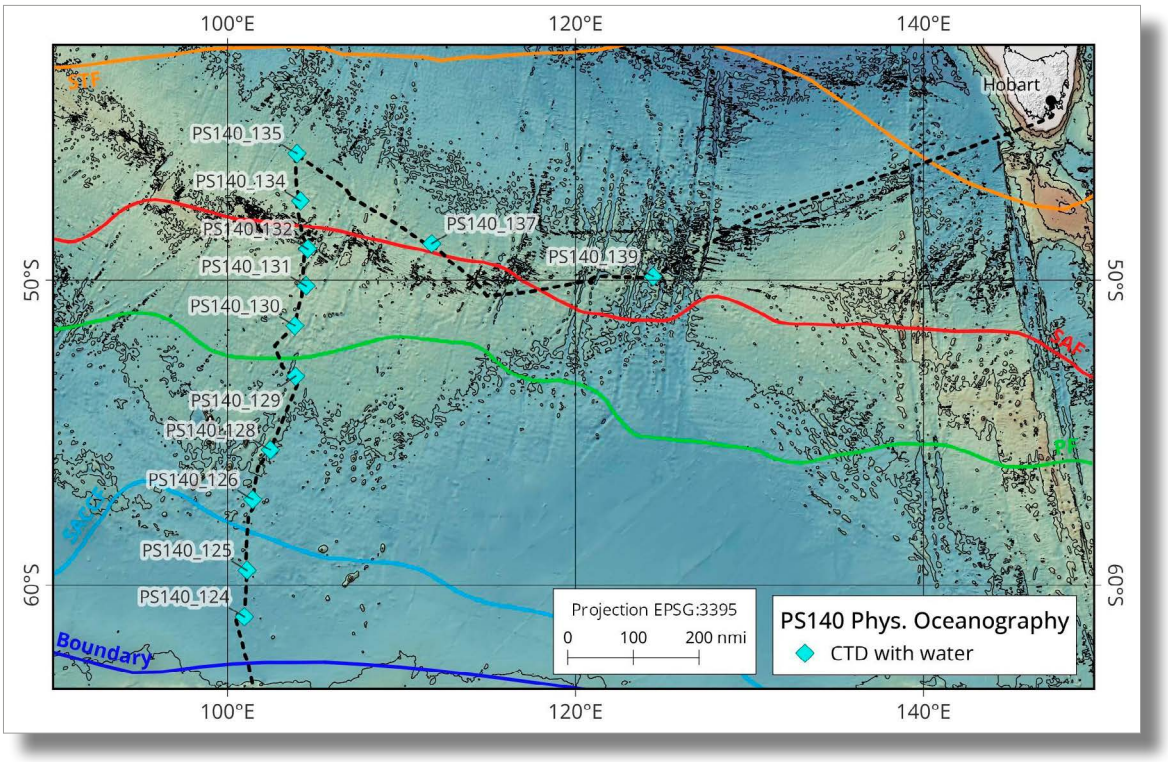

Fig. 3.4: Eastern Indian Ocean transect stations covered during transit north and then east on the way to Hobart. Also shown are the major Southern Ocean fronts (STF: Subtropical Front; SAF: Subantarctic Front; PF: Polar Front; SACCF: Southern Front of the ACC; Boundary: Southern boundary of the ACC).

CTD-PS

The standard sensor configuration of the CTD system throughout the cruise consisted of two temperature sensors, two conductivity cells, a pressure sensor, two oxygen sensors, one fluorescence sensor, and a transmissiometer (see Tab. 3.1 for more details).

Two Acoustic Doppler Current Profilers were attached to the rosette as well; more information can be found in the respective subsection below.

The usual procedure for a CTD deployment was as follows: lowering the rosette to 20 m, waiting for the CTD pump to turn on, heaving back to the surface. Then the downcast started by lowering the rosette with up to 1.0 m/s. The lowering speed was reduced when approaching the sea floor. The casts were stopped 10 m above ground.

For water sampling purposes the Niskin bottles were fired on the upcast after waiting for 60 seconds at each target depth for both sampling the ‘true’ ambient water mass and also allowing for lagging sensors to adjust. These water samples are partly used for calibrating the salinity. Results from on-board salinometry are presented in the subsequent section.

CTD data was preliminary processed onboard using the ManageCTD software from DE.AWI that is based on the Seabird software SeaSave. Post-processing of the CTD data and alignment with the salinometry data is conducted by AU.CSIRO-ENVIRONMENT and DE.AWI.

Tab. 3.1: Sensor configurations for the CTD-PS system used during PS140.

	SN	Calibration Date	Channel	Description
CTD	485			SBE 911plus
Temperature (primary)	1338	22.06.2022	F0	SBE3plus
Conductivity (primary)	3173	23.06.2022	F1	SBE4c
Pressure	0485	14.11.2017	F2	SBE9
Temperature	1374	22.06.2022	F3	SBE3plus
Conductivity	3590	23.06.2022	F4	SBE4c
Oxygen (primary)	4402	20.05.2023	V0	SBE43
Oxygen	4401	20.05.2023	V1	SBE43
Altimeter	46611	--	V2	SBE 171740
Fluorescence	1853	16.11.2021	V3	WETLabs ECO CDOM Fluorometer
Beam Transmission	1220	07.09.2022	V5	WETLabs C-Star
Lowered Acoustic Doppler Current Profiler (LADCP)	23292 and 23293			Teledyne RD Instruments WHM300-I-UG500

Tab. 3.2: Meta-data of all CTD stations from PS140 and the corresponding LADCP profile numbers. The station names refer to the file numbers and headers of the CTD data and correspond to the DSHIP entries.

Station	Event Time	Depth (m)	Lat (deg)	Lon (deg)	LADCP	Comment
PS140_1-2	30.11.2023 18:49:38	4270	-39.066	28.248	No data	
PS140_2-1	02.12.2023 02:46:34	4465	-41.712	31.641	No data	
PS140_3-1	03.12.2023 18:33:52	2992	-43.006	38.154	No data	
PS140_6-1	07.12.2023 06:50:38	4457	-50.540	51.162	No data	
PS140_8-1	08.12.2023 09:33:07	4475	-52.755	55.731	No data	
PS140_10-3	09.12.2023 17:01:19	4326	-53.452	57.578	No data	
PS140_11-5	11.12.2023 16:07:09	2309	-55.608	65.608	No data	
PS140_12-1	12.12.2023 16:39:29	4449	-58.164	72.114	No data	
PS140_13-5	13.12.2023 16:13:06	1195	-59.153	75.976	No data	
PS140_14-1	14.12.2023 12:30:27	3872	-62.929	76.080	No data	

Station	Event Time	Depth (m)	Lat (deg)	Lon (deg)	LADCP	Comment
PS140_15-1	16.12.2023 00:29:16	2865	-66.374	77.058	No data	
PS140_16-1	18.12.2023 19:42:24	842	-68.685	76.744	No data	
PS140_17-1	19.12.2023 11:44:40	1437	-68.931	77.312	No data	
PS140_19-2	20.12.2023 15:08:15	519	-68.141	75.679	No data	
PS140_20-1	21.12.2023 01:24:19	467	-67.702	75.377	No data	
PS140_21-1	21.12.2023 04:44:18	430	-67.250	75.050	No data	
PS140_22-1	21.12.2023 07:38:18	399	-67.114	75.039	No data	
PS140_23-1	21.12.2023 09:14:32	383	-66.980	75.033	No data	
PS140_24-1	21.12.2023 10:40:24	1024	-66.900	75.017	No data	
PS140_25-1	21.12.2023 13:04:48	1991	-66.720	74.999	No data	
PS140_26-1	22.12.2023 07:50:01	556	-67.232	73.159	17	
PS140_27-1	22.12.2023 16:35:42	530	-67.017	72.333	18	
PS140_28-1	22.12.2023 18:44:18	541	-67.000	71.660	19	
PS140_29-1	22.12.2023 20:35:28	477	-67.000	71.000	20	
PS140_30-1	22.12.2023 23:16:29	518	-66.817	70.867	21	
PS140_31-1	23.12.2023 00:27:08	991	-66.775	70.863	22	
PS140_32-1	23.12.2023 02:45:06	1833	-66.614	70.764	23	
PS140_36-1	23.12.2023 19:59:59	422	-67.497	71.149	24	
PS140_37-1	24.12.2023 01:16:48	501	-67.999	70.941	25	
PS140_38-1	24.12.2023 04:19:06	359	-68.088	70.388	26	
PS140_39-1	24.12.2023 06:20:43	225	-68.185	69.888	27	
PS140_40-1	24.12.2023 07:31:49	214	-68.295	69.870	28	
PS140_41-1	25.12.2023 22:50:13	689	-68.468	70.120	29	
PS140_42-1	26.12.2023 01:36:40	409	-68.664	70.468	30	

Station	Event Time	Depth (m)	Lat (deg)	Lon (deg)	LADCP	Comment
PS140_43-1	26.12.2023 03:40:01	1235	-68.516	70.282	31	
PS140_44-1	26.12.2023 13:28:34	700	-68.569	70.834	32	
PS140_45-1	26.12.2023 15:16:59	561	-68.568	71.291	33	
PS140_46-1	26.12.2023 18:13:05	410	-68.546	71.588	34	
PS140_47-1	26.12.2023 20:07:15	501	-68.500	72.039	35	
PS140_48-1	26.12.2023 22:09:39	567	-68.565	72.514	36	
PS140_50-1	27.12.2023 12:54:31	660	-67.968	71.785	37	
PS140_51-1	27.12.2023 15:30:45	711	-67.950	72.481	39	
PS140_53-1	28.12.2023 22:58:54	732	-68.163	72.945	40	
PS140_57-1	29.12.2023 08:48:02	710	-68.682	72.831	41	
PS140_58-1	29.12.2023 12:10:27	748	-68.578	73.178	42	
PS140_59-1	29.12.2023 14:24:50	761	-68.606	73.617	43	
PS140_60-1	29.12.2023 17:23:21	768	-68.745	73.922	45	
PS140_61-1	29.12.2023 20:55:40	696	-68.869	74.212	46	
PS140_62-1	29.12.2023 22:51:37	762	-69.006	74.314	47	
PS140_63-1	30.12.2023 01:15:57	829	-69.141	74.570	48	
PS140_64-1	30.12.2023 06:10:04	837	-69.273	74.777	49	
PS140_66-1	01.01.2024 11:32:45	715	-69.324	74.189	50	
PS140_67-1	01.01.2024 17:47:28	793	-69.337	74.418	51	
PS140_68-1	01.01.2024 19:57:06	771	-69.347	74.622	52	
PS140_69-1	01.01.2024 21:14:05	694	-69.367	74.798	54	
PS140_70-1	01.01.2024 23:58:19	676	-69.317	75.113	55	
PS140_73-1	02.01.2024 11:53:58	725	-68.857	75.599	56	
PS140_74-1	02.01.2024 20:45:24	1207	-69.247	76.516	57	

Station	Event Time	Depth (m)	Lat (deg)	Lon (deg)	LADCP	Comment
PS140_77-1	04.01.2024 04:53:17	1019	-68.726	77.703	58	
PS140_80-1	04.01.2024 22:07:41	734	-67.823	78.246	59	
PS140_82-1	05.01.2024 08:24:57	1614	-67.228	80.536	60	
PS140_88-1	08.01.2024 05:18:58	719	-66.054	95.464	61	
PS140_90-1	08.01.2024 07:53:40	1031	-65.806	95.403	62	
PS140_92-1	08.01.2024 12:39:53	540	-65.569	95.214	63	
PS140_99-1	08.01.2024 20:43:10	233	-64.570	96.419	64	
PS140_107-1	09.01.2024 11:08:22	539	-64.371	99.556	66	
PS140_110-1	09.01.2024 17:16:25	493	-64.729	100.274	70	
PS140_112-1	09.01.2024 19:58:33	520	-65.001	100.005	71	
PS140_114-1	09.01.2024 23:29:44	412	-65.332	99.961	72	
PS140_116-1	10.01.2024 01:22:00	542	-65.593	99.853	73	
PS140_117-1	10.01.2024 04:08:13	350	-65.717	99.749	74	
PS140_118-1	10.01.2024 06:30:30	604	-65.872	99.679	75	
PS140_123-1	10.01.2024 23:54:10	1399	-63.689	100.774	76	
PS140_124-5	12.01.2024 13:13:31	4515	-60.901	100.944	77	
PS140_125-4	13.01.2024 10:36:47	4159	-59.546	101.125	78	
PS140_126-3	14.01.2024 19:09:30	4235	-57.431	101.417	79	
PS140_128-1	15.01.2024 18:02:57	3809	-55.872	102.470	80	
PS140_129-1	16.01.2024 18:16:25	3712	-53.422	103.922	81	
PS140_130-1	17.01.2024 20:07:00	3159	-51.653	103.882	82	
PS140_131-3	19.01.2024 00:02:48	3291	-50.224	104.511	83	
PS140_132-1	19.01.2024 15:56:29	3126	-48.822	104.615	84	
PS140_134-3	20.01.2024 22:59:42	3395	-46.974	104.225	85	File name: PS140_133-3

Station	Event Time	Depth (m)	Lat (deg)	Lon (deg)	LADCP	Comment
PS140_135-1	21.01.2024 16:20:40	3632	-45.074	103.994	86	
PS140_137-1	23.01.2024 14:26:22	3568	-48.626	111.746	87	
PS140_139-2	26.01.2024 01:07:54	3465	-49.858	124.442	88	

Salinometry

We obtained high precision salinity measurements with an Optimare Precision Salinometer (OPS, SN 006) for potential recalibration of the conductivity sensors. The samples were taken from the Niskin bottles of both the regular CTD (CTD-PS) and the NIOZ-owned Ultra Clean CTD (UC-CTD, see Chapter 4). Before taking the actual sample, the bottles and rubber lid were rinsed 3 times. Then the bottles were closed, sealed (crimped) with an aluminium cap or waxed, and stored at room temperature for at least 12 h.

The day before a measurement session, the salinity bottles were heated in a water bath to approximately 30° C, and then left to cool down for about 12 h. The pressure within the bottles was released with an injection needle directly after the warm bath. Before using the OPS, the samples were shaken thoroughly for overcoming any stratification in the bottle. While sampled by the OPS, the opening of the bottles was sealed with parafilm to inhibit evaporation. The metal inlet tube of the OPS was cleaned with a Kim-wipe between samples.

A salinometry session starts with the standardization of the OPS using standard seawater. The respective bottle was sealed with the original cap and regularly sampled at the end of each session again. Each salinity measurement of a water sample from the Niskin bottles is calculated from the average of three individual OPS measurements that are allowed to differ by less than 0.0005 PSU. The salinity values measured by the two sensors of the CTD (Sal00 and Sal11) are calculated from the mean of 49 data scans recorded at the time of closing the Niskin bottle. A detailed error analysis will be conducted after the expedition.

Lowered ADCP

Two 300 kHz RDI Workhorse ADCPs were mounted on the rosette to act as lowered ADCPs (LADCP). The LADCP consists of the two 300 kHz ADCPs and a battery container. Communication was established to a computer in the winch room via two cables (for master and slave). The wall-installed cables COM1 and COM2 were used. The ADCPs were operated using the GUI of the LADCP tool V1.7 from GEOMAR. The LADCP computer time was synchronized with the ships NTP server directly. Specifically, they use a bin size of 10 m, a maximum range of 200 m, beam coordinates, no blanking after transmission, narrow band processing, and a timing of the master and slave such that the acoustic energy of the master is separated by 0.55 seconds from the acoustic energy of the slave. The Master (downward looking device) and slave (upward looking device) data file names consist of the station number (three digits), an abbreviation indicating the viewing direction (UP for upward and DN for downward) and a running number with three digits beginning with 000, representing the file number, in case there are multiple files (e.g., 001DN000.000 and 001UP000.000). These files were stored in a folder named according to the station number. Also log files documenting all actions conducted as starting (with configurations), stopping and downloading were kept. The LADCP profiles have been processed using MatLab scripts provided by GEOMAR, using navigational, SADCP

and CTD data. Due to technical issues there is no data available for stations 1 to 25. The match up for CTD cast to LADCP profile number is shown in Table 3.2.

Ship ADCP

The ship Acoustic Doppler Current Profiler (SADCP) was in operation from 26 November 2023 06:15 UTC until entering the 12 nm territorial waters of Tasmania at the end of the cruise when passing 144°E, unless South African territorial waters were passed on the transect south or *Polarstern* was breaking through fast ice. The RDI Ocean Surveyor instrument (150 kHz) was mounted at an angle of 45 degrees in the 'Kastenkiel' of *Polarstern* and provides a continuous time series of profiles of the ocean current velocity in the upper 300 m of the water column while underway. The instrument was configured in narrowband mode and set up to use a 4 m bin size (configuration file cmd_OS150NB_trigger_off.txt), covering a range from 15 m to around 200 – 300 m depth with varying data quality depending on sea state, ship speed and the presence of back-scatterers in the water column.

Overall, the system functioned without any issues and all data was collected entirely in the data files (file format: PS140[three digit deployment number]_000[three digit file number].ENX, *.ENR, *.ENS, *.N1R, *.N2R, *.NMS, *.STA, *.LTA, *.VMO, *.LOG), as we did not apply any changes to the instrument configuration.

The setup of navigational input was used from the vessel's GPS system.

The software VmDas (Teledyne RD Instruments) was used to set the ADCP's operating parameters and to record the data. Finally, the data conversion was done using Matlab routines of the Ocean Surveyor Sputum Interpreter (OSSI) version 1.9 (osheader.m, osdatasip.m, osrefine.m, osbottom.m). The finishing processing will be done on land.

XBT

36 Deep Blue Expandable Thermobathymographs (XBT) manufactured by Lockheed Martin were deployed in the East Antarctic shelf region to complement the CTD profiling (see Tab. 3.3), using the AU.CSIRO-ENVIRONMENT XBT deck unit Quoll SN 228, and a handheld launcher. The deployment was performed from the ship's stern and dependent on the ice condition either on portside or rear. Repeated observations were conducted in case of premature wire break due to sea ice conditions. The XBT probes measure temperature as a function of time which can then be related to depth that is calculated via the known fall speed in the water column. For most casts the profiling worked well and a thorough analysis will be conducted after the voyage.

Post-processing of the XBT profiles is conducted by AU.CSIRO-ENVIRONMENT.

Tab. 3.3: Meta-data of all XBT stations from PS140. The station names refer to the DSHIP entries.

Station	Serial Nr.	Event Time (UTC)	Latitude (deg)	Longitude (deg)
PS140_79-1	1231569	2024-01-04 19:38:51	-68.1731	77.7100
PS140_81-1	1231573	2024-01-05 03:24:14	-67.6036	79.2786
PS140_83-1	1231578	2024-01-05 19:14:24	-66.1407	80.2122
PS140_83-2	1231577	2024-01-05 19:18:49	-66.1225	80.2114
PS140_84-1	1231574	2024-01-05 19:35:45	-66.0715	80.2194
PS140_85-1	1231571	2024-01-05 19:54:41	-66.0234	80.2208

Station	Serial Nr.	Event Time (UTC)	Latitude (deg)	Longitude (deg)
PS140_86-1	1231575	2024-01-05 20:13:51	-65.9761	80.2189
PS140_87-1	1231570	2024-01-05 20:27:21	-65.9401	80.2055
PS140_89-1	1231579	2024-01-08 06:28:04	-65.9290	95.4319
PS140_91-1	1231572	2024-01-08 11:30:57	-65.6892	95.3083
PS140_93-1	1231576	2024-01-08 14:37:30	-65.4067	95.3159
PS140_94-1	1231580	2024-01-08 15:23:39	-65.2485	95.4133
PS140_95-1	1195357	2024-01-08 16:11:57	-65.0828	95.5145
PS140_96-1	1195358	2024-01-08 17:01:09	-64.9068	95.6154
PS140_97-1	1195354	2024-01-08 17:56:12	-64.7794	95.8445
PS140_98-1	1195356	2024-01-08 18:44:09	-64.4687	96.1562
no DSHIP entry	1195359	2024-01-08 22:26:00	-64.4593	96.6785
PS140_100-1	1195353	2024-01-08 22:34:05	-64.4593	96.7053
PS140_101-1	1195352	2024-01-09 00:29:12	-64.2787	97.1291
PS140_102-1	1195349	2024-01-09 01:58:12	-64.1241	97.4181
PS140_103-1	1195348	2024-01-09 04:52:04	-64.1324	98.1769
PS140_104-1	1195355	2024-01-09 06:24:55	-64.1426	98.5504
PS140_105-1	1195351	2024-01-09 08:07:38	-64.2197	98.8682
PS140_106-1	1195350	2024-01-09 09:11:53	-64.2902	99.1610
PS140_106-1	1252085	2024-01-09 09:20:43	-64.2891	99.1827
PS140_108-1	1252077	2024-01-09 14:26:42	-64.5076	99.7950
PS140_108-1	1252081	2024-01-09 14:35:58	-64.5211	99.8402
PS140_109-1	1252086	2024-01-09 15:45:14	-64.5715	100.1505
PS140_109-1	1252087	2024-01-09 15:49:35	-64.5789	100.1549
PS140_111-1	1252079	2024-01-09 18:28:01	-64.8757	100.2759
PS140_113-1	1252083	2024-01-09 22:20:59	-65.1700	99.9998
PS140_115-1	1252078	2024-01-10 00:20:30	-65.4570	99.9821
PS140_119-1	1252082	2024-01-10 17:14:07	-64.3346	100.5464
PS140_120-1	1252084	2024-01-10 17:36:38	-64.2734	100.5540
PS140_121-1	1252088	2024-01-10 18:11:53	-64.1865	100.5246
PS140_122-1	1252080	2024-01-10 18:51:26	-64.1161	100.5171

ARGO float deployment

Eight ARVOR/Provor floats were deployed in collaboration with the Bundesamt fuer Seeschifffahrt und Hydographie (BSH) and AWI. The deployment protocol is shown below. The deployment was performed according to NKE instruments deployment guidelines and combined with a CTD station whenever possible.

Preliminary results

CTD

The hydrographic structure of the Southern Ocean water column as observed during our cruise is shown in Figure 3.5 for the western Indian transect going south from Cape Town towards Prydz Bay, and in Figure 3.6 during transit from Denman Glacier to ~45°S (eastern Indian transect). Note the very comparable physical water mass properties that are typical for the Southern Ocean. Following Sloyan and Rintoul (2001) and Iudicone et al. (2008), the water masses can be distinguished based on their neutral densities (γ^n). Waters in the neutral density range 26 kg m^{-3} to 27.8 kg m^{-3} can be defined as Intermediate Waters (i.e. Subantarctic Mode Water and Antarctic Intermediate Water), a neutral density range 27.8-28.0 defines Upper Circumpolar Deep water, 28.0 kg m^{-3}-28.2 kg m^{-3} refers to Lower Circumpolar Deep Water, and a neutral density above 28.2 kg m^{-3} in the Southern Ocean is found in Antarctic Bottom Water. Note that the AABW variety in the western and eastern Indian transects differ. While the western section is dominated by AABW sourced from the Weddell Sea and Cape Darnley, the eastern section is dominated Adélie Land- and Ross Sea-sourced AABW (Solodoch et al. 2022). The lower water column between these transects is separated by the bathymetric high of the Kerguelen Plateau.

Figure 3.7 shows a Temperature-Salinity plot for a selection of stations for the different regions visited during the voyage. In grey are the profiles from the first transect with higher surface temperatures decreasing with latitude, and the presence of cold and dense AABW at the bottom. Stations from Prydz Bay (orange) show potentially supercooled water (temperature less than the surface freezing point, blue line). The presence of mCDW at the Denman glacier (green) is shown by the increase in temperature towards the bottom.

Tab. 3.4: Float deployment protocol.

Float S/N	**AI2600-23DE012**	**AI3500-23DE001**	**AI3500-23DE002**	**AI3500-23DE003**	**AI2600-23DE101**	**AI3500-23DE102**	**AI3500-23DE103**	**AI3500-23DE104**
WMO	2903793	1902598	6990527	4903669				
Lat	-51.984	-46.996	-50.525	-48.998	-68.000	-68.578	-68.923	-67.228
Lon	53.968	42.989	51.160	45.997	70.935	73.180	77.318	80.543
Activation date/time [UTC]	07.12.2023 21:44:00	5.12.2023 12:10:00	07.12.2023 11:36:00	6.12.2023 3:12:00	24.12.2023 02:23:00	29.12.2023 12:14:00	19.12.2023 19:34:00	05.01.2024 13:40:00
Deployment date/time UTC]	07.12.2023 21:55:00	5.12.2023 12:36:44 PM	07.12.2023 11:45:00 AM	6.12.2023 3:21:50 AM	24.12.2023 02:46:00	29.12.2023 12:33:07	19.12.2023 19:48:00	05.01.2024 14:02:00
method	manual	manual	manual	manual	manual	manual	manual	manual
Ships speed [kts]	4	5	4	5	4	2	4	4
Wind speed [Bf]	6	8	8	8	2	6	4	3
Sea State (calm, smooth, etc.)	chill	rocky	rocky	rocky	calm	very flat	smooth	calm
Water depth [m]	4183	3535	4456	4347	483	749	912	1590
CTD Profile (Station No., CTD cast)	-	-	PS140 _06_001	-	PS140 _036_01	PS140 _058_01	PS140 _017_01	PS140 _082_01

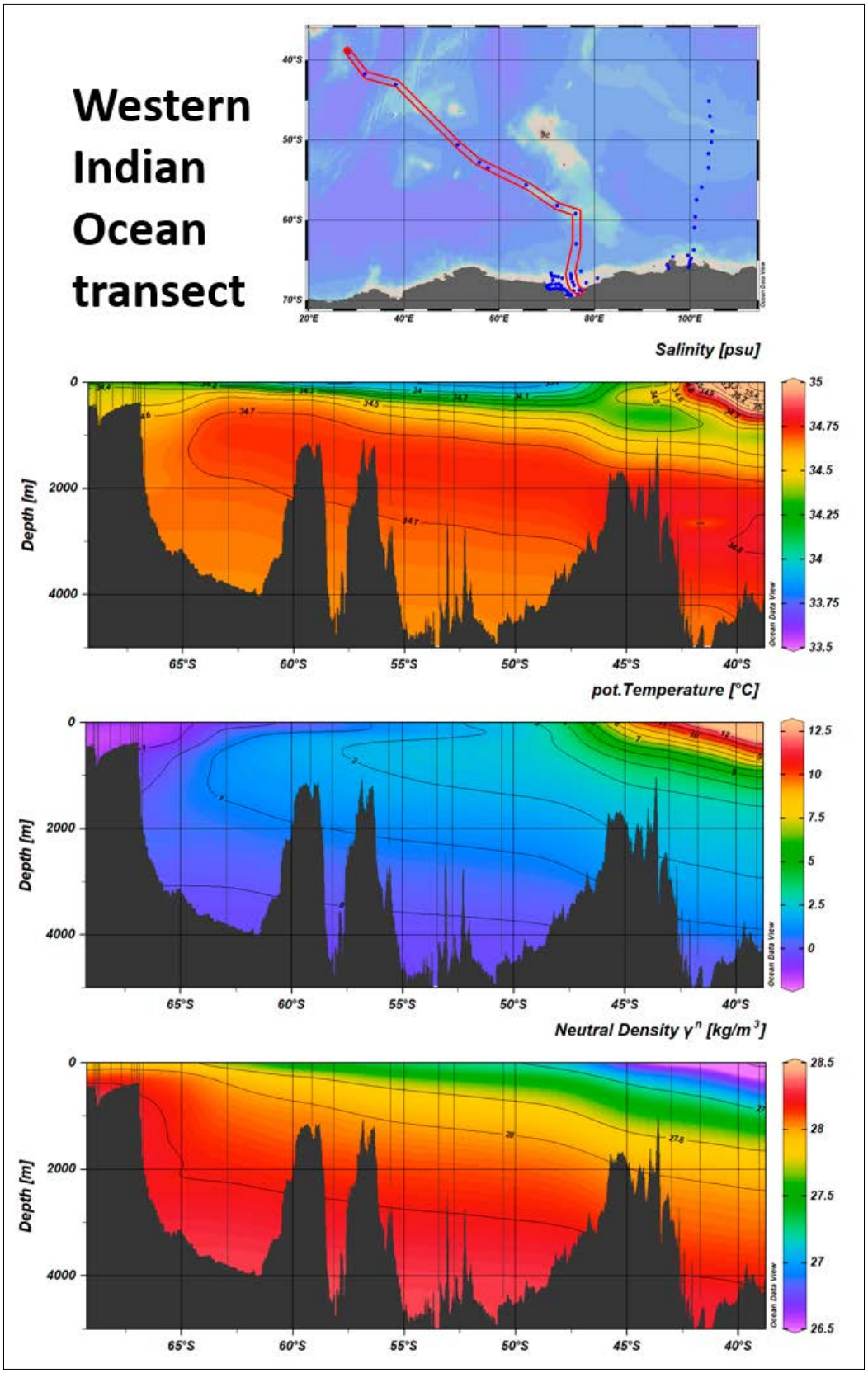

Fig. 3.5: Hydrographic section of the Indian Ocean water column as observed during transit from Cape town to Prydz Bay (western Indian Ocean transect) shown as a function of latitude. The map in the top panel shows the section defined for this figure, besides salinity, potential temperature and neutral density (γ^n).

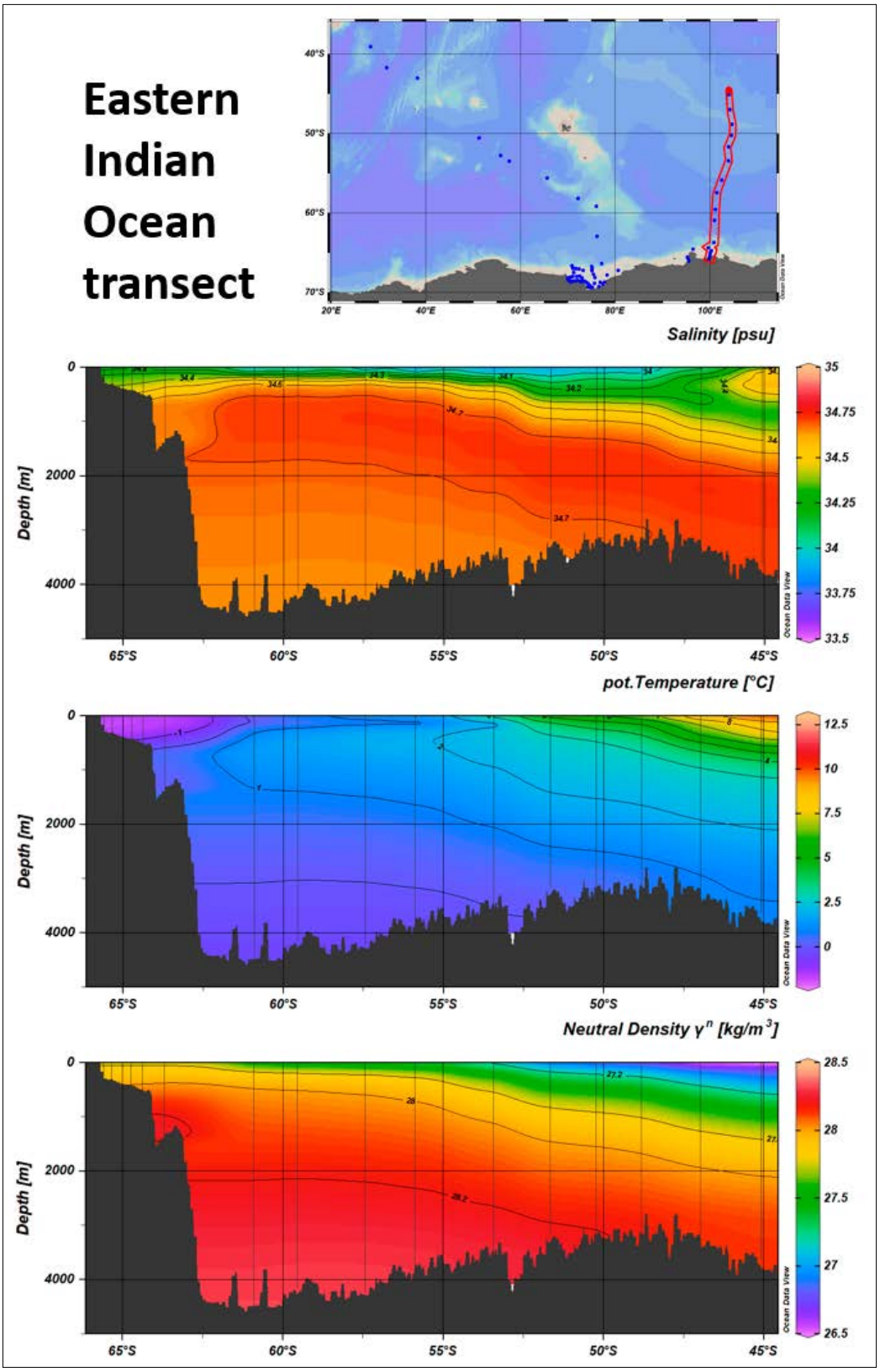

Fig. 3.6: Hydrographic section of the Indian Ocean water column as observed during transit from Denman Glacier to ~45°S heading north at around 100-105°E (eastern Indian Ocean transect). The map in the top panel shows the section defined for this figure, besides salinity, potential temperature and neutral density (γ^n). Note the very comparable meridional water mass properties between the western and eastern transects, which are typical for the Southern Ocean.

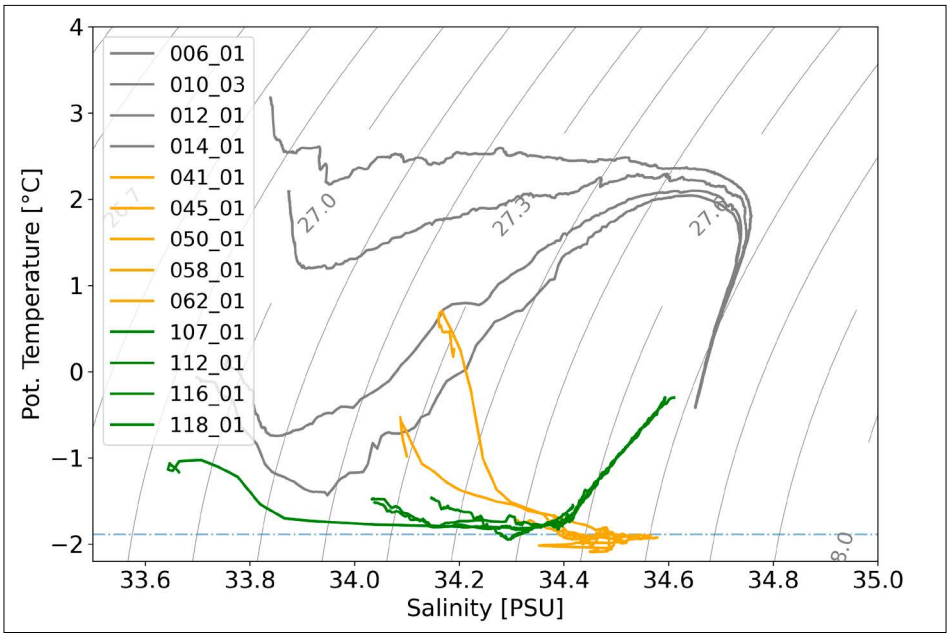

Fig. 3.7: Temperature-Salinity plot for a selection of transit (grey), Prydz Bay (orange) and Denman (green) stations. Isobars are shown as thin black lines in the background and the surface freezing temperature in dotted-dashed lightblue. The legend displays the corresponding station number.

LADCP

Figure 3.8 shows the zonal (a) and meridional (b) velocities measured by the lowered ADCP along a section across the shelf break in western Prydz Bay (c). Zonal velocities reveal the presence and extent of the Antarctic Slope Current (ASC) as a bottom-intensified westward current. There are two visible cores of the ASC with in the profiles at station 031 and 032, one is found at around 300m depth, and the other at 600m depth with velocities of up to 0.2 m/s. The current appears strongest where the gradient in the topography is strongest.

Meridional velocities indicate a southward inflow in the area of the shelf break which could indicate a potential inflow of warm water. The velocities are reversed to northward flow further south. It should be noted that the continental slope is not entirely zonal, meaning that an along-slope ASC will have a meridional velocity component as well. A decomposition into along-slope and across-slope velocities will be necessary to properly disentangle the ASC from cross-shelf transport.

In the post-cruise analysis, the velocities will be combined with CTD data to investigate the role of the ASC, and the meridional flow in the overflow of DSW from the continental shelf into the open ocean that will then contribute to AABW, and the inflow of warm mCDW.

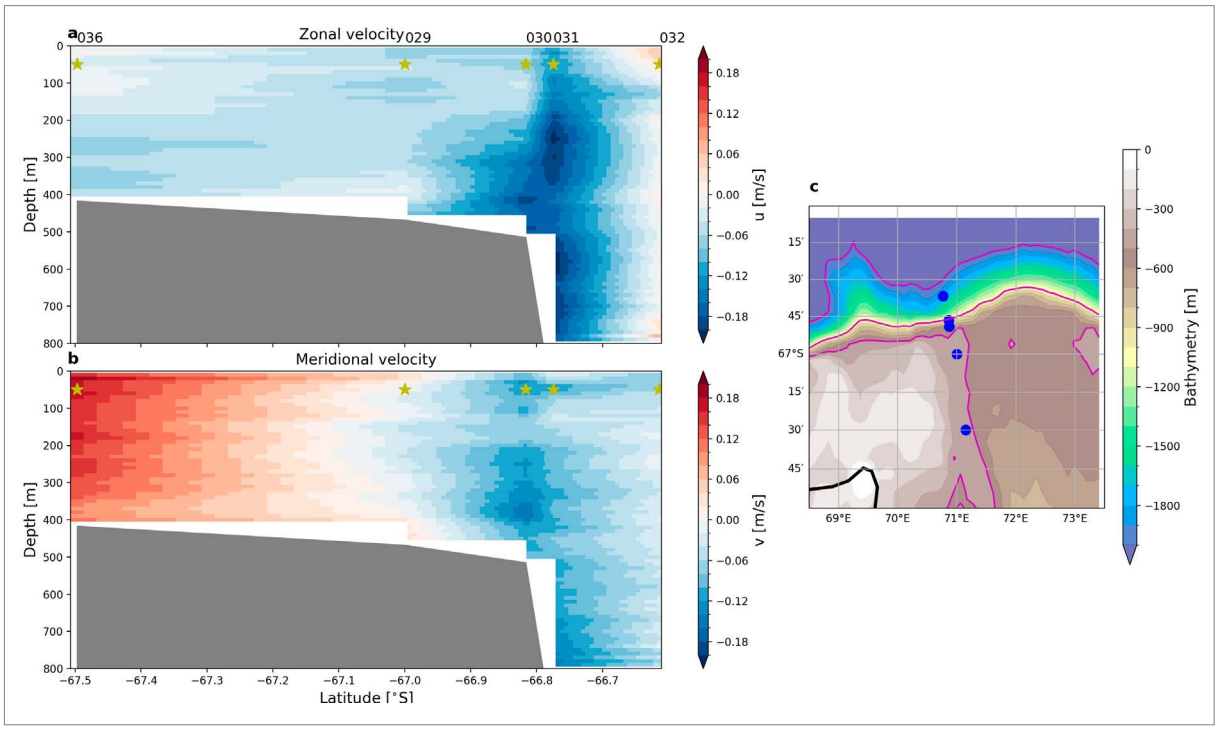

Fig: 3.8: Zonal (a) and meridional (b) velocities measured by the LADCP across the section shown in c. c) Blue dots indicate locations of LADCP measurements. Magenta lines indicate the 400, 1,000 & 2,000m isobaths. Negative velocities in (a) denote a net westward flow, negative values in (b) a net southward flow direction.

XBT

A section of temperature profiles from XBTs deployed across the continental shelf break northwest of the west ice shelf is shown in Figure 3.9. Warm CDW of up to 2°C is present at depth below 300m offshore while the continental shelf is occupied mainly by cold water close to the surface freezing point. Temperatures near the bottom of the continental shelf show a small warming, indicating some warm water intrusions of mCDW from the deep ocean towards the shelf. The shallowest profile of the section was conducted at 500m depth but bathymetry datasets and bathymetry data from this cruise indicates that the continental shelf is even shallower just south of the section, with depth of 300m and less in some places (Fig. 3.8). This is shallower than the depth of mCDW in this transect, indicating that it is unlikely for mCDW to access far onto the shelf in this location. Bathymetric data does, however, suggest the presence of a deeper trough connecting the shelf break towards the West ice shelf further east (Fig. 3.8) that could provide an inflow pathway for warm water under similar hydrographic conditions as in this transect. Due to extensive sea ice cover that area was inaccessible during this voyage.

The temperature observations show a strong horizontal temperature gradient with sloping isotherms in the area of the shelf break. This indicates the presence of a strong Antarctic slope front, associated with a horizontal density gradient and a strong ASC that is intensifying towards the bottom, similar to what was found in Prydz Bay (Fig. 3.7). As density is primarily controlled by salinity in polar oceans, salinity measurements would be necessary to verify this hypothesis.

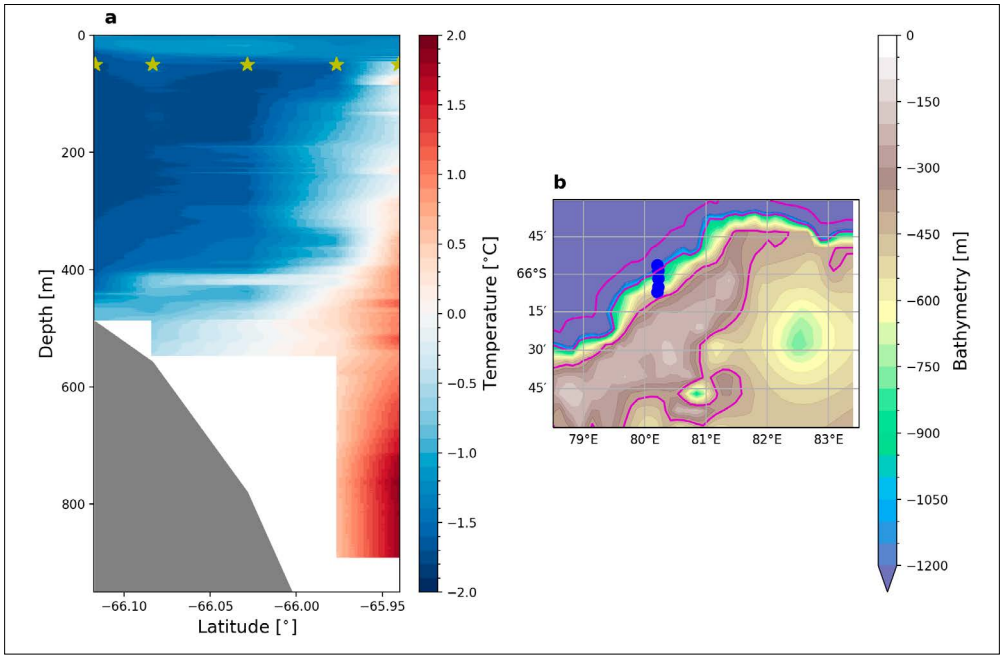

Fig. 3.9: a) Temperature section across the continental shelf break. XBT drop locations indicated by the yellow asterixes. b) Locations of the deployment. Magenta lines indicate the 400, 1,000 and 2,000m isobaths.

Data management

The raw CTD data and the velocity data from the LADCP and SADCP will be made available through the World Data Center PANGAEA Data Publisher for Earth & Environmental Science (https://www.pangaea.de) within two years after the cruise. The finally processed CTD and velocity data will also be made available through PANGAEA when processing has been completed. By default, the CC-BY license will be applied.

This expedition was supported by the Helmholtz Research Programme “Changing Earth – Sustaining our Future” Topic 2, Subtopic 2.1, 2.2, 2.3 and 2.4. It further contributes to Topic 6, Subtopic 6.1 and 6.2.

In all publications, based on this cruise, the one of the relevant Grant Numbers referring to the seawater work (i.e., AWI_PS140_01, AWI_PS140_02, AWI_PS140_10, AWI_PS140_11, AWI_PS140_12) will be quoted and the following *Polarstern* article will be cited:

Alfred-Wegener-Institut Helmholtz-Zentrum für Polar- und Meeresforschung (2017) Polar Research and Supply Vessel POLARSTERN Operated by the Alfred-Wegener-Institute. Journal of large-scale research facilities, 3, A119. http://dx.doi.org/10.17815/jlsrf-3-163.

References

Herraiz-Borreguero Lγ & Naveira Garabato A (2022) Poleward shift of Circumpolar Deep Water threatens the East Antarctic Ice Sheet. Nature Climate Change 12(8):728–734. https://doi.org/10.1038/s41558-022-01424-3

Herraiz-Borreguero L, Coleman R, Allison I, Rintoul SR, Craven M & Williams GD (2015) Circulation of modified Circumpolar Deep Water and basal melt beneath the Amery Ice Shelf, East Antarctica. Journal of Geophysical Research: Oceans 120(4):3098–3112. https://doi.org/10.1002/2015JC010697

Iudicone D, Madec G and McDougall TJ, 2008: Water-Mass Transformations in a Neutral Density Framework and the Key Role of Light Penetration. J. Phys. Oceanogr. 38:1357–1376, https://doi.org/10.1175/2007JPO3464.1

Meijers A J, Klocker A, Bindoff N L, Williams G D & Marsland SJ (2010) The circulation and water masses of the Antarctic shelf and continental slope between 30 and 80°E. Deep Sea Research Part II: Topical Studies in Oceanography 57(9-10):723–737. https://doi.org/10.1016/j.dsr2.2009.04.019

Ohshima K I, Fukamachi Y, Williams GD, Nihashi S, Roquet F, Kitade Y, . . . Wakatsuchi M (2013) Antarctic Bottom Water production by intense sea-ice formation in the Cape Darnley Polynya. Nature Geoscience 6(3):235–240. https://doi.org/10.1038/ngeo1738

Orsi A H, Whitworth T & Nowlin WD (1995) On the meridional extent and fronts of the Antarctic Circumpolar Current. Deep Sea Research Part1: Oceanographic Research Pages 42(5):641–673. https://doi.org/10.1016/0967-0637(95)00021-W

Purkey S G, Smethie W M, Gebbie G, Gordon A L, Sonnerup RE, Warner M J & Bullister J L (2018) A Synoptic View of the Ventilation and Circulation of Antarctic Bottom Water from Chlorofluorocarbons and Natural Tracers. Annual Review of Marine Science 10: 503–527. https://doi.org/10.1146/annurev-marine-121916-063414

Sloyan BM and Rintoul SR (2001) Circulation, Renewal, and Modification of Antarctic Mode and Intermediate Water. J. Phys. Oceanogr. 31:1005–1030, https://doi.org/10.1175/1520-0485(2001)031<1005:CRAMOA>2.0.CO;2

Solodoch A, Stewart A L, Hogg A M, Morrison A K, Kiss A E, Thompson A F, et al. (2022) How does Antarctic Bottom Water cross the Southern Ocean? Geophysical Research Letters 49:e2021GL097211. https://doi.org/10.1029/2021GL097211

van Wijk E M, Rintoul SR, Wallace L O, Ribeiro N & Herraiz-Borreguero L (2022) Vulnerability of Denman Glacier to Ocean Heat Flux Revealed by Profiling Float Observations. Geophysical Research Letters 49(18). https://doi.org/10.1029/2022GL100460

Williams G D, Herraiz-Borreguero L, Roquet F, Tamura T, Ohshima KI, Fukamachi Y, . . . Hindell M (2016). The suppression of Antarctic bottom water formation by melting ice shelves in Prydz Bay. Nature Communications 7(1):12577. https://doi.org/10.1038/ncomms12577

Williams G D, Nicol S, Aoki S, Meijers AJ, Bindoff NL, Iijima Y, . . . Klocker A (2010). Surface oceanography of BROKE-West, along the Antarctic margin of the south-west Indian Ocean (30–80E). Deep Sea Research Part II: Topical Studies in Oceanography 57(9-10):738–757. https://doi.org/10.1016/j.dsr2.2009.04.02

4. CHEMICAL CHARACTERISATION OF THE SOUTHERN OCEAN WATER COLUMN AND EAST ANTARCTIC SHELF WATERS

Marcus Gutjahr[1], Rob Middag[2,3], Huang Huang[4], Wytze Lenstra[5], Layla Creac'h[6], Annika Oetjens[7], Ole Rieke[7], Florine Kooij[2,3], Robin van Dijk[3], David Menzel[1], Patrick Deprie[1], Kathrin Groß[1], Manuel Ehnis[6], Fabian Schneider[6], Manuel Ruben[8], Lester Lembke-Jene[8], Samuel Sellmaier[8] Jasmin Stimpfle[8], Marrit Jacob[8]

Not on board: Jörg Lippold[6], Gesine Mollenhauer[8], Tobias Steinhoff[1], Patrick Blaser[9], Norbert Frank[6], Hermann Bange[1], Caroline Slomp[5], Willem van de Poll[3], Laura Herraiz-Borreguero[10], Markus Janout[8], Sandra Tippenhauer[8]

[1]DE.GEOMAR
[2]NL.NIOZ
[3]NL.UNI-GRONINGEN
[4]CN.SUN-YAT-SEN-ZHUHAI
[5]NL.UNI-RADBOUD
[6]DE.UNI-HEIDELBERG
[7]AU.UNI-TASMANIA
[8]DE.AWI
[9]CH.UNI-LAUSANNE
[10]AU.CSIRO-ENVIRONMENT

Grant-No. AWI_PS140_00 (AWI_PS140_01, AWI_PS140_02, AWI_PS140_10)

Outline

The comprehensive study of a series of chemical parameters in the Southern Ocean is one of the key objectives of our current EASI-2 expedition. Following the physical oceanographic characterisation of water masses in the study area (Chapter 3), investigation of chemical oceanographic parameters will allow identification of trace metal sourcing and cycling within the various SO water masses. To this end we collected water samples for the analyses of macro- and micronutrients, a wide range of minor and trace elemental concentrations, many stable, radiogenic or radioactive isotope systems ($\delta^{11}B$, $\delta^{13}C$, $F^{14}C$, $\delta^{18}O$, $^{41}Ca/Ca$, $\delta^{56}Fe$, $^{87}Sr/^{86}Sr$, $^{143}Nd/^{144}Nd$, $^{206,207,208}Pb/^{204}Pb$, $\delta^{234}U$), as well as carbonate system parameters (Total Alkalinity and Dissolved Inorganic Carbon). Sampling was carried out in a transect from Cape Town to Prydz Bay (Western Indian Ocean Transect), at many sites within Prydz Bay, during transit along the Davis Sea stretching from Prydz Bay to the east of the Shackleton Ice Shelf (~100°E), and along a transect north between 100 and 105°E, from 65°S to 45°S (Eastern Indian Ocean Transect). Both a regular (non-trace metal clean) water sampler and the NIOZ trace metal clean water sampler "Titan" were used in combination. Samples obtained during this expedition will be further purified and processed in laboratories at GEOMAR Helmholtz Centre for Ocean Research Kiel, NIOZ Texel, the University of Groningen, Heidelberg University, and the Alfred Wegener Institute, Helmholtz Centre for Polar and Marine Research (AWI) in Bremerhaven. Particular focus is placed on the transfer of anthropogenically sourced Pb to Antarctic waters, as well as an assessment of particularly contamination-prone transition metals. Neodymium isotopes will provide further water mass sourcing and water mass mixing information, while radiocarbon measurements provide information on deep water ventilation rates. Since such water transects have not yet been carried out in the study area the outcome of this cruise will substantially expand our knowledge on key trace metal concentrations and their isotopic signatures in the Indian sector of the Southern Ocean. Chemical oceanographic insights derived from this cruise will further allow trace metal reconstructions on co-sampled sediments in order to assess Pleistocene SO overturning and trace metal circulation states (Chapter 5).

Objectives

The Indian sector of the SO is the arguably least explored and understood sector of the SO. It borders the marine-based East Antarctic Ice Sheet, which is increasingly exposed to corrosive warm modified Circumpolar Deep Water (mCDW) such as in the area of the Denman Glacier (Herraiz-Borreguero and Garabato, 2022; Ribeiro et al., 2021; van Wijk et al., 2022). This not only has consequences for EAIS dynamics but also for trace element (isotope) cycling. Chemical oceanographic work to be carried out with samples from this expedition will allow us to quantify the current state of the SO water column trace metal budget. Chemical exchange processes at the seafloor are particularly important since the seafloor may be a source for a whole range of major, minor and trace elements. We further want to connect elemental budgets with carbonate system parameters, with potentially added information towards aspects of the marine carbon cycle. Last but not least, the water column and benthic porewater work will be further extended by the sampling of sediment-containing continental ice (containing Antarctic rock debris) that PI M. Gutjahr is carrying out in cooperation with the land geology group onboard PS140 (Chapter 6). Below, we will introduce aspects related to each proxy of interest.

Lead input and its dispersal in the Southern Ocean

The human impact on the marine environment is extreme and mankind already altered natural biogeochemical cycles substantially (Hader et al., 2020; Mahowald et al., 2018), even though the impact on the Antarctic ecosystem via pollution seemingly is as yet not as dramatic when compared to other regions (Clarke and Harris, 2003). Atmospheric emissions of lead (Pb) are a prime example for anthropogenic metal pollution and transient atmospheric fluxes of Pb have long been monitored (Duce et al., 1991; Schaule and Patterson, 1981). During the late 1980s, the global total Pb flux to the oceans was on the order of 0.24 mg per square metre and year (Duce et al., 1991). The majority was deposited in the North Atlantic, while dust fluxes in the South Indian Ocean were estimated at 0.05 mg/m^{2}yr. This Pb flux led to a Pb deposition budget of 89x109 g/yr globally and 2.4 x109 g/yr in the South Indian Ocean. These numbers comprise both natural and anthropogenically sourced Pb but are clearly dominated by anthropogenic Pb sourcing. The phasing out of leaded gasoline between 1975 and 1995 resulted in remarkable modern-day water column Pb concentration gradients in the North Atlantic, where at present highest dissolved Pb concentrations are observed in the intermediate depth water column (Noble et al., 2015). These are water masses enriched in Pb that were in contact with the atmosphere decades ago when anthropogenic Pb emissions from Northern Hemisphere sources were still substantially higher than today. This North Atlantic subsurface concentration maximum equally highlights the transient behaviour of anthropogenic and natural Pb sourcing and its short residence time in seawater. The intermediate water Pb concentration peak in the North Atlantic also demonstrates that anthropogenic Pb emissions to the atmosphere have been decreasing in circum-North Atlantic areas, in contrast to other parts of the world such as the North Indian Ocean where surface water Pb concentrations define maxima because of continuously increasing Pb emissions in India, China and South Africa (Echegoyen et al., 2014; Lee et al., 2015).

While the generally lower Pb emissions in the Southern Ocean are more difficult to detect, these can be sensitively traced in Antarctic snow and ice. Antarctic snow deposited in the Hercules Névé plateau in Victoria Land (Antarctica) between 2012-15 still contained more than 90% Pb of noncrustal origin (Han et al., 2022). Combining these recent observations with previous data, the authors suggested that Pb pollution in Antarctica has not significantly decreased until recently, despite continued international efforts to reduce Pb emissions in the Southern Hemisphere during the corresponding period (see also Bertinetti et al., 2020) The Pb isotopic fingerprints in Victoria Land point to major Pb sourcing from South America, and particularly Brazil and Chile have become major sources of anthropogenic Pb in East Antarctic

areas bordering the Pacific sector of the Southern Ocean (Han et al., 2022). Conversely, anthropogenic Pb in the Indian sector of the Southern Ocean is dominantly of South African origin (Boye et al., 2012; Lee et al., 2015; Schlosser et al., 2019).

Lead is a very particle-reactive element with an associated short residence time in seawater. According to a study using ^{210}Pb, the average residence time within the upper 2,000 m is in the order of 48 years, yet with large differences between high- and low-productivity regions (Henderson and Maier-Reimer, 2002). The residence time of Pb in the surface Indian Ocean is shorter than one year, while dissolved Pb in the deep Northern Indian Ocean has a residence time of 6-10 years (Sarin et al., 1994). Given that anthropogenic Pb sources also generate a regional water mass sourcing signal, it should be possible to distinguish anthropogenic Pb sourcing from major input sources such as India, China, or South Africa (Bollhöfer and Rosman, 2000, 2001; Flament et al., 2002). All these anthropogenic Pb isotope signatures will equally be substantially different compared with regional natural (Antarctic) Pb isotope source signatures.

In terms of ocean current and water mass configuration, the Southern Ocean presents an ideal laboratory to study how anthropogenic Pb sourced from the lower latitudes is transferred southward and eastward within various water masses. Given that anthropogenic sourcing of Pb is a very regional phenomenon, we should be able to sensitively trace the continental sources of Pb in each part of the Southern Ocean, particularly given the short residence time in the order of only a few years to decades. In order to resolve water mass sourcing by means of Pb, it is essential to study its isotopic composition and not only the dissolved Pb concentration. Lee et al. (2015) who presented the first in-depth study of natural and anthropogenic Pb distribution in the Indian Ocean demonstrated that Pb isotopic compositions measured at the deepest water depths of the most southern station contained compositions closest to natural Fe-Mn crust compositions, but still contained an anthropogenic component.

Over the past decades the southern hemisphere westerlies intensified (Boning et al., 2008). This, in turn, led to stronger vertical mixing, and as a result, also more efficient entrainment of atmospherically deposited anthropogenic Pb into intermediate water depths of the ACC within the Southern Ocean (Schlosser et al., 2019). This also coincided with a southerly displacement of the southern hemisphere westerly wind belt at least in the Pacific sector of the Southern Ocean, while displacements in the ACC frontal system in the Indian sector seem to be more strongly controlled by regional changes in ocean circulation (Kim and Orsi, 2014). Overall, the strengthening of the westerly wind belt alongside its displacement to higher southern latitudes will lead to accelerated Pb transfer to the Antarctic zone of the Southern Ocean.

The last point investigated is the generally poorly understood benthic Pb cycling in the marine environment. Some elements such as neodymium were shown to be released from marine sediments to overlying bottom water (Abbott et al., 2015; Du et al., 2022). While such a scenario is less likely important for Pb because of its higher particle reactivity, potential exchange of Pb between dissolved and particulate phase has been mentioned (Lee et al., 2015). While this aspect may seem less important to readers outside the paleoceanographic community, it is a crucial process indeed since exchange between particulate and dissolved Pb in sedimentary porewaters in the worst-case could lead to alteration of originally precipitated seawater-sourced Pb isotope signatures. A previous record published from the last two glacial terminations suggest that the authigenic Pb isotope signature in Southern Ocean sediments is immune to such authigenic diagenesis (Huang et al., 2020; Huang et al., 2021), yet this needs further proof from modern meaningful case studies. And such case studies can only be realised in remote sub-glacial settings such as proposed here. This research objective is targeted with continental ice sampling containing detrital sediments that is presented in Chapter 6.

Tracing water mass sourcing with neodymium isotopes

A secondary major target for PS140 is the study of neodymium (Nd) isotope systematics within the water column. Neodymium isotopes are among the best provenance markers for individual water masses. Neodymium belongs to the group of Rare Earth Elements (REE) and is systematically incorporated in continental and oceanic crust with unique isotopic signatures. Neodymium isotopes are also an increasingly employed tool to investigate the origin and flow path of water masses in the oceans today and in the past. Analogously to Pb, this trace metal is supplied to the oceans via physico-chemical weathering on land and at the seafloor in shallow marine and continental rise settings. A latest modelling study reported that the relative contributions of Nd to seawater are ~60% via boundary/benthic additions (i.e., from the sediments to bottom water), ~32% through riverine inputs, and ~9% from partial dissolution of dust in the water column (Pöppelmeier et al., 2020). The Nd isotope signature is thereby reflecting the isotopic signal of the material dissolving on land, within the water column (dust), or at the seafloor. As a consequence, water masses in contact with the ocean margin often successively change their isotopic composition along their flow path, but in the open ocean Nd isotopic compositions remain constant unless a parcel of water is mixed with another parcel of water with a different isotopic composition. Neodymium can hence be categorized as behaving semi-conservatively in seawater with a mean global residence time of about 690 years (Pöppelmeier et al., 2020).

To the west of the Kerguelen Plateau, the AABW exported into deep Atlantic and Indian Ocean today are predominately sourced from the areas in the southwest Weddell Sea and Prydz Bay regions (Solodoch et al., 2022). To the east of the Kerguelen Plateau, a different variety of AABW fills abyssal parts of the SO that is mainly sourced from Adélie Land and the Ross Sea further to the east (Solodoch et al., 2022). The PIs have sampled seawater in the southern and north-western Weddell Sea and in the western flank of Prydz Bay during previous cruises for analyses of Nd isotopes and its concentration during PS111 in 2018, PS118 in 2019 and PS128 in 2022. Preliminary Nd data has already provided insights into the Nd isotopic and concentration behaviours in these areas, also highlighting discrete hotspots of Nd addition to bottom waters, most clearly resolvable along the margins of the eastern Antarctic Peninsula and East Antarctica within the Indian sector. The work to be realised during PS140 will extend the Nd database to the key unsampled East Antarctic areas, e.g., Prydz Bay and the Antarctic shelf areas to the east, for a comprehensive understanding of the quasi-conservative behaviour of Nd isotope signatures in the SO.

Specifically, the marine geochemistry team onboard PS140 will assess the feasibility of using seawater Nd isotope signatures as a water mass tracer in the Indian Ocean sector of the Southern Ocean. We will compare actual seawater Nd isotope data in the water column with the standard physical oceanographic parameters and oxygen concentrations. In order to better constrain the non-conservative behaviour of Nd, we also targeted the seawater-sediment interface by collecting Nd isotope and REE concentration data in the porewater, authigenic and detrital fractions of the surface sediments at many locations throughout the cruise. The benthic fluxes of Nd into the bottom water will be quantified via combined water column and sedimentary data at various sites covering the Antarctic continental shelf, Antarctic continental slope and seafloor in the open ocean. The results will largely improve our knowledge regarding the Nd isotope geochemical cycle in the SO.

It is also worth noting that the Prydz Bay-sourced Dense Shelf Water (DSW), which is one of the precursors of Cape Darnley AABW, is the last global deep water endmember of which the Nd isotope signature is still undetermined. Precise measurements of its Nd isotope signature implemented during PS140 will allow us to reconstruct back into past glacial cycles the evolution of Prydz Bay-sourced DSW export. Marine sediments contain an authigenic Fe-Mn

oxyhydroxide fraction that preserves the bottom water Nd isotope signatures and we can extract this bottom water signature with a gentle reductive solution (Huang et al., 2021). This objective will be realised by targeting marine sediments that will be obtained in close cooperation with the Marine Geology group during PS140 (Chapter 5). The reconstruction of Prydz Bay-sourced AABW variability will provide essential information about the interactive mechanisms between past East Antarctic Ice Sheet dynamics and the formation and export of AABW.

Transition metals

Marine primary productivity exerts a key control on global climate. Trace metal availability limits primary productivity in many ocean regions, influencing ecosystem dynamics and (anthropogenic) carbon sequestration. Specifically, Fe, Mn, Ni, Cu, Zn and Co, are key micro-nutrients for marine organisms. Notably in high latitude oceans, the availability of these bio-essential trace metals, and especially Fe and Mn, can limit phytoplankton productivity and control the microbial community composition (Finkel et al., 2010; Schoffman et al., 2016). This makes it critical to understand the key sources of trace metals in surface waters. Recent evidence suggests that, besides atmospheric input and upwelling, lateral transport of trace metals released from continental margin sediments and glacial melt is an important source of trace metals in the open ocean (Homoky et al., 2016; Lenstra et al., 2019; Lenstra et al., 2022; Seyitmuhammedov et al., 2021; Shi et al., 2019). For many marine areas, but especially in high-latitude regions where glaciers supply particulate trace metals to continental shelves (Raiswell et al., 2018; van Manen et al., 2022), insight in the sedimentary mobilization and its impact on the water column is still lacking. Consequently, current global scale models that are used to assess the potential impacts of climate change on ocean biogeochemistry, and vice versa, cannot reproduce present-day oceanic trace metal distributions and, hence, vary widely in their predictions (Tagliabue et al., 2016). Given ongoing rapid climate change at high latitudes, it is crucial to obtain a better predictive and quantitative insight into trace metal input from shelf sediments in these regions.

Specifically, we will characterize the water column using trace metal clean techniques (Middag et al., 2015; Rijkenberg et al., 2015), sample for the relevant water column parameters (including trace metals and lead isotopes), followed by analysis of selected trace metal concentrations and isotopic compositions in the water column and near the sediment (e.g. Lenstra et al., 2019; van Manen et al., 2022). The ensuing data interpretations would not just be standalone research outcomes but are needed to successfully complete the overall mission of EASI-2, understanding the role of the EAIS and nearby seas and ocean in past, current and future climate scenarios.

Notably, we will assess the role of Antarctic shelf sediments and glacial melt as a source of bio-available Fe, Mn, Ni, Cu, Zn and Co to offshore waters. We will also compare this trace metal release from shelves to release from deep ocean sediments. The benthic fluxes of bioavailable trace metals and their controls will be quantified using a combination of the water column data from this project and sediment and porewater analyses and sediment incubations in project AWI_PS140_10, Biotrace. Overall, the research is expected to provide key novel insights into the processes that could make the EAIS a driver of future sea level rise. The results will also greatly improve our knowledge of the trace metal fluxes of continental margin sediments to the ocean.

Assessing sediment cycling and benthic fluxes for transition metals

Iron (Fe) and manganese (Mn), among other trace metals, are key micro-nutrients for marine phytoplankton. The availability of these bio-essential trace metals in oceanic surface waters can (co)-limit primary productivity (Moore et al., 2013; Browning et al., 2021). This makes it critical to understand the key sources of these trace metals to oceanic surface waters. Recent

evidence points towards continental margin sediments as an important source of Fe and Mn to the surface ocean (Lam and Bishop, 2008; Tagliabue et al., 2009). It is therefore of key importance to understand the mechanisms that control the benthic supply of Fe and Mn to the ocean, especially at high latitude regions where Fe and Mn limit primary productivity. During EASI-2 we therefore combined high resolution porewater sampling with benthic flux experiments. Additionally, with onboard incubations we quantified the importance of macrofauna in the release of (trace) nutrients from the sediment. Overall, the combination of sediment analysis and the determination of benthic fluxes is expected to greatly improve our mechanistic understanding of the supply of trace metals from the continental shelf to the Southern Ocean.

Porewater extractions will also be performed for several other trace metal concentration measurements (various TE, REE, Pb, U, Th), as well as boron, strontium and possibly lead isotopic analyses.

Uranium isotopes in Antarctic waters

Uranium (U) and its natural radioactive isotopes have been proposed as a tracer in oceanography for more than 60 years (Ku et al., 1977). Their utility stem from the ^{238}U decay into ^{234}U and ^{230}Th, providing measures of time for processes such as particle scavenging and continental weathering as well as carbonate formation in the recent geologic past (Bourdon et al., 2003). More recently, redox-driven $^{238}U/^{235}U$ isotope fractionation was recognized providing a potential proxy of ocean anoxia (Kipp et al., 2022). Note, U behaves conservatively in seawater with a mean residence time > 400 kyr in the Ocean allowing inferences of global balances and regional processes. Also important is the potential strong regional influence on the ^{234}U-excess as demonstrated in studies of semi-closed ocean basins, yielding a visible signal of elevated ^{234}U-excess from river discharge or submerged groundwaters (Andersen et al., 2007; Border, 2020). Consequently, studies of the regional U isotopic composition of seawater regarding the $^{238}U/^{235}U$ ratio as well as the excess of ^{234}U can inform on ocean anoxia, weathering patterns, and freshwater discharge which gives the U proxy a new utility in paleoceanography. Here, we will collect samples representing the southern hemisphere balance of water injected in the Antarctic Circumpolar Current and its potentially visible influences from regional freshwater release and sedimentological isotope fractionation imprinted on the seawater $^{238}U/^{235}U$ ratio and ^{234}U-excess. This is of particular interest as the U isotope balance of the south polar Ocean has not been studied so far.

$^{41}Ca/Ca$ in seawater

Calcium-41 (half-life $t_{1/2}$ ~1.0 X 10^6 years) has been suggested as a new tool for radiometric dating in the range of 10^5 to 10^6 years since 1970s (Henning et al., 1987). However, due to the low abundance of ^{41}Ca in the natural environment, resulting in an approximate $^{41}Ca/Ca$ below 10^{-15}, there are almost no reliable data of its natural abundance. In 2023, a novel Atom-trap trace analysis (ATTA) method achieved to measure $^{41}Ca/Ca$ ratios below the range of 10^{-16} to 10^{-15}, making the determination of $^{41}Ca/Ca$ in environmental samples possible (Xia et al., 2023). Because Ca has a very long residence time in the ocean (over 500 ka), the seawater $^{41}Ca/Ca$ ratio is supposed to be homogeneous in the ocean. Therefore, determining the seawater $^{41}Ca/Ca$ ratio may become an excellent tool for dating marine samples in the future. During this cruise, we sampled seawater for measuring the first SO $^{41}Ca/Ca$ ratio.

Radiocarbon in seawater

Global climate is critically sensitive to physical and biogeochemical dynamics in the subpolar Southern Ocean, since it is here that deep, carbon-rich layers of the world ocean outcrop and exchange carbon with the atmosphere (e.g., MacGilchrist et al., 2019). It is also here that much of anthropogenic carbon is taken up by the ocean, and glacial ocean carbon storage in the deep

Southern Ocean is well established (e.g., Brovkin et al., 2012). Changes in Southern Ocean carbon uptake and its export to depth are thus strongly impacting the global carbon cycle. The Southern Ocean's role in anthropogenic carbon uptake has long been identified (Caldeira and Duffy, 2000), and it has been suspected that climate warming reduced the efficiency of this anthropogenic carbon uptake. More recently, the strength of this carbon sink has been described to have re-invigorated (Landschützer et al., 2015).

The distribution of deep ocean fraction modern ($F^{14}C$) values of dissolved inorganic carbon (DIC) are often used to illustrate the rate of deep ocean circulation, as radiocarbon is an invaluable tool to trace exchange processes in the carbon cycle and to estimate time in closed reservoirs. For instance, $F^{14}C$ of DIC can be used to map the uptake of atmospheric CO_2 into the ocean, or reflect input of aged carbon from the sea floor originating, e.g., from geologic sources or by degradation of old organic carbon (Ruben et al., 2023). Despite its usefulness, high-resolution profiles of $F^{14}C$ of DIC in the water column are scarce, in particular for the Southern Ocean, and near the Antarctic continental margin, albeit the occurrence of deep-water formation at these locations. The current state of knowledge is based on a large international effort, the World Ocean Circulation Experiment conducted in the early 2000s. We will sample at all CTD stations to significantly expand the existing data base of DIC $F^{14}C$ in the Southern Ocean, to detect deep-water formation and export and to investigate potential decadal-scale changes in carbon uptake.

The radiocarbon signature of pore water DIC has been used to infer the age of remineralized organic matter in sediment (Dumoulin et al., 2022) or dissolved carbonates (Martin et al., 2000), and it has been proposed that in extreme environments such as deep brine pools, inverse diffusion into the sediment might impact pore water $F^{14}C$ (Sivan and Lazar, 2002). Gradients of DIC $F^{14}C$ in the uppermost sediments and across the sediment-water interface will in any case have an impact on bottom water DIC $F^{14}C$, which in turn will be incorporated by benthic foraminifera, commonly used as paleo-proxy carriers. In close collaboration with the marine geology group, we will study this system of complex interaction by sampling pore waters at selected sites and determining isotopic compositions and concentrations of DIC.

Carbonate System Parameters (TA and DIC), seawater $\delta^{13}C$ and $\delta^{18}O$

Any change in the marine carbon pool can be readily quantified via measurement of selected carbonate system parameters. At least two out of six carbonate system parameters are required in order to constrain all essential carbonate system variables (i.e. CO_2, HCO_3^-, CO_3^{2-}, H^+, DIC, TA). During PS140 we determined total alkalinity (TA) either underway as well as in all individual bottled water samples. Seawater TA was titrated onboard with help of a CONTROS HydroFIA™-TA, from 4H-JENA engineering. In addition to TA, discrete samples for Dissolved Inorganic Carbon (DIC) were collected in order to provide the required second carbonate system parameter. Since planktic carbonates (e.g. foraminifera) are equally expected to be collected during the cruise, a direct assessment of seawater chemistry using for example the boron isotope proxy will be possible. The DIC budget will hence not only provide insights into current changes in the dissolved Southern Ocean carbon budget but also allow calibration of sedimentary carbonate system proxies, essential for any paleoceanographic applications following EASI-2. Moreover, TA was also manually titrated onboard PS140 from extracted marine porewaters for the detection of diagenetic redox processes in surface sediments. Last but not least, at each water sampling station additional aliquots were taken for shore-based analyses of DIC $\delta^{13}C$, as well as seawater $\delta^{18}O$.

Methane and nitrous oxide in seawater

Following carbon dioxide (CO_2), nitrous oxide (N_2O) and methane (CH_4) are the most important natural greenhouse gases (IPCC, 2021). Moreover, CH_4 and N_2O are involved in stratospheric

ozone depletion (WMO, 2018). N_2O, in view of the ongoing atmospheric decrease of the chlorofluorocarbons, is expected to become the most important ozone-depleting compound of the 21st century (Ravishankara et al., 2009). When it comes to what we know of the ocean as a source of these gases, our knowledge is patchy and uncertainty ranges are significant. Estimates of oceanic CH_4 emissions suffer from significant uncertainties: although the ocean could contribute a minor, but still significant, 1% of global CH_4 emissions, uncertainties are in the range of at least ± 50% (IPCC, 2021). Oceanic N_2O emission estimates indicate that the open and coastal oceans may contribute between 13% and 44% of the natural and anthropogenic N_2O sources combined (IPCC, 2021). Oceanic emissions of both CH_4 and N_2O are largely determined by the balance of microbial production (i.e. nitrification, denitrification and methanogenesis) and consumption processes (denitrification and CH_4 oxidation) (Bakker et al., 2014). In the case of CH_4, microbial consumption is thought to be very effective and thus consumes a large fraction of the gas produced *in-situ* allowing only a small fraction to escape into the atmosphere. In contrast to the majority of the oceanic regions, the Southern Ocean is undersaturated with CH_4 and thus seems to act as a sink for atmospheric CH_4 (see e.g. Ye et al., 2023). However, only a few studies have addressed the distributions of CH_4 and N_2O in the water column of the Indian Ocean sector of the Southern Ocean and the Prydz Bay so far.

Work at sea

Seawater, porewater and MUC-sediment sampling

Seawater sampling during PS140 was carried out at 53 out of 85 realised regular CTD stations. The sampling areas either fall within the western Indian transect, many shelf sites within and to the north and east of Prydz Bay, the Shackleton Ice Shelf area and Denman Glacier, and the eastern Indian transect heading north between 100-105°E (Fig. 4.1 to Fig. 4.4). Depending on condition at each station, water sampling varied. At 17 stations, only the regular and clean CTD were employed. At 29 stations, the regular and clean CTD were used as well as MUC water collected. At five stations only the regular CTD and MUC water was collected. Finally, at the last two stations of the cruise only aliquots for trace metal and nutrient analyses were sampled. An overview is shown in Table 4.1.

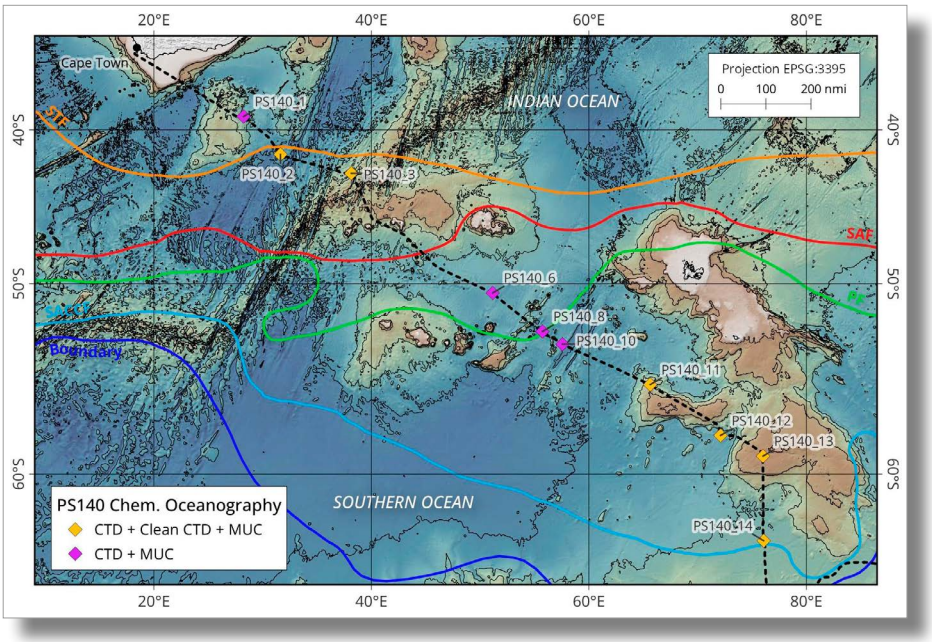

Fig. 4.1: Chemical oceanographic sampling along the West Indian Ocean Transect going south. Also shown are the major Southern Ocean fronts (STF: Subtropical Front; SAF: Subantarctic Front; PF: Polar Front; SACCF: Southern Front of the ACC; Boundary: Southern boundary of the ACC).

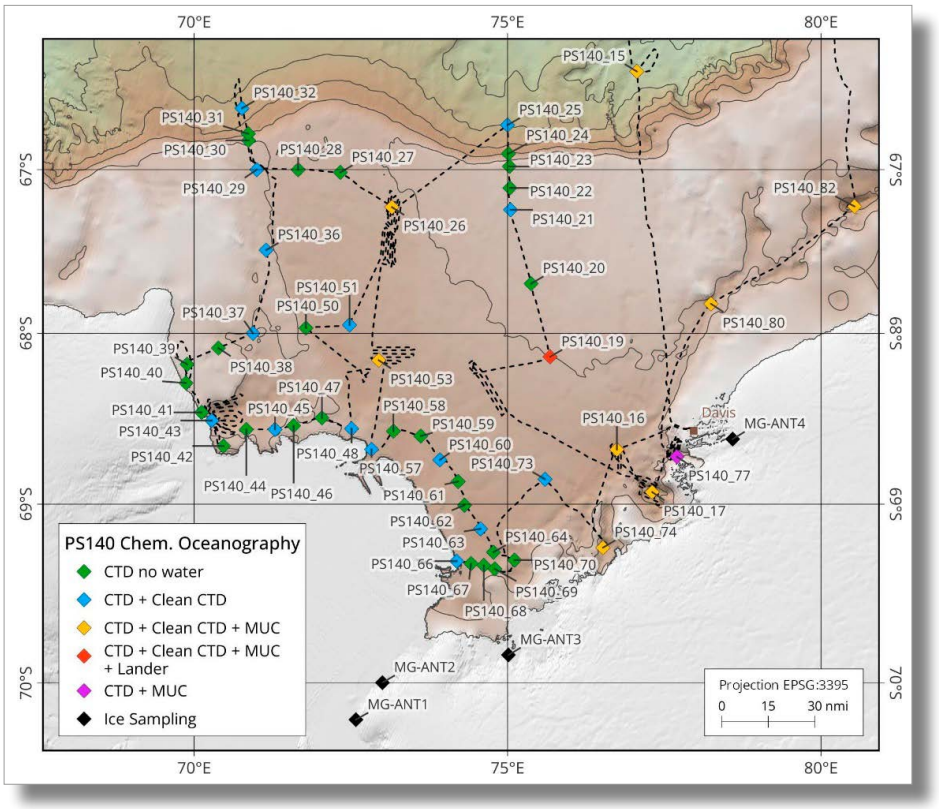

Fig. 4.2: Chemical oceanographic stations covered in the Prydz Bay area

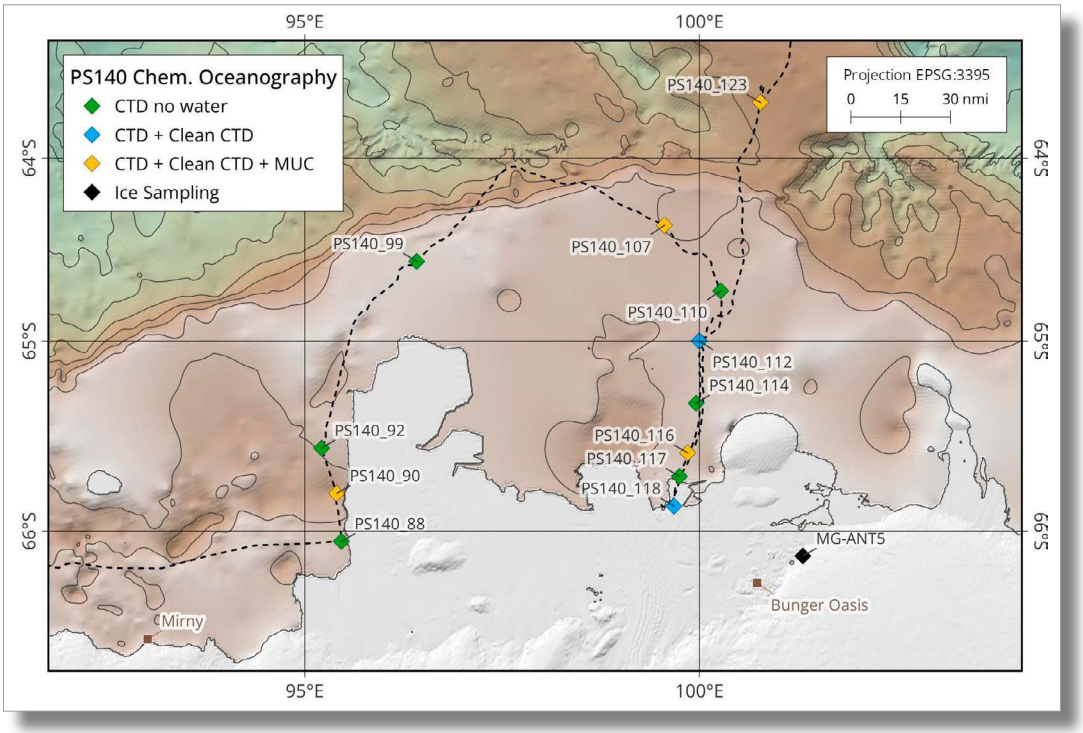

Fig. 4.3: Chemical oceanographic sampling around the Shackleton Ice Shelf and in front of the Denman Glacier.

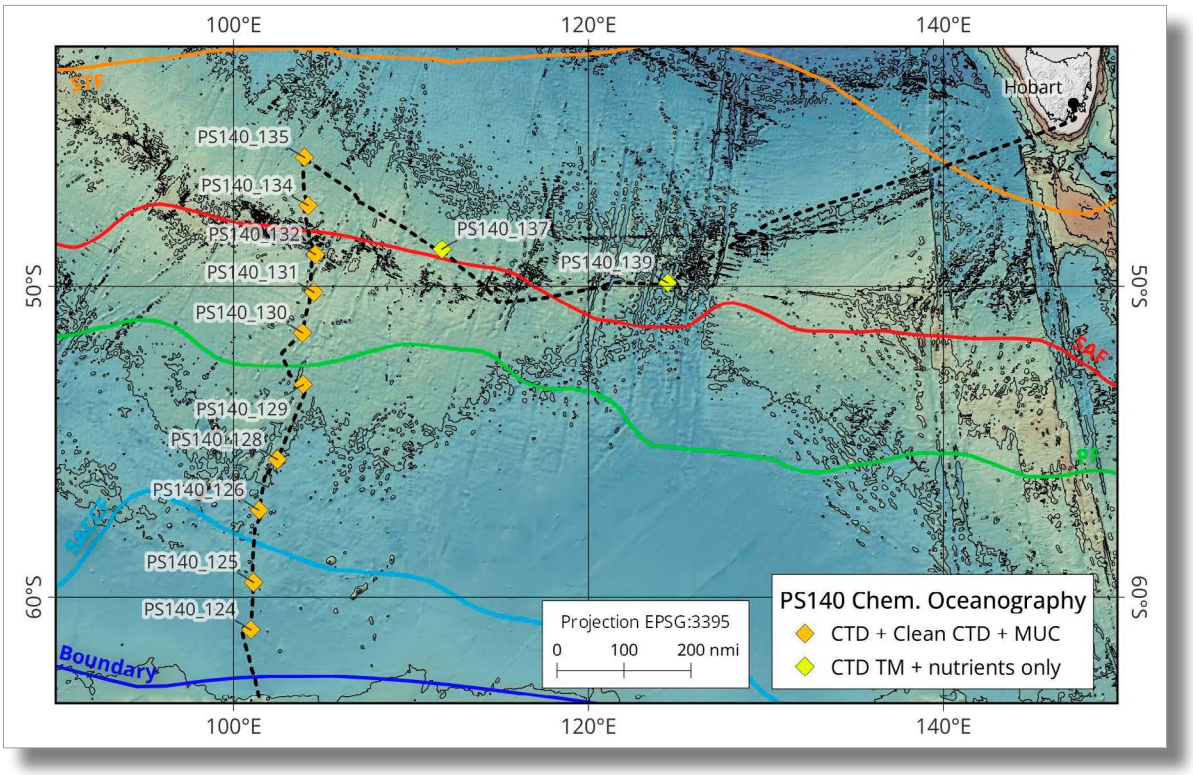

Fig. 4.4: Chemical oceanographic sampling along the Eastern Indian Ocean Transect.

Tab. 4.1: Overview of all CTD stations illustrating respective sampling protocols

Station Number	Station name	Water depth (m)	Decimal Lat.	Decimal Lon.
Water sampling with Regular and Clean CTD without MUC water collection				
PS140_21	W CTD inflow mCDW2	402	-67.247	75.052
PS140_25	W inflow mCDW5	2000	-66.719	75.000
PS140_29	W outflow DSW3	469	-67.000	71.000
PS140_32	W outflow DSW6	1833	-66.614	70.764
PS140_36	W outflow DSW mid shelf revised	422	-67.497	71.149
PS140_37	W upper mid shelf DSW revised	505	-68.000	70.940
PS140_43	Full MacKenzie Polynia 4	1245	-68.517	70.236
PS140_45	W Amery IS 3	562	-68.568	71.291
PS140_48	W Amery IS 6	650	-68.565	72.517
PS140_51	W LEACOV mid shelf	713	-67.947	72.477
PS140_57	W Amery IS 7	731	-68.684	72.831
PS140_60	W Amery IS 10	766	-68.736	73.906
PS140_63	W Amery IS 13	841	-69.144	74.560
PS140_66	W Amery IS 17 revised	714	-69.324	74.189
PS140_73	Water and MN target 3a	725	-68.861	75.597
PS140_112	W Denman IS 3	420	-65.000	100.000
PS140_118	W Denman IS 7	626	-65.872	99.680

Station Number	Station name	Water depth (m)	Decimal Lat.	Decimal Lon.
Water sampling with Regular and Clean CTD including MUC water collection				
PS140_2	W-STF1	4479	-41.710	31.640
PS140_3	W-STF2	2995	-42.984	38.153
PS140_11	W-POOZ2	2295	-55.614	65.640
PS140_12	W-SIZ1	4450	-58.170	72.110
PS140_13	W-SIZ2	1184	-59.160	76.014
PS140_14	W-SIZ3	3871	-63.000	76.060
PS140_15	W-SSZ1	2933	-66.060	76.900
PS140_16	NBP0101-JPC24 revisited	825	-68.694	76.709
PS140_17	Full Great Gully Experience	1430	-68.929	77.305
PS140_19	Full OE Target 1 INCL. BENTHIC LANDER	502	-68.146	75.693
PS140_26	Full OE Target 6	545	-67.235	73.172
PS140_53	Full OE target 4a/4b	730	-68.163	72.945
PS140_74	Full Diatom Valley	850	-69.250	76.599
PS140_80	Transit to WIS 1	713	-67.819	78.247
PS140_82	Transit to WIS 2	1619	-67.228	80.536
PS140_90	W Shackleton IS West2	1024	-65.806	95.403
PS140_107	W Denman IS 1	540	-64.372	99.559
PS140_116	W Denman IS 5	542	-65.591	99.849
PS140_123	W&SED (ca. -63/100)	1372	-63.687	100.772
PS140_124	E-SIZ1	4515	-60.896	100.974
PS140_125	E-SIZ2	4170	-59.569	101.124
PS140_126	E-POOZ1	4224	-57.443	101.450
PS140_128	E-POOZ2b	3836	-55.873	102.467
PS140_129	E-APF1	3723	-53.442	103.090
PS140_130	E-APF2	3200	-51.651	103.868
PS140_131	E-PFZ1	3200	-50.205	104.523
PS140_132	E-PFZ2	3141	-48.822	104.616
PS140_134	EIR1	3257	-46.968	104.199
PS140_135	EIR2	3631	-45.073	103.994
Water sampling with Regular CTD only but including MUC water collection				
PS140_1	W-STZ1	4285	-39.048	28.245
PS140_6	Gutwetterstation	4450	-50.500	51.000
PS140_8	W-APF1 (Polar front)	4477	-53.000	56.300
PS140_10	W-POOZ1a	4330	-53.410	57.732
PS140_77	Heli Shuttle Station	1018	-68.726	77.704
Water sampling with Regular CTD only for trace metal and nutrient concentrations				
PS140_137	EIR3	3565	-48.627	111.747
PS140_139	E-SAZ2 revised	3700	-49.897	124.300
Water sampling with Clean CTD only				
PS140_9	Clean CTD test 500 m	4534	-53.258	57.173

Station Number	Station name	Water depth (m)	Decimal Lat.	Decimal Lon.
Regular CTD stations without any water sampling (physical oceanography only, see Chapter 3)				
PS140_20	NW CTD inflow mCDW1	444	-67.698	75.378
PS140_22	NW CTD inflow mCDW2b	399	-67.115	75.038
PS140_23	NW CTD inflow mCDW3	366	-66.979	75.026
PS140_24	NW CTD inflow mCDW4	1020	-66.898	75.021
PS140_27	NW CTD outflow DSW1	528	-67.017	72.333
PS140_28	NW CTD outflow DSW2	523	-67.000	71.660
PS140_30	NW CTD outflow DSW4	590	-66.817	70.889
PS140_31	NW CTD outflow DSW5	1020	-66.775	70.865
PS140_38	NW CTD MacKenzie outflow	372	-68.088	70.388
PS140_39	NW MacKenzie polynia 1	300	-68.185	69.887
PS140_40	NW MacKenzie polynia 2	350	-68.296	69.869
PS140_41	NW MacKenzie polynia 3	720	-68.470	70.111
PS140_42	NW Amery IS 1	470	-68.664	70.470
PS140_44	NW Amery IS 2	700	-68.568	70.838
PS140_46	NW Amery IS 4	408	-68.546	71.589
PS140_47	NW Amery IS 5	440	-68.496	72.058
PS140_50	NW ISW mid-shelf west	636	-67.969	71.784
PS140_58	NW Amery IS 8	746	-68.578	73.180
PS140_59	NW Amery IS 9	761	-68.607	73.622
PS140_61	NW Amery IS 11	670	-68.868	74.175
PS140_62	NW Amery IS 12	808	-69.006	74.309
PS140_64	NW Amery IS 14	837	-69.273	74.728
PS140_67	NW Amery IS 16 revised	793	-69.337	74.339
PS140_68	NW Amery IS 15	745	-69.347	74.622
PS140_69	NW Amery IS 19 revised	674	-69.368	74.418
PS140_70	NW Amery IS 20 icehole (be precise)	710	-69.317	75.112
PS140_88	NW Shackleton IS West1	720	-66.054	95.464
PS140_92	NW Shackleton IS West3	533	-65.569	95.214
PS140_99	NW Shackleton IS West4	231	-64.569	96.424
PS140_110	NW Denman IS 2	480	-64.730	100.272
PS140_114	NW Denman IS 4	413	-65.332	99.959
PS140_117	NW Denman IS 6	350	-65.717	99.746

Seawater sampling from the Clean CTD

Titan is the NIOZ facility for obtaining CTD data as well as samples for trace element analyses without contaminating the samples. This sampling system was developed at NIOZ in 2005 allowing efficient sampling of seawater under ultraclean conditions (de Baar et al., 2008). It consists of a rectangular shaped all titanium frame which is fitted with a CTD system in a titanium housing and 24 pristine samplers (Rijkenberg et al., 2015). After recovery, the complete system is immediately placed inside a clean-air laboratory unit for sub-sampling and remains there until its next deployment. The temperature inside the container was maintained as close to the water temperature as possible and was usually below 4°C. For this expedition

the system was deployed from a non-conducting 11 mm dyneema rope and data was logged and bottles closed with an SBE-17 auto fire module. Besides an SBE-9+, there were an oxygen sensor, an altimeter and a combined fluorescence and turbidity sensor on the system.

The system was deployed 50 times of which 3 deployments failed (see Appendix Tab. 4.2). The first deployment came up with open bottles and the SBE-17 switched off. The system log indicated this was due to low battery during the downcast, even though the battery voltage was more than sufficient back on deck. Analysis of the data indicated the altimeter gave highly variable readings during below ~2,000 m and suspecting a faulty sensor or connection, this sensor was disconnected. Given that the cable and connection for the altimeter and oxygen sensor was shared on the SBE-9 and we did not have a dummy plug for the altimeter end of the cable, this also meant no oxygen data. However, this did fix the problem and no more problems were encountered with the SBE-17. However, we ran into the problem of sampler bottles not closing on station PS140_8. Flushing all the lines of the pressure barrel (used for the hydraulic closing of the samplers was followed by a successful test to 500 m (station PS140_9), but at the subsequent deep station the bottles did not close again. The pressure barrel was replaced with a spare part and from then on, no more problems were encountered. From station PS140_16 onward, the oxygen sensor was functional as well again after a replacement cable was located that could connect the sensor directly to the SBE9 without the need for connecting the altimeter.

On board, the CTD-data was preliminarily processed. The data consists of all measured parameters (pressure, temperature, conductivity, dissolved oxygen, fluorescence and turbidity) and will undergo later quality control and calibration where necessary. Sampler bottles were closed and sub-samples taken from 12 to 23 depths, depending on water depth and water volumes required.

Depending on the fluorescence, samples for phytoplankton pigments and photosynthetic efficiency (Fv/Fm) were taken at up to 3 depths in the upper water column (~100m). Pigments can resolve phytoplankton composition roughly to the taxonomic level. Furthermore, their abundance is a useful estimate for algal biomass (e.g. chlorophyll a). After filtration of 2-4 L of the water collected from the clean CTD, using a 47 mm GF/F filter under mild vacuum (<0.2 mBar), samples were snap frozen in liquid nitrogen and stored at -80°C. Analysis will be completed at the University of Groningen, the Netherlands, by high performance liquid chromatography (HPLC). Fast repetition rate fluorometry (FRRf) measurements were done for up to 3 depths in the upper water column (~100 m). FRRf measures photosynthetic characteristics related to the efficiency of electron transport by photosystem 2. The characteristics were measured after a minimum of 30 min dark incubation and during a series of irradiance exposures (photosynthesis vs irradiance curves; 8 levels of 40 sec, each up to 1,000 µmol photons m-2 s-1). Changes in photosystem II (PSII; part of the photosynthesis pathway) characteristics are indicative for nutrient limitation (particularly iron limitation) and taxonomic composition. Additionally, water was sampled for bio assays and experiments at selected stations (see Chapters 7 and 8).

Samples for macro nutrients (silicate, phosphate, nitrite and nitrate) where taken at every sampled depth in high-density polyethylene syringes (Terumo®) with a three way valve. This syringe was subsequently used to filter the water over a 0.2 µm Acrodisc® filter and subsamples were transferred into 5 ml polyethylene vials (ponyvials) after rinsing three times with the sample before being capped and stored at -20 °C (phosphate, nitrite and nitrate) or 4 °C (silicate). These samples will be analysed at NIOZ afterwards.

For dissolved metal concentrations and isotopes, samples from all sampled depths were filtered over a 0.2 µm PES Acropak filter under 0.5 bar inline filtered nitrogen pressure directly from the pristine polypropylene samples. For dissolved metals, samples were collected in acid cleaned 125 ml LDPE bottles (Nalgene). All samples were acidified to ~1.8 pH immediately after filtration

using ultra clean HCL to 0.024 M (Normatom Ultrapure, VWR) in a clean flow bench and double bagged in LDPE resealable bags. Samples will be transported back to the shore-based laboratory for Multi-Element (ME) determination that will give the concentrations of Cd, Co, Cu, Fe, Mn, Ni, Zn, Ti, Y, La, Pb, and Ga. This analysis will be done using a SeaFAST system and a High-Resolution Sector Field Inductively Coupled Plasma Mass Spectrometer (HR-ICP-MS) (Middag et al., 2023). For every sampled depth, an additional sample was collected in acid cleaned 500 ml LDPE bottles and acidified as described above. This sample will be stored as an archive sample. Larger volumes were collected for stable metal isotopes (e.g. Fe, Zn and Cd), 4 L in the upper 100 – 125 m (5 depths), 2 L samples at the two subsequent depths and 1 L samples deeper in the water column as the concentrations are expected to be lower at the shallower depths. Samples will be processed for isotope ratios using previously published techniques, i.e. chemical processing with Nobias PA-1 chelating resin and analysis by double spike mass spectrometry using a Thermo Neptune MC-ICPMS (Conway et al., 2013). A separate sample was collected for Pb isotopes and ^{41}Ca/Ca at selected depth in 3 L and 1 L acid cleaned LDPE bottles (neoLab Migge GmbH, Niskin). These samples will be transported to NIOZ for Pb extraction from the seawater matrix, followed by further elemental purification and isotopic measurements at GEOMAR Helmholtz Centre for Ocean Research Kiel.

At all stations until station PS140_43, samples were taken for iron binding ligands from all sampled depths. This water was sampled as for the metals and isotopes in 250 ml LDPE bottles, but these were filled about 80% and frozen at -20°C without any acidification. These samples will be transported to GEOMAR for competitive ligand exchange -cathodic stripping voltammetry (CLE-CSV) analysis in the lab of Prof Sylvia Sander.

For particulate organic carbon and particulate organic nitrogen (POC and PON) sampling, 1-5 L unfiltered seawater was collected from 12 depths per station. These samples were stored at 4 °C until filtration (within several hrs) and filtered through pre-combusted 25 mm glass microfiber filters (GF/75; 0.3 µm) using a mild vacuum pump system (< 0.2 mbar). After filtration, the filters were wrapped in aluminium foil and frozen at -20°C. The C/N analysis will be conducted in the shore-based laboratory at NIOZ using a Thermo-Interscience Flash EA1112 Series Elemental Analyzer (Thermo Scientific). At the same 12 depths, a maximum of six litre (i.e. up to 6 L for deep waters and less for surface waters) of unfiltered seawater was collected for particulate metals.

For particulate trace metals, unfiltered samples were collected in 10L, acid cleaned, carboys (VWR Collection) and stored in dark plastic bags close to the ambient seawater temperature until the moment of filtration.

Before the expedition, 25 mm poly-ether-sulfone (PES) disc filters (0.45 µm Pall Supor) were cleaned by heating them at 60°C for 24h in 3x sub-boiled distilled 1.2M HCl (VWR Chemicals – AnalaR NORMAPUR) and rinsing them 5 times with MQ water (18.2 MΩ) (Ohnemus et al., 2014). Filters were stored in MQ water (18.2 MΩ) until use. Filtrations were started within a maximum of two hours after sampling (Cutter et al., 2017). Before the start of the filtrations, the PES filters were placed in acid-cleaned polypropylene filter holders (Advantec). Filter holders were placed on the caps (Nalgene) of the carboys using polypropylene luer-locks (Cole-Palmer). Carboys were then hung upside down onto the CTD frame using a custom-made polypropylene carboy frame. Filtration was done under nitrogen gas pressure (0.3 bar overpressure). Samples were filtered for a maximum of 2 hours and checked regularly for leaks. For each filter, filtered water was collected into a waste container for subsequent quantification of the amount of seawater that passed the filter. Right after starting the filtration, a subsample of each filtrate was collected in 60 ml acid cleaned LDPE sampling bottles for analysis of dissolved metals in this fraction. After filtration, excess seawater on top of the filters was removed by gentle air pressure. In the clean laboratory, under the fume hood, the filters

were removed from the filter holders and were folded in half, placed in a clean Eppendorf tube and stored frozen (-20°C) until analysis. Particulate metals analysis will be subjected to acid digestion at NIOZ and elemental composition will be quantified using the Element 2 HR-ICP-MS.

Oxygen isotopes ($\delta^{18}O$) were sampled in 2 mL glass vials from stations PS140_12 till station PS140_125, in the upper water column in the deep ocean and over the entire water column for the shelf stations. $\delta^{18}O$ will be analysed using a stable isotope ratio mass spectrometer at NIOZ. The data will be used to quantify the oceanic freshwater input in the study region from rivers and glacial melt.

For bioassays, unfiltered water was filled in trace metal clean incubation bottles as soon as possible after the sampling system was back in the container. Subsequently, bottles were transported to a temperature controlled (2°C) lab container for further processing. To determine vitamin B12 concentrations, 0.2µm filtered seawater was taken from the same depth as water for bioassays was taken (see chapter 7).

To assess phytoplankton community composition and the functional range of associated bacteria, 1L of seawater was taken at 6 stations (stations 9, 14, 124, 126, 129, 131) for assessment of phytoplankton taxonomic composition (18S rRNA DNA metabarcoding) and analysis of bacterial metagenomics. The samples were taken from the depth with maximum chlorophyll (see table xx) and 500-900ml were filtered in series over a 3µm polycarbonate filter (18S analysis) and then a 0.2µm filter (bacterial metagenomics). Filters were treated with SL1 buffer for preservation of DNA, flash frozen, and kept at -80°C. Sample processing and sequencing will commence on land (see Chapter 8).

Seawater sampling from the regular CTD

The seawater sampling operations with the regular CTD were carried out at 54 stations (Tab. 4.1). At each station, two Niskin bottles were used to sample seawater at each selected water depth and our sampling programme focused of the following topical groups:

Oxygen concentration analyses

Seawater sampling for oxygen concentration measurements was the first sampling carried out with both the regular CTD, as well as with the clean CTD. The oxygen concentrations of water samples from the regular and clean CTD were both measured using Winkler titration to (a) cross-validate the oxygen sensor derived concentrations of the CTD, and (b) to test whether the sampled water depth in these two different systems match. The oxygen concentrations in multicore water were also determined by Winkler titration, while the oxygen levels in both the MUC water and underlying porewater were also measured by optical fiber using Pyroscience sensor spots which were stuck inside the MUC tube at a 2.5 cm resolution. However, due to the limited amount of titration solution onboard the Winkler titration were skipped at certain stations as indicated in Appendix Table 4.1.

Water sampling for REE and uranium isotope analysis

The content in the Niskin bottles was filtered directly at the rosette sampler. Seawater samples of 500 mL (for REE) and 125 mL (for U) were filtered through 0.45 µm capsule filters into acid-cleaned wide-neck bottles. They were acidified to a pH of ~2 with concentrated HCl and stored for further analyses in Heidelberg and Kiel.

Nd isotopic compositions (eNd)

All the seawater from the second bottle (12 litres) was collected for Nd isotopic analyses. Filtered seawater samples were collected in 20 L collapsible canisters, acidified to a pH of ~2 with approximately 8 mL of concentrated HCl, and 0.6 mL $FeCl_3$ solution. Following another 8 to 24 hours of equilibration time, concentrated ammonia solution was added to the samples raising the seawater pH to 8-9 (all reagents used were either distilled or of suprapure quality). The addition of ammonia led to precipitation of Fe from solution, co-precipitating Nd. The precipitates settled at the bottom of each collapsible container, and the supernatant was siphoned off. The collapsible containers could then be acid-cleaned onboard, and reused for another CTD deployment. Sample solutions were first transferred into 1 liter wide-neck bottles, later into 50 mL centrifuge vials and centrifuged onboard to collect the seawater precipitates within the centrifuge vials. All remaining supernatant could then be discarded. In total 392 Nd isotope samples were prepared from CTD sampled depths. Samples will be further processed in the clean laboratory facilities of GEOMAR Helmholtz Centre for Ocean Research Kiel.

A similar approach was taken for bottom seawater sampled from Multicores. Here, overlying water was collected from as many MUC as possible, usually resulting in three to eight liters, subsequently filtered in the chemistry laboratory onboard *Polarstern*, and then treated in a similar manner as the CTD seawater samples above. Overall, 35 MUC water samples were processed during PS140 (see Appendix Tab. 4.3).

Underway and discrete total alkalinity analysis

Semi-continuous measurements of Total Alkalinity (TA) were performed in the surface water along the cruise track. Seawater was drawn from the keel of the ship at a depth of approx. 10.8 m using a membrane pump and fed into the ship's main pump line. A water flow was branched off from this and passed through a cross-flow filter (pore size 0.2 µm; volume approx. 200 ml) to remove particulate matter and air bubbles. The measurement was performed using a CONTROS HydroFIA TA system from 4H-JENA engineering GmbH. At 30-minute intervals, sub-samples were automatically pumped from the continuous water flow and measured via titration in single determination. The system's accuracy was verified at weekly intervals through multiple determinations of a certified reference solution for oceanic CO_2 measurements (procured from Dickson Laboratory, UCSD, La Jolla/CA, USA). In total, approximately 1200 underway surface TA measurements were conducted. Additionally, discrete TA measurements were carried out on all individual bottle samples from the CTD to obtain water column profiles. The measurement of discrete samples will be verified onshore through manual titration. Due to lower sample volumes, alkalinity from sediment pore water samples extracted from the Multicores were measured manually by colorimetric titration onboard. IAPSO Standard Seawater P164 was titrated three times prior to the pore water samples for calibration. HCl was added to the prepared sample-indicator solution to determine the TA of the sample. Manual titrations were performed at 32 Multicorer stations with a depth ranging from 24 to 42 cm. Marine pore water samples were collected in discrete 2 cm steps resulting in a total of 12 to 22 titration measurements per station.

Water sampling for nutrients, DIC concentration, $\delta^{18}O$, DIC $\delta^{13}C$, and DIC $F^{14}C$.

We sampled seawater from a total of 54 CTD stations with the rosette sampler deployments, for the characterization of modern physical ($\delta^{18}O$) and chemical (PO_4, DIC, NO_3, $\delta^{13}C$, and $F^{14}C$) oceanographic parameters. The choice of stations and sampled water depth was made in accordance to the water sampling program for REE and εNd analyses.

Samples for isotope and nutrient analyses were taken according to standard protocols immediately after the CTD rosette was retrieved into the hangar of Polarstern. Clean glass

bottles with screw lids were flushed with seawater from the Niskin bottles, before fully filling the bottles bubble-free in overflow without air reservoir. From each bottle depth sampled we took the following standard series of samples: (1) one 50 mL glass bottle for oxygen isotope analysis, (2) one 250 mL glass bottle for Dissolved Inorganic Carbon (DIC) concentrations, (3) one 25 mL glass bottle for stable carbon isotope analysis of DIC ($\delta^{13}C_{DIC}$), (4) a 12 mL glass bottle for DIC $F^{14}C$ analysis, and (5) one 15 ml PE plastic tube with screw caps for phosphate and nitrate concentrations in the filtered seawater. All samples for DIC measurement were fixed with saturated $HgCl_2$ solution under a fume hood to stop biological activity. All glass bottles with screw caps were sealed airtight after sampling with a heated stearin/beeswax mixture to inhibit gas leakage during long-term storage. Samples were thereafter stored refrigerated in the cold rooms at +4°C (stable isotopes and $F^{14}C$) or deep-frozen at –20°C (nutrients). Because of the shortage of 250 mL glass bottles, DIC concentration samples at Station PS140_67 and from station PS140_125 to PS140_137 were taken in 12 mL vials and poisoned with 50 µL $HgCL_2$. Station PS140_67 and PS140_137 were sampled in higher resolution to obtain isotope end-members of the water column at 22 sampling depth for DIC concentration, DIC $\delta^{13}C$, DIC $F^{14}C$, and $\delta^{18}O$. PS140_67 was located right at the ice-shelf edge covering glacial water outflow over 790 m of water depths. PS140_137 was located north of the polar front in the southern Indian Ocean at a maximum water depth of 3,560 m.

Seawater sampling for methane and nitrous oxide

During transit from Cape Town to Antarctica (Station PS140_01 – PS140_15) and the beginning of the South-North Transit towards Hobart (Station PS140_118 – PS140_123), sampling was focused on the mixed layer, particularly targeting the chlorophyll maximum. During the time in Prydz Bay and the Davis Sea (Station PS140_16 – PS140_116), sampling was conducted at the surface (1 – 5 m) and throughout the water column, with on average sampling from six water depths per station (Appendix Tab. 4.4).

The water samples for CH_4 and N_2O were taken as soon as possible, right after the O_2 sampling to minimize the risk of gas exchange with ambient air. At each sampled depth, triplicate samples for CH_4 and N_2O were obtained, employing 20 ml vials from one Niskin bottle. The vials were rinsed and an air bubble free sampling was ensured. Right after sampling the vials were closed tight with a crimp. To stop microbial processes, 50 µl $HgCl_2$ was injected in each vial via a syringe with gauche needle, with pressure compensation achieved using a second syringe. The samples were shaken and stored in the dark and at room temperature afterwards.

MUC-sediment and sedimentary porewater sampling

Porewater oxygen and pH measurements

Oxygen concentrations and pH were measured by optical fiber in the MUC water and porewaters using PyroScience contactless sensors. These sensors were glued inside a core barrel at a 2.5 cm resolution and repetitively used during the entire cruise. The measurements were performed as soon as possible after the MUC was back on deck, using a PyroScience FireSting®-PRO optical multi-analyte meter. Once the measurements were completed, the sediment was gently removed from the barrel and sieved for macro-fauna. These measurements were generally performed at every station, except when we encountered some technical problems related to the laptop/software towards the beginning of the expedition, and at the end of the cruise when the sensors were too damaged (due to the > 25 deployments) to give reliable results.

Marine sedimentary porewater extraction using rhizomes

In addition, pore water was extracted from a separate core at 13 MUC stations (see Appendix Tabs. 4.3 and 4.8) using rhizomes to generate three 2 mL aliquots for dissolved inorganic carbon (DIC) analysis. Aliquots were preserved by $HgCl_2$ (10µL) poisoning for later analysis for DIC concentration, $\delta^{13}C$, and $F^{14}C$. Samples were sealed with heated stearin/beeswax mixture to inhibit gas leakage during long-term storage and refrigerated at 4°C. At 5 of the MUC sites porewater pH was determined using a pH-meter.

Anoxic sediment sampling and porewater extraction (GEOMAR)

A total of 24 surface sediment MUC stations were sampled for combined bottom water and sediment surface proxy analyses to be carried out at GEOMAR Kiel. These were chosen in combination with CTD stations (see Appendix Tab. 4.3). One sediment core from each MUC deployment was used for these purposes. They were sampled in 2 cm intervals under oxygen-free argon atmosphere in a glove bag, aliquoting a small fraction for measurements of sedimentary physical properties at GEOMAR Kiel, and using the rest for porewater extraction. Per 2-centimeter interval one 50 mL centrifuge vial could be filled. These were centrifuged for 60 to 90 minutes onboard *Polarstern* prior to filtration through a 0.2 µm filter and transfer of porewaters for (a) alkalinity, (b) nutrient and ion chromatography (IC) analyses, and (c) trace metal concentration measurements. Alkalinity was measured onboard, while nutrients/ ICsamples (frozen) and trace elemental aliquots (filtered and acidified with 100 µL HCl) will be analyzed in Kiel.

At 10 stations, one additional MUC was used to test the application of DGT® probes (i.e. active filter surfaces by a commercial manufacturer designed to extract 2+ and 3+ trace metals from porewaters) in sediments. DGT® sediment probes were taken from their packing, washed with deionized water, placed within a multicore and left to collect trace metals from the MUC for at least a total of 72 hours at 4°C. DGT® probes were then removed from the sediments and any attached sediment was washed off with deionized water. The DGT probes were placed in plastic bags for further processing at GEOMAR Kiel. The respective MUC was frozen and returned to the Marine Geology group.

MUC sediment sampling and porewater extraction under argon atmosphere (anoxic), onboard and lander incubations (Radboud University)

For selected stations (Appendix Tab. 4.5), one core was taken for core slicing under anoxic conditions. After multicore retrieval this 1 core was brought directly to a temperature controlled labcontainer (set at 4 °C). Here the core was subsequently brought under an anoxic atmosphere in an argon filled glovebag. Within the glovebag, two 30 ml bottom water samples were taken and closed with a threeway valve. The remaining overlying water was removed with a syringe. Subsequently the sediment was sliced into 50 ml centrifuge tubes according to the following resolution: 0-10 cm every 1 cm; 10-30 cm every 2 cm; below 30 cm until the bottom of the core every 4 cm. After core slicing the samples were centrifuged for 45 minutes at 4,000 rpm at 2°C.

After centrifugation of the samples the 50 ml centrifuge tubes together with the two bottom water samples were brought under an anoxic atmosphere in a second argon filled glovebag for filtration and subsampling of the porewater according to the subsample scheme in Appendix Table 4.6. In the glovebag the porewater was poured into 30 ml syringes with a 0.45 µm nylon filter on top. The first 3 ml of porewater were filtered into a 15 ml centrifuge tube for NH_4^+ determination and to rinse the nylon filter for any NO_x contamination. After that ca. 1 ml was filtered into the NO_x centrifuge tube. Subsequently the rest of the porewater was filtered into the centrifuge tube for NH_4^+ determination. From this tube 0.5 ml was pipetted into 2 ml zn-acetate solution for H_2S as quickly as possible to avoid outgassing of H_2S. Subsamples for H_2S were

only taken at selected stations (Appendix Tab. 4.6). After this was carried out for all porewater samples the porewater in the 15 ml NH_4^+ centrifuge tubes were further subsampled for IC/ alkalinity and ME according to the scheme in Appendix Table 4.6.

After subsampling, samples were stored at either 4 or -20 °C (Appendix Tab. 4.6). The remaining sediment samples in the 50 ml centrifuge tubes were stored in aluminum bags filled with argon at -20 °C. Samples for total alkalinity, determined by titration, were measured within 24 hours of sample collection and the remaining sample (0.5 ml) was stored as 4 °C. Aliquots of porewater for sites presented in Appendix Table 4.5 will be shared with GEOMAR.

Oxic sediment sampling (porosity and DNA)

For selected stations (Appendix Tabs. 4.3 and 4.5), one core was taken for core slicing under oxic conditions. After core retrieval the core was directly brought into a temperature-controlled lab container set at 4 °C. Here the core was sliced withing 3 hours of core retrieval according to the following resolution: 0-10 cm every 1 cm; 10-30 cm every 2 cm; below 30 cm until the bottom of the core every 4 cm. For the first 10 cm subsamples from the middle of the core were taken, to avoid the impact of smearing on the sediment close to the core liner, with a spatula into an Eppendorf tube and were subsequently frozen at -80 °C. The remaining sediment was sliced into a pre-weighted 50 ml centrifuge tube for the determination of porosity and then stored at -20 °C.

Onboard core incubations

Onboard incubations were performed at selected sites (Appendix Tab. 4.5) to determine the rates of nutrient and trace metal release from the sediment and to determine bioirrigation rates in the sediment. After core retrieval one core per station was directly brought into a temperature-controlled room (4 °C). The volume of overlying water was adjusted to 300 ml and a tube connected to an aquarium pump was placed in the overlying water to establish homogeneous conditions and to keep the water oxygenated. Sodium bromide (NaBr) was added to the overlying water to increase the bromide concentrations approximately by 10 times. The cores were incubated for 2 days. Samples of the overlying water were taken at three time points (t=0, t=1 day and t = 2 days) to determine the benthic release of nutrients and trace metals from the sediment. Samples for NO_x and $NH4^+$ were stored at -20°C. Samples that will be measured by ICP-OES and ICP-MS were acidified with 10 µl suprapur HCl per ml of samples and stored at 4 °C. After the two-day incubation the core was sliced into 50 ml centrifuge tubes. The first 10 cm were sliced in 1 cm resolution and from 10 to 18 cm the resolution changed to 2 cm. Subsequently the samples were centrifuged for 15 minutes at 4000 rpm and the porewater was filtered through a 0.45 µm nylon filter into pony vials. The filtered porewater samples were stored at 4 °C.

Sieving for macrobenthos

For selected sites (Appendix Tab. 4.5) 1 core was sieved withing 24 hours of core retrieval. Samples were sieved using a 500 µm mesh size handheld sieve. After sieving samples were collected within a 50 ml centrifuge tube and were fixed with either ca. 4% formaldehyde or 96% ethanol. After sample collection samples were stored at 4 °C.

Benthic lander deployment

In-situ benthic fluxes of nutrients and trace metals were measured on site PS140_19 using a MiniChamber Lander System (Unisense) equipped with a metal-free polycarbonate incubation chamber (30 x 30 x 35 cm; (surface of 0.09 m^2)) and a set of twelve 50 mL plastic syringes controlled by an autosampler and connected to the chamber with plastic tubing. The adjustable

feet of the lander enabled the incubation chamber to sink 7 cm into the sediment, leaving a water volume of ca. 25.2 L in the chamber. The sequence programmed on the MiniChamber Lander was started within minutes before lander deployment. After 45 minutes the stirrer, which is attached to the lid of the chamber started. 1 hour after lander deployment started, the lid of the chamber was closed. The stirrer attached to the lid constantly mixed the water in the chamber to keep the incubated water homogeneous. Each deployment consisted of 6 timepoints (55 minutes apart from each other). For each timepoint two syringes of 30 mL were filled to ensure enough water was collected for all analysis. A small septum in the lid of the chamber ensured replacement of the water that was withdrawn. Upon retrieval the samples were filtered over 0.45 µm nylon filters and subsampled in different vials for various analysis (Appendix Tab. 4.7). During the deployment the benthic lander was likely moved by sea ice after ca. 4 hours.

Preliminary results

REE, uranium and neodymium isotopes in seawater

The REE, uranium and neodymium isotopes will need further processing prior to mass spectrometric measurements at Heidelberg university and GEOMAR Kiel.

Oxygen and salinity

In total Winkler titrations were carried out at 26 stations on the regular and clean CTD water samples, as well as 17 individual assessments on MUC water. Most of the oxygen concentrations resulting from the regular and clean CTD are consistent. The MUC oxygen concentrations were almost always within error of oxygen concentrations of the lowermost CTD sample.

With the exception of oxygen and salinity, for all parameters sampled from the Clean CTD, further processing is needed in the shore-based labs prior to analysis.

Total alkalinity analysis (underway TA analyses)

Approximately 2250 underway measurements of total alkalinity in the surface water were performed along the cruise track. Outliers in the data were removed using a simple filter code. The preliminary data set of total alkalinity measurements is plotted in Figure 4.5. Gaps in the recording are primarily attributed to device malfunction, because of air in the flow-through system. The measured values in the open ocean as well as Prydz Bay correspond to the expected surface values. On the Antarctic shelf, relatively low values were recorded between approximately 80–100°E.

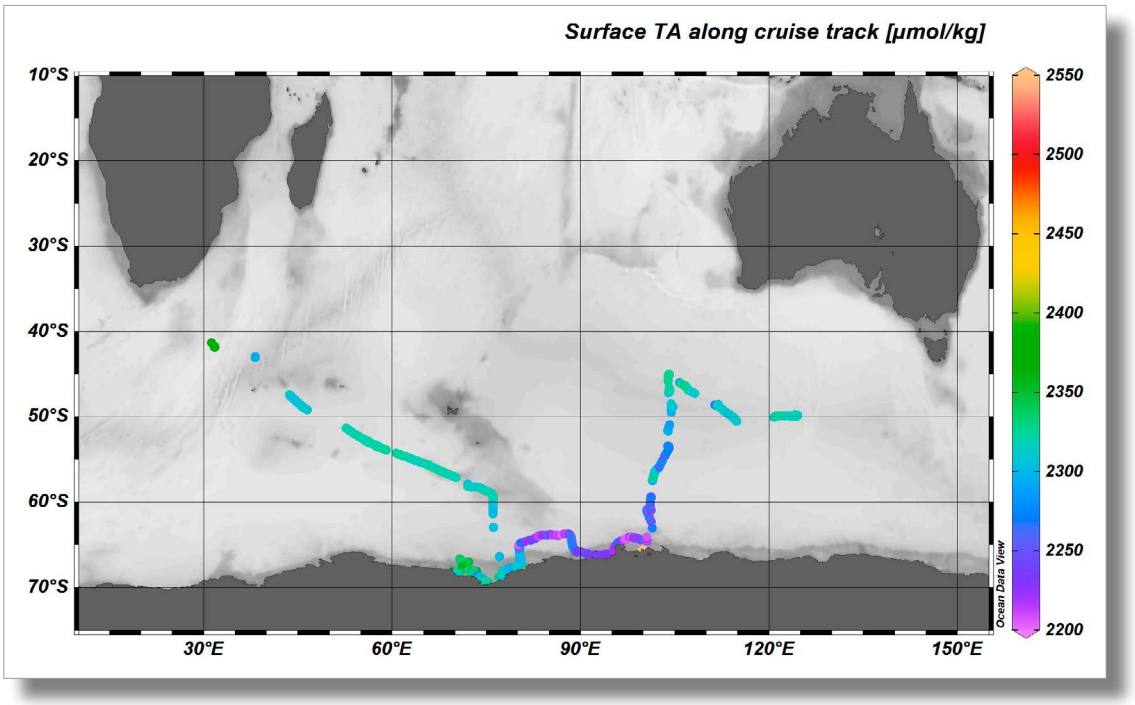

Fig. 4.5: Semi-continuous measurements of total alkalinity in the surface water along the cruise track of PS140.

MUC porewater sampling under anoxic conditions (glove bag)

Marine pore water samples extracted from Multicorer cores of the surface sediment were titrated manually onboard at 41 stations (see Appendix Tabs. 4.3 and 4.5). The results of the manual total alkalinity titration for station PS140_53 and PS140_107 are plotted in Figure 4.6. Most stations show expected total alkalinity values and an increasing TA with depth. Station PS140_75 has exceptionally high TA values up to 16 µmol/kg. Outliers in the data can be attributed to air bubbles in the tube connecting the titration unit to the sample-indicator solution.

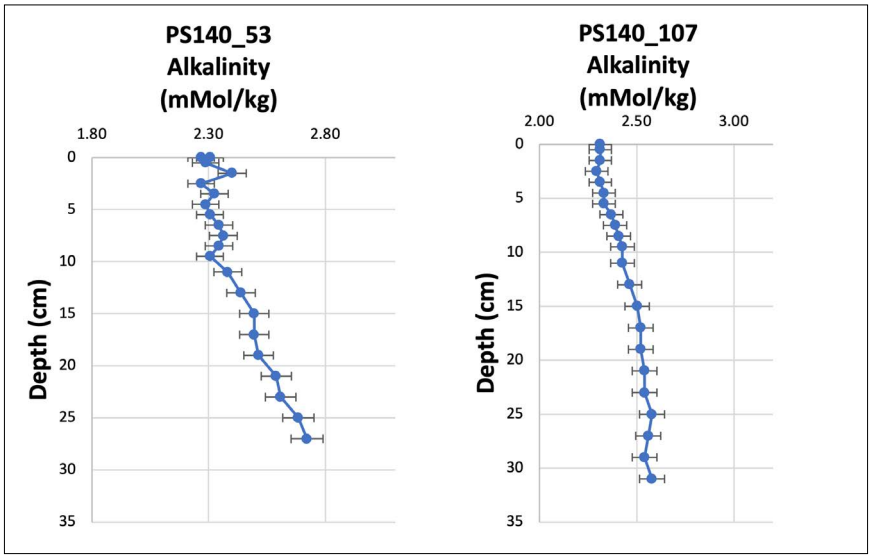

Fig. 4.6: Discrete total alkalinity measurement of marine pore water samples extracted from Multicorer core of the surface sediment at sites PS140_53 (Prydz Bay) and PS140_107 (Dotson Ice shelf). Error bars indicate uncertainties based on triplicate titration of a standard.

Porewater oxygen and pH measurements

The use of the contactless sensors for the measurements of oxygen concentrations and pH worked efficiently, and provided immediate data at a high resolution. The measured oxygen concentrations ranged between 0 to 11 mg/L (Fig. 4.7). The measured pH exhibited moderate variations, ranging from 7.4 to 8.4 (Fig. 4.8). At some stations, the porewater (extracted with rhizomes) pH was also measured using a WTW 3310 pH-meter with an InLab Micro electrode (Mettler Toledo), from another core of the same multi-core deployment. The pH values obtained using the sensors partially deviate from the values of the pH-meter by up to 0.3 pH units (Fig. 4.8), but we consider the observed offset reasonable considering the small pH-variations observed, and the fact that the measurements were not performed on the exact same sediment core.

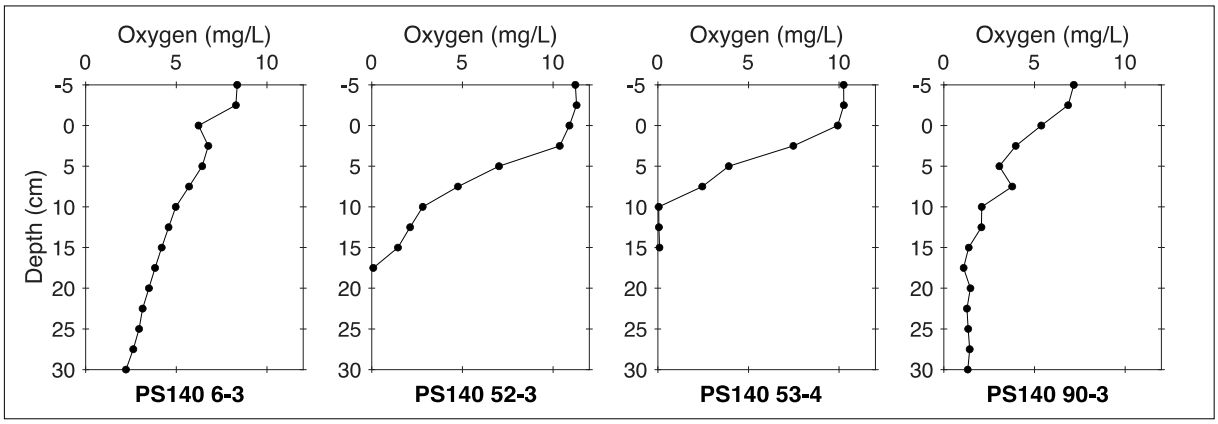

Fig. 4.7: Sediment porewater oxygen concentrations obtained using PyroScience contactless oxygen sensors.

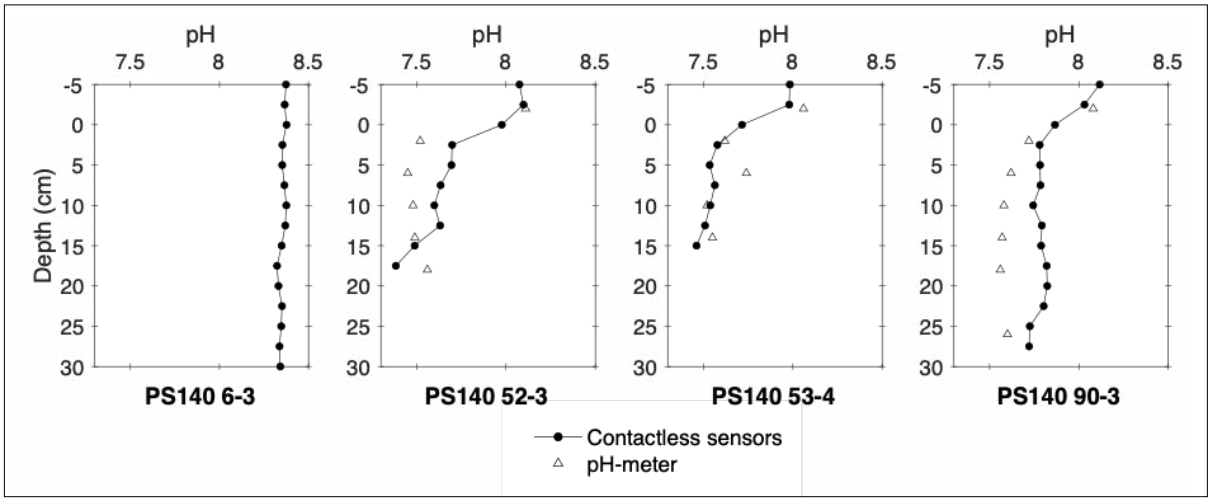

Fig. 4.8: Sediment porewater pH values obtained using PyroScience contactless pH sensors (circles) and pH-meter (triangles)

Data management

Environmental data will be archived, published and disseminated according to international standards by the World Data Center PANGAEA Data Publisher for Earth & Environmental Science (https://www.pangaea.de) within two years after the end of the expedition at the latest. By default, the CC-BY license will be applied.

This work was partly supported by the Deutsche Forschungsgemeinschaft (DFG) in the framework of the priority program SPP 1158 “Antarctic Research with comparative investigations in Arctic ice areas” by the grant GU 1017/9-1 as well as LI 1815/14-1 and contributes to the Helmholtz Research Programme “Changing Earth – Sustaining our Future” Topic 2, Subtopics 2.1, 2.2, 2.3 and 2.4.

Molecular data (DNA and RNA data) will be archived, published and disseminated within one of the repositories of the International Nucleotide Sequence Data Collaboration (INSDC, www.insdc.org) comprising of EMBL-EBI/ENA, GenBank and DDBJ).

Any other data will be submitted to an appropriate long-term archive that provides unique and stable identifiers for the datasets and allows open online access to the data.

In all publications based on this expedition, the corresponding **AWI Grant No.** shown below will be cited:

Research Focus	AWI Grant Number	Lead PI
Seawater isotopes, porewater and nutrients	AWI_PS140_01	Marcus Gutjahr
Transition metals in seawater	AWI_PS140_02	Rob Middag
Bio Trace	AWI_PS140_10	Caroline Slomp / Wytze Lenstra

Besides quoting the AWI grant number the following publication will be cited:

Alfred-Wegener-Institut Helmholtz-Zentrum für Polar- und Meeresforschung (2017) Polar Research and Supply Vessel POLARSTERN Operated by the Alfred-Wegener-Institute. Journal of large-scale research facilities, 3, A119. http://dx.doi.org/10.17815/jlsrf-3-163.

Acknowledgements

We would like to thank the German Research Foundation (DFG) for funding of the trace metal clean seawater sampling for Pb isotopes within the scope of the DFG priority programme 1158 ”Antarctic Research” (Grant Numbers GU 1017/9-1 and LI 1815/14-1). We are grateful also to Yvonne Schulze Tenberge (AWI) for the production of all bathymetric figures included in Chapter 4.

References

Abbott AN, Haley BA, McManus J (2015) Bottoms up: Sedimentary control of the deep North Pacific Ocean’s εNd signature. Geology 43:1035–1035. https://doi.org/10.1130/G37114.1

Andersen MB, Stirling CH, Porcelli D, Halliday AN, Andersson PS, Baskaran M (2007) The tracing of riverine U in Arctic seawater with very precise $^{234}U/^{238}U$ measurements. Earth Planet Sci Lett 259:171–185. https://doi.org/10.1016/j.epsl.2007.04.051

Bakker DCE, Bange HW, Gruber N, Johannessen T, Upstill-Goddard RC, Borges AV, Delille B, Löscher CR, Naqvi SWA, Omar AM, Santana-Casiano JM (2014) Air-sea interactions of natural long-lived greenhouse gases (CO_2, N_2O, CH_4) in a changing climate, in Liss P.S., Johnson M.T. eds., Ocean-Atmosphere Interactions of Gases and Particles. Heidelberg: Springer: 113–169. https://doi.org/10.1007/978-3-642-25643-1_3

Bertinetti S, Ardini F, Vecchio MA, Caiazzo L, Grotti M (2020) Isotopic analysis of snow from Dome C indicates changes in the source of atmospheric lead over the last fifty years in East Antarctica. Chemosphere 255:126858. https://doi.org/10.1016/j.chemosphere.2020.126858

Bollhöfer A, Rosman, KJR (2000) Isotopic source signatures for atmospheric lead: The Southern Hemisphere. Geochim Cosmochim Acta 64:3251-3262. https://doi.org/10.1016/S0016-7037(00)00436-1

Bollhöfer A, Rosman KJR, (2001) Isotopic source signatures for atmospheric lead: The Northern Hemisphere. Geochimi Cosmochim Acta 65:1727–1740. https://doi.org/10.1016/S0016-7037(00)00630-X

Boning CW, Dispert A, Visbeck M, Rintoul SR, Schwarzkopf FU (2008) The response of the Antarctic Circumpolar Current to recent climate change. Nat Geosci 1:864–869. https://doi.org/10.1038/ngeo362

Border EC (2020) Variability of $\delta^{234}U$ in the Mediterranean Sea, Amazon Estuary, and Atlantic Ocean, Faculty of Physics and Astronomy. University Heidelberg, Heidelberg, p. 124. Available from: https://d-nb.info/1215758243/34

Bourdon B, Henderson GM, Lundstrom, CC, Turner S (2003) Uranium-series Geochemistry. De Gruyter, Berlin, 125. https://doi.org/10.1515/9781501509308

Boye M, Wake BD, Garcia PL, Bown J, Baker AR, Achterberg EP (2012) Distributions of dissolved trace metals (Cd, Cu, Mn, Pb, Ag) in the southeastern Atlantic and the Southern Ocean. Biogeosciences 9:3231–3246. https://doi.org/10.5194/bg-9-3231-2012

Brovkin V, Ganopolski A, Archier D, Munhoven G (2012) Glacial CO_2 cycle as a succession of key physical and biogeochemical processes. Clim Past 8:251–264. https://doi.org/10.5194/cp-8-251-2012

Browning TJ, Achterberg EP, Engel A, Mawji E (2021) Manganese co-limitation of phytoplankton growth and major nutrient drawdown in the Southern Ocean. Nat Commun 12:1–9. https://doi.org/10.1038/s41467-021-21122-6

Caldeira K, Duffy PB (2000) The role of the Southern Ocean in uptake and storage of Anthropogenic carbon dioxide. Science 287(5453):620–622. https://doi.org/10.1126/science.287.5453.620

Clarke A, Harris, CM (2003) Polar marine ecosystems: major threats and future change. Environ Conserv 30:1–25. https://doi.org/10.1017/S0376892903000018

Conway, T.M., A.D. Rosenberg, J.F. Adkins, S.G. John (2013) A new method for precise determination of iron, zinc and cadmium stable isotope ratios in seawater by double-spike mass spectrometry, Analytica Chimica Acta, Volume 793, 44-52, https://doi.org/10.1016/j.aca.2013.07.025.

De Baar HJW, Timmermans KR, Laan P, De Porto HH, Ober S, Blom JJ, Bakker MC, Schilling J, Sarthou G, Smit MG, Klunder M (2008) Titan: A new facility for ultraclean sampling of trace elements and isotopes in the deep oceans in the international Geotraces program. Mar Chem 111:4–21. https://doi.org/10.1016/j.marchem.2007.07.009

Du J, Haley BA, Mix AC, Abbott AN, McManus J, Vance D (2022) Reactive-transport modelling of neodymium and its radiogenic isotope in deep-sea sediments: The roles of authigenesis, marine silicate weathering and reverse weathering. Earth Planet Sci Lett 596:117792. https://doi.org/10.1016/j.epsl.2022.117792

Duce RA, Liss PS, Merrill JT, Atlas EL, Buat-Menard P, Hicks BB, Miller JM, Prospero JM, Arimoto R, Church TM, Ellis W, Galloway JN, Hansen L, Jickells TD, Knap AH, Reinhardt KH, Schneider B, Soudine A, Tokos JJ, Tsunogai S, Wollast R, Zhou M (1991) The atmospheric input of trace species to the world ocean. Glob Biogeochem Cycle 5:193–259. https://doi.org/10.1029/91GB01778

Dumoulin J-P, Rabouille C, Pourtout S, Bombled B, Lansard B, Caffy I, Hain S, Perron M, Sieudat M, Thellier B, Delqué-Količ Moreau C, Beck L (2022) Identification in pore waters of recycled sediment organic matter using the dual isotopic composition of carbon ($\delta^{13}C$ and $\Delta^{14}C$): New data from the continental shelf influenced by the Rhône River. Radiocarbon 64(6):1617–1627. https://doi.org/10.1017/RDC.2022.71

Echegoyen Y, Boyle EA, Lee JM, Gamo T, Obata H, Norisuye K (2014) Recent distribution of lead in the Indian Ocean reflects the impact of regional emissions. Proc Natl Acad Sci USA 111:15328–15331. https://doi.org/10.1073/pnas.1417370111

Finkel ZV, Beardall J, Flynn KJ, Quigg A, Rees TAV, Raven JA (2010) Phytoplankton in a changing world: cell size and elemental stoichiometry. J Plankton Res 32:119–137. https://doi.org/10.1093/plankt/fbp098

Flament P, Bertho ML, Deboudt K, Veron A, Puskaric E (2002) European isotopic signatures for lead in atmospheric aerosols: a source apportionment based upon Pb-206 /Pb-207 ratios. Sci Total Environ 296:35–57. https://doi.org/10.1016/S0048-9697(02)00021-9

Hader DP, Banaszak AT, Villafane VE, Narvarte MA, Gonzalez RA, Helbling, EW (2020) Anthropogenic pollution of aquatic ecosystems: Emerging problems with global implications. Sci Total Environ 713. https://doi.org/10.1016/j.scitotenv.2020.136586

Han C, Kim S, Lee AH, Han Y, Lee S, Chang C, Hong S, Jung H, Hong SB, Lee J, Hur SD (2022) Variations in lead isotopes in Antarctic snow from northern Victoria Land during 2012-2015. Environ Res Commun 4. https://doi.org/10.1088/2515-7620/ac6cd1

Henning W, Bell WA, Billquist PJ, Glagola BG, Kutschera W, Liu Z, Lucas HF, Paul M, Rehm KE, Yntema JL (1987) Calcium-41 Concentration in terrestrial materials: prospects for dating of pleistocene samples. Science 236:725–727. https://doi.org//10.1126/science.236.4802.725

Henderson GM, Maier-Reimer E (2002) Advection and removal of ^{210}Pb and stable Pb isotopes in the oceans: a general circulation model study. Geochim Cosmochim Acta 66:257–272. https://doi.org/10.1016/S0016-7037(01)00779-7

Herraiz-Borreguero L, Garabato I (2022) Poleward shift of Circumpolar Deep Water threatens the East Antarctic Ice Sheet. Nat Clim Change 12, 728-734. https://doi.org/10.1038/s41558-022-01424-3

Homoky WB, Weber T, Berelson WM, Conway TM, Henderson GM, van Hulten M, Jeandel C, Severmann S, Tagliabue A (2016) Quantifying trace element and isotope fluxes at the ocean–sediment boundary: a review. Philos Trans R Soc A 374(2081):20160246. https://doi.org/10.1098/rsta.2016.0246

Huang H, Gutjahr M, Eisenhauer A, Kuhn G (2020) No detectable Weddell Sea Antarctic Bottom Water export during the Last and Penultimate Glacial Maximum. Nat Commun 11:424. https://doi.org/10.1038/s41467-020-14302-3

Huang, H, Gutjahr M, Kuhn G, Hathorne EC, Eisenhauer A (2021) Efficient extraction of past seawater Pb and Nd isotope signatures from Southern Ocean sediments. Geochem Geophys Geosyst 22: e2020GC009287. https://doi.org/10.1029/2020GC009287

IPCC (2021) Climate Change 2021: The Physical Science Basis. Contribution of Working Group I to the Sixth Assessment Report of the Intergovernmental Panel on Climate Change. Cambridge, UK and New York, NY, USA: Cambridge University Press. https://dx.doi.org/10.1017/9781009157896

Kim YS, Orsi AH (2014) On the Variability of Antarctic Circumpolar Current Fronts Inferred from 1992-2011 Altimetry. J Phys Oceanogr 44:3054–3071. https://doi.org/10.1175/JPO-D-13-0217.1

Kipp MA, Li HY, Ellwood MJ, John SG, Middag R, Adkins JF, Tissot FLH (2022) U-238, U-235 and U-234 in seawater and deep-sea corals: A high-precision reappraisal. Geochim Cosmochim Ac 336, 231-248. https://doi.org/10.1016/j.gca.2022.09.018

Ku T-L, Knauss KG, Mathieu GG (1977) Uranium in open ocean: concentration and isotopic composition. Deep Sea Res 24:1005–1017. https://doi.org/10.1016/0146-6291(77)90571-9

Lam PJ, Bishop JKB (2008) The continental margin is a key source of iron to the HNLC North Pacific Ocean. Geophys Res Lett 35. https://doi.org/10.1029/2008GL033294

Landschützer P, Gruber N, Haumann FA, Rödenbeck C, Bakker DCE, van Heuven S, Hoppema M, Metzl N, Sweeney C, Takahashi T, Tilbrook B, Wanninkhof R (2015) The reinvigoration of the Southern Ocean carbon sink. Science *349*(6253):1221–1224. https://doi.org/10.1126/science.aab2620

Lee J-ML, Boyle EA, Gamob T, Obata H, Norisuye K, Echegoyen Y (2015) Impact of anthropogenic Pb and ocean circulation on the recent distribution of Pb isotopes in the Indian Ocean. Geochim Cosmochim Acta 170:126–144. https://doi.org/10.1016/j.gca.2015.08.013

Lenstra WK, Hermans M, Séguret MJM, Witbaard R, Behrends T, Dijkstra N, van Helmond NAGM, Kraal P, Laan P, Rijkenberg MJA, Severmann S, Teacă A, Slomp CP (2019) The shelf-to-basin iron shuttle in the Black Sea revisited. Chem.Geol 511:314–341. https://doi.org/10.1016/j.epsl.2014.04.030

Lenstra WK, van Helmond NAGM, Żygadłowska OM, van Zummeren R, Witbaard R, Slomp CP (2022) Sediments as a Source of Iron, Manganese, Cobalt and Nickel to Continental Shelf Waters (Louisiana, Gulf of Mexico). Front Mar Sci 9:811953. https://doi.org/10.3389/fmars.2022.811953

MacGilchrist GA, Naveira Garabato AV, Brown PJ, Jullion L, Bacon S, Bakker DCE, Hoppema M, Meredith MP, Torres-Valdés S (2019) Reframing the carbon cycle of the subpolar Southern Ocean. Sci Adv eaav6410. https://doi.org/10.1126/sciadv.aav6410

Mahowald NM, Hamilton DS, Mackey KRM, Moore JK, Baker AR, Scanza RA, Zhang Y (2018) Aerosol trace metal leaching and impacts on marine microorganisms. Nat Commun 9. https://doi.org/10.1038/s41467-018-04970-7

Martin WR, McNichol AP, McCorkle DC (2000) The radiocarbon age of calcite dissolving at the sea floor: Estimates from pore water data. Geochim Cosmochim Acta 64(8):1391–1404. https://doi.org/10.1016/S0016-7037(99)00424-X

Meijers AJS, Klocker A, Bindoff NL, Williams GD, Marsland SJ (2010). The circulation and water masses of the Antarctic shelf and continental slope between 30 and 80°E. Deep Sea Res Part II Top Stud Oceanogr 57:723-737. https://doi.org/10.1016/j.dsr2.2009.04.019

Middag R, Séférian R, Conway TM, John SG, Bruland KW, de Baar HJW (2015) Intercomparison of dissolved trace elements at the Bermuda Atlantic Time Series station. Mar Chem 177, Part 3, 476–489. https://doi.org/10.1016/j.marchem.2015.06.014

Middag R, Zitoun R, Conway TM (2023) Trace Metals, in: Blasco, J., Tovar-Sanchez, A. (Eds.), Marine Analytical Chemistry. Springer, Cham, Switzerland. https://dx.doi.org/10.1007/978-3-031-14486-8_3

Moore C M, Mills MM, Arrigo KR, Berman-Frank I, Bopp L, Boyd PW, Galbraith ED, Geider RJ, Guieu C, Jaccard SL, Jickells TD, Roche JL, Lenton TM, Mahowald NM, Marañón E, Marinov I, Moore JK, Nakatsuka T, Oschlies A, Saito M, Thingstad TF, Tsuda A, Ulloa O (2013) Processes and patterns of oceanic nutrient limitation. Nat Geosci 6(9):701–710. https://doi.org/10.1038/ngeo1765

Noble AE, Echegoyen-Sanz Y, Boyle EA, Ohnemus DC, Lam PJ, Kayser R, Reuer M, Wu JF, Smethie W (2015) Dynamic variability of dissolved Pb and Pb isotope composition from the US North Atlantic GEOTRACES transect. Deep Sea Res Part II Top Stud Oceanogr 116:208–225. https://doi.org/10.1016/j.dsr2.2014.11.011

Ohnemus Daniel C, Auro Maureen E, Sherrell Robert M, Lagerström Maria, Morton Peter L, Twining Benjamin S, Rauschenberg Sara, Lam Phoebe J, (2014), Laboratory intercomparison of marine particulate digestions including Piranha: a novel chemical method for dissolution of polyethersulfone filters, Limnology and Oceanography: Methods, 12. https://doi.org/10.4319/lom.2014.12.530

Pöppelmeier F, Gutjahr M, Blaser P, Oppo DW, Jaccard SL, Regelous M, Huang KF, Süfke F, Lippold J (2020) Water mass gradients of the mid-depth Southwest Atlantic during the past 25,000 years. Earth Planet Sci Lett 531:115963. https://doi.org/10.1016/j.epsl.2019.115963

Raiswell R, Hawkings J, Elsenousy A, Death R, Tranter M, Wadham J (2018) Iron in Glacial Systems: Speciation, Reactivity, Freezing Behavior, and Alteration During Transport. Front Earth Sci 6. https://doi.org/10.3389/feart.2018.00222

Ravishankara AR, Daniel JS, Portmann RW (2009) Nitrous oxide (N_2O): The dominant ozone-depleting substance emitted in the 21st century. Science 326:123–125. https://doi.org/10.1126/science.1176985

Ribeiro N, Herraiz-Borreguero L, Rintoul SR, McMahon CR, Hindell M, Harcourt R & Williams G (2021). Warm modified Circumpolar Deep Water intrusions drive ice shelf melt and inhibit Dense Shelf Water formation in Vincennes Bay, East Antarctica. Journal of Geophysical Research: Oceans, 126, e2020JC016998. https://doi.org/10.1029/2020JC016998

Rijkenberg MJA, de Baar HJW, Bakker K, Gerringa LJA, Keijzer E, Laan M, Laan P, Middag R, Ober S, van Ooijen J, Ossebaar S, van Weerlee EM, Smit MG (2015) "PRISTINE", a new high volume sampler for ultraclean sampling of trace metals and isotopes. Mar Chem 177, Part 3:501–509. https://doi.org/10.1016/j.marchem.2015.07.001

Ruben, M., Hefter, J., Schubotz, F. et al. (2023) Fossil organic carbon utilization in marine Arctic fjord sediments by subsurface micro-organisms. Nat. Geosci. 16:625–630. https://doi.org/10.1038/s41561-023-01198-z

Sarin MM, Rengarajan R, Somayajulu BLK (1994) Natural radionuclides in the Arabian Sea and Bay of Beng–l - distribution and evaluation of particle scavenging processes. Proc Indian Acad Sci Earth Panet Sci 103:211–235. https://doi.org/10.1007/BF02839537

Schaule BK, Patterson CC (1981) Lead concentrations in the northeast Pacif–c - evidence for global anthropogenic perturbations. Earth Planet Sci Lett 54:97–116. https://doi.org/10.1016/0012-821X(81)90072-8

Schlosser C, Karstensen J, Woodward EMS (2019) Distribution of dissolved and leachable particulate Pb in the water column along the GEOTRACES section GA10 in the South Atlantic. Deep Sea Res Part I Oceanogr Res Pap 148:132–142. https://doi.org/10.1016/j.dsr.2019.05.001

Schoffman H, Lis H, Shaked Y, Keren N (2016) Iron–Nutrient Interactions within Phytoplankton. Front Plant Sci 7, 1223. https://doi.org/10.3389/fpls.2016.01223

Seyitmuhammedov K, Stirling CH, Reid MR, van Hale R, Laan P, Arrigo KR, van Dijken G, Alderkamp A-C, Middag R (2021) The distribution of Fe across the shelf of the Western Antarctic Peninsula at the start of the phytoplankton growing season. Mar Chem 104066. https://doi.org/10.1016/j.marchem.2021.104066

Sivan O, Lazar B (2002) ^{14}C excess in deep-sea sediments porewater driven by diffusi–n - Southeast Mediterranean. Limn Oceanogr 47(2):565–570. https://doi.org/10.4319/lo.2002.47.2.0565

Shi X, Wei L, Hong Q, Liu L, Wang Y, Shi X, Ye Y, Cai P (2019) Large benthic fluxes of dissolved iron in China coastal seas revealed by $^{224}Ra/^{228}Th$ disequilibria. Geochim Cosmochim Acta 260:49–61. https://doi.org/10.1016/j.gca.2019.06.026

Solodoch A, Stewart AL, Hogg AM, Morrison AK, Kiss AE, Thompson AF, Purkey SG, Cimoli L (2022. How Does Antarctic Bottom Water Cross the Southern Ocean? Geophys Res Lett 49. https://doi.org/10.1029/2021GL097211

Tagliabue A, Bopp L, Aumont O (2009) Evaluating the importance of atmospheric and sedimentary iron sources to Southern Ocean biogeochemistry. Geophys Res Lett 36, 1–5.

Tagliabue A, Aumont O, DeAth R, Dunne JP, Dutkiewicz S, Galbraith E, Misumi K, Moore JK, Ridgwell A, Sherman E, Stock C, Vichi M, Völker C, Yool A (2016) How well do global ocean biogeochemistry models simulate dissolved iron distributions? Global Biogeochem Cycles 30, 149-174. https://doi.org/10.1029/2009GL038914

van Manen M, Aoki S, Brussaard CPD, Conway TM, Eich C, Gerringa LJA, Jung J, Kim T-W, Lee S, Lee Y, Reichart G-J, Tian H-A, Wille F, Middag R (2022) The role of the Dotson Ice Shelf and Circumpolar Deep Water as driver and source of dissolved and particulate iron and manganese in the Amundsen Sea polynya, Southern Ocean. Mar Chem 246:104161. https://doi.org/10.1016/j.marchem.2022.104161

van Wijk EM, Rintoul SR, Wallace LO, Ribeiro N & Herraiz-Borreguero L (2022). Vulnerability of Denman Glacier to ocean heat flux revealed by profiling float observations. Geophysical Research Letters 49: e2022GL100460. https://doi.org/10.1029/2022GL100460

WMO (World Meteorological Organization) (2018) Scientific assessment of ozone depletion: 2018. Global Ozone Research and Monitoring Project – Report No. 58, 588 Geneva, Switzerland. http://ozone.unep.org/science/assessment/sap

Xia TY, Sun WW, Ebser S, et al. Atom-trap trace analysis of $^{41}Ca/Ca$ down to the 10^{-17} level. Nat. Phys. 19:904–908 (2023). https://doi.org/10.1038/s41567-023-01969-w

Ye W, Arévalo-Martínez DL, Li Y, Wen J, He H, Zhang J, Liu J, Wu M, Zhan L (2023) Significant methane undersaturation during austral summer in the Ross Sea (Southern Ocean). Limnol Oceanogr Lett 8(2):305–312. https://doi.org/10.1002/lol2.10315

5. MARINE GEOLOGY AND PALEOCEANOGRAPHY

Oliver Esper[1], Lester Lembke-Jene[1], Eleni Anagnostou[2], Marcello Arevalo Gonzalez[3], Nazanin Asadi[4], Tarik Bozkuyu[1,4], Johanna Brehmer-Moltmann[1,4], Katrin Ederer[1], Götz Hoeppe[5], Alina Ivanova[1,4], Norbert Lensch[1], Niklas Kubik[1], Denise Otto[1,4], Manuel Ruben[1], Valea Schumacher[1], Vivian Marissa Sinnen[1], Silla Thomsen[1,4], Marcus Gutjahr[2]

not on board: Ralf Tiedemann[1], Frank Lamy[1], Juliane Müller[1], Thomas Frederichs[4], Johann Klages[1]

[1]DE.AWI
[2]DE.GEOMAR
[3]CL.SERV-EXPLORATION
[4]DE.UNI-BREMEN
[5]CA.UNI-WATERLOO

Grant-No. AWI_PS140_03

Objectives and scientific programme

The Antarctic Circumpolar Current (ACC) is the world's largest current system and connects all three major basins of the global ocean (i.e., the Pacific, Atlantic and Indian Ocean), and therefore integrates and responds to climate signals across the globe (e.g. Talley, 2013). Through upwelling and formation of new water masses, the ACC affects the global meridional overturning circulation (MOC) (Marshall and Speer, 2012) and the stability of Antarctica's ice sheets. Atmosphere-ocean-cryosphere interactions play an important role for understanding processes and feedbacks of past and future climate change, with the subantarctic SO providing the major link between Antarctica and the low latitudes. In the SO, these interactions are believed to control sea-ice cover, ice-sheet dynamics, upper ocean stratification, biological nutrient utilization, upwelling rates of deep-water, and to play a key role in explaining the variability in atmospheric CO_2 concentrations. Further major atmospheric forcing via the Southern Westerly Winds (SWW) impact the upwelling of carbon-rich deep-water masses in the SO affecting atmospheric CO_2 (Anderson et al., 2009).

The East Antarctic Ice Sheet (EAIS) holds a potential contribution of 53 m to global sea level, of which currently 19 m form part of grounded continental ice below sea level (Fretwell et al., 2013). Past sea level estimates for the most recent warmer-than-present interglacials strongly suggest that parts of the EAIS are susceptible to enhanced melting under elevated radiative forcing (Wilson et al., 2018). The most important process leading to melting of marine based portions of both the EAIS and WAIS is submarine basal melting (Depoorter et al., 2013). At present the marine portions of the EAIS are largely shielded from basal melting through the presence of the westward flowing Antarctic Slope Current (Williams et al., 2010) forming a thermal buffer zone around most of the EAIS with near freezing temperatures (see also Fig. 2). The presence of this current prevents incursions of warmer Lower Circumpolar Deep Water (LCDW) diverted south from the eastward flowing Antarctic Circumpolar Current (ACC) that currently erodes large portions of the WAIS (Pritchard et al., 2012; Wåhlin et al., 2020).

Past changes in current strength and transport of the ACC are fragmentary reconstructed and only for limited late Pleistocene time intervals. In the Drake Passage (DP), a significant glacial decrease in DP throughflow combined with reduced current velocities has been identified (e.g., Lamy et al. 2015), most likely regulated by variations in the SWW field over the subantarctic zone and changes in Antarctic sea ice extent. In contrast, a 500,000-year record from the Indian sector of the SO suggests that the ACC was weak during warm stages and strong during glacial epochs (Mazaud et al., 2010). The latitudinal positions of the oceanic fronts are not very well constrained in the Indian sector of the Southern Ocean during glacial/interglacial variations or even on millennial to centennial timescales during the last glacial to Holocene transition. This is largely due to the very remote locality of this part of the SO. However, like no other sector in the SO, the Indian sector offers a unique opportunity for reconstructing changes in SO circulation that responded to or have been forced by past variations in EAIS dynamics. This is because of bathymetric highs (shallow water depth), the Kerguelen Plateau and the Southeast Indian Ridge, covering a latitudinal range from 65° to 45°S, which allows for coring of carbonate-rich sediment cores. The application of carbonate-based proxies doubles the library of proxies that can be used to reconstruct climatic and oceanographic changes, e.g. latitudinal changes in the oceanic fronts as well as variations in deep water chemistry and circulation. This possibility will greatly improve the reliability of our reconstructions and statements about the period of the last interglacials (Marine Isotope Stages (MIS) 5, 7, 9, 11), while during glacial periods a northward movement of subantarctic water masses up to <44° S may have occurred (Nürnberg and Groeneveld, 2006). Instead Chase et al. (2003) concluded that a significant northward shift of the fronts in the SW Pacific during the last glacial is not feasible, as in particular the expected enhanced opal accumulation north of the glacial Polar Front (PF) has not been documented. Whether this finding is also valid for the Indian sector of the SO, or whether there was a steepening of hydrographic gradients during the glacial period, can only be clarified by examining the sediment core transects retrieved during PS140. The large majority of studies to date focused on the most extreme climatic transitions, most commonly the last (18-11 ka BP) or penultimate (137-129 ka BP) glacial terminations. The gradual oceanographic process of transitioning from an interglacial into a glacial circulation mode is much less well known, not to mention the detailed processes at work during re-partitioning of atmospheric carbon dioxide into a glacial abyssal ocean reservoir (Sigman et al., 2010).

The deep SO experienced major circulation changes on glacial/interglacial timescales, with significantly reduced overturning dynamics during peak glacial intervals (e.g. Adkins, 2013; Hasenfratz et al., 2019). A recent study presented evidence for cessation of Weddell Sea-sourced AABW export into the Atlantic sector of the SO (Huang et al., 2020) whereas AABW export into the Indian sector of the SO may still have been possible given the bathymetry of the Weddell-Enderby abyssal plane if AABW was indeed formed during extreme glacial climate. While AABW formation is generally assumed to take place in glacial climate, its presence has never been unambiguously proven apart from indirect evidence. The two transects of sediment cores sampled during PS140 allow a much better quantification of the export of AABW into the Indian Ocean and the import of CDW into the Southern Ocean during the last glacial cycles. In this context, geological work has been carried out in the Prydz Bay area, and along the Antarctic coasts of the Cooperation Sea and the Davis Sea to reveal past geological processes in vicinity of the East Antarctic Ice Sheet (EAIS). Particular attention is paid to processes that are related to basal ice shelf melting, including Warm Deep Water (WDW) intrusions into the ice shelf cavities and feedback mechanisms (e.g. freshening, sea-ice cover) that control the formation and extent of Antarctic Bottom Water (AABW).

The overall goal of PS140 was to enhance our understanding of Quaternary processes as well as the orbital to submillenial-scale evolution of ice-ocean-climate interactions during deglacial warming and climate intervals that were warmer than today. Therefore, we probed Subantarctic

and Antarctic marine sediment archives along two latitudinal transects across the fronts of the ACC, one in the western Indian sector and one in the eastern Indian sector of the Southern Ocean. The coring sites for sampling of late Pleistocene sediments were chosen aiming to collect information on changes of the oceanic fronts and prevailing climate in response to ice sheet variability over the last glacial cycles. The palaeoceanographic approaches focus on sediment cores from the SO frontal system between Cape Town, Hobart, and Antarctica. Similar to previous information from other sediment cores of the western Indian sector (e.g., Marion Dufresne expeditions in the 1980´s and 1990´s and *Polarstern* cruises ANT-XI/4 and ANT-XXIII/9) we estimated that cores recovered at the transect locations of PS140 document up to 300-800 kyr. Such material is crucial for addressing a number of current hypotheses regarding the importance of ocean-atmosphere-cryosphere dynamics in affecting global ocean circulation, atmospheric pCO_2, and climate. Pleistocene to Holocene variations in ACC dynamics, near-surface temperatures salinity and nutrient concentrations, are to be determined with a multi-proxy approach. The regional changes in their gradients are intended to decipher fluctuations in heat and salt transfer, and provide additional information on the position of oceanic fronts and the wind field for certain time slices. Their vertical gradients are used to reconstruct the stratification of the upper ocean. These changes in stratification are the basis for understanding ocean-atmosphere gas exchange (CO_2) and for deciphering the subantarctic intermediate and mode water formation. The boron isotopic and B/Ca application will be a powerful tool to gauge the SO carbon budget over the investigated timescales, most importantly with regard to the glacial sequestration of respired atmospheric carbon in the deep SO and subsequent release during glacial terminations (Martinez-Boti et al., 2015; Moy et al., 2019).

An important backbone to validate these hypotheses is the development of high-resolution age models. Precise timeframes are required to allow for comparisons with other existing high-resolution climate proxy records derived from sediment and ice cores. We will apply a variety of stratigraphic methods, including marine oxygen isotope stratigraphy, ^{14}C-dating techniques, $^{230}Th_{xs}$-based chronostratigraphy, cross-correlation of proxy records with other well-dated records (e.g., ice-cores), paleomagnetics and tephrachronology.

ACC strength changes will be reconstructed by sedimentological and geochemical methods (sortable silt, XRF (e.g. Wu et al., 2021; 2023). Sea surface, intermediate and deep-water temperatures will be based on Mg/Ca paleothermometry of planktic and benthic foraminifers (Nürnberg et al., 2000), the organic biomarker-based indices alkenones TEX^L_{86} and RI-OH' (Ho et al., 2014; Lamping et al., 2021; Park et al., 2019) and diatom transfer functions (Esper and Gersonde, 2014a). Sea-ice reconstructions will be based on analyses and intercomparisons of specific biomarker lipids (highly branched isoprenoids) and diatom assemblages (Esper and Gersonde, 2014b). These studies will allow to assess the role of "Warm Deep Water" in ice-shelf melting and the response of the Southern Ocean and sea ice to meltwater-induced freshening. A multi-proxy approach is required to reconstruct and understand the system (Rickli et al., 2014; Borchers et al., 2016; Vorrath et al., 2019). We will reconstruct changes in sea-ice production, biogenic productivity, sediment provenance based on detrital Nd and Pb isotope compositions as well as Rare Earth Element signatures indicative of the provenance of currently derived and ice-transported material as well as past regional changes in overturning circulation. Sedimentary authigenic Pb isotopes will provide insights on past changes in the provenance of water mass. Changes in ocean stratification are the basis for understanding ocean-atmosphere gas exchange (CO_2) (e.g., based on multispecies foraminiferal oxygen, carbon and boron isotopes, B/Ca ratios) and for deciphering the subantarctic intermediate and mode water formation, complimenting the isotope geochemical approaches outlined above.

The calcite shells of the planktic foraminifers dwelling in the upper ocean have a high preservation potential in the sediment and are therefore an important tool for paleo-reconstructions. The elemental and stable isotopic compositions of the foraminiferal calcite shell are important proxies

to reconstruct past ocean temperature or salinity. Pteropods are marine planktic gastropods that are found globally in the ocean, comprising two orders: the Gymnosomata (naked pteropods) and Thecosomata (shelled pteropods), which are separated by their morphology, behaviour and position in the marine food web. Pteropods are an important prey for predators, while also contributing to the downward flux of inorganic and organic carbon through the ballasting effects of their fecal pellets and mucous nets, daily migrations and mass mortality events, burying the shells at the seafloor. Pteropod shells consist of aragonite, making them more susceptible to ocean acidification than other shelled marine plankton such as foraminifers and coccolithophores with calcitic shells. Despite their ecological and biogeochemical importance, essential details about pteropod global biomass distribution are not well resolved. Another gap in knowledge constitutes the trace elemental and stable isotopic composition of pteropods, which only few studies have addressed to date.

Our studies also aim to significantly improve our understanding of past EAIS extent, its flow and retreat patterns, and the related bed processes that controlled ice flow primarily since the last glacial to the Holocene (Klages et al., 2016; 2017). We will integrate and link bathymetric, seismic, marine geological, and modelling competence to map and document temporal changes in grounding line dynamics since the LGM on the Antarctic shelf.

We have addressed our sites under the following research questions:

- **What is the state of AABW formation and export during Pleistocene glacial and extreme interglacial climate under elevated melting?** Given current knowledge, we predict that AABW will be severely reduced and possibly absent both during extreme glacial and interglacial boundary conditions (e.g. Huang et al., 2020).
- **Will a southward moving ACC eventually lead to cessation of AABW formation? Did this happen in the past and what were the consequences?** The ACC was tentatively moving south over the past decades (Chapman et al., 2020) yet results are in parts conflicting. We expect that such latitudinal shifts likewise occurred at glacial-interglacial and shorter centennial to millennial scale time frames.
- **How drastically shifted were SO fronts during glacial and interglacial climate in the Indian sector of the SO?** The absolute position of fronts is very likely to change depending on climate state (Fyfe and Saenko, 2006). However, this will vary spatially also as a function of bathymetry (Sokolov and Rintoul, 2009).
- **Which marine ecosystem responses are likely during AABW weakening due to elevated EAIS melting, lowered bottom-water ventilation and altered nutrient delivery to the SO?** The present-day micro-nutrient inventory of the water column can be set in context with past proxy records. We postulate that AABW weakening will have an effect on the marine ecosystem. However, the degree of which is largely unknown to date.
- **What is the offshore expression of chronological land-based deglacial EAIS retreat constraints?** The retreat of near-shore continental ice will take place during times of climatic warming that also involves palaeocirculation and palaeoproductivity changes. We will aim to link Antarctic shore- and shelf-based, as well as offshore records. How reliably can we use offshore records in older sedimentary sequences to reconstruct glacial processes on land preceding the LGM?
- **What is the distribution of pteropod/foraminifer species and biomass and their geochemical composition in the Indian sector of the Southern Ocean in the upper 500 m of the water column?** We aim to assess of the fractionation of trace elements and stable isotopes between pteropod/foraminiferal shells and the surrounding water masses.

Work at sea

Marine sediment echosounding (PARASOUND P70)

Bathymetric and hydroacoustic surveys were used to identify core locations containing ideally undisturbed sediment sequences, as well as sites with high sediment accumulation. We focused on potential sites that comprise the last 500 ka or less in the upper 20 m of the sediment archive, as well as grounding lines, moraines and scour marks. The survey work was aimed at:

- enable the selection of coring stations based on acoustic patterns and backscatter,
- obtain different pattern of high-resolution acoustic stratigraphy useful for lateral correlation over shorter and longer distances thereby aiding correlation of sediment cores retrieved during the cruise,
- improve information on the sediment distribution in the Indian Ocean sector of the Southern Ocean and near Antarctica in Prydz Bay.

Instruments

Sub-bottom profiles were recorded with the hull-mounted Deep-Sea Sediment Echosounder PARASOUND (Teledyne Reson, Bremen, Germany), system PS3-P70. This system generates two primary, high-frequency acoustic signals with slightly differing frequencies selectable in a range of 18-24 kHz (PLF, PHF). Due to the non-linear acoustic behaviour of water, the so-called “Parametric Effect”, two secondary harmonic frequencies (SLF, SHF) are generated in the water column of which one is the difference (SLF) and the other the sum (SHF), respectively. As a result of the longer wavelength, the secondary low frequency signal (SLF) is able to penetrate the sediment column as deep as for example a 4 kHz signal (up to 200 m depending on sediment conditions), whereas the vertical resolution still corresponds to the primary high frequency signal (PHF), and thus about some decimeters in sediments. The secondary high frequency (SHF) can be used for detection of bubbles in the water column.

The primary signals are emitted in a narrow beam of 4°, but at high power. That has the advantage that the pulse penetrating he sediment is generated within the narrow beam of the primary frequencies, and thereby providing a very high lateral resolution.

The system, however, has its limitations in imaging rough sea floor topographies or submarine ridges with slopes steeper than 4°. Here, the signal energy reflected from the small inclined footprint on the seafloor is scattered from the lateral range of the receiving transducers in the hull of the vessel. As a consequence, only few reflections from the seafloor are recorded, i.e., even fewer from the sub-bottom.

Survey settings

During expedition PS140, a 22.5 kHz setting was used as the Primary High Frequency (PHF), to avoid interferences with the Hydrosweep (Bathymetry) system (see chapter 3). This had to be switched to 19 kHz during the course of the cruise to adapt to more challenging terrain. The Secondary Low Frequency (SLF) was set to 4 kHz. Depending on the properties of the sea-floor surface and sediments our settings enabled an imaging of the sub-bottom down to 150 m, and with a vertical resolution of about 30 cm. The combined signal has a beam width of ~4°. The resulting beam’s footprint on the sea bottom is about 7 % of the water depth.

The system was controlled using the program Hydromap Control. Live data visualisation and data storage was performed with the Parastore software. Every hour, screenshots of the profiles were stored and made directly accessible on a public directory.

Sub-bottom profiling

During expedition PS140, digital data acquisition and storage were switched on after *Polarstern* left the EEZ of South Africa on 30 November 2023 at 00:01h UTC, and was switched off finally on 28 January 2023 at 20:42h UTC, when the ship reached the EEZ of Australia at the end of the expedition. Additionally, the EEZ of South African islands was passed from 4 December, 10:00h UTC until 5 December, 12:11h UTC, during which the Parasound was turned of as well. Data acquisition took place during all times on transit, and while surveying in the main study area to provide information for station planning and sediment coring sites. “Parasound” profiling was carried out in a 24-hour/7-day shift mode, and the data recorded were promptly made available for site selection and cruise planning.

While steaming, the quasi-equidistant transmission mode for signal transmission was used most of the time, occasionally the transmission mode was set to single pulse. The desired time interval between signal transmissions was set between 500 and 2000 ms. During station work, the transmission mode was set to single pulse in order to reduce data volume. The system was operator-controlled during PS140 (watch keeping). Book keeping was carried out including basic PARASOUND system settings, some navigation information, various kinds of remarks. The system depth source was set to PARASOUND PHF, the multibeam echosounder HYSROSWEEP DS2 or manual. Depth measurements in steep slope areas were, however, not always stable and occasional failures occurred. Difficulties were encountered in the beginning with the automatic depth detection, this was transitionally fixed by using the manual system depth mode. Eventually, this problem was resolved by the Teledyne remote access helpline service.

The daily routine included the subsequent processing steps that are meanwhile established as a standardised workflow consisting of (a) acquisition of data in the internal PARASOUND ASD and PS3 formats, (b) conversion of PS3 to standard SGY format, (c) extraction of navigation data and conversion to standard UKOOA format, (d) preparation for storage in Pangaea, and (e) performance of a preliminary processing of data and visualisation with Kingdom software.

Mitigation for marine mammals

The mitigation regulations for profiling operations consisted of visual observations for marine mammals by observers, following the mitigation protocol predefined by Germany’s Federal Environment Agency (Umweltbundesamt – UBA).

In detail, the mitigation actions comprised:

1. Start of sounding only after at least 15 min. marine mammal observer (MMO) watch without sightings of marine mammals.
2. After interruptions of more than 30 min, the Parasound P70 sediment echosounder has to be restarted with reduced pulse rate (“Whale Warning Mode”).
3. When sounding is needed **on station**, continuous MMO watches by two persons has to be performed on the bridge. Sounding has to be stopped whenever marine mammals were sighted in the water closer than 100 m to the ship. Restart only after 15 min without sightings of marine mammals as in 1.
4. Pulse rate and sounding operations have to be reduced appropriate to a scientific necessary level and water depth.
5. During the operation of the sediment echosounder **on stations** closer than 500 m to large icebergs, shelf-ice edges, and coasts, and whales are observed in between the ship and the obstacle, sounding has to be stopped. Sounding can be restarted after 15 min without sightings as in 1.

6. If opportunistic sightings of whales between ship's course and icebergs, shelf-ice edges, and coasts, the ship has to keep a distance of > 500 m.
7. Every exception of following this mitigation regulations will have to be documented in a report.

All actions and reasons concerning switching on and off the system, and events concerning MMO calls are documented in the Appendix Table 5.1 (PS140 Parasound Log). For MMO calls during Parasound sounding ON station, an extra documentation is attached in the Appendix as well, stating the two responsible MMO on duty and actions.

Plankton and Surface Sediment Sampling

The standard plankton and surface sediment sampling program included the operation of the Plankton Net, the Multi-Net, and underway filtration of pumped surface seawater.

Plankton Multi-Net Sampling

During the cruise, plankton was collected vertically using a multiple closing plankton net (Hydrobios Kiel, nominal mouth area of 0,25 m^2) with five nets (55 µm mesh size for calcitic plankton), allowing stratified vertical sampling of five depth intervals (Fig. 5.1).

Fig. 5.1: Deployment and retrieval of Hydrobios Multi-Net during PS140

A total of 28 stations were sampled (Fig. 5.2). For foraminiferal and pteropod analyses one tow was cast at each station between 500 m water depth and the surface. The sampling intervals of the net were chosen according to the water mass distribution at the sampling site and the deep chlorophyll maximum. In addition, at 11 stations a single plankton net with 41µm net mesh size and 10 µm net beaker mesh size has been deployed to collect phytoplankton of the upper 100 m of the water column (Fig. 5.2).

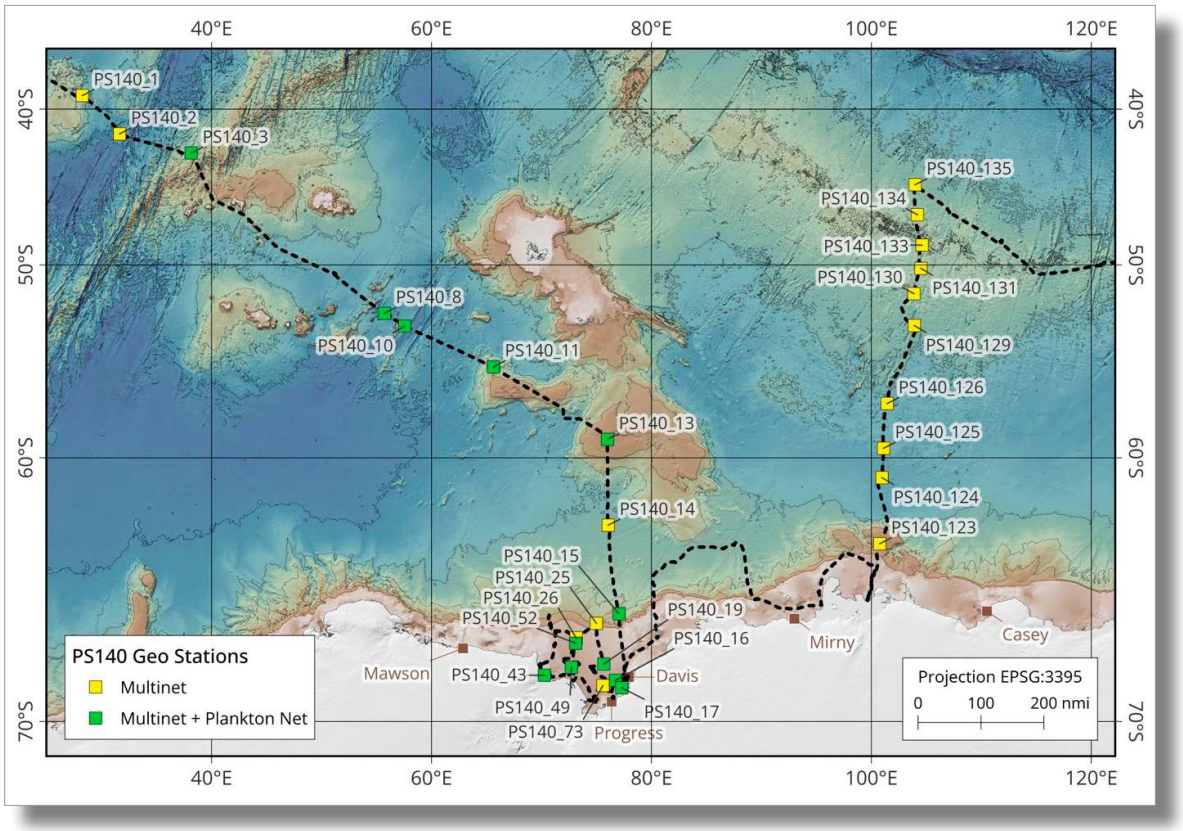

Fig. 5.2: Overview of all sampled multinet and plankton net stations covered during PS140

Slacking was carried out at a speed of 0.5 m/s and hoisting at 0.3 m/s. After each haul the nets were washed with sea water and the net cups were rinsed with filtered sea water. The residue of the net cups containing the plankton >100 µm was fixed with a filtered seawater – ethanol (50:50) mix and stored at 4°C. Calcifying plankton will be sorted and counted from sampling bottles after return to the home laboratory. At all multinet stations, CTD data will be used for fluorescence information in the water column (a measure of the chlorophyll concentration).

Underway membrane pump plankton filtration

Living planktic organisms (e.g., diatoms, coccoliths, silicoflagellates, etc.) were collected in the near-surface water during the cruise along routes of varying filtering length, dependent on the varying phytoplankton concentration (see Appendix Tab. 5.2). The surface water was taken with the ship's membrane pump from 11m water depth and filtered with a cellulose nitrate filter of 0.45 µm filter size. The filter was placed inside a stainless-steel In-Line Filter Holder combined with a flowmeter. Up to three times a day, a specific amount of water has been filtered. Those filters have been air-dried afterward. Parts of the dried filters were used for microscopic inspection on board. For this purpose, a square centimeter of the filter was cut out and embedded on a microscopic slide with NORLAND adhesive No. 61. A total of 41 samples were obtained this way (Fig. 5.3). Inspection was done with a Zeiss Axioplan II microscope at x630 magnification. The rest of the dried filters were wrapped in paper envelopes and were packed in Whirlpack bags for further treatment and analysis.

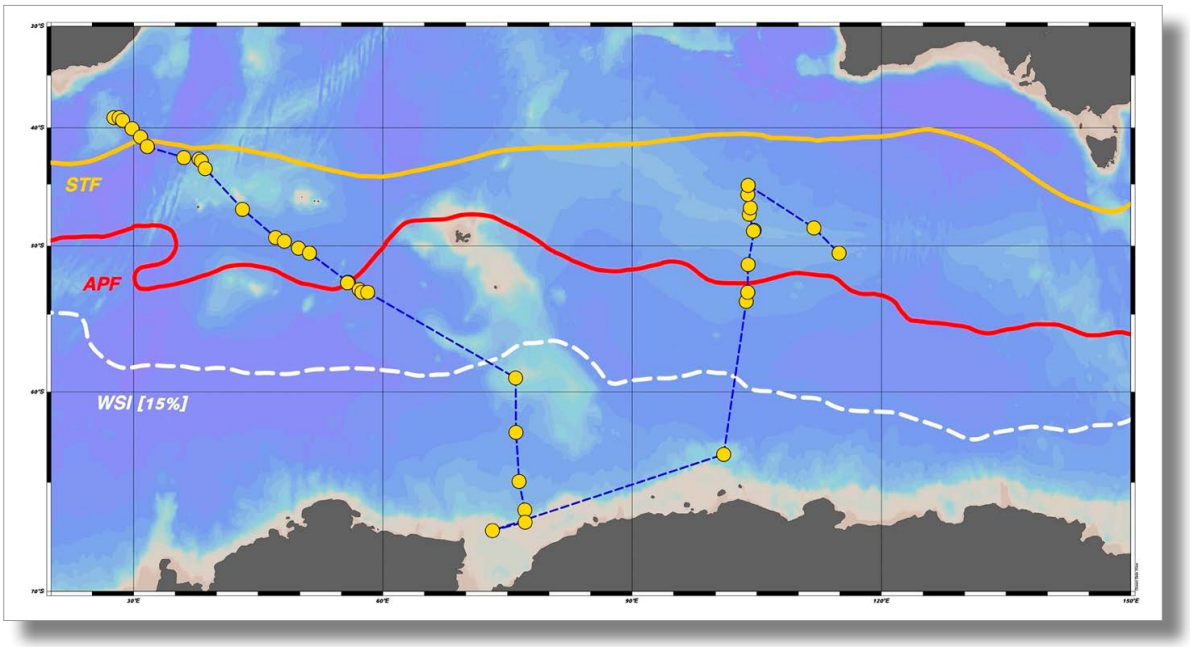

Fig. 5.3: Map of 41 starting points of the filtration route along the cruise track of PS140

Sediment Surface Sampling

Surface and near-surface sediment sampling during PS140 was carried out at 50 stations with a Multicorer (MUC) (Fig. 5.4) or a Giant Box Corer (GBC). The 12-tubes multicorer (MUC67; manufactured by Fa. Wuttke, Henstedt-Ulzburg, Germany), with an inner tube diameter of 6 cm and a length of 60 cm, was deployed at 44 stations and usually recovered undisturbed surface sediments and overlying bottom water. Apart from an initial test run, all MUC but two deployments successfully recovered surface sediments.

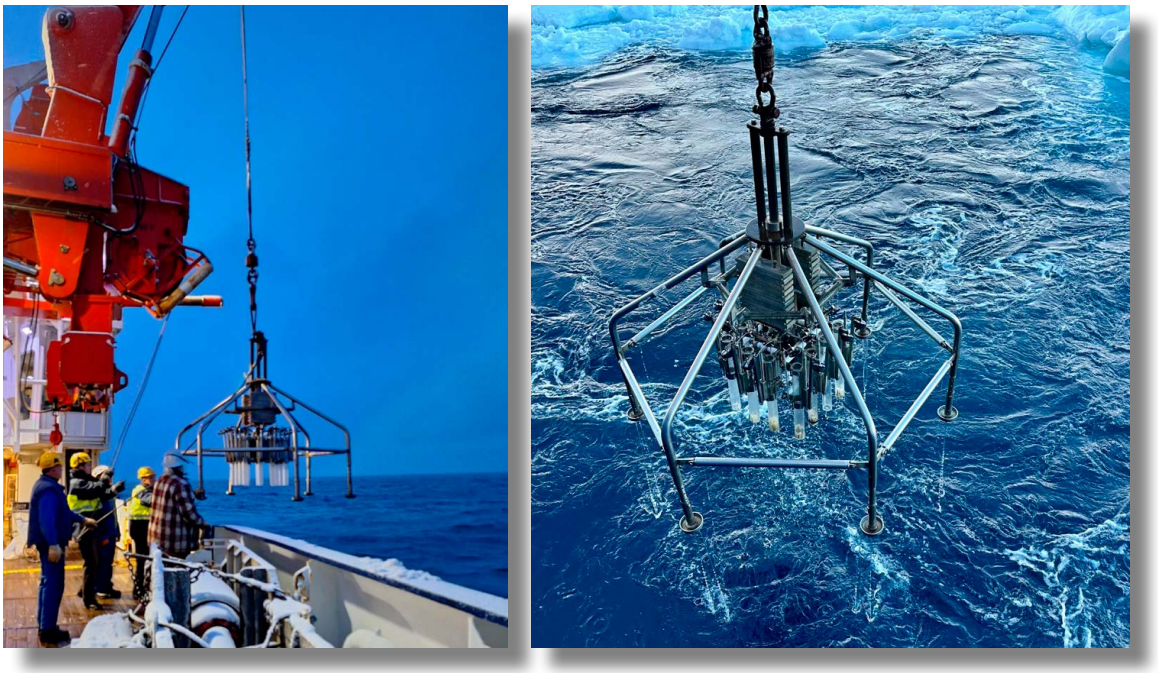

Fig. 5.4: Deployment Multi-Corer (Fa. Wuttke) with 67 mm diameter during PS140 in Prydz Bay with moderate sea-ice conditions.

On average, all 12 tubes recovered intact sediments, with average penetration depths around 30 cm (Fig. 5.5) in the transect areas. On the continental shelf, more MUC deployments failed to recover sediment, due to hard surfaces or substrate problems. Overpenetration of the MUC67 occurred at station PS140_16-3, PS1240_16-4 and PS140-74-3, and was likely related to the occurrence of very soft, biosiliceous sediments. On these stations, only four MUC cores were deep-frozen as entire cores, designated as ARC I – IV.

Fig. 5.5: Examples of photo-documented MUC tubes retrieved at station PS140_14-4 (left) and PS140131-2 (right). Note the evident optical differences in bio-silicous-terrigenou vs. carbonate-dominated sedimentary facies

Besides the “small” MUC with 12 x 63 mm tubes, the “large” MUC with 8 x 100 mm tubes was deployed on several occasions. The “large” MUC was equipped with a camera system to transmit a live video feed via an optical fiber (LWL) to the ship during deployment of the device (further on named as “TV-MUC”). The power supply for the system is provided by a Coax cable with LWL (>600 V). The video has a resolution of 1440i and was recorded with 60 transmissions. On several deployments, the video system failed to transmit a continuous video signal while lowering through the water column, due to insolation failure of the camera connector or problems with the optical fiber. Only two deployments, PS140_26-3 and -5, and PS140_34-1, were successful regarding the video transmission and allowed the digital recording of the MuC release on the sea floor (Fig. 5.6 and 5.7). During the other occasions, however, even after a blackout of the video system, the MUC deployment could retrieve multiple sediment cores by applying known sea floor detection techniques (tension relief recorder). In most cases undisturbed surface sediments and overlying bottom water were recovered. An overview over all sampled MUC stations as well as their recovery can be found in Figure 5.8.

The TV-MUC was lowered with an average speed of 1 m/s to about a few meters above seafloor where it was stopped for a few minutes to observe the sediment surface with the camera system. The lowering to the seafloor continued with a speed of 0.5 m/s until the cable tension monitored bottom contact. The multicorer was left on the seafloor for a few seconds before being pulled out of the sediment with a speed of 0.5 m/s and subsequently heaved with 1 m/s.

Fig. 5.6: TV-MUC deployment at station PS140_26-3, still from video at bottom penetration, at this site krill was abundant and relatively homogenous sedimentary surface facies.

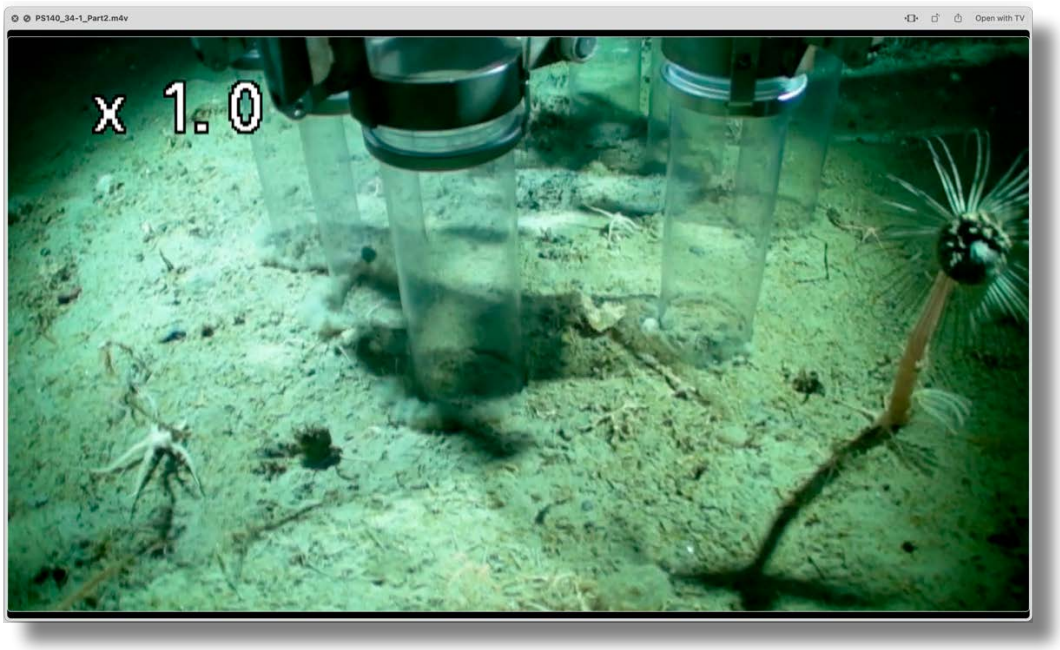

Fig. 5.7: TV-MUC deployment at station PS140_34-1, still from video at bottom penetration, note the relatively abundant benthic macrofauna on this site.

Immediately after recovery of the device, supernatant water was sampled at each station for stable isotopes ($\delta^{13}C$ and $\delta^{18}O$), Nd isotopes (see Chapter 4) and ^{14}C from the two assigned Benthos (BEN I and II) tubes. Stable isotope samples were collected as duplicates in 50 ml and 100 ml glass bottles with screw tops. For radiocarbon analyses, 125 ml of water from the same MUC tube were sampled in pre-combusted glass vials, which were poisoned with $HgCl_2$ and closed gas-tight using screw lids immediately after sampling.

For documentation, all MUC tubes were photographed (e.g., Fig. 5.5). Except the MUC tubes designated as Archive-MUCs, all MUC tubes were sampled immediately after recovery to avoid degradation of organic compounds. All MUC deployments were sampled quantitatively, except for the tubes designated for direct shipboard work by the geochemistry/chemical oceanography group that targeted marine porewater (see Chapter 4). The number of tubes used for marine porewater studies varied between two and six tubes, depending on location, water depth and work area. For multi-disciplinary investigations of the recovered sediments, the remaining multicorer tubes were sampled according to the following scheme:

Tab. 5.1: Allocation and sampling of MUC tubes for different post-cruise investigations.

# Tubes	Working Group	Sampling	Storage
1	Sedimentology (SED)	1 cm slices in Whirlpack bags	4°C
2	Benthos (BEN I+II)	1 cm slices in Kautex bottles (0-6 cm) & Whirlpack bags (6 cm to bottom)	4°C
1	Biomarker BIO	1 cm slices in glass vials covered with Al foil	-20°C
1	Plankton (PLA)	1 cm slices in Whirlpack bags	4°C
1	Micropaleontology (MPAL)	1 cm slices in Whirlpack bags	4°C
1	Porewater sampling WG Wytze (POW)	1 cm slices in Whirlpack bags if not sampled by MG	4°C
1	Paleo DNA (DNA)	Entire MUC tube deep frozen, stored wrapped in aluminum foil in evacuated and sealed plastic bag	–20°C
1	Physical properties (PP)	1 cm slices in Whirlpack bags	4°C
1	Porewater Sampling Sensor Tube (PWS)	Sample immediately given to external (NIOZ) users	4°C
1	General Porewater Sampling (POR)	Smaples for external users, if not needed cut in 1 cm slices and stored in WP bags	4°C
1	Archive (ARC)	Entire MUC tube deep frozen, stored wrapped in aluminum foil in evacuated and sealed plastic bag	-20°C

The giant box corer (GBC; volume of sample 50*50*60 cm (manufactured by Fa. Wuttke, Henstedt-Ulzburg, Germany) was unsuccessfully deployed on station PS140_18-1 and -2 on the continental shelf of Prydz Bay. Failure was due to problems with the releasing mechanism.

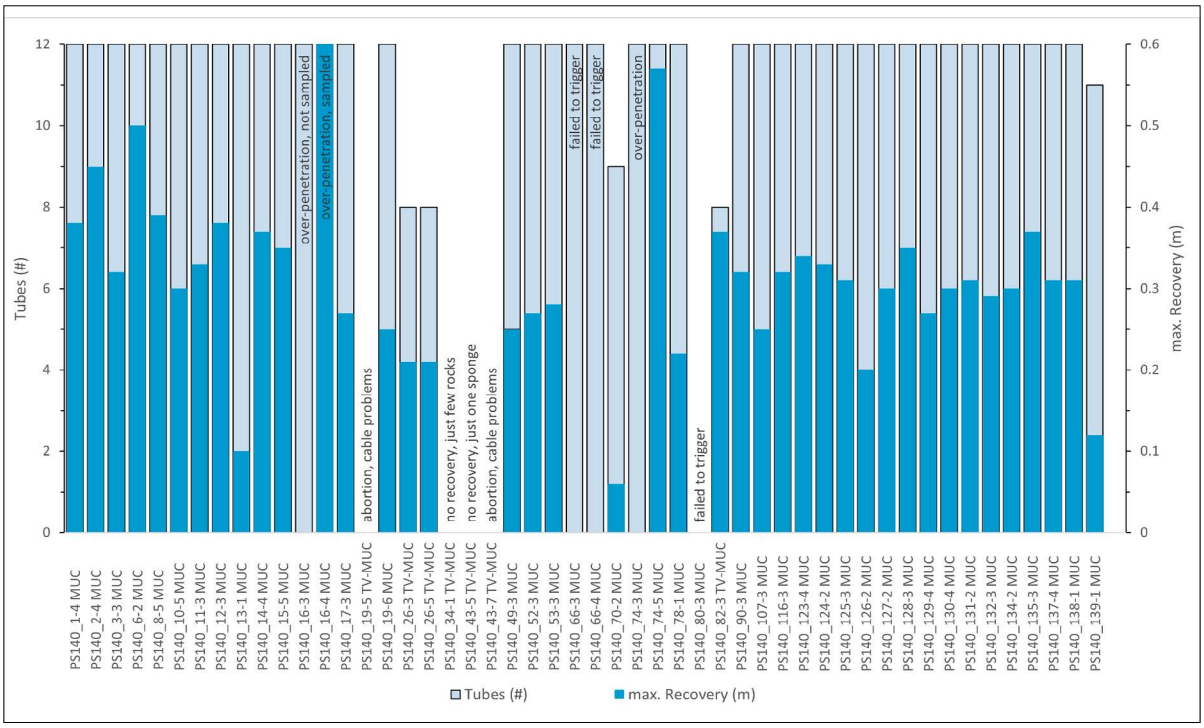

Fig. 5.8: Recovery of 12-tubes Multicorer (MUC) and 8 Tubes TV-Multicorer (TV-MUC) on PS140 stations. Light blue bars show the number of tubes that recovered sediment (left axis), the dark blue bars indicate the maximum recovery (right axis).

Sediment coring and core documentation

Two main sediment coring devices were applied during cruise PS140. The first was a gravity corer (GC), which consists of a 2.3 t weight and an up to 25 m long steel pipe (in 5 m-barrel-increments). The gravity corer was lowered to depth at a speed of 1.0 to 1.2 m/s. The device remained in the sediments for ~30 seconds to allow for penetration until it was heaved with a speed of 0.2 m/s out of the seafloor and with 1.2 m/s back to the ship´s working deck. Penetration into and release from the sediments were monitored through the cable tension.

For *ad hoc* deployments in order to gain a quick impression of the sediment consistency, we used a short gravity corer, with 5 m to 8 m steel pipe length. Here we did not make use of the ship's core handling rack.

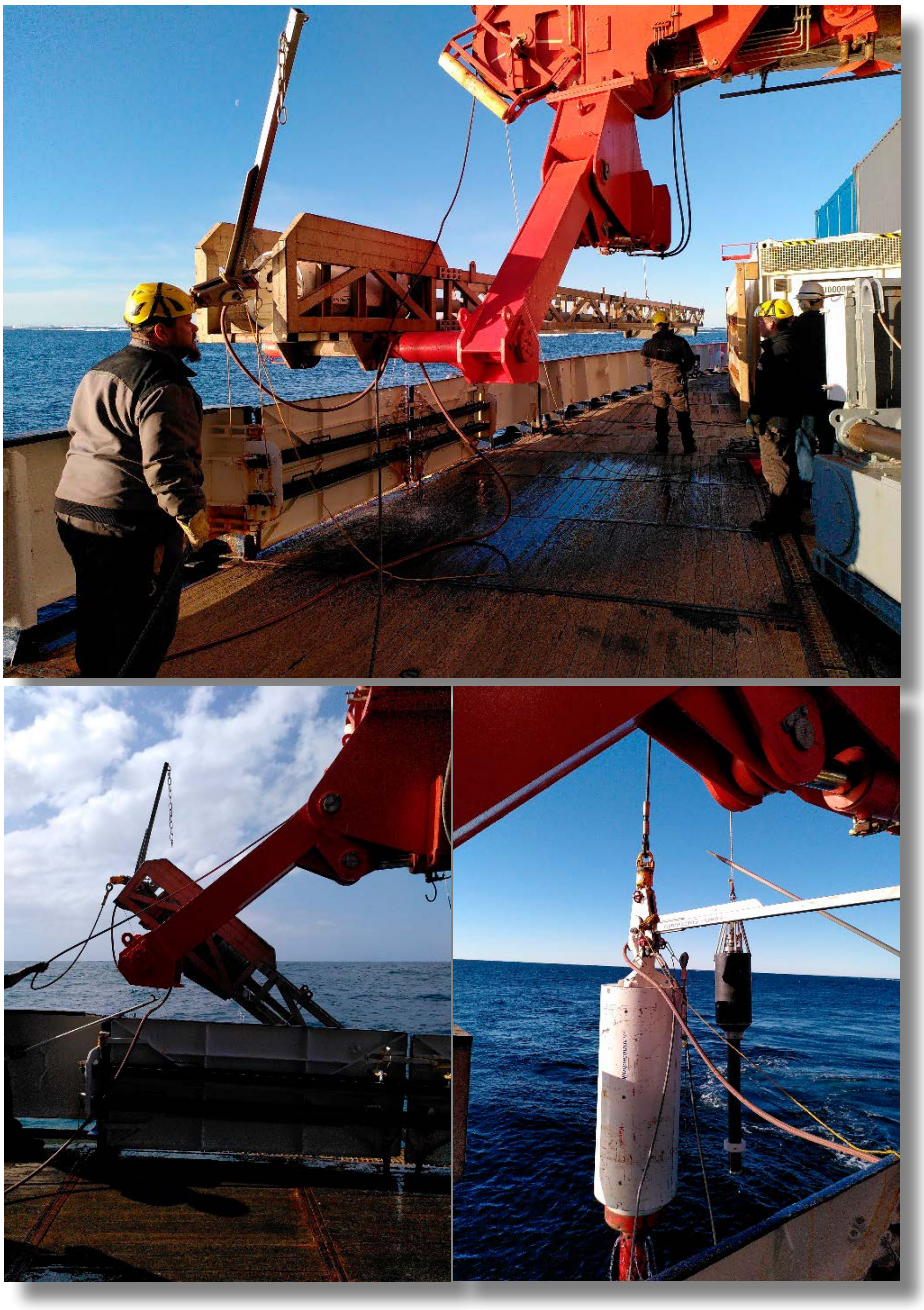

Fig. 5.9: Polarstern´s core handling rack system to deploy long coring devices, here the piston corer

In addition to gravity coring, we used both AWI piston coring systems, with diameters of 90 mm (PC 90) and 125mm (PC-125). Both coring devices were acquired from Fa. Kawohl-Marinetechnik (Fig. 5.9, 5.10). Equipped with a split piston, the maximum length of both assembled piston core stands aboard *Polarstern* is 25 m (in 5 m increments). The barrel´s head weight for PC-125 is ca. 2.8 t. The piston corer with 90mm diameter was only used for the first stations, from station PS140_14-5 onwards the piston corer with 125 mm diameter was used for more sediment yield. The piston corer was lowered and heaved at a winch speed of 1.2 m/s. A 1 m-long pilot (trigger) core is attached to the piston corer by a steel rope via a release mechanism (Fig. 5.9). Upon contact with the seafloor, the pilot core triggers the release of the main device, which then free-falls into the sediment and allows deeper penetration into the sediments, rather than a gravity corer. To allow for a deep penetration, the piston corer was

left at the seafloor for about 30 seconds, then hieved with 0.2 m/s until it was pulled out of the sediment. Hieving activates the split piston, which allows for better core recovery (Fig. 5.10).

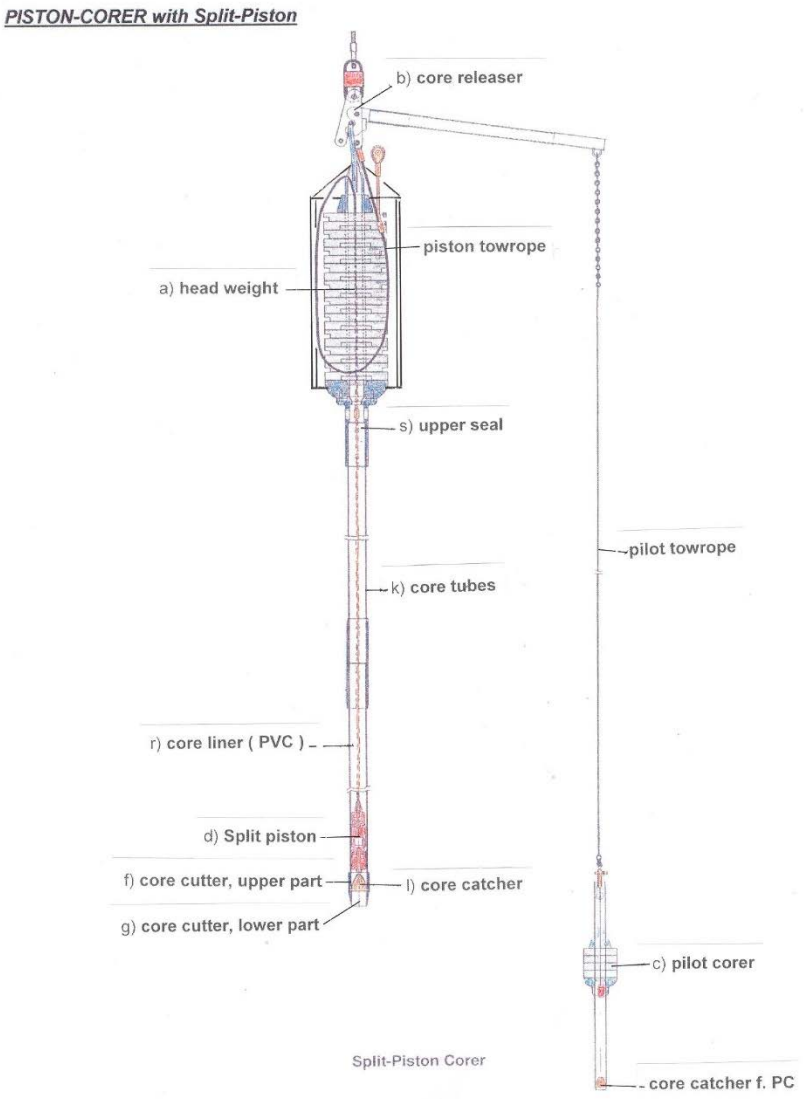

Fig. 5.10: Setup of the AWI piston corer (PC) from Fa. Kawohl-Marinetechnik with release mechanism b), split piston d) and pilot corer c).

In total, 22 piston corers (PC) with core barrel lengths between 15 and 25 m, 26 gravity corers (GC) with lengths between five and eight metres, and one Kasten Corer (KC) with a device length of 5.75 m were used to recover long sedimentary sequences (Tab. 5.3). All different coring systems were primarily deployed via the core handling rack (Kernabsatzgestell) using winch 72.1 with a diameter of 18 mm. 44 deployments were successful and resulted in a total core recovery of ca. 409 m (Fig. 5.11). In addition, 14.92 m were recovered from the Trigger Corer (TC). The gear types and the length of the coring devices were chosen based on sediment acoustic profiles acquired with the PARASOUND shallow sub-bottom profiling system, considering acoustic patterns such as the strength of characteristic reflectors, their spacing, and the total sub-bottom penetration (see above).

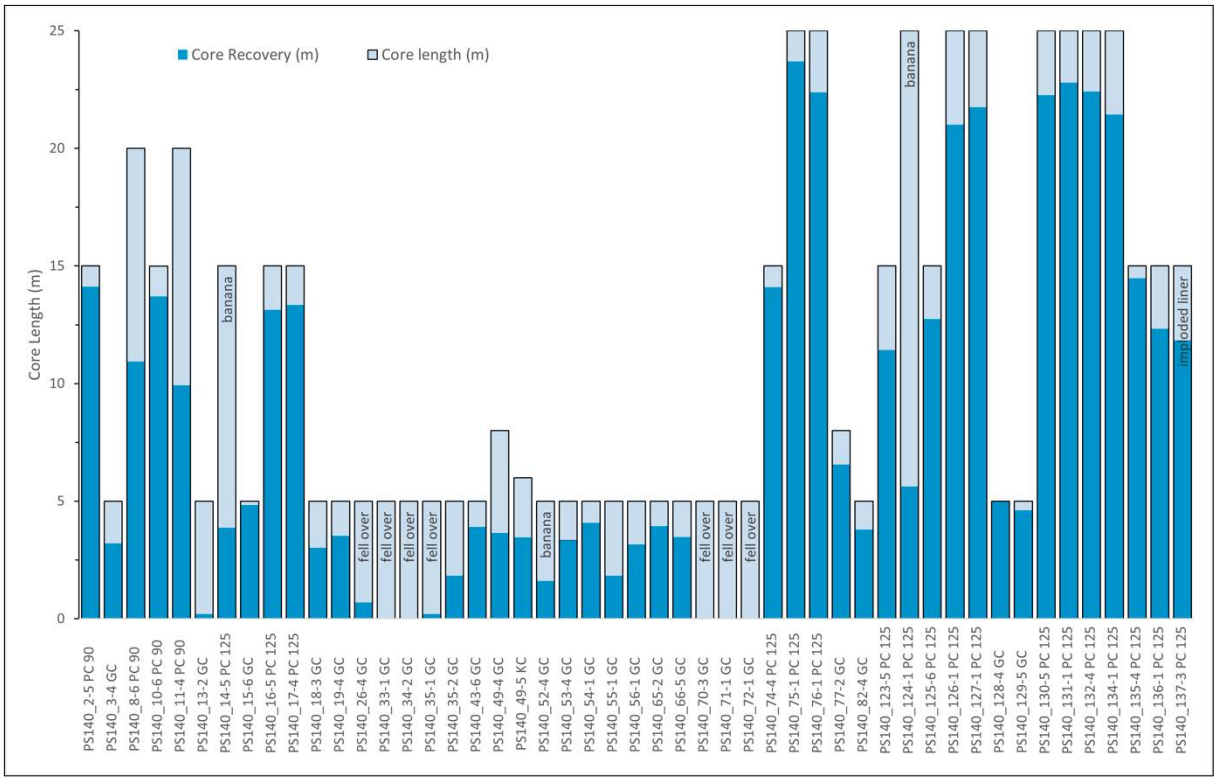

Fig. 5.11: PS140 sediment core recovery (m) in consecutive order of stations. Light blue shading: Length of deployed coring device (m). Dark blue shading: Absolute core recovery in (m).

Sediment core handling

After being placed on deck, the core catcher of the coring device was removed and stored with its sediment material being stored in labeled plastic bags. The 5 m-long PVC-liner sections were pulled out of the steel core barrels, thereafter immediately marked with latin numbers (I, II, III, IV, etc.) and yellow tape on their bottom end. The numbered sections were brought into the laboratory and cut into 1 m long segments. Before closing the core segments with plastic caps, smear slides were taken from each segment base in order to conduct biostratigraphic analyses. Sediment cores were cut into 1 m whole-round sections and each section one also marked with yellow tape on the bottom end. Labeling of the 1-m PVC sections was carried out according to the following scheme that was also used for the storage containers (D-tubes) and the end caps (Fig. 5.12):

- Cruise number; station number; number of the device at station (e.g. PS140_07-2)
- Label A for archive half; label W for working half
- Arrow, pointing to the bottom of the section
- Depth interval (in cm)
- Label Top/Base

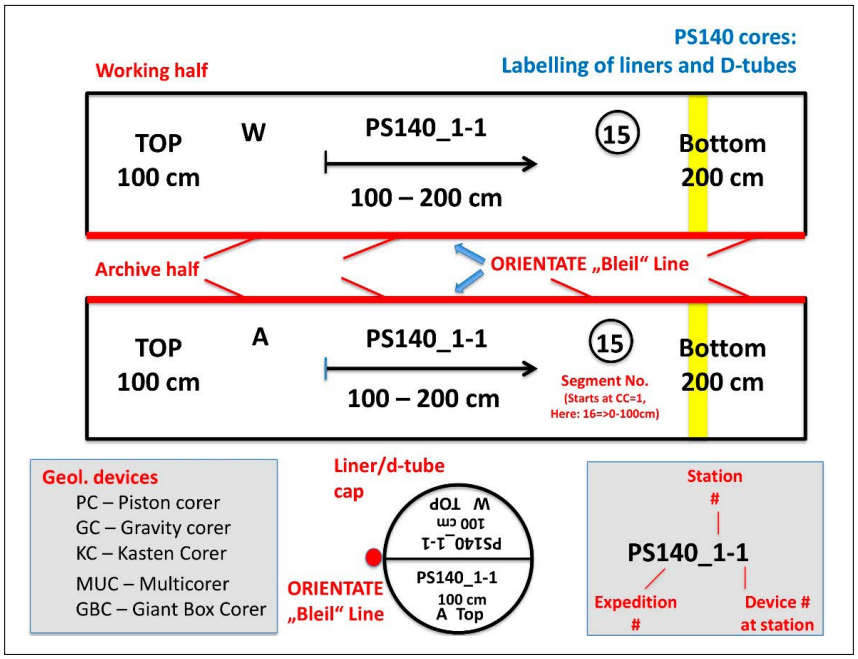

Fig. 5.12: Labeling scheme for liners, D-tubes, and liner caps

Prior to storage at 4° C, all core sections were analyzed for physical properties of the entire core using a Multi-Sensor-Core-Logger (MSCL-S, Geotek Ltd.). The MSCL device provides data at 1 cm depth intervals of wet-bulk density, porosity, p-wave velocity and magnetic susceptibility.

The largest diameter coring device deployed during PS140 was a 5.75 m Kasten Core (KC) consisting of one 5.75 m segment. The KC´s rectangular shape has a footprint of 30x30 cm, attached to a 2.8 t weight barrel. Due to its large diameter, the KC has a four-times higher sediment recovery compared to the PC. Upon recovery, one of the two angle sections of the KC were removed to allow access to the sediments. Prior to sampling, the outermost sediments layers were removed, which may have been disturbed by the coring process. To sample the recovered sediments, four rows of rectangular plastic boxes (98*15*7 cm), 3 rows of smaller rectangular plastic boxes (98*7*7 cm) and 1 row of U-channels (for paleomagnetic studies) were pushed into the sediments according to a pre-defined sampling scheme (Fig. 5.13).

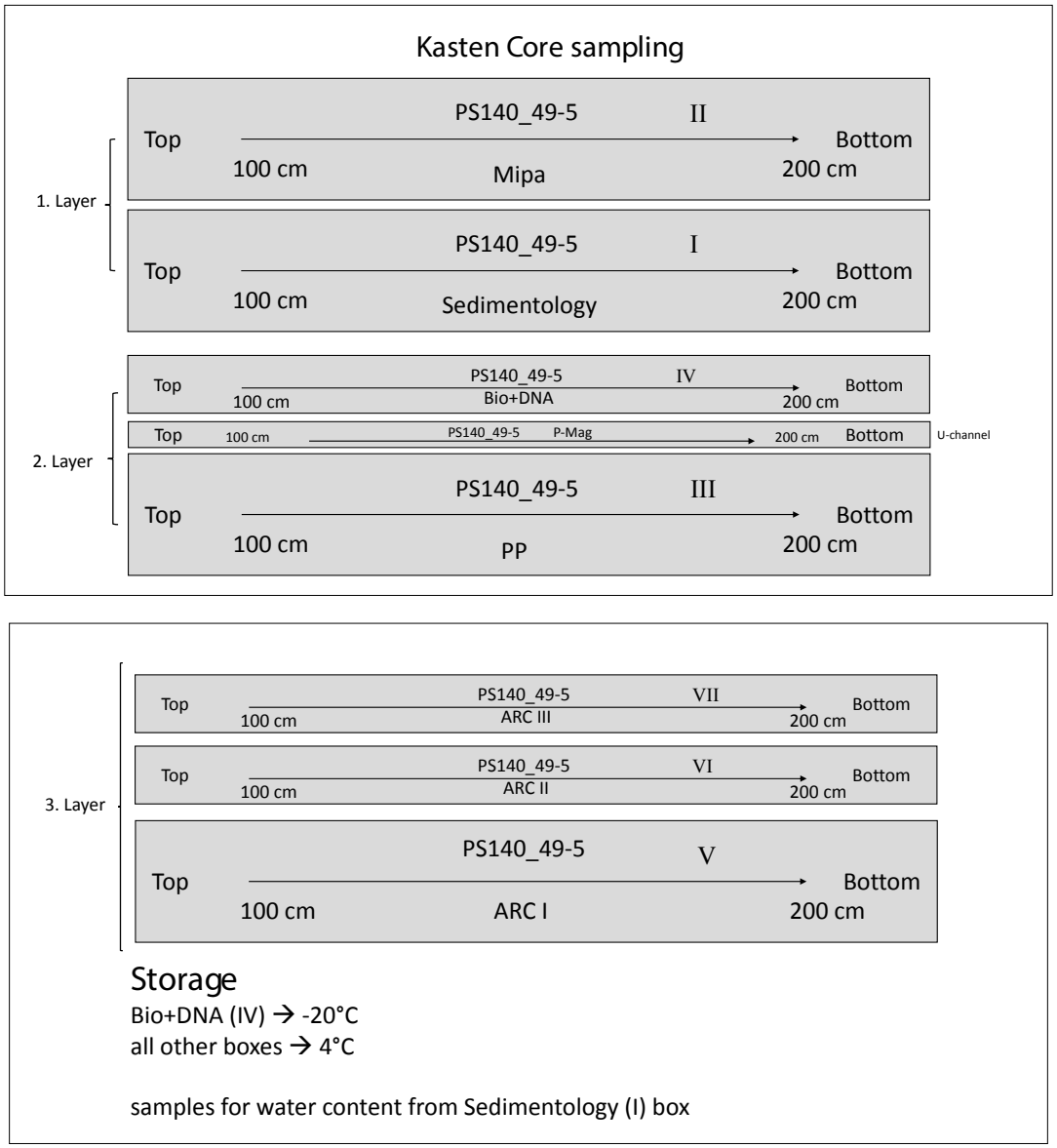

Fig. 5.13: Sampling scheme for Kasten Corer that was used during PS140.

Multisensor core logging and physical properties measurements

We carried out Multi Sensor Core Logging (MSCL) as initial non-destructive measurement on all obtained sediment cores with a diameter of 125 mm. Major lithological changes are often evident in logging data and thus give information on variations in biogenic opal or carbonate as well as terrigenous sediment content. These results enable the calculation of key parameters like sediment thickness or continuity of distribution around coring locations and serves for core-to-core correlations as well.

The following parameters were measured on whole-round core sections: magnetic susceptibility, sound velocity of the pressure wave (vP), and the gamma ray attenuation, later calibrated as wet bulk density (WBD). Physical properties of the sediments expressed as wet bulk density, p-wave velocity and magnetic susceptibility were measured on all collected sediment cores using a GEOTEK multi-sensor core logger (MSCL). In addition, the core diameter was measured for

data processing. The parameters listed in the logger settings of the MSCL software (version 6) and given in Table 5.2 were used for calibration that was conducted following the Geotek MSCL manual and established procedures (Gunn and Best, 1998; Best and Gunn, 1999). An AWI MSCL instrument was used for continuous whole-round core section measurements with a 1 cm resolution. All physical property data were qualitatively controlled on board, and faulty values, e.g. at core section boundaries, were flagged in output files. In order to obtain true volume-corrected $\varkappa$ (Kappa) magnetic susceptibility in (10^{-6} SI-units) values, the processed magnetic susceptibility sensor data were processed drift and volume corrected and multiplied by the correction factor (Tab. 5.2).

MSCL measurements will be validated at a later stage with shore-based analyses, hence individual sediment samples were taken from all cores opened with 10 cubic centimetre plastic syringes at 10 cm sample spacing for physical property measurements (water content, sediment density) and further geochemical, sedimentological and mineralogical investigations. To calculate sediment fluxes and mass accumulation rates of specific compounds, the water content and the sediment density will be measured on individual samples taken from the cores that were opened during the cruise. Onshore at AWI, all individual physical properties samples shall be weighed, freeze-dried and milled. Water content, bulk-, grain-, wet-, and dry-bulk-densities, and the porosity shall be determined.

Tab. 5.2: Sensors and parameter settings for measurements with the GEOTEK multi-sensor core logger during PS140.

P-wave velocity and core diameter
Rolling transducers Transmitter pulse frequency: 250 kHz P-wave travel time offset: 19.5 µs (PC125, 125 cm outer diam., 2*3.7 mm liner thickness) P-wave travel time offset: 18.5 µs (PC125, 125 cm outer diam., 2*2.5 mm liner thickness) Temperature = 20 °C, salinity = 35 psu, not corrected for water depth and in situ temperature; calibrated with water core of known temperature and theoretical sound velocity.
Density
Gamma ray source: Cs-137; activity: 370 MBq, Serial No. 0874/13 Aperture diameter: 5.0 mm Gamma ray detector: 3rd generation; count time 5 s Gamma ray attenuation measurement and density calculation with equation type $y=Ax^2+Bx+C$, (Coefficients A, B, and C determined with measurements on calibration cores).
Fractional porosity
Mineral grain density = 2.65, water density = 1.026
Magnetic susceptibility (MS)
Coil sensors: BARTINGTON MS-3, Ser. Nr. 0582, and Ser. Nr. 716 (coil sensor) Nominal inner coil diameter: 14 cm Coil diameter: 14.8 cm (factors B, Den and LD were deactivated in the GEOTEK processing software). Alternating field frequency: 565 Hz, count time 5 s, precision $0.1 * 10^{-5}$ (SI)
Core thickness measurement
Laser detection

Core opening and sampling, Visual core description

After the measurement of the physical properties using the GEOTEK multi-sensor core logger for un-split core sections, cores were selected for opening and sampling based on initial biostratigraphic and physical property analyses. Routinely, the 1 m-core sections were split lengthwise into a working (W) and an archive (A) half (Fig. 5.14 and 5.15). In total, ~141 core meters were opened and sampled. Core segments, which were not opened during the expedition, were stored in reefer containers at a temperature of 4° C for transport.

Core images, descriptions of sediment properties and smear slide investigations of the cores opened on board allow to initially characterize the sediments. However, some of the sediment cores remain unsplit until arrival at port and subsequent processing onshore. Sampling of the MUC sediment records (1 cm slices) into combusted glass vials (biomarker) and Whirlpack sampling bags took place onboard. Samples designated for biomarker studies and ancient DNA analyses at home laboratories were stored frozen (–20° C). At most sites, MUC cores were equally sampled for their trace metal and Pb isotope budget, both in porewaters as well as the particulate phase (see also Chapter 4).

Fig. 5.14: Splitting of a core section in working and archive halves, using the Fa. Marinetechnik Kawohl vibration saw tool

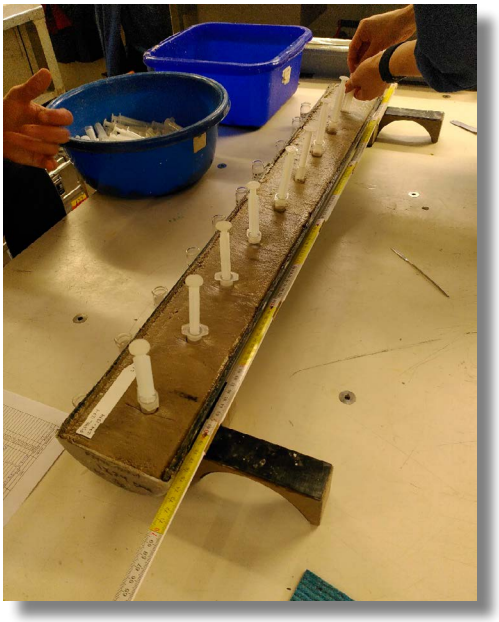

Fig. 5.15: Sampling of the working half in 10 cm distances with syringes of 10 mm diameter

After opening and splitting of the cores, the core sections were photographed.

The work halves were used for taking shipboard samples (~10 cc) designated for measurements of physical properties and bulk parameters (contents of $CaCO_3$, total organic carbon, and biogenic silica) studies were taken each 10 cm from the working halves (Fig. 5.15). These bulk parameter samples (~6 – 10 cm^3 in volume each) were taken by 10 cm^2 plastic syringe cylinders with cut-off tips and stored in glass vials.

The archive halves were described visually (see below). Sediment colors were determined using the "Munsell Soil Color Chart". The sediment core descriptions, visualized as lithologs, comprise information on lithogenic and biogenic sediment composition, as well as the inventory of sediment textures and structures. Lithologs were generated according to observations from visual core inspection in verification with shipboard core logging, core photography, and findings from microscopic smear-slide analysis. Based on the standard IODP classification scheme (Fig. 5.16) and following the lithological classification of Mazzullo et al. (1998), we used the APPLECORE software package with a custom-made lithological file to digitalize all visual core descriptions. We used a principal name and additional minor or major modifiers to describe the composition, texture and features of the sediments. The principal name identifies the degree of consolidation (induration) as well as the granular sediment class. Further characteristics like the occurrence of disturbances, slumps, turbiditic structures, as well as the occurrence of macro- and microfossils, ichnofossils, dropstones, shell fragments, tephra layers, laminae, pyrite or iron sulfides etc. were reported in the core descriptions both in text and annotated with symbols on the VCDs.

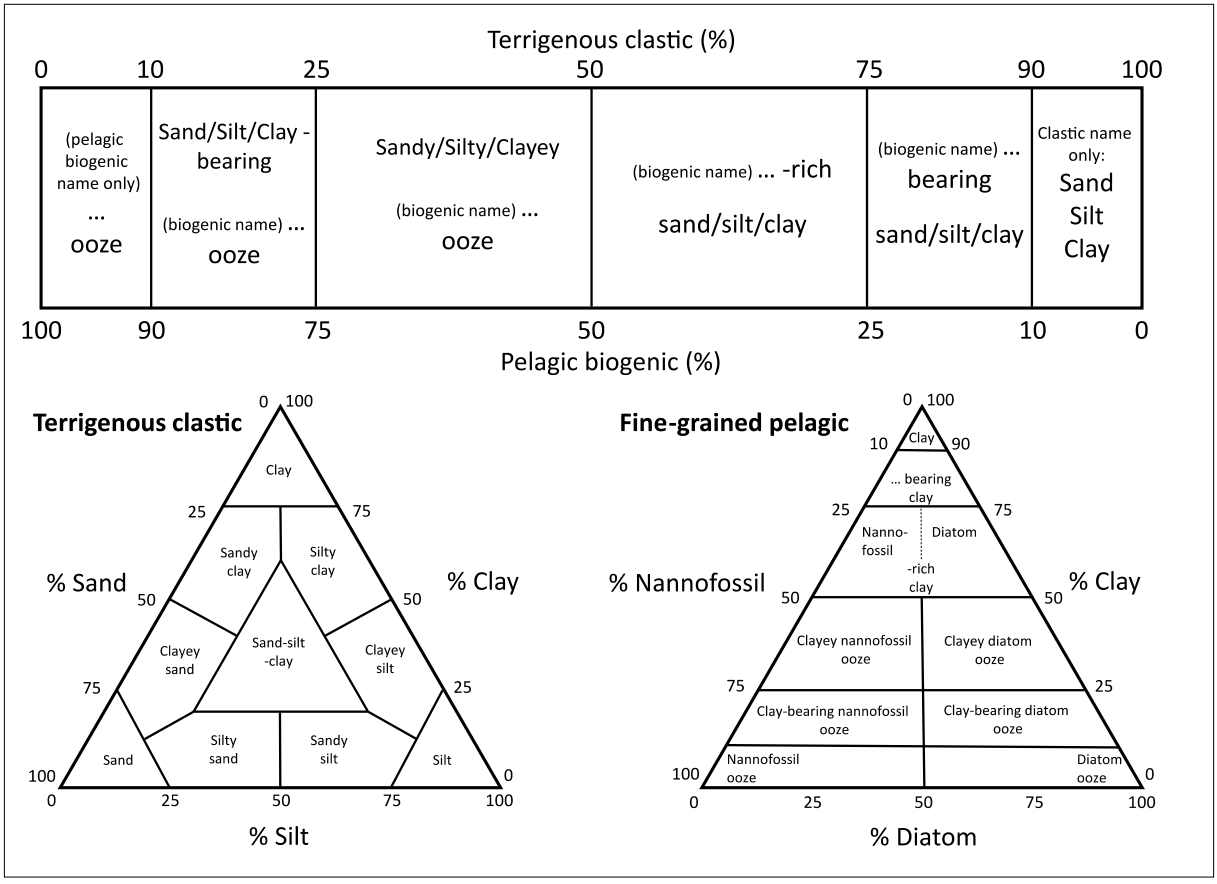

Fig. 5.16: Overview of classification scheme used for shipboard visual core description, derived from IODP and ODP classification schemes (Marsaglia et al., 2013, 2015)

We complemented the Visual Core Description by microscopic analysis of sediment smear slides from major lithologies found in the individual cores. Smear slides were prepared and examined under transmitted light with a Leitz Otrthoplan petrographic microscope (100 to 630X magnification), allowing mineral determination under both plane-polarized and cross-polarized light. Smear-slide analysis of bulk sediment was undertaken to check sediment composition and for the identification of diatoms and radiolarians that bear biostratigraphic information. Where possible, maximum ages were determined from core catcher samples at the base of each core, and in some cases, samples within cores were examined to refine age determination.

Finally, all core sections were packed in transparent cling wrap, placed into plastic D-tubes or vacuum bags, sealed and stored in reefer containers at ~4°C.

Tab. 5.3: Gravity and piston core stations during PS140.

Station Number	Gear (Type /Length)	Latitude (°)	Longitude (°)	Water depth (Hydro-sweep)	Core recovery (m)	TC recovery (m)	Opened/ described
Area 1							
PS140_2-5	PC 90 (15m)	41°42.624‘S	031°38.400‘E	4458	14.11	0.84	
PS140_3-4	GC (5m)	42°59.991‘S	038°09.096‘E	2983	3.21		X
PS140_8-6	PC 90 (20m)	52°45.264‘S	055°43.822‘E	4470	10.94	0.65	
PS140_10-6	PC 90 (15m)	53°27.110‘S	057°34.655‘E	4327	13.70	0.48	
PS140_11-4	PC 125 (15m)	55°36.804‘S	065°38.273‘E	2296	9.92	0.76	X
PS140_13-2	GC (5m)	59°09.640‘S	076°00.879‘E	1184	0.20		
PS140_14-5	PC 125 (15m)	62°55.695‘S	076°04.873‘E	3836	3.87	0.90	
PS140_15-6	GC (5m)	66°22.715‘S	077°03.879‘E	2830	4.83		
PS140_16-5	PC 125 (15m)	68°41.084‘S	076°44.668‘E	817	13.13	unknown	
PS140_17-4	PC 125 (15m)	68°55.863‘S	077°18.588‘E	1416	13.34	0.31	
PS140_18-3	GC (5m)	68°14.293‘S	074°28.565‘E	602	3.01		
PS140_19-4	GC (5m)	68°08.451‘S	075°40.734‘E	502	3.52		
PS140_26-4	GC (5m)	67°13.926‘S	073°09.307‘E	555	0.69		
PS140_33-1	GC (5m)	66°38.222‘S	070°47.267‘E	1742	0.00		
PS140_34-2	GC (5m)	66°56.488‘S	070°55.803‘E	500	0.00		
PS140_35-1	GC (5m)	66°59.645‘S	071°07.471‘E	518	0.2		
PS140_35-2	GC (5m)	66°59.552‘S	071°07.623‘E	505	1.83		
PS140_43-6	GC (5m)	68°30.915‘S	070°16.881‘E	1239	3.9		
PS140_49-4	GC (8m)	68°15.031‘S	072°43.838‘E	771	3.64		X
PS140_49-5	KC (6m)	68°15.029‘S	072°43.843‘E	771	3.45		X
PS140_52-4	GC (5m)	67°25.457‘S	073°07.017‘E	593	1.61		
PS140_53-4	GC (5m)	68°09.625‘S	072°56.755‘E	731	3.34		
PS140_54-1	GC (5m)	68°09.668‘S	072°59.377‘E	696	4.08		
PS140_55-1	GC (5m)	68°09.668‘S	073°00.249‘E	669	1.82		
PS140_56-1	GC (5m)	68°09.683‘S	073°02.910‘E	684	3.16		
PS140_65-2	GC (5m)	69°19.006‘S	075°06.756‘E	675	3.93		
PS140_66-5	GC (5m)	69°19.414‘S	074°11.357‘E	714	3.47		
PS140_70-3	GC (5m)	69°19.048‘S	075°06.765‘E	676	0.00		
PS140_71-1	GC (5m)	69°18.312‘S	075°04.318‘E	705	0.00		
PS140_72-1	GC (5m)	69°18.259‘S	075°00.924‘E	773	0.00		
PS140_74-4	PC 125 (15m)	69°14.821‘S	076°31.357‘E	1235	14.09	0.95	

Station Number	Gear (Type /Length)	Latitude (°)	Longitude (°)	Water depth (Hydro-sweep)	Core recovery (m)	TC recovery (m)	Opened/ described
PS140_75-1	PC 125 (25m)	68°43.256‘S	076°40.825‘E	843	23.70	0.85	
PS140_76-1	PC 125 (25m)	68°56.560‘S	077°19.927‘E	1404	22.38	0.99	
PS140_77-2	GC (8m)	68°43.570‘S	077°42.235‘E	1017	6.55		
PS140_82-4	GC (5m)	67°13.682‘S	080°32.200‘E	1613	3.79		
PS140_123-5	PC 125 (15m)	63°41.335‘S	100°46.428‘E	1400	11.42	0.83	X
PS140_124-1	PC 125 (25m)	60°53.791‘S	100°58.451‘E	4515	5.63	0.87	
PS140_125-6	PC 125 (15m)	59°34.139‘S	101°07.433‘E	4166	12.73	0.30	X
PS140_126-1	PC 125 (25m)	57°26.602‘S	101°27.022‘E	4225	21.00	0.55	X
PS140_127-1	PC 125 (25m)	56°25.222‘S	101°46.805‘E	3884	21.75	0.50	X
PS140_128-4	GC (5m)	55°52.380‘S	102°28.102‘E	3799	4.97		X
PS140_129-5	GC (5m)	53°26.516‘S	103°54.507‘E	3914	4.61		X
PS140_130-5	PC 125 (25m)	51°39.172‘S	103°52.905‘E	3167	22.26	0.81	
PS140_131-1	PC 125 (25m)	50°12.275‘S	104°31.354‘E	3112	22.80	0.50	X
PS140_132-4	PC 125 (25m)	48°49.350‘S	104°36.914‘E	3129	22.42	0.89	
PS140_134-1	PC 125 (25m)	46°58.089‘S	104°11.895‘E	3327	21.43	0.66	X
PS140_135-4	PC 125 (15m)	45°04.414‘S	103°59.662‘E	3640	14.48	0.60	
PS140_136-1	PC 125 (15m)	46°51.259‘S	107°06.129‘E	3365	12.33	0.88	
PS140_137-3	PC 125 (15m)	48°37.550‘S	111°44.748‘E	3567	11.84	0.80	

Micropaleontology and Biostratigraphy

The three study areas (Western Indian Ocean Transect, Prydz Bay, and Eastern Indian Ocean Transect) are characterized by diatom-rich sediments. Sediment cores taken with piston and gravity corers in the study areas provide continuous records useful for biostratigraphy. Smear slide samples from every core section were prepared by embedding a smeared toothpick sediment sample with NORLAND Optical Adhesive No. 61 on a microscopic slide. The slides were examined under transmitted light with a Zeiss Axioplan II microscope at a magnification of 630x, allowing for the identification of diatom species for relative abundance estimations. A qualitative estimate of the relative abundance of age-determining diatom species is based on Zielinski and Gersonde (2002). The preservation state of the diatom assemblage has been distinguished between poor, moderate, and good (Zielinski, 1993; *cf*. Fig. 5.17).

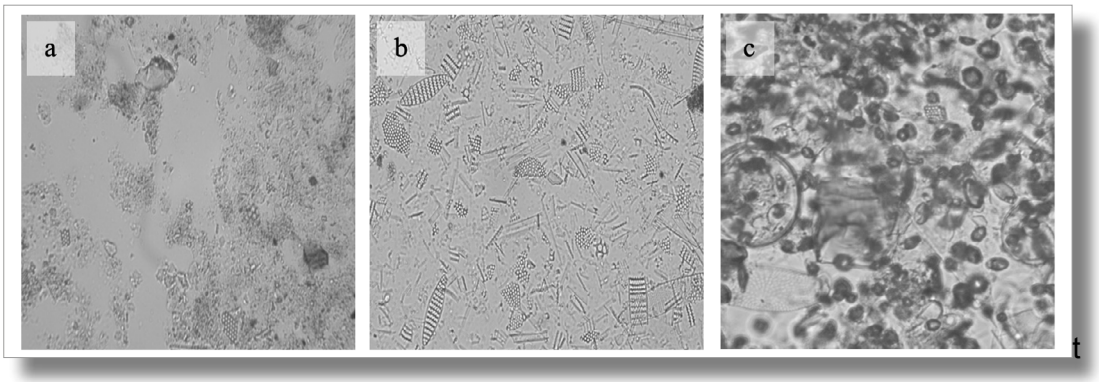

Fig. 5.17: Pictures of dominating diatom preservation states encountered in PS140 core sediments; a: poor; b: moderate; c: extraordinary.

Preliminary (expected) results

Preliminary results

With the sediments recovered during PS140, we aim to resolve glacial-interglacial, as well as millennial-scale variations in ACC dynamics, AABW formation and export, East Antarctic marginal seas ice extent, glacial deep Southern Ocean carbon storage, as well as sediment sourcing and bottom-water oxygenation levels that include the most extreme late Pleistocene interglacials MIS 5e (Clark et al. 2020) and MIS 11 (Raymo and Mitrovica 2012, Wilson et al. 2018).

Station works were carried out in three designated working areas: Western Indian Ocean Transect (Fig. 5.18 and 5.19), Prydz Bay (Fig. 5.20), Eastern Indian Ocean Transect (Fig. 5.21-5.23). Along the NW-SE western Indian Ocean transect we retrieved seven sediment records crossing the major oceanic frontal systems. The material obtained from sediment records will be used to reconstruct changes in AABW dynamics and glacial-interglacial geographic shifts in the Southern Ocean frontal system. In the Prydz Bay Area, we covered transects particularly in the vicinity of the Amery Ice Shelf edge. In close proximity to the EAIS, we complemented previous shelf coring campaigns carried out during PS128 in the Nielsen Basin to the west in order to define the extent and timing of grounded ice beneath and offshore the EAIS across a wide range of different ice stream systems. This work to constrain the past extent and retreat pattern of grounded ice and its timing since the LGM will continue along the coast of the Davis and Mawson seas by combining information from multibeam and sediment echosounders with appropriate coring locations (KC and GC) on selected shelf sectors during the forthcoming expedition PS141. Along a S-N transect across the sea ice margin and the oceanic fronts of the eastern Pacific sector up to the Southeast Indian Ridge, we performed an extensive sediment coring program, targeting sites distributed in water depths between 2,000 m and more than 4,000 m to reconstruct the vertical water mass structure and the different physical and chemical signatures of intermediate to deep water masses.

At selected stations along both transects and the proximal ice shelf locations, the sediment sampling was complemented by multinet and plankton net hauls (Fig. 5.2). Undisturbed surface sediments, reflecting the most recent sedimentary and environmental conditions in our study area, provide an important avenue for the calibration of microfossil and geochemical proxies against observational data. This is important as new proxies evolve continuously, and testing their applicability and reliability, e.g. as sea surface temperature or sea ice proxies, is a crucial step within paleoceanographic and paleoclimate research. The multicorer permits the recovery of up to 12 surface sediment samples and the uppermost 30 to 40 cm of sediment, which encompass the most recent geological history. The surface sediments recovered during *Polarstern* Expedition PS140 thus constitute a highly valuable reference data set for the evaluation of different proxies' response to varying polar oceanic domains and polar frontal connected sea ice – glacier – ocean systems. Additionally, these near-surface samples are indispensable for generating uninterrupted records up to the most recent past, in cases where the uppermost part of a gravity or piston core is disturbed or missing. By combining proxy records from both the multicorer and the piston/gravity corer, a complete sedimentary sequence and hence, stratigraphy can be established.

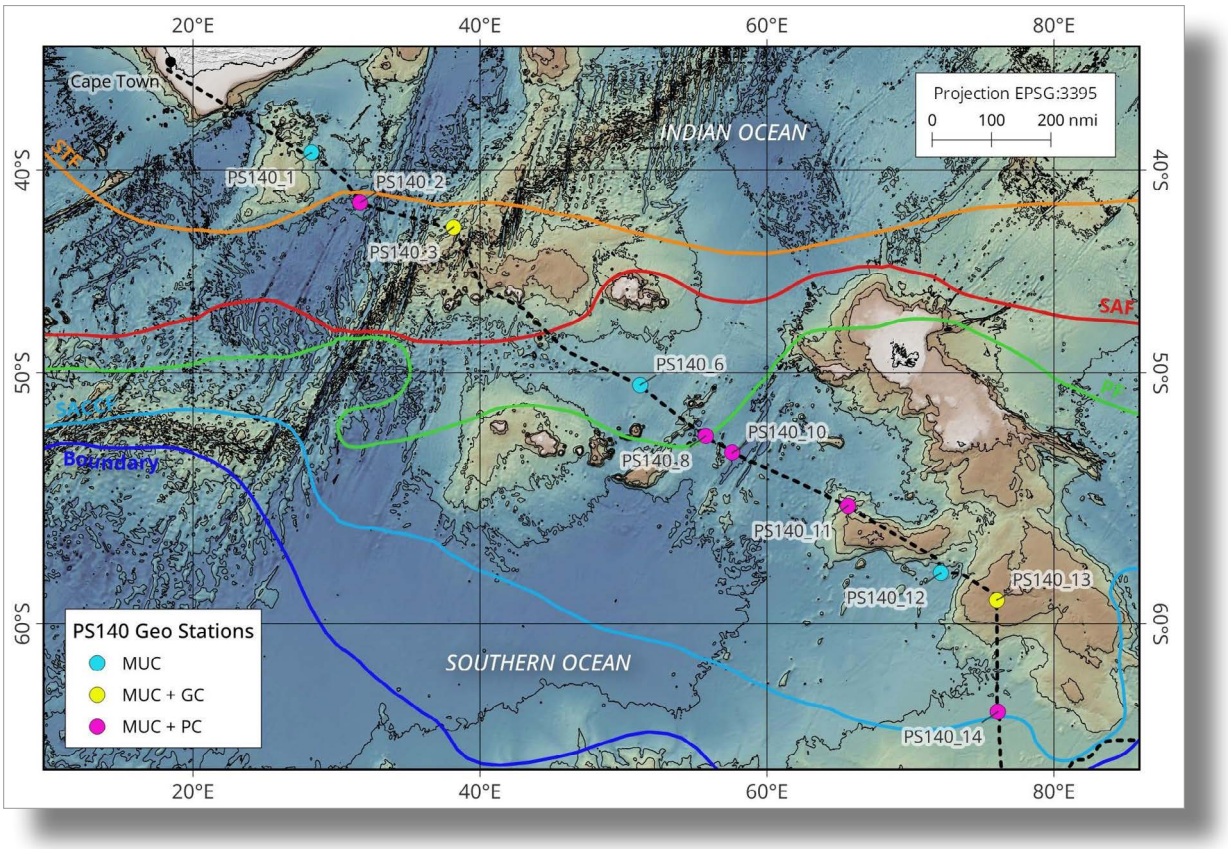

Fig. 5.18: Overview of multicorer (MUC) and giant box corer (GKG) stations along the West Indian Ocean Transect.

In general, our expedition provides new data and samples from key regions of the Indian sector of the Southern Ocean and along the East Antarctic continental margin that will enhance our understanding of processes related to interactions in the ice-ocean-bedrock-climate system. This should improve our assessment of future ice sheet instability and associated changes in Southern Ocean circulation and ventilation. On board, the combination of bathymetric and subsurface sediment features (parasound) in combination with core descriptions already provided information on sedimentary structures and their morphological history in relation to former ice coverage, sub-ice hydrological conditions (sub-glacial lakes, meltwater channels), ice-flow dynamics and possible past natural collapses of ice shelves. The transect of sediment cores sampled during PS140 allows a better quantification of the export of AABW into the Indian Ocean and the import of CDW into the Southern Ocean during the last glacial cycles.

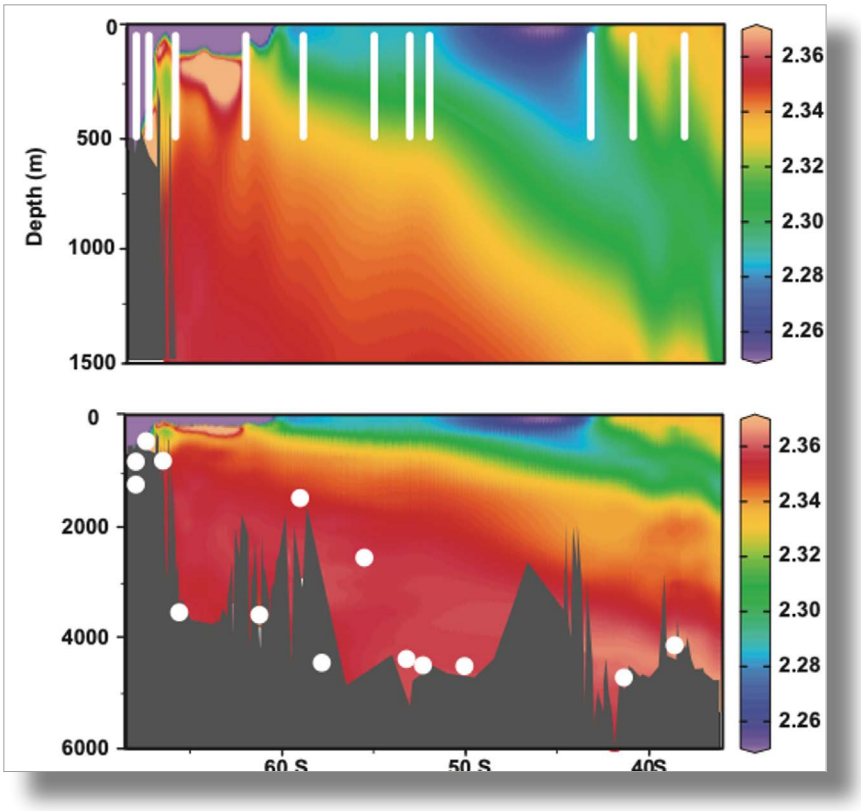

Fig. 5.19: Section along the cruise track on the Western Indian Ocean Transect, projected onto latitude. Shown are GLODAP 2.2-based atlas values of alkalinity in mmol/kg, with locations of station sampling. Upper panel shows enlarged upper 1,500 m of water column. White lines mark deployments of multi-net for plankton sampling. White dots in lower panel show stations with MUC and core sampling. Note that dots were projected onto the plane of the transect and thus do not always show accurate bottom topography.

Western Indian Ocean Transect

Two sediment cores of the Western Indian Ocean Transect have been split and described on board. The sediment of these two cores exhibits a transition from carbonate-rich (PS140_3-4) towards biogenic opal-rich (PS140_11-4) sediments. The northern core (PS140_3-4) is dominated by grayish to yellowish colored diatom-bearing nannofossil ooze with minor amounts of foraminifer fragments decreasing towards the top of the core. Generally, three boundaries have been recognized mainly based on color changes. Core PS140_3-4 is characterized by low to moderate bioturbation with two layers of intense bioturbation.

The lithology of the southern core (PS140_11-4) is characterized by several alternating layers of white to yellowish diatom ooze with minor foraminifers throughout the core. In total, seven boundaries have been distinguished based on gradual color changes only. Variations in color are not clearly related to lithological variations. Light grayish diatom ooze with foraminifers and carbonate fragments (927 – 992 cm) differs clearly from the remaining sediment color. The bioturbation index changes throughout the core from none to intensive.

Micropaleontology and Biostratigraphy

Research sites of the Western Indian Ocean Transect exhibit an N-S transition from carbonate-rich (PS140_2-5 and PS140_3-4) towards opal-rich sediments (PS140_8-6 to PS140_14-5),

which are produced by diatoms with minor amounts of radiolarians. Additionally, coccoliths and foraminifers comprise a small amount of biogenic calcite preserved in the core segments. The poor diatom preservation (Figure 5.17a) in carbonate-rich sediments in the Subantarctic Zone (SAZ) did not allow to obtain a continuous diatom record useful for biostratigraphy. Generally, the preservation state of diatoms along the Western Indian Ocean Transect sediment core segments can be described as poor-moderate to moderate (Fig. 5.17), except for diatom assemblages of cores PS140_8-6 and PS140_10-6, which have moderate-good diatom preservation. The lithological composition of core sediments varies from nannofossil ooze (PS140_2-5 and PS140_3-4) to diatom ooze (PS140_8-6, PS140_10-6, and PS140_11-4) to silty mud with some diatom fragments. Warm water diatoms, such as *Alveus marinus*, *Roperia tesselata, and Fragilariopsis doliolus,* were encountered in carbonate-dominated sediment cores (e.g., PS140_2-5) of the SAZ only. Southward from the Subantarctic Front (SAF), typical warmer water taxa such as *Hemidiscus cuneiformis*, *Thalassionema nitzschioides*, *Thalassiosira oestrupii,* and *Azpetia tabularis* are found in most sediment samples. The assemblage composition observed in diatom-rich sediments of the opal belt (SAF to POOZ) is dominated by *Fragilariopsis kerguelensis* (usually most abundant near the Antarctic Polar Front; APF) and *Thalassiosira lentiginosa* (Permanent Open Ocean Zone; POOZ). Other taxa encountered more southward include typical sea ice indicators such as *Fragilariopsis curta, Fragilariopsis vanheurckii, Fragilariopsis obliquecostata, Fragilariopsis ritscheri* and *Actinocyclus actinochilus*.

Tab. 5.4: Summary of preliminary biostratigraphic results for all cores with sediment recovery >5 m from Western Indian Transect. Abbreviation: (N), north of Subantarctic Front; (S), south of Subantarctic Front.

Datum	**MIS**	**Age (Ma)**	**Core depth* (cm) of PS140**				
			3-4	**8-6**	**10-6**	**11-4**	**14-5†**
Core Length			**321**	**1094**	**1370**	**992**	**387**
LOD Rouxia leventerae	6	0.13		300	971		
LOD Hemidiscus karstenii	7	0.18 – 0.19	321		1071	399	
LOD Rouxia constricta	8	0.24 – 0.30 (0.28, S), 0.44 – 0.64 (N)		894			87
FAOD Hemidiscus karstenii	11	0.42					
LOD Actinocyclus ingens	12	0.36 – 0.42 (0.38, S), 0.45 – 0.51 (N)		1094		792	
LAOD Actinocyclus ingens	16	0.56 – 0.64 (N), 0.64 – 0.7 (S)				992	
LOD Thalassiosira elliptipora	18	0.61 – 0.82					187

Biostratigraphic results for all cores along the Western Indian Ocean Transect with sediment recovery >5 m are summarized in Table 5.4 For the biostratigraphic age estimation, the last occurrence datum (LOD), first abundant occurrence datum (FAOD), and last abundant

occurrence datum (LAOD) of several index diatom taxa have been used according to Zielinski and Gersonde (2002). Noticeably, the age estimations were restrained by the general preservation state of diatoms. During the Western Indian Transect, the micropaleontological examination of the core catcher sediments or their subsequent segment sediments revealed age estimates from 0.19 Ma (PS140_3-4) to a potential 0.82 Ma (PS140_14-5). Reworked or turbiditic mass flows along slopes encountered, e.g., in core PS140_14-5, need to be addressed carefully.

Prydz Bay Shelf and Shackleton Ice Shelf Areas

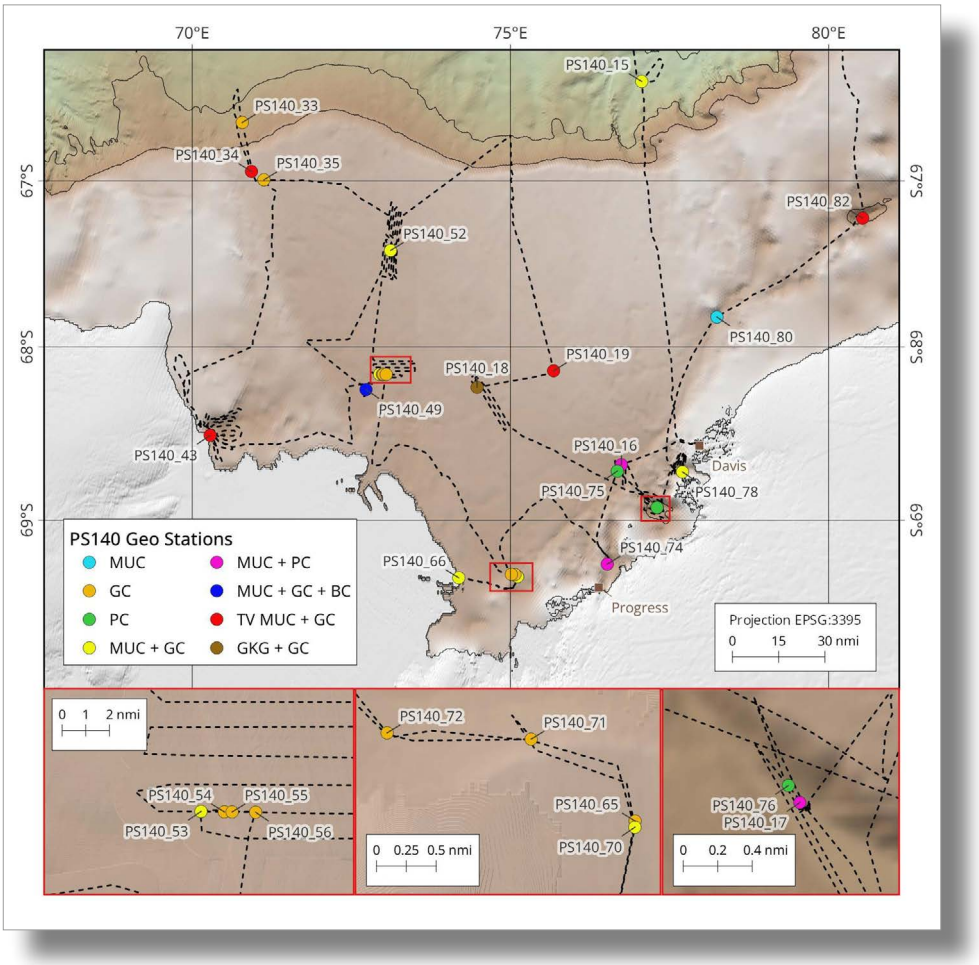

Fig. 5.20: Overview of multicorer (MUC), gravity corer (GC), piston corer (PC), box corer (BC) and giant box corer (GKG) stations in the Prydz bay area. Inserts show detailed station locations along small-scale features that were addressed during coring operations.

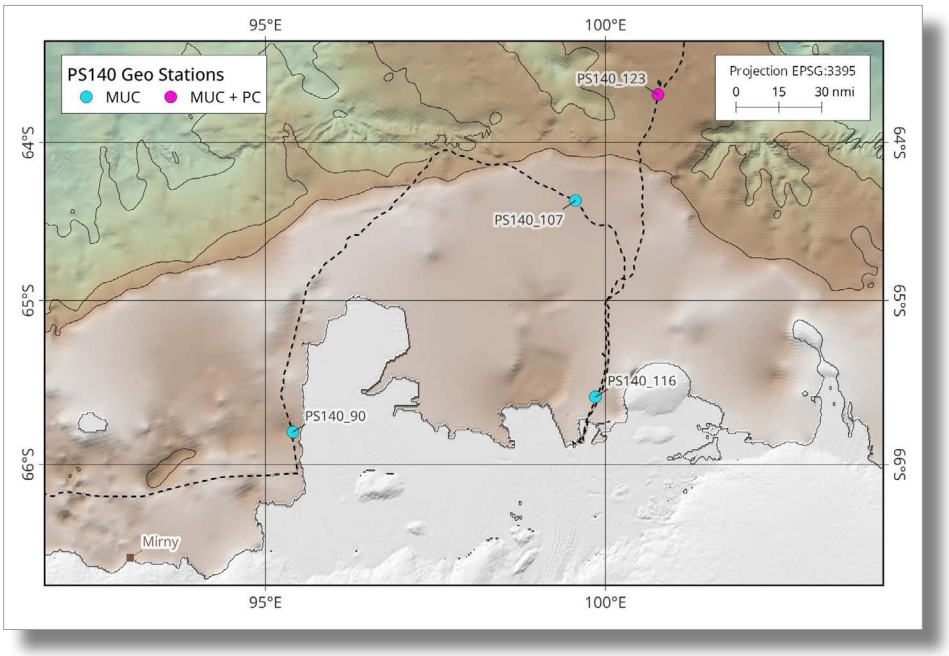

Fig. 5.21: Overview of multicorer (MUC) and piston corer (PC) stations in the Shackleton Ice Shelf area.

Lithology

The only Kasten corer applied during PS140 in the Pryzd Bay, with a total sediment recovery of 336 cm, was split and described on board. The bottom layer of the Kasten corer is mainly composed of diatomaceous ooze with intermixed terrigenous components. It is overlain by two terrigenous sequences, the lower one composed of silty clay, the upper one consists of clay with several minerals such as glauconite, pyrite and vivianite. Remarkable is the appearance of foraminifers. The top of the core exhibits diatom ooze with sponge spicules and minor clay components. Dropstones were recognized only in the two terrigenous sequences.

Piston core PS140_123-5 retrieved from the continental slope off Prydz Bay consists of alternating sequences of diatomaceous ooze dominated sediments and terrigenous mud dominated sediments with transitional parts of intermixed character.

Micropaleontology and Biostratigraphy

Short (up to 5m length) gravity cores (PS140_15-6, PS140_18-3 to PS140_72-1, PS140_77-2 to PS140_82-4) from the Prydz Bay area exhibit a classic sediment succession from a base diamicton, overlain by postglacial till and a top layer composed of diatomaceous mud, restraining the general age assignment to younger than 16 ka. The diatomaceous mud mainly consists of *F. kerguelensis* (3-15 %), *T. lentiginosa* (3-15 %) and *Thalassiothrix antarctica* (15 %). In contrast, the long (up to 22m length) piston cores (PS140_16-5, PS140_17-4, PS140_74-4 to PS140_76-1) exhibit higher postglacial sedimentation rates, leading to high abundant good to extraordinary preserved diatoms. The most prevalent shelf diatom assemblages herein are dominated by *Chaetoceros* spp. (15-30 %), *F. curta* (15-30 %), *F. obliquecostata* (3-15 %), *F. vanheurckii* (3-15 %) and *Corethron pennatum* (15-60 %). Generally, biostratigraphic age estimations were impossible due to lacking index diatom taxa. This also applies to cores near or at the shelf slope (PS140_15 and PS140_123). Here, reworked material restrains the age assignment.

Eastern Indian Ocean Transect

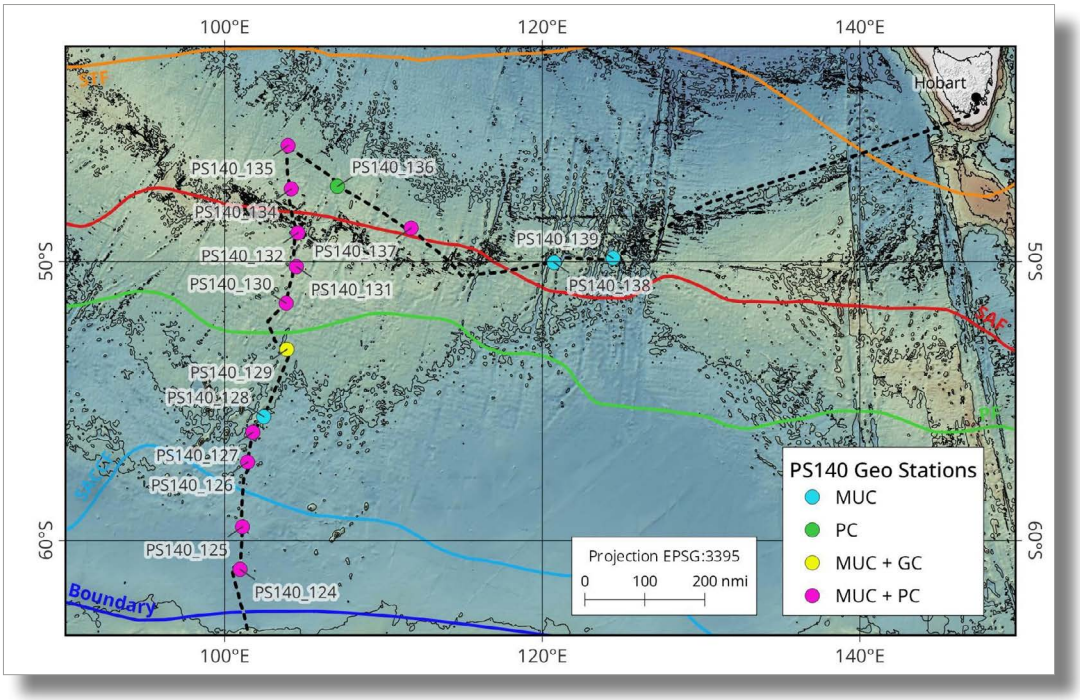

Fig. 5.22: Overview of multicorer (MUC) and giant box corer (GKG) stations along the East Indian Ocean Transect.

Lithology

Seven sediment cores of the Eastern Indian Ocean Transect have been split and described on board. The southernmost core PS140_125-6 is dominated by diatomaceous ooze with alternating minor terrigenous components (sand to clay), which are responsible for significant color changes from greenish gray in the lower part and dark gray in the middle part to yellowish brown in the top part. The next core on the transect, PS140_126-1, is mainly composed of olive gray to gray diatom ooze in the lower core and yellowish brown to gray diatom ooze in the upper core, due to varying abundance of terrigenous components. The following core, PS140_127-1, is dominated by diatomaceous ooze with minor terrigenous components, with irregularly alternating color sequences of olive gray and grayish brown. The next core following northward, PS140_128-4, is mainly composed of very dark gray diatomaceous ooze, interrupted irregularly by grayish green and light olive brown laminated bands. On top of the core, light gray diatomaceous ooze prevails. The next core, PS140_129-5, is dominated by olive gray to yellowish brown diatomaceous ooze with minor terrigenous components.

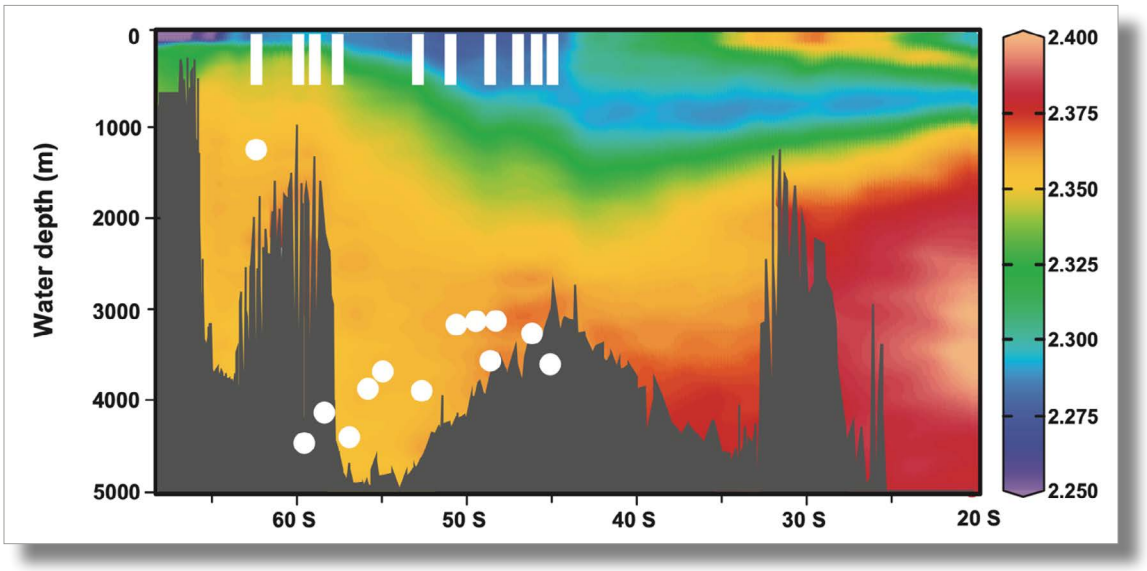

Fig. 5.23: Section along the cruise track on the EIOT, projected onto 100° E latitude. Shown are GLODAP 2.2-based atlas values of alkalinity in mmol/kg are shown, with locations of station sampling. White lines mark deployments of multi-net for plankton sampling. White dots show stations with MUC and core sampling. Note that dots were projected onto the plane of the transect and thus do not always show accurate bottom topography.

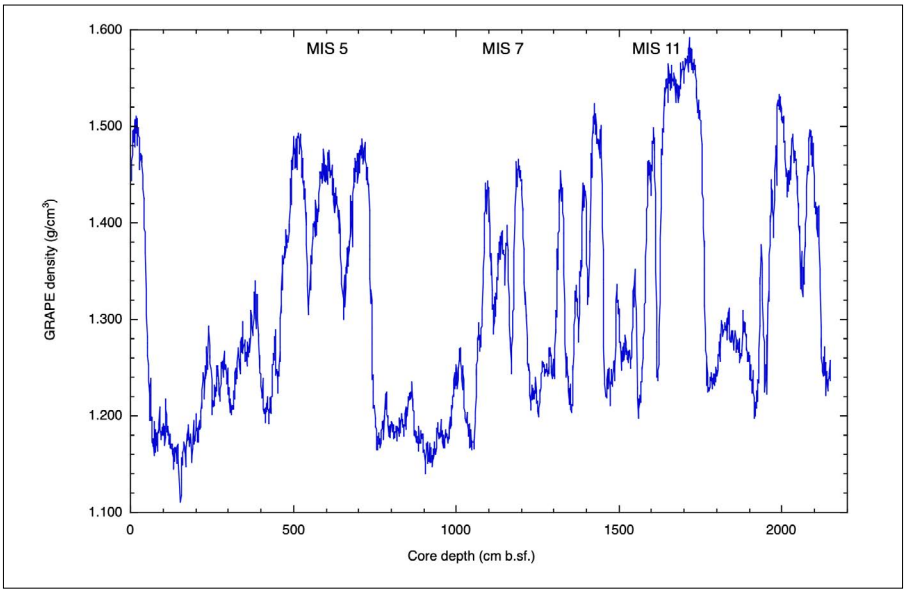

Fig. 5.24: Exemplary density data of piston core PS140_134-1, located within the subantarctic frontal zone on the Eastern Indian Ocean Transect. Gamma-ray attenuation-derived density values shown against core depth in cm below surface. Higher densities tentatively allocated to carbonate-rich, interglacial facies, whereas colder intervals are dominated by lighter diatom oozes. Preliminiary assignments of Marine Isotope Stages (MIS) are given on top based on shipboard correlation and biostratigraphic data.

The occurrence of diatomaceous gravely to sandy mud overlain by a thin layer of nannofossil ooze at the base of the core is remarkable. The northernmost core PS140_134-1 is characterized

by alternating sequences of white to light greenish grey foraminifera-bearing nannofossil ooze and light grey diatom ooze. These alterations, likely derived from lateral migrations of the subantarctic frontal system are clearly visible in changes in logging-derived GRAPE densities (Fig. 5.24).

Micropaleontology and Biostratigraphy

Similar to the Western Indian Transect, the diatom assemblages of the Eastern Indian Transect (Sites PS140_124 to PS140_137) show a congruent diatom preservation pattern. Right to the north of the continental slope, in the southern SIZ, the diatom assemblage of core PS140_124-1 is strongly affected by preservation and dilution with terrigenous particles. In the sediment cores along the cruise track from the northern SIZ to the APF, increased numbers of diatom species associated with sea ice, such as *Fragilariopsis curta* and *Actinocyclus actinochilus* were observed. In the following, sediments of the POOZ and PFZ reveal diverse diatom assemblages composed mainly of species like *F. kerguelensis, T. lentiginosa*, *Eucampia antarctica*, *Thalassiothrix antarctica*, and *F. separanda*. Northern cores from the SAZ (PS140_134-1 to PS140_137-3) exhibit various sediment sections with a high amount of carbonate composed of coccoliths and foraminifers, either alternating or mixing with a high abundance of diatoms. Thus, in interglacial times, diatom assemblages are highly diluted by overwhelmingly abundant nannofossils.

Biostratigraphic results for all Eastern Indian Ocean Transect cores with sediment recovery >5 m are summarized in Table 5.5. The same index diatom taxa as for the Western Indian Transit have been used. Noticeably, the age estimates were restrained by the preservation state of diatom valves, especially during glacial periods.

Tab. 5.5: Summary of biostratigraphic results for all cores with sediment recovery >5 m from Eastern Indian Transect. Abbreviation: (N), north of Subantarctic Front; (S), south of Subantarctic Front.

Datum	**MIS**	**Age (Ma)**	**Core depth* (cm) of PS140**						
			123-5 †	**124-1 †**	**125-6**	**126-1**	**127-1**	**128-4**	**129-5**
Core length			**1142**	**563**	**1273**	**2100**	**2175**	**497**	**461**
LOD *Rouxia leventerae*	6	0.13							
LOD *Hemidiscus karstenii*	7	0.18 – 0.19			1273	1300			
LOD *Rouxia constricta*	8	0.24 – 0.30 (0.28, S), 0.44 – 0.64 (N)							
FAOD *Hemidiscus karstenii*	11	0.42							
LOD *Actinocyclus ingens*	12	0.36 – 0.42 (0.38, S), 0.45 – 0.51 (N)	546			2100	2175		
LAOD *Actinocyclus ingens*	16	0.56 0.64 (N), 0.64 – 0.7 (S)							61
LOD *Thalassiosira elliptipora*	18	0.61 – 0.82	643						461

Poor diatom preservation

CC to top modern diatoms

Datum	MIS	Age (Ma)	Core depth* (cm) of PS140						
			130-5	131-1	132-4	134-1	135-4	136-1	137-4
Core length			**2226**	**2208**	**2242**	**2143**	**1448**	**1233**	**1184**
LOD *Rouxia leventerae*	6	0.13					947		
LOD *Hemidiscus karstenii*	7	0.18 – 0.19	CC to top modern diatoms	CC to top modern diatoms	CC to top modern diatoms	1144	1046	333	
LOD *Rouxia constricta*	8	0.24 – 0.30 (0.28, S), 0.44 – 0.64 (N)				1944			
FAOD *Hemidiscus karstenii*	11	0.42						633	
LOD *Actinocyclus ingens*	12	0.36 – 0.42 (0.38, S), 0.45 – 0.51 (N)						633	
LAOD *Actinocyclus ingens*	16	0.56 0.64 (N), 0.64 – 0.7 (S)				2143			
LOD *Thalassiosira elliptipora*	18	0.61 – 0.82						733	

**** Smear slides taken at segment boundaries † reworked***

Along the Eastern Indian Ocean Transect, the micropaleontological studies are mainly based on core catcher sediment samples and individual segment sediment samples. Age estimates reached 0.19 Ma (PS140_125-6 and PS140_126-1) to a potential of 0.82 Ma (PS140_123-5) in the transect. The poor preservation of diatom valves in core PS140_123-5 does not allow for any age assignment. Due to the lack of index diatom taxa, the biostratigraphic age assignment was impossible for cores PS140_124-1, PS140_130-1, PS140_131-5, and PS140_132-4. The cores contain modern diatom assemblages throughout. The relative abundance of 1% *Thalassiosira elliptipora* (LOD) in cores PS140_123-5, PS140_129-5, and PS140_136-1 constrains the age to a maximum of 0.82 Ma.

Sample and data management

The entire international community involved in the planned expedition will have immediate and preferential access to the cruise report, to shipboard data and samples retrieved. The availability of expedition data and samples may remain restricted to others not directly involved in the project. After a moratorium period that protects the interests of the project partners, the scientific community will have access to data and samples.

In principle, AWI's research data policy follows the principles for the responsible handling of research data, which are based on the recommendations of the Helmholtz Association for guidelines on the management of research data, on the Guidelines of the European Commission on Data Management according to the FAIR principles and the guidelines of the Deutsche Forschungsgemeinschaft on handling research data.

AWI publishes at least the primary scientific data as soon as possible. The open-access cruise report is published shortly after the cruise in the AWI series "Reports on Polar and Marine Research". All data must be archived in a publicly accessible, citable long-term repository two years after collection. The archived data may be under moratorium for a maximum of two additional years. In addition, appropriate moratorium periods must be applied for and recorded

in the data management plan. After the embargo periods have expired, the data must be made public immediately and actively using the FAIR principles. All data connected to the sediment sampling (core photos, visual core descriptions) will be stored in the PANGAEA Data Publisher for Earth & Environmental Science database (https://www.pangaea.de), operated as an open-access library by the AWI and the Center for Marine Environmental Sciences, University of Bremen (MARUM) within two years after the end of the cruise at the latest. By default, the CC-BY license will be applied.

Sediment samples and cores collected during Polarstern expedition PS140 shall be archived in the AWI Core Repository, which is operated by the Marine Geology department since 1983. Cores are stored in sealed D-tubes at 4° C and an air humidity limited at 35 %. The repository is open to the scientific community for sampling after the moratorium periods ´and subject to ongoing work by the shipboard and shore-based PS140 Science Party.

Any other data will be submitted to an appropriate long-term archive that provides unique and stable identifiers for the datasets and allows open online access to the data.

This work contributes to the Helmholtz Research Programme “Changing Earth – Sustaining our Future” Topic 2, Subtopics 2.1, 2.2, 2.3, and 2.4. It further contributes to Topic 6, Subtopic 6.1 and 6.2.

In all publications, based on this cruise, the Grant No. AWI_PS140_03 will be quoted and the following Polarstern article will be cited: Alfred-Wegener-Institut Helmholtz-Zentrum für Polar- und Meeresforschung (2017) Polar Research and Supply Vessel POLARSTERN Operated by the Alfred-Wegener-Institute. Journal of large-scale research facilities, 3, A119. http://dx.doi.org/10.17815/jlsrf-3-163.

References

Adkins JF (2013) The role of deep ocean circulation in setting glacial climates. Paleoceanogr 28:539–561. https://doi.org/10.1002/palo.20046

Anderson RF, Ali S, Bradtmiller LI, Nielsen SHH, Fleisher MQ, Anderson BE, Burckle LH (2009) Wind-driven upwelling in the Southern Ocean and the deglacial rise in atmospheric CO_2. Science 323: 1443–1448. https://doi.org/10.1126/science.1167441

Best AI, Gunn DE (1999) Calibration of marine sediment core loggers for quantitative acoustic impedance studies. Mar Geol 160:137–146. https://doi.org/10.1016/S0025-3227(99)00017-1

Borchers A, Dietze E, Kuhn G, Esper O, Voigt I, Hartmann K, Diekman, B (2016) Holocene ice dynamics and bottom-water formation associated with Cape Darnley polynya activity recorded in Burton Basin, East Antarctica. Mar Geophys Res 37(1), 49-70. https://doi.org/10.1007/s11001-015-9254-z

Chapman CC, Lea MA, Meyer A, Sallée JB, Hindell M (2020) Defining Southern Ocean fronts and their influence on biological and physical processes in a changing climate. Nat Clim Change 10(3):209–219. https://doi.org/10.1038/s41558-020-0705-4

Chase Z, Anderson RF, Fleisher MQ, Kubik PW (2003) Accumulation of biogenic and lithogenic material in the Pacific sector of the Southern Ocean during the past 40,000 years. Deep-Sea Research Part II: Topical Studies in Oceanography 50:799–832. https://doi.org/10.1016/s0967-0645(02)00595-7

Clark PU, He F, Golledge NR, Mitrovica JX, Dutton A, Hoffman JS, Dendy S (2020) Oceanic forcing of penultimate deglacial and last interglacial sea-level rise. Nature 577(7792):660–664. https://doi.org/10.1038/s41586-020-1931-7

Depoorter MA, Bamber JL, Griggs JA, Lenaerts JTM, Ligtenberg SRM, van den Broeke MR, Moholdt G (2013) Calving fluxes and basal melt rates of Antarctic ice shelves. Nature 502:89–92. https://doi.org/10.1038/nature12567

Esper O, Gersonde R (2014a) Quaternary surface water temperature estimations: New diatom transfer functions for the Southern Ocean. Palaeogeogr, Palaeoclimatol, Palaeoecol 414:1–19. https://doi.org/10.1016/j.paleo.2014.08.008

Esper O, Gersonde R (2014b) New tools for the reconstruction of Pleistocene Antarctic sea ice. Palaeogeogr Palaeoclimatol Palaeoecol 399:260–283. https://doi.org/10.1016/j.palaeo.2014.01.019

Fretwell P, Pritchard HD, Vaughan DG, Bamber JL, Barrand NE, Bell R, Bianchi C, Bingham RG, Blankenship DD, Casassa G, Catania G, Callens D, Conway H, Cook AJ, Corr HFJ, Damaske D, Damm V, Ferraccioli F, Forsberg R, Fujita S, Gim Y, Gogineni P, Griggs JA, Hindmarsh RCA, Holmlund P, Holt JW, Jacobel RW, Jenkins A, Jokat W, Jordan T, King EC, Kohler J, Krabill W, Riger-Kusk M, Langley KA, Leitchenkov G, Leuschen C, Luyendyk BP, Matsuoka K, Mouginot J, Nitsche FO, Nogi Y, Nost OA, Popov SV, Rignot E, Rippin DM, Rivera A, Roberts J, Ross N, Siegert MJ, Smith AM, Steinhage D, Studinger M, Sun B, Tinto BK, Welch BC, Wilson D, Young DA, Xiangbin C, Zirizzotti A (2013) Bedmap2: improved ice bed, surface and thickness datasets for Antarctica. The Cryosphere 7:375–393. https://doi.org/10.5194/tc-7-375-2013

Fyfe JC, Saenko OA (2006) Simulated changes in the extratropical Southern Hemisphere winds and currents. Geophys Res Let 33(6). https://doi.org/10.1029/2005GL025332

Gunn DE, Best AI (1998) A new automated non-destructive system for high resolution multi-sensor core logging of open sediment cores. Geo Mar Let 18:70–77. https://doi.org/10.1007/s003670050054

Hasenfratz AP, Jaccard SL, Martinez-Garcia A, Sigman DM, Hodell DA, Vance D, Bernasconi SM, Kleiven HF, Haumann FA, Haug GH (2019) The residence time of Southern Ocean surface waters and the 100,000-year ice age cycle. Science 363:1080–1084. https://doi.org/10.1126/science.aat7067

Ho SL et al (2014) Appraisal of TEX86 and thermometries in subpolar and polar regions. Geochim Cosmochim Acta 131:213–226. https://doi.org/10.1016/j.gca.2014.01.001

Huang H, Gutjahr M, Eisenhauer A, Kuhn G (2020) No detectable Weddell Sea Antarctic Bottom Water export during the Last and Penultimate Glacial Maximum. Nature Com 11, 424. https://doi.org/10.1038/s41467-020-14302-3

Klages JP, Kuhn G, Hillenbrand CD, Graham AG, Smith JA, Larter RD, Gohl K (2016). A glacial landform assemblage from an inter-ice stream setting in the eastern Amundsen Sea Embayment, West Antarctica. Geol Soc Lond Mem 46:349–352. https://doi.org/10.1144/M46.147

Klages JP et al. (2017) Limited grounding-line advance onto the West Antarctic continental shelf in the easternmost Amundsen Sea Embayment during the last glacial period. PLOS ONE 12(7): (e0181593). https://doi.org/10.1371/journal.pone.0181593

Lamping N, Müller J, Hefter J, Mollenhauer G, Haas C, Shi X, Vorrath ME, Lohmann G, Hillenbrand CD (2021) Evaluation of lipid biomarkers as proxies for sea ice and ocean temperatures along the Antarctic continental margin. Clim Past 17:2305–2326. https://doi.org/10.5194/cp-17-2305-2021

Lamy F, Arz HW, Kilian R, Lange CB, Lembke-Jene L, Wengler M, Kaiser J, Baeza-Urrea O, Hall IR, Harada N, Tiedemann R (2015) Glacial reduction and millennial-scale variations in Drake Passage throughflow. Proceedings of the National Academy of Sciences 112:13496–13501. https://doi.org/10.1073/pnas.1509203112.

Marshall J and Speer K (2012) Closure of the meridional overturning circulation through Southern Ocean upwelling. Nature Geosci 5, 171-180. https://doi.org/10.1038/ngeo1391

Martinez-Boti MA, Marino G, Foster GL, Ziveri P, Henehan MJ, Rae JWB, Mortyn PG, Vance D (2015) Boron isotope evidence for oceanic carbon dioxide leakage during the last deglaciation. Nature 518: 219–222. https://doi.org/10.1038/nature14155

Marsaglia K, Milliken K, Doran L (2013) IODP digital reference for smear slide analysis of marine mud. Part 1: Methodology and atlas of siliciclastic and volcanogenic components. IODP Technical Note 1. https://doi.org/10.2204/iodp.tn.1.2013

Marsaglia K, Milliken K, Leckie RM, Tentori D, Doran L (2015) IODP Smear Slide Digital Reference for Sediment Analysis of Marine Mud. Part 2: Methodology and Atlas of Biogenic Components. IODP Technical Note 2. https://doi.org/10.14379/iodp.tn.2.2015

Mazaud A, Michel E, Dewilde F, Turon JL (2010) Variations of the Antarctic Circumpolar Current intensity during the past 500 ka. Geochem Geophys Geosyst 11, Q08007. https://doi.org/10.1029/2010gc003033

Mazullo J, Graham AG (1988) Handbook for shipboard sedimentologists. Ocean Drilling Programm Technical Note No. 8, Texas A&M University, College Station, U.S.A. https://doi.org/10.2973/odp.tn.8.1988

Moy AD, Palmer MR, Howard WR, Bijma J, Cooper MJ, Calvo E, Pelejero C, Gagan MK, Chalk TB (2019) Varied contribution of the Southern Ocean to deglacial atmospheric CO_2 rise. Nature Geoscience 12:1006–1011. https://doi.org/10.1038/s41561-019-0473-9

Nürnberg D, Müller A, Schneider RR (2000) Paleo-sea surface temperature calculations in the equatorial east Atlantic from Mg/Ca ratios in planktic foraminifera: A comparison to sea surface temperature estimates from U37K‘, oxygen isotopes, and foraminiferal transfer function. Paleoceanogr 15(1): 124–134. https://doi.org/10.1029/1999PA000370

Nürnberg D, Groeneveld J (2006) Pleistocene variability of the Subtropical Convergence at East Tasman Plateau: Evidence from planktonic foraminiferal Mg/Ca (ODP Site 1172A). Geoche Geophys Geosyst 7:Q04P11. https://doi.org/10.1029/2005gc000984

Park E, Hefter J, Fischer G, Iversen MH, Ramondenc S, Nöthig EM, Mollenhauer G (2019) Seasonality of archaeal lipid flux and GDGT-based thermometry in sinking particles of high-latitude oceans: Fram Strait (79°N) and Antarctic Polar Front (50°S). Biogeosci 16:2247–2268. https://doi.org/10.5194/bg-16-2247-2019

Pritchard HD, Ligtenberg SRM, Fricker HA, Vaughan DG, van den Broeke MR, Padman L (2012) Antarctic ice-sheet loss driven by basal melting of ice shelves. Nature 484:502–505. https://doi.org/10.1038/nature10968

Raymo ME, Mitrovica JX (2012) Collapse of polar ice sheets during the stage 11 interglacial. Nature 483(7390):453–456. https://doi.org/10.1038/NGEO1118

Rickli J, Gutjahr M, Vance D, Fischer-Gödde M, Hillenbrand CD, Kuhn G (2014) Neodymium and hafnium boundary contributions to seawater along the West Antarctic continental margin. Earth Planet Sci Lett 394, 99-110. https://doi.org/10.1016/j.epsl.2014.03.008

Sigman DM, Hain MP, Haug GH (2010) The polar ocean and glacial cycles in atmospheric CO_2 concentration. Nature 466:47–55. https://doi.org/10.1038/nature09149

Sokolov S, Rintoul SR (2009) Circumpolar structure and distribution of the Antarctic Circumpolar Current fronts: 1. Mean circumpolar paths. J Geophys Res Oceans, 114(C11). https://doi.org/10.1029/2008JC005108

Talley LD (2013) Closure of the Global Overturning Circulation Through the Indian, Pacific, and Southern Oceans: Schematics and Transports. Oceanogr 26:80–97. https://doi.org/0.5670/oceanog.2013.07

Vorrath ME, Müller J, Esper O, Mollenhauer G, Haas C, Schefuß E, Fahl K (2019) Highly branched isoprenoids for Southern Ocean sea ice reconstructions: a pilot study from the Western Antarctic Peninsula. Biogeosci 16:2961–2981. https://doi.org/10.5194/bg-16-2961-2019

Wåhlin AK, Steiger N, Darelius E, Assmann KM, Glessmer MS, Ha HK, Herraiz-Borreguero L, Heuzé C, Jenkins A, Kim TW, Mazur AK, Sommeria J, Viboud S (2020) Ice front blocking of ocean heat transport to an Antarctic ice shelf. Nature 578:568–571. https://doi.org/10.1038/s41586-020-2014-5

Williams GD, Nicol S, Aoki S, Meijers AJS, Bindoff NL, Iijima Y, Marsland SJ, Klocker A (2010) Surface oceanography of BROKE-West, along the Antarctic margin of the south-west Indian Ocean (30–80°E). Deep Sea Res II: Top Stud Oceanogr 57:738–757. https://doi.org/10.1016/j.dsr2.2009.04.020

Wilson DJ, Bertram RA, Needham EF, van de Flierdt T, Welsh KJ, McKay RM, Mazumder A, Riesselman CR, Jimenez-Espejo FJ, Escutia C (2018) Ice loss from the East Antarctic Ice Sheet during late Pleistocene interglacials. Nature 561:383–386. https://doi.org/10.1038/s41586-018-0501-8

Wu S, Lembke-Jene L, Lamy F, Arz HW, Nowaczyk N, Xiao, W, Zhang X, Hass HC, Titschack J, Zheng X, Liu J, Dumm L, Diekmann B, Nürnberg D, Tiedemann R, Kuhn, G (2021). Orbital-and millennial-scale Antarctic Circumpolar Current variability in Drake Passage over the past 140,000 years. Nature Com 12(1):3948. https://doi.org/10.1038/s41467-021-24264-9

Wu S, Kuhn G, Arz HW, Lembke-Jene L, Tiedemann R, Lamy F, Diekmann B (2022) Late Quaternary terrigenous sediment supply in the Drake Passage in response to Patagonian and Antarctic ice dynamics. Global Planet Change 104024. https://doi.org/10.1016/j.gloplacha.2022.104024.

Zielinski, U (1993) Quantitative Bestimmung von Paläoumweltparametern des Antarktischen Oberflächenwassers im Spätquartär anhand von Transferfunktionen mit Diatomeen = Quantitative estimation of palaeoenvironmental parameters of the Antarctic surface water in the Late Quaternary using transfer functions with diatoms , PhD thesis, Bremen, Univ., Diss., 1993. Ber Polarforschung 126:1–148. http://hdl.handle.net/10013/epic.10127.d007

Zielinski U, Gersonde, R (2002). Plio–Pleistocene diatom biostratigraphy from ODP Leg 177, Atlantic sector of the Southern Ocean. Mar Micropaleontol 45(3-4):225–268. https://doi.org/10.1016/S0377-8398(02)00031-2

6. LAND GEOLOGY AND GEODESY

Martin Melles[1], Niklas Leicher[1], Jacob Feller[1], Benjamin Schröter[2], Matt Jeromson[3], Goran Boren[4], Marcus Gutjahr[5]

not on board: Sonja Berg[1], Bernd Wagner[1], Mirko Scheinert[2], Duanne White[3], Krystyna Saunders[6], Matt King[7], Kate Selway[7], Tobias Stål[7], Anya Reading[7], Damian Gore[8], John Gibson[9]

[1]DE.University of Cologne
[2]DE.Dresden Univ of Technology
[3]AU.University of Canberra [4]AU. University Adelaide
[5]DE.GEOMAR Kiel
[6]AU.ANSTO Sydney
[7]AU.Univ. of Tasmania, Hobart
[8]AU.Macquarie Univ. Sydney
[9]AU.Austr. Antarctic Div., Hobart

Grant-No. AWI_PS140_04

Outline

Geological and geodetic field work on land within the scope of the expedition PS140 (EASI- 2) was concentrated on the Vestfold Hills, an ice-free area of 413 km^2 in Princess Elizabeth Land at the eastern margin of Prydz Bay (Figs. 6.1 and 6.2B). A temporary field camp was set up there and used to core lake and fjord sediment records and to obtain complementary data and samples on land, with the overall objective to contribute to a better understanding of the glacial, climatic and sea-level histories of the region (see Subchapter 6.1). Subsequently, the Gaussberg in Wilhelm II Land (GAUS), Gillis Island in Queen Mary Land (CAD3) and Bunger Hills in Wilkes Land (Fig. 6.1) were visited on day trips by helicopter in order to maintain and set up GNSS (Global Navigation Satellite Systems) stations, sample erratics for exposure dating or sample sediment-bearing ice for sediment provenance analyses (see Subchapter 6.2).

The field work in Vestfold Hills was conducted by a group of six persons from the University of Cologne and the Technical University Dresden, Germany, as well as the University of Canberra and the University Adelaide, Australia. The work was logistically supported by the Australian Antarctic Expedition (AAD), which operates the research station “Davis” in the Vestfold Hills (Fig. 6.2). And it was complemented by the sampling of sediment-bearing ice at five localities under involving the GEOMAR in Kiel, Germany. The analyses of the data and samples obtained will involve additional scientists from additional institutions.

6.1 Ice sheet instability in Vestfold Hills – history and control

Objectives

The Prydz Bay is a key area to investigate the stability or instability of the East Antarctic Ice Sheet (EAIS). This bay forms the terminus of the Lambert Glacier-Amery Ice Shelf ice-drainage system, which drains about 16 % of the grounded EAIS (Fricker et al., 2000). The topography of Prydz Bay is highly overdeepened, landward sloping and relatively smooth at 100 km scales, making the area particularly prone to marine ice-sheet instability (White et al., 2022). Marine geological data and ice sheet models provide a basic understanding of the large-scale areal extent and flow pattern of the EAIS on the Prydz Bay shelf during the Last Glacial Maximum (LGM) and deglaciation (e.g., Domack et al., 1998; Golledge et al., 2012; Guitard et

al., 2016). However, the data base still is rather poor with respect to the chronology of the reconstructed changes. Moreover, very little is known about past ice thicknesses, postglacial ice advances, and the regional climatic and sea-level changes that may have influenced the glacial history. This information can best be obtained by comprehensive paleoenvironmental investigations in currently ice-free areas along the Antarctic coastline, which are most proximal to the current ice edge, such as the Vestfold Hills (Fig. 6.2).

The fieldwork in Vestfold Hills on PS140 aimed at a better understanding of the regional glacial history and the factors that have controlled past glaciological changes.

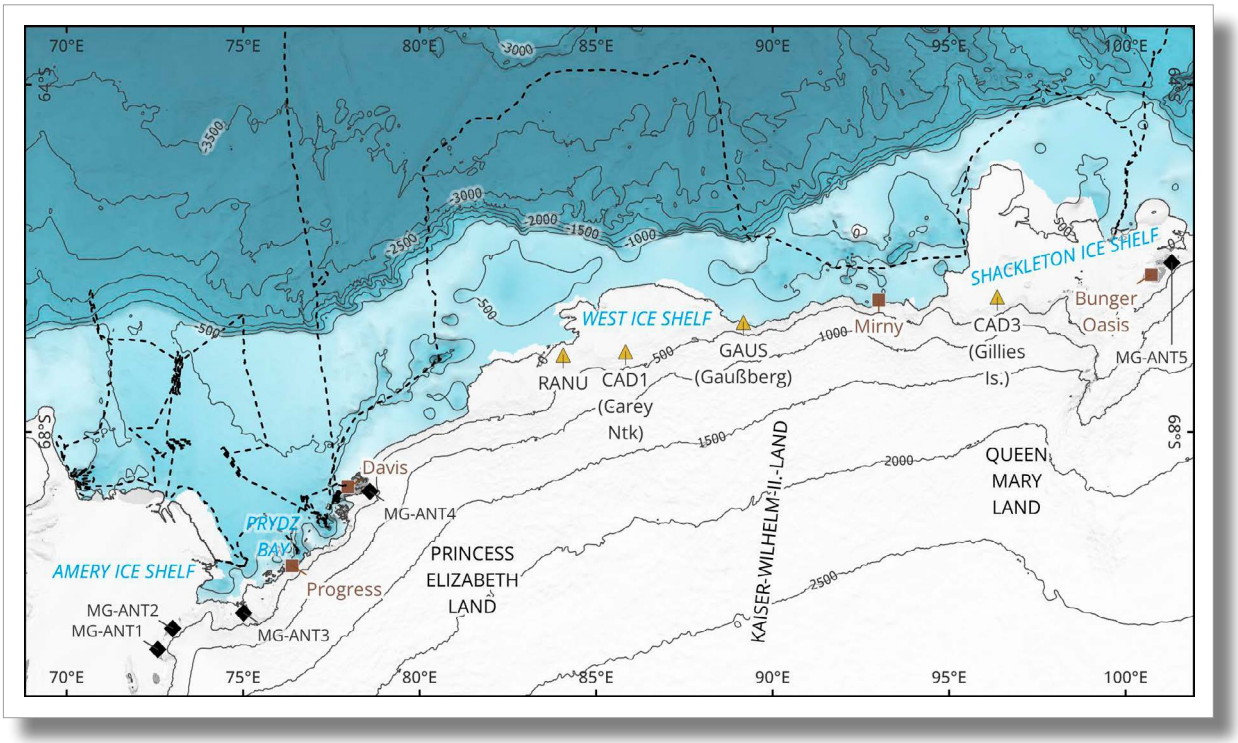

Fig. 6.1: Overview map showing the location of Vestfold Hills, the main land working area on PS140, along with the offshore bathymetry and cruise track of Polarstern and other geographical terms and locations mentioned in the text.

They are driven by the hypotheses that the Late Quaternary ice sheet history of the oasis was more complex than indicated by the existing dataand that the ice sheet dynamics were controlled by internal as well as external forcing mechanisms. These hypotheses shall be tested by answering the following central research questions:

Q1 What was the maximum extent and thickness of the LGM ice coverage?

It is not yet clear, whether Vestfold Hills was entirely ice covered during the LGM (White et al., 2022). Gibson et al., (2009) deduced ice-free settings at the northwestern corner of the oases from presumed continuous sedimentation in a saline lake. This, however, has not yet been confirmed by geomorphological features or cosmogenic exposure ages in that area, and it is in conflict with an ice thickness of more than ~500 m that has been modelled based on relative uplift curves (e.g., Zwartz et al., 1998).

Q2 When and how quick did deglaciation commence, how far did the ice retreat, and did ice re-advances take place?

The ice retreat over currently ice-free areas of Vestfold Hills is to some degree tracked by maximum ^{14}C ages of postglacial sediments and cosmogenic exposure ages (e.g., White et al., 2022). Very little, on the other hand, is known about potential ice sheet re-advances. The only one documented is the Chelnok Advance of the Sørsdal Glacier to the south of Vestfold (Fig. 6.2B), which probably had a minor lateral expansion and still is poorly dated (e.g., Kiernan et al., 2002). Ice retreats beyond the modern ice margin, which are known to have occurred in other East Antarctic oases (e.g., Goodwin 1996), have not yet been detected in Vestfold Hills.

Q3 Did unglaciated areas also exist during MIS 3 or earlier warm phases?

There is no evidence yet for the existence of ice-free areas in Vestfold Hills prior to the LGM. For Marine Isotope Stage (MIS) 3, ice sheet models hindcast an expanded EAIS, largely driven by lower sea levels and reduced rates of sub-ice shelf melt (e.g. Pollard & Deconto, 2009). However, this is in contrast to MIS 3 raised beaches in Lützow-Holm Bay (~40°E; Miura et al., 1998) and MIS 3 lake sediments in Rauer Group (to the west of Vestfold; Berg et al., 2016). Pre-LGM sediments were also cored in Windmill Islands (~110°E; Cremer et al., 2003), but their dating to MIS 3 or an earlier interglacial is ambiguous.

Q4 Did local climatic changes initiate or follow ice retreats and advances?

The mid-Holocene ice margin retreat in Vestfold Hills correlates with increased temperatures, which are indicated in diatom assemblages and foraminifera concentrations (e.g., White et al., 2022; McMinn et al., 2001; Gibson et al., 2009). However, the age control is insufficient to identify leads or lags, i.e. it is not solved yet, whether the ice retreat was caused by the temperature rise, due to increasing melt rates, or has led to the temperature rise, due to additional exposure of dark land areas. Moreover, nothing is known about temperature changes during earlier movements of the ice margin and about potential influences of regional precipitation changes on the ice sheet behaviour.

Q5 What do changes in relative sea level reveal about the glacial history?

Changes in the relative sea level in coastal areas of Antarctica on the one hand provide information on former ice loads, due to glacial-isostatic adjustment (GIA) of the crust (e.g., Whitehouse et al., 2012), and on the other hand may influence the ice sheet behaviour by changing grounding line positions. In Vestfold Hills, relatively detailed information on past sea-level changes was already obtained from raised beaches and abandoned penguin colonies on land, as well as marine sediments in modern lakes and lacustrine sediments in modern marine basins (e.g., Zwartz et al., 1998; Hodgson et al., 2016). However, the available data still have larger gaps, in particular concerning the late glacial history, when sea level was below modern, and are not sufficiently well traced by the available GIA models.

Q6 Did the sea-ice coverage and oceanic circulation on the shelf influence the ice sheet dynamics in Vestfold?

In contrast to other oases such as Bunger Hills, the Vestfold Hills are in direct contact with the open ocean (Figs. 6.1 and 6.2B). Nonetheless, it has never been investigated which influence the oceanic properties had on the glacial history of the oasis. Possible impacts include warm-water intrusions with associated subaquatic ice melt (e.g., Pritchard et al., 2012) and the stabilization of the ice margin against calving by the sea-ice cover (Gomez-Fell et al., 2022).

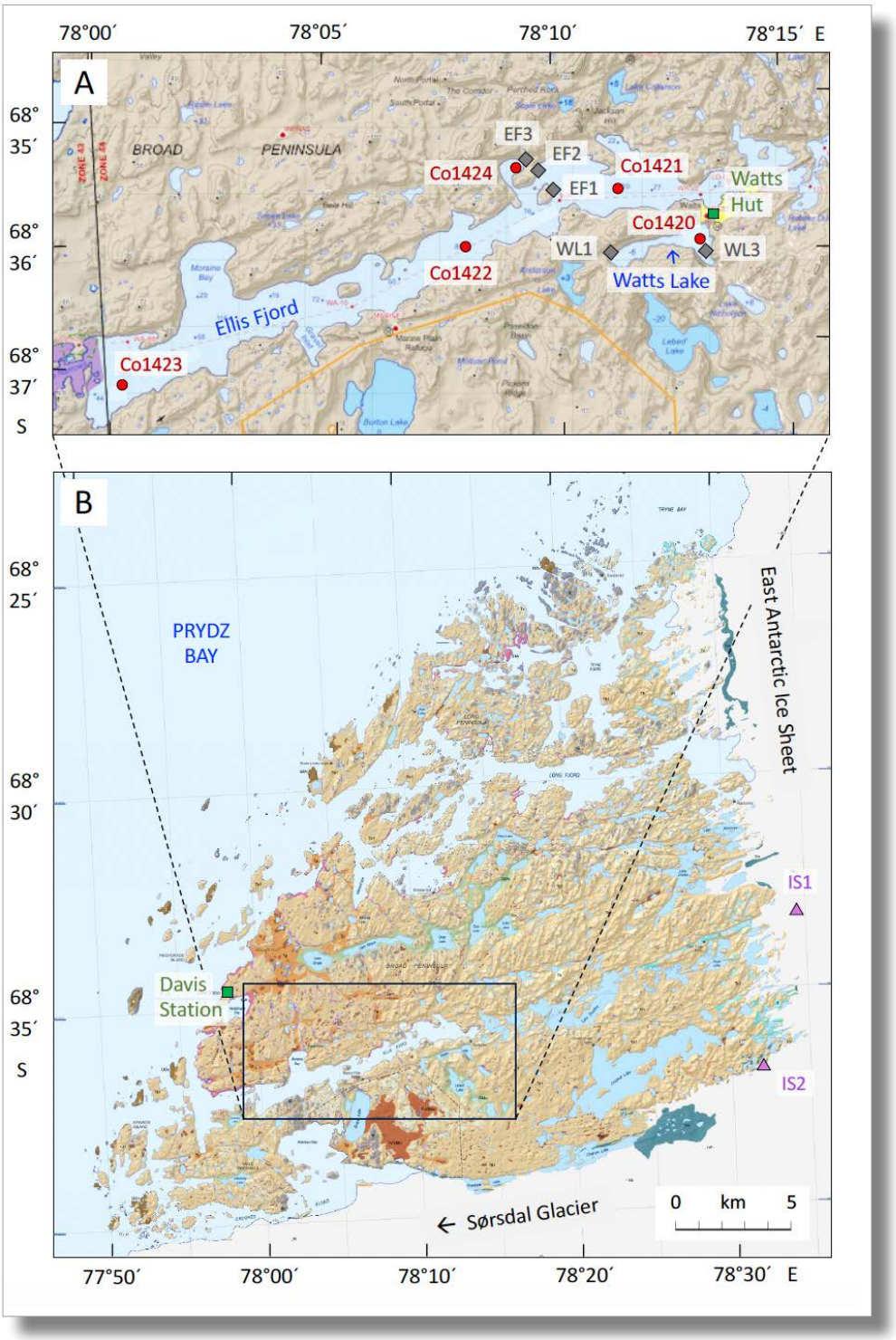

Fig. 6.2. (A) Map of the main working area in the southern part of Vestfold Hills (after Australian Antarctic Data Center 2021a and b) and (B) overview map of the entire Vestfold Hills (after McLennan et al., 2020), showing the locations of Davis Station and Watts Hut (green squares), lake and fjord sediment cores (red circles), samples from raised beach ridges (grey diamonds) and samples of sediment-bearing ice (violet triangles). Station IS2 corresponds to MG-ANT3 (see Tab. 6.10).

Q7 Which impacts did glaciological and morphological characteristics have on the glacial history?

Deglaciation and postglacial advances of the EAIS, as documented on the shelf and in ice-free coastal areas, were clearly asynchronous (Mackintosh et al., 2014). This may be due to individual climatic and relative sea-level histories in the different regions, but also to glaciological and morphological peculiarities. For instance, the more rapid post-LGM ice retreat at Vestfold Hills compared to other oases may be due to the over-deepened Svenner Channel on the adjacent shelf (O´Brien et al., 2015), which may have supported the grounding line retreat and subglacial erosion. Further support may have come from the fast-flowing Sørsdal Glacier to the south of Vestfold Hills, since dynamic outlet glaciers are believed to be more sensitive to climate and sea-level changes than areas with slow ice-sheet flow (White et al., 2011).

Work conducted and preliminary results

Field work in the Vestfolds Hills was carried out for 19 days, from 17 December 2023 to 4 January 2024, from a field camp that was set up at Watts Hut of the AAD (Figs. 6.2A and 6.3). Transport between *Polarstern* and the camp was by helicopters stationed onboard *Polarstern*. The freight, consisting of field equipment, consumables and personnel, comprised a total of ca. 3.6 tons. Local transport was on foot and on Ellis Fjord by snowmobile.

Lake and fjord sediment coring

Sediment coring was conducted at Watts Lake and at Ellis Fjord (Fig. 6.2A), using the 1.5 to 1.6 m thick lake and fjord ice cover as platform. The sediment records were recovered by gravity corer (GC) and percussion piston corer (PC, both UWITEC, Austria), which were operated with a tripod through ice holes of 10-inch diameter that were drilled with a motorized ice auger (Eskimo, USA) (Fig. 6.4A, B).

Fig. 6.3: Field camp at Watts Hut in the southern part of Vestfold Hills (for location see Fig. 6.2A): (A) view from the east, with Watts Lake at the left margin, (B) view from the west, with Lake Druzhby in the back

The gravity corer was employed for proper sampling of the sediment-water boundary and the soft uppermost sediment decimeters (Fig. 6.4C). The corer is run with transparent PVC tubes of 120 or 60 cm length and 6.3 cm outer diameter, equipped with one or two weights of about 4 kg each, depending on sediment properties. The corer sinks into the sediment by its own weight. During pull out, the upper end of the core tube is closed by a lid and a ball is towed underneath the lower end by an elastic strap, acting as a core catcher.

Deeper sediments were recovered with the percussion piston corer. This corer consists of 3 m long core barrels and an inner PVC tube (liner) of 6.3 cm outer diameter. The corer can sample sediments from defined depths by controlled release of the piston, which is fixed in the core cutter at the lower end of the corer during its way through both the water column and overlaying deposits. By recovering successive or overlapping sediment sections, sequences of more than 3 m can be obtained. Matching and correlation of overlapping core parts can lead to continuous composite cores without core gaps due to core catcher or core losses. Table 6.1 and Figure 6.5 provide overviews of the core segments recovered in Vestfold Hills at PS140 (EASI-2). There, piston cores from overlapping sections were alternately taken through ice holes some 5 m away from each other, in order to exclude coring of sediments that became disturbed by the core run before.

The piston corer is deployed with three ropes, which are operated by hand winches (Fig. 6.4A): (i) With one rope (5 mm kevlar) the piston corer is moved through the water column and pulled out of the sediment at the end of the coring process. For a reduced load, this rope is run by a pulley tackle with an idler pulley at the top of the gear. (ii) A second rope (8 mm plastic) is used to lift and drop a hammer weight that slides along a hammer rod and forces the corer in deeper sediments when pitching a basal plate at the lower rod end. Extension rods can be screwed in between the hammer rod and the core barrel to ensure that the hammering takes place in the water column and not in the sediment. (iii) The third rope (5 mm steel) is connected to the piston. By fixing the rope and building up tension on it by further lowering the gear releases the piston in the core cutter and lets the corer slide along the piston into the sediments to be sampled. In this way, a negative pressure is built up in the tube, supporting the retrieval of an undisturbed, representative sediment sequence.

To prevent sediment loss at the base of the coring tube the piston corer was operated with two different core catchers. In most cases, a hydraulic catcher was employed, which closes the corer, when the piston reaches the head of the coring tube. There, the piston displaces remaining water and pumps it between the liner and the core tube into a rubber sleeve in the catcher, which inflates and thereby closes the core tube. According to this construction, this core catcher can work only if the core tube is completely filled with sediment, in order to reach its final position within the head. Moreover, the rubber sleeve can be disturbed by coarse angular particles. Hence, whenever it was expected that the coring process stops earlier or that particularly coarse-grained sediments will be penetrated, as being the case for core segments Co1420-14 and Co1423-7 (Tab. 6.1), a core catcher was used consisting of flexible steel lamella attached to the inner wall of a metal cylinder at its lower end. When using this core catcher, the sediment pushes the lamella against the cylinder wall during penetration, but is held in the core tube by the closing of the lamella on withdrawal.

Fig. 6.4: Photos from Ellis Fjord illustrating parts of the work techniques.
(A) Piston coring with the tripod through an ice hole, (B) drilling the 1.5 to 1.6 m thick ice cover,
(C) gravity core showing clear bottom water above undisturbed surface sediment,
(D) transport of parts of the technique to the next coring site.

For initial observations of grain-size distribution, diatom assemblages and possible lithological changes, a total of 21 smear slides were prepared from the core catcher samples on *Polarstern*, and inspected with a light microscope at 10x and 40x magnification.

Watts Lake

Watts Lake to the south of Watts Hut today has a length of about 1.6 km and is separated by a narrow sill into two basins (Fig. 6.2A). The surface area amounts to 0.38 km^2 and the lake level is located 5.8 m below sea level (Pickard et al., 1986). Watts Lake has a salinity of 2.2 to 2.5 ‰ (Gibson et al., 1998; Roberts & McMinn 1998). The maximum water depth recorded is 35.9 m and the water column has been found thermally stratified with an anoxic layer below 29 m depth (Pickard et al., 1986) but also holomictic (Roberts & McMinn 1998).

Tab. 6.1: Sediment cores recovered during PS140 from Watts Lake and Ellis Fjord by gravity corer (GC) and percussion piston corer (PC). The indicated recovery excludes the core catcher samples at the bottom of piston cores, which are of about 10 cm long.

Core no. Site	- Run	Lake/ Fjord	Position Latitude [S]	Position Longitude [E]	Water depth [m]	Date	Gear	Recovery from - to [cm]
Co1420	-1	Watts Lake	68°36´12.0´´	78°13´11.1´´	35.9	18.12.2023	GC	0 - 76
	-2					19.12.2023	GC	0 - 75
	-3					19.12.2023	GC	0 - 46
	-4					19.12.2023	PC	0 - 292
	-5					19.12.2023	PC	300 - 597
	-6					20.12.2023	PC	600 - 889
	-7					20.12.2023	PC	900 - 1192
	-8					21.12.2023	PC	1200 - 1313
	-9					21.12.2023	GC	0 - 70
	-10					21.12.2023	PC	0 - 252
	-11					22.12.2023	PC	200 - 495
	-12					22.12.2023	PC	500 - 796
	-13					22.12.2023	PC	800 - 1092
	-14					22.12.2023	PC	1100 - 1136
Co1421	-1	Ellis Fjord	68°35´45.4´´	78°11´27.5´´	110.0	23.12.2023	GC	0 - 87
	-2					24.12.2023	GC	54 - 158
	-3					24.12.2023	GC	4 - 117
	-4					24.12.2023	GC	0 - 106
	-5					24.12.2023	PC	0 - 277
	-6					24.12.2023	PC	100 - 392
	-7					25.12.2023	PC	300 - 573
	-8					26.12.2023	PC	500 - 791
	-9					27.12.2023	PC	700 - 976
	-10					27.12.2023	PC	900 - 1190
	-11					27.12.2023	PC	1100 - 1254
Co1422	-1	Ellis Fjord	68°36´10.7´´	78°08´04.9´´	85.2	28.12.2023	GC	0 - 99
	-2					28.12.2023	GC	0 - 90
	-3					28.12.2023	PC	0 - 245
	-4					29.12.2023	PC	100 - 391
	-5					29.12.2023	PC	300 - 588
	-6					29.12.2023	PC	500 - 789
Co1423	-1	Ellis Fjord	68°37´10.2´´	78°00´23.9´´	109.0	30.12.2023	GC	0 - 55
	-2					30.12.2023	GC	0 - 64
	-3					30.12.2023	PC	0 - 258
	-4					31.12.2023	PC	100 - 388
	-5					01.01.2024	PC	300 - 591
	-6					01.01.2024	PC	500 - 793
	-7					02.01.2024	PC	700 - 856
Co1424	-1	Ellis Fjord	68°35´32.0´´	78°09´12.0´´	4.8	02.01.2024	GC	0 - 45
	-2					02.01.2024	GC	0 - 32
	-3					02.01.2024	PC	0 - 289
	-4					02.01.2024	PC	300 - 592

Marine and lacustrine sediments exposed in the catchment prove that Watts Lake was a marine inlet during the early to mid Holocene (Adamson and Pickard 1983; Pickard et al., 1986). A sea-level highstand is well reflected by an erosional terrace about 9 m above present lake level (*cf*. Fig. 6.7C). Isostatic uplift isolated the inlet from the sea and led to the development of a fresh-water lake some time between 4700 and 2800 ^{14}C yr BP (Pickard et al., 1986). Subsequently, decreased melt-water supply caused a lowering of the lake level beneath sea level. The only core as yet available from Watts Lake was recovered from 33 m water depth in the eastern basin (Zwartz et al., 1998). The core has a length of 2.7 m and a basal age of 4700 ^{14}C yr BP. It suggests the transition from marine to freshwater in only 14 cm sediment depth, dated to have occurred between 3800 and 3400 ^{14}C yr BP.

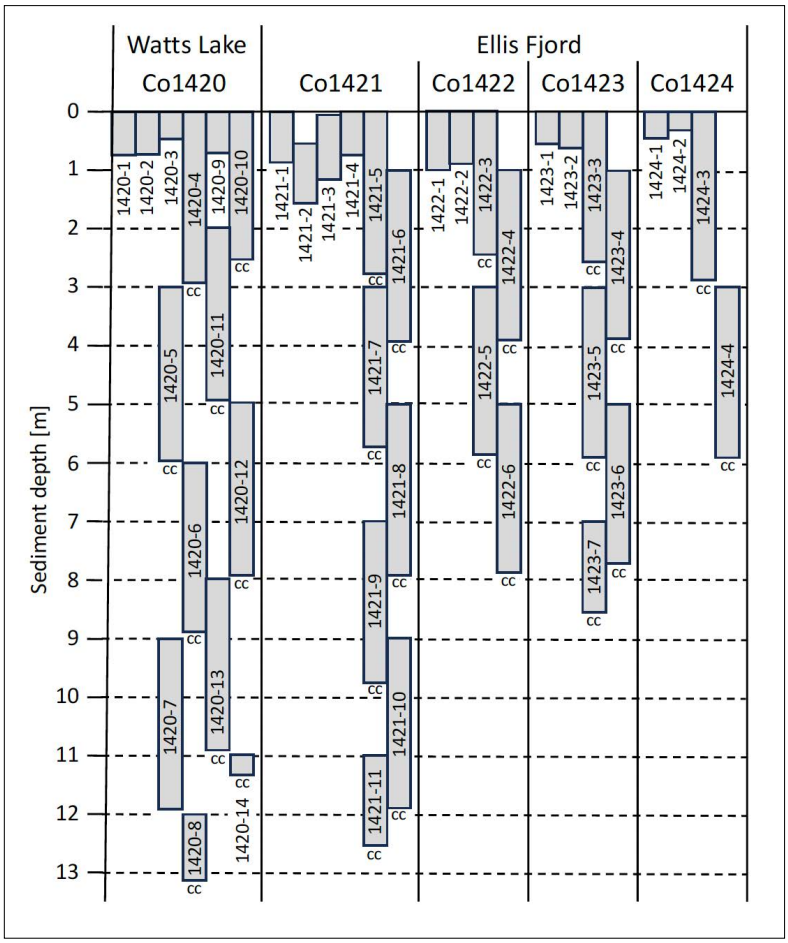

Fig. 6.5: Recovery of gravity cores and percussion piston cores (sediment in PVC tubes indicated by grey rectangles, core catcher material by cc) at the coring sites Co1420 to Co1424 in Watts Lake and Ellis Fjord.

Coring at site Co1420 in Watts Lake comprises four gravity cores and ten piston cores down to a sediment depth of 13.2 m (Tab. 6.1, Fig. 6.5). Until about 12 m depth the sediment mainly consists of dark greenish sapropels, which strongly smell of H_2S and reflect anoxic deposition. Marine diatoms in the respective core catcher samples, including the uppermost one (~3 m sediment depth), indicate a relatively recent transition from marine to lacustrine conditions, thereby supporting respective findings by Zwartz et al., (1998). Below ca. 12 m, clastic sediments of variable grain size were cored, which probably reflect deposition in a proglacial environment and may contain a till deposited from grounded ice.

Ellis Fjord

Ellis Fjord is a narrow, about 11 km long fjord between Mule Peninsula and Broad Peninsula in the southern Vestfold Hills (Fig. 6.1), which is ice covered for 11 to 12 months of the year. The bathymetry and hydrology of Ellis Fjord were first investigated in detail by Gallagher and Burton (1988). The data show that the fjord is subdivided into several basins with water depths of up to 117 m, which are separated by sills having depths of 1 to 30 m (Fig. 6.6). The fjord waters are full marine, showing increasing salinities with increasing depth. The two eastern-most basins are meromictic and have anoxic bottom waters. The degree of water mixing in Ellis Fjord is dependent on the degree of ice formation (Gibson 1999). Also the modern biology and sedimentation in the fjord are intensively studied and well understood (e.g., Marchant et al., 1987; Kirkwood and Burton 1988; McMinn and Hodgson 1993; McMinn et al., 1995, 1998; McMinn 1996).

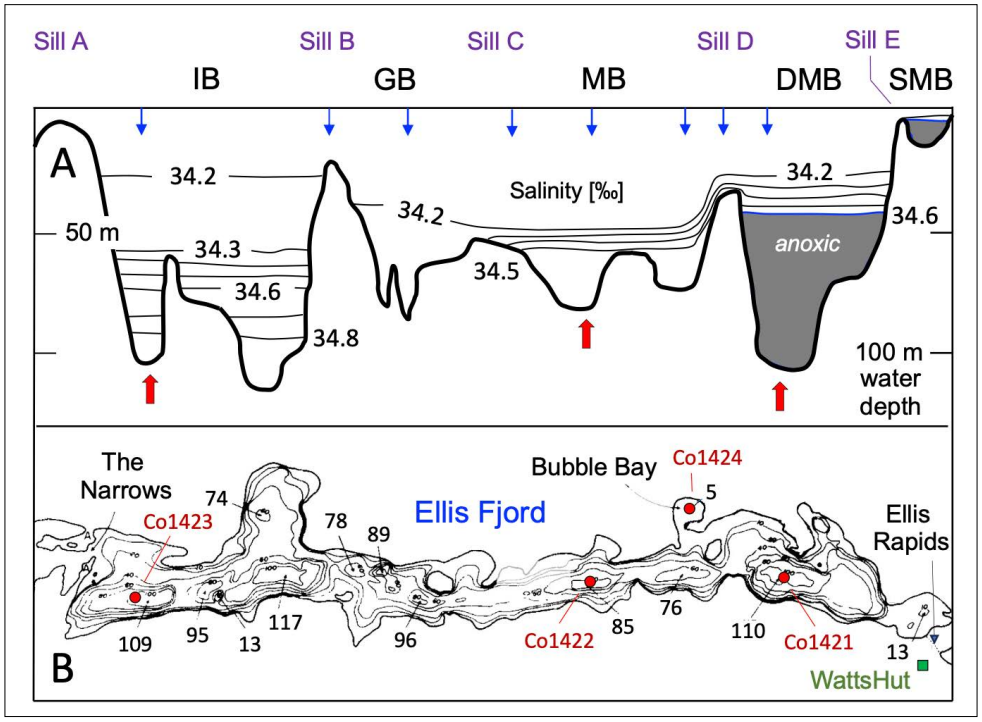

Fig. 6.6: Hydrological and bathymetric data from Gallagher and Burton (1988). (A) Salinity on 3 June 1985 along the axis of central and eastern Ellis Fjord, with the locations of hydrological stations (blue arrows), PS140 coring sites (red arrows) and the major basins (IB = Inner Basin, GB = Gravel Basin, MB = Middle Basin, DMB = Deep Meromictic Basin, SMB = Small Meromictic Basin) separated by sills (Sill A to Sill E). (B) Bathymetric map of central and eastern Ellis Fjord, with the locations of the PS140 coring sites (red dots)

Information on the history of Ellis Fjord is restricted to the late Holocene. It is based on the fossil assemblages (diatoms, dinoflagellates, sea urchins) as well as the organic and inorganic geochemistry of sediment cores of up to 4.1 m length and 4500 ^{14}C yr BP age, which were mainly taken from the anoxic basins in the eastern fjord (Bird et al., 1991; McMinn et al., 2001; Damsté et al., 2007; Boere et al., 2009). The results suggest that the deposition in Ellis Fjord during the late Holocene to a large extent was influenced by the sea-ice history, which in turn was controlled by changes in atmospheric temperatures.

On PS140 (EASI-2), coring on Ellis Fjord was carried out at four sites, three in deep basins and one in a small lagoon at the northern shore of the fjord (Figs. 6.2A and 6.6). At site Co1421 in

the Deep Meromictic Basin four gravity cores and seven overlapping piston cores provide a continuous sediment record down to 12.6 m depth (Tab. 6.1, Fig. 6.5). The sediment mainly consists of dark greenish sapropel. Sediment dominated by clastic components only occurs in the lowermost sediment decimeters, consisting of well sorted gravel in the core catcher. Similar successions, but with diamictons at the core bases, were recovered at sites Co1422 and Co1423 in the currently oxic Middle Basin and Inner Basin. These records comprise four and five piston cores, respectively, as well as two gravity cores each. At site Co1424 in the lagoon, which is named ´Bubble Bay´ in Gallagher and Burton (1988), two gravity cores were recovered, complemented by two piston cores. There, the piston cores do not overlap and do not reach clastic sediments underneath the sapropels cored.

Smear slides from the core catcher samples reveal that the sapropels in Ellis Fjord contain a diverse marine diatom community, including ice algae (*Eucampia Antarctica*), benthic diatoms (*Cocconeis stauroneiformis*) and planktonic diatoms (*Chaetoceros*) (O. Esper, pers. comm. 2024), as well as dinoflagellates, sponge spicules and foraminifera. Besides, poorly sorted and poorly rounded clastic components occur throughout all cores, increasing with depth and with proximity to the ocean. In the deepest core catcher samples from the clastic sediments the biogenic remains are much less if not absent.

Hence, the new coring of deep basins in Ellis Fjord for the first time provides sediment records spanning the entire fjord history since its deglaciation. The records shall shed new light on the deglaciation history along the 7.5 km long transect from Co1421 to Co1423 (Fig. 6.2A), but also on the postglacial ecological and climatic development of the fjord. The lagoon record from site Co1424, in contrast, only covers parts of the postglacial history. However, it nicely complements the deep basin cores by providing insights into the variability of shallow-water sedimentation, and it shall be compared to information that will be derived from raised beaches at its eastern shore (site EF3, see below).

Planned laboratory analyses and expected information

The sediment cores recovered from Watts Lake and Ellis Fjord were kept at slightly positive temperatures and stored in the dark until further processing in the laboratory. This applies to the PVC tubes as well as 50 ml vials, which were used to store single samples from the core catchers. The PVC tubes were cut into up to 1 m long pieces in the field, in order to fit into the foam boxes used for transport. They were sealed with plastic caps and tape to keep them water- and airtight.

The multi-disciplinary laboratory investigation of the sediment cores has different objectives in order to answer the research questions outlined and explained above. For instance, if one or more of the cores has penetrated into pre-glacial sediments, this would be the first evidence for ice-free areas prior to the LGM in the southern Vestfold Hills, allowing for investigations of the deposition times and of the environmental conditions that have existed (Q3). The oldest ages of the postglacial sediments in the cores probably will confirm at least partial ice coverage during the LGM (Q1) but also provide unprecedented information on the time of deglaciation at the individual sites and the speed of ice retreat between the sites (Q2). Whether the ice had retreated beyond the modern ice margin, and whether ice re-advances have taken place (Q2), shall be derived from facies changes (glacial, ice-proximal, ice-distal) in the sedimentary records. Besides, marine-limnic and limnic-marine transitions in the records, and the water depths at the sills separating the basins and subbasins, shall provide new information on the relative sea-level history of the oasis (Q5), which is rather well known for changes above the modern level during the Holocene, but not at all for the changes below the modern level during the Late Glacial (Zwartz et al., 1998; Hodgson et al., 2016). Finally, the sediment cores shall be

investigated for sedimentological, chemical and biogenic indications for climatic changes, both in temperature and precipitation, and their dependence on ice-sheet or ocean proximity (Q4).

The paleoenvironmental findings from Vestfold Hills shall eventually be put into a wider East Antarctic context, based on published data and new findings from the EASI expeditions PS128, PS140 and PS141. This on the one hand concerns the history of the adjacent ocean, in particular the sea-ice coverage and oceanic circulation and their potential impacts on the glacial history of the oasis (Q6). On the other hand, comparisons of the history but also glaciological and morphological characteristics of Vestfold Hills with respective information from other oases further east and west shall shed a new light on the impact of regional peculiarities on the stability of the EAIS on land (Q7).

Independent of the paleoenvironmental analyses, one gravity core each from the sites Co1420 in Watts Lake and Co1421 in the Deep Meromictic Basin of Ellis Fjord shall be analysed by Krystyna Saunders (ANSTO, Sydney) for plutonium (^{239}Pu and ^{240}Pu) concentrations and atom ratios (^{240}Pu/^{239}Pu). The analyses aim to test whether these anthropogenic radionuclides, which were released into the atmosphere by aerial nuclear weapon detonations between 1945 and 1980, have become deposited in the Antarctic environment, as proven to be the case for instance in Tasmania (Harrison et al., 2021). The analyses include lead-210 (^{210}Pb) measurements on the sediments to obtain the necessary sediment chronology and determine changes in sediment accumulation rates.

Surveys and sampling on land

Sampling of sediments in the catchment of Watts Lake

The investigation of the sediment record cored from deep waters in Watts Lake (see above) shall be compared to the findings made concerning the environmental history of this basin based upon marine and lacustrine sediments exposed in the lake´s catchment (Adamson and Pickard 1983; Pickard et al., 1986). In oder to complement these data, we took additional samples from four land sites, WL-1 and WL-2 at the northeastern lake shore and WL-3 and WL-4 at the southeastern lake shore (Fig. 6.7, Tab. 6.2).

Site WL-1 represents the highest elevation of marine sediments at the northeastern shore of Watts Lake. A basal diamicton was sampled there, as well as an overlaying orange sand and a marine, fossil-bearing sediment layer (Fig. 6.7A). Radiocarbon dating of calcareous fossils at the base of the marine sediments may provide good age control for the initial marine inundation of the basin following deglaciation. Similar information is expected from the radiocarbon age of a reddish shell, which was extracted from fossil-poor gravelly sand that overlays a basal diamicton at site WL-2 (Fig. 6.7B). Further upwards, the record at site WL-2 consists of orange sand and silty sand layers, which may have become formed by fluvial sediment supply, before a lacustrine stage developed that is clearly reflected by the formation of algae mats. Age control on the latter transitions shall be obtained by luminescence dating of the silty sand and radiocarbon dating of the lowermost algae mats.

At site WL-3, widely intact mollusc shells (probably *Laternula Elliptica*), often still connected, occur in growing/living position (Fig. 6.7C and -D) and were sampled. Upwards, the sediments contain successively less intact and more broken shells. At site WL-4 (Fig. 6.7E) the uppermost shell-bearing sediments were sampled from a dug trench in about 30 cm depth. Radiocarbon dating of the shell fragments and potentially other marine fossils may shed new light on the altitudes and times of the marine limit in the area of Watts Lake.

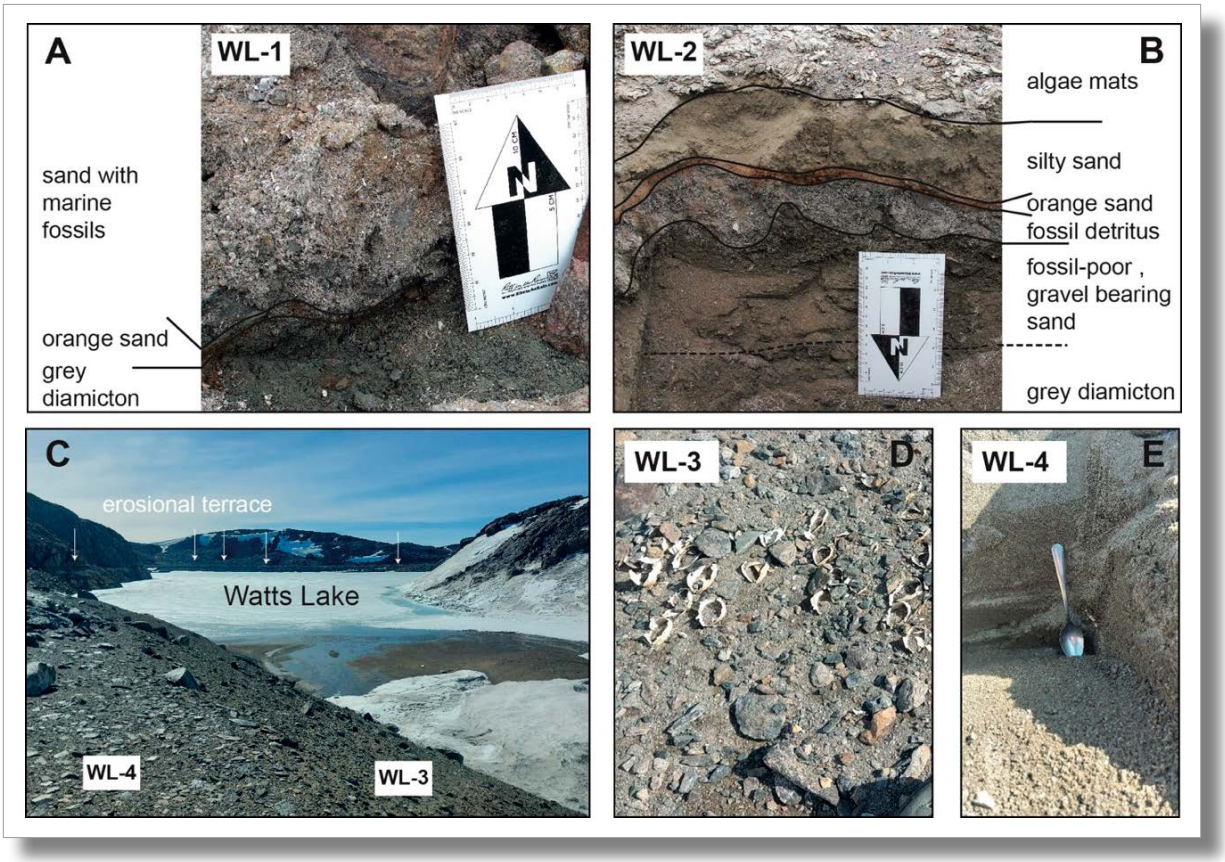

Fig. 6.7: Sediment sampling in the catchment of Watts Lake. (A) Diamicton, orange sand and initial marine sediment with fossils at site WL-1, (B) section from a diamicton to algae mats at site WL-2, (C) slope towards southeastern Watts Lake with locations of sites WL-3 and WL-4 and of the erosional terrace at the southern and northern lake shores, (D) mollusks (probably Laternula Elliptica) in growing position at site WL-3, (E) uppermost sand with marine fossil fragments at site WL-4.

Tab. 6.2: Sediment samples taken in the catchment of Watts Lake (OSL = optically stimulated luminescence dating).

Site - Sample	Latitude [S]	Longitude [E]	Sediment	Sample
WL-1 -1	68°36´04.0´´	78°13´19.0´´	grey diamicton	bulk
-2			orange sand	bulk
-3			sand with marine fossils	bulk
WL-2 -1	68°36´04.2´´	78°13´18.8´´	fossil-poor gravelly sand	bulk
-2			sediment rich in fossil detritus	bulk
-3			orange sand	bulk
-4			olive silty sand	bulk
-5			algae mats	bulk
-6			olive silty sand	tube for OSL
-7			olive silty sand	bulk for dose rate
-8			fossil-poor gravelly sand	shell (Ant. scallop)
WL-3	68°36´27.0´´	78°13´30.0´´	marine sand	mollusc shell
WL-4	68°36´27.0´´	78°13´30.0´´	marine sand	shell fragments

Survey and sampling of raised beaches

Raised beach ridges are paleoshorelines that represent a lowering of sea level. This may be due to eustatic, evaporative, or isostatic sea level changes through time. In ice marginal environments, the beach ridges are often a product of sea ice-beach interaction and related to glacial-isostatic adjustment (GIA). GIA occurs over extended periods of time. In areas near ice sheets today, it results in a lowering of sea level relative to land, since Antarctica is still rebounding from the significant ice-mass removal resulting from the deglaciation period that followed the LGM. Understanding this rate of uplift has implications for modelling ice sheet dynamics and sea-level rise, but accurate rates are difficult to acquire due to the limited ways the processes in the past may be assessed. Here, we aim to utilise raised beach ridges at Watts Lake and Ellis Fjord in the Vestfold Hills, to calculate the rate and degree of regional rebound by dating these geomorphic features on a beach face.

We sampled one raised beach site at the western shore of Watts Lake (WL1) and three at Ellis Fjord: one at the eastern shore of an island west of Co1421 (EF1), one at the northern shore (EF2) and one at the eastern shore of the lagoon at the northern coastline of the fjord (EF1, Fig. 6.2A, Table 6.3). The ridges at Ellis Fjord should primarily be the result of GIA and eustatic sea level changes. Until around 4700 ^{14}C yr BP, Watts Lake was also marine (Pickard et al., 1986), thus ridge formation would also have been GIA or eustacy related. Subsequent GIA formed a sill, isolating Watts Lake from the ocean. Following 4700 ^{14}C yr BP, we would expect topographic changes in the beach profile to be the result of lake lowering due to evaporation.

We surveyed the beach ridges by collecting elevation data from GNSS receivers and using handheld lidar to assess the extent of elevation change. Subsurface data were obtained via ground penetrating radar (GPR) and logging of sampling pits. Sand was sampled for optically stimulated luminescence (OSL) dating and calcareous shell material for radiocarbon (^{14}C) dating.

Elevation data – To generate elevation data, we employed two methods: GNSS techniques with the aid of ground control points (GCPs) and Lidar (Fig. 6.8). The GCPs are 15x15 cm black squares with 5 cm wide reflective tape attached in an arrowhead shape. The GCP arrows were placed facing approximately north at the relevant sites across the beach (sampling sites and truthing points for the lidar) that required accurate GPS and elevation data. The base of the GNSS antenna pole was placed on the inside centre of the arrow when collecting the GNSS data for each point. The GNSS set up and data collection is described in more detail in the subchapter “Geodetic measurements” below.

Tab. 6.3: Samples taken from raised beaches. EF1 had no physical samples taken (only LiDAR and GPR), so included is the general location. Coordinates and elevation are from a Galaxy A73 using the app HandyGPS (OSL = optically stimulated luminescence dating).

Site ID	Sample ID	Sample type	Date	Latitude [S]	Longitude [E]	Elevation [m]
WL1	OB1	OSL Pit	19.12.2023	68°36´16.9´´	78°11´11.8´´	-5
	OB2	OSL Pit	19.12.2023	68°36´17.6´´	78°11´09.7´´	-1
	OB3	OSL Pit	19.12.2023	68°36´17.6´´	78°11´09.0´´	2
	OB4	OSL Pit	19.12.2023	68°36´17.6´´	78°11´07.4´´	3
	Seaweed	Fossil	19.12.2023	68°36´16.9´´	78°11´12.1´´	-3
EF1		Location	24.12.2023	68°35´46.3´´	78°10´01.4´´	9
EF2	OB1	OSL Attempt	28.12.2023	68°35´34.4´´	78°09´42.9´´	4
	OB2	OSL Pit	28.12.2023	68°35´34.4´´	78°09´42.4´´	6

Site ID	Sample ID	Sample type	Date	Latitude [S]	Longitude [E]	Elevation [m]
	OB3	OSL Pit	28.12.2023	68°35´34.4´´	78°09´41.9´´	6
	OB4	OSL Pit	28.12.2023	68°35´34.4´´	78°09´41.6´´	4
EF3	OB1	OSL Pit and shell	01.01.2024	68°35´30.1´´	78°09´29.1´´	11
	OB2	OSL Pit and shell	01.01.2024	68°35´29.8´´	78°09´30.1´´	2
	OB3	OSL Pit and shell	01.01.2024	68°35´29.8´´	78°09´31.7´´	6
	OB4	OSL Pit and shell	01.01.2024	68°35´29.4´´	78°09´33.9´´	8
	OB5	OSL Pit and shell	01.01.2024	68°35´29.8´´	78°09´36.3´´	9
	OB6	OSL Pit	01.01.2024	68°35´29.0´´	78°09´38.1´´	6
	Shell1	Shell for ^{14}C	02.01.2024	68°35´29.0´´	78°09´30.1´´	1

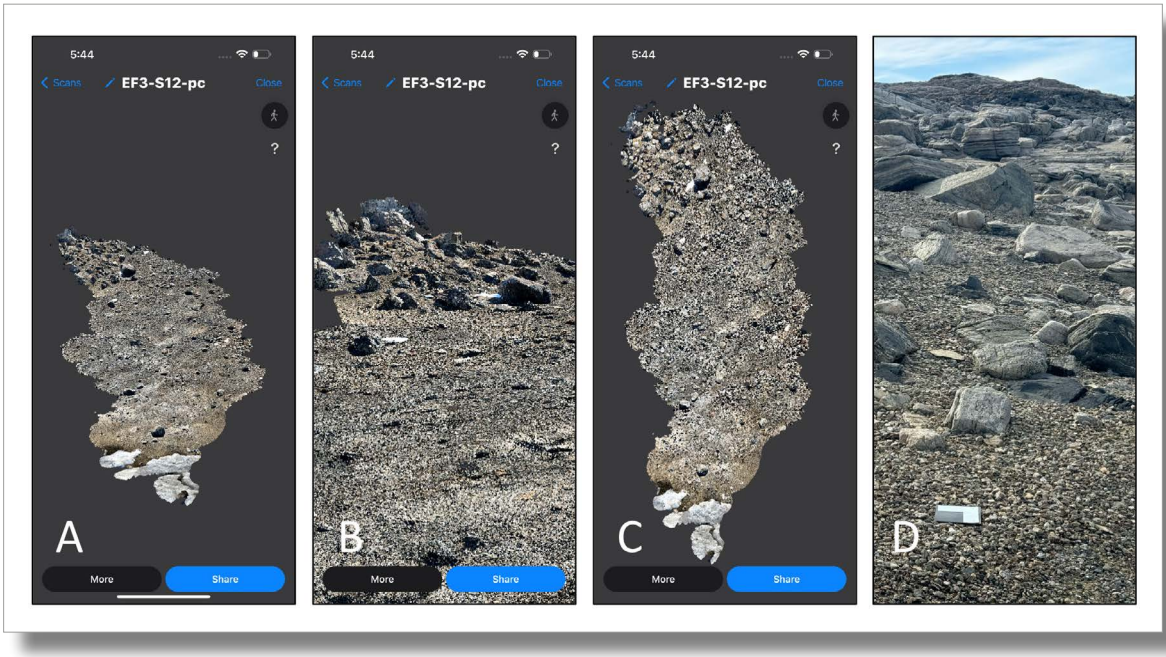

Fig. 6.8: Elevation measurements of raised beaches. (A) to (C): Examples of raw, colourised LiDAR point cloud data models taken as screenshots from the iPhone. (D) Example of GCP placement with arrow pointing north. All examples are from site EF3 (for location see Fig. 6.2A).

The lidar data was taken using an iPhone 15 Pro Max attached to a DJI OM 6 extendable gimbal. The free application “3d Scanner App” was used to collect the data. We primarily employed Point Cloud mode when conducting large beach scans (Fig. 6.8A-C), but Lidar Advanced mode was sometimes used. We walked the site, aiming the camera and lidar scanner towards the ground – collecting data within about a 5 m range. Point cloud scanning was limited to approximately 15 minutes of data collection, each beach required multiple scans (between 2 and 18). The method was time consuming, with EF3 (the largest site) taking around 5 hours to complete. However, there were no structured walking paths, employing these may have decreased collection time.

In the raw data, we see drift in the horizontal and vertical axes through the scan. The GCPs, however, have been placed with the aim to correct for this drift in post processing, and multiple GPCs were imaged during each scan (Fig. 6.8D). The reflective tape on the GCPs will be picked

up as having a high intensity in the lidar scans and, during post cruise processing, the shape of the arrow should be observable. With this, the coordinates and elevation data should be applied to the inside of the arrow, correcting for the observed drift. Once the scans are corrected and combined during post cruise processing, they can be used to assess the geomorphology of the beach and the elevation change of paleoshorelines through the Holocene.

Subsurface imaging – We used ground penetrating radar (GPR) to image the subsurface (Fig. 6.9). This is important when sediment structure variations are expected from different geomorphic features. We employed a sled-mounted Mala GX 160 MHz GPR antennae at each beach, taking between two and five transect scans. In some cases, this was used to aid sampling, but will primarily be used to assess subsurface structure to complement the lidar surface data. Besides, we dug a pit at the top of each targeted beach ridge. The pits ranged from 25 to 50 cm deep. The sediments exposed were photo documented and described.

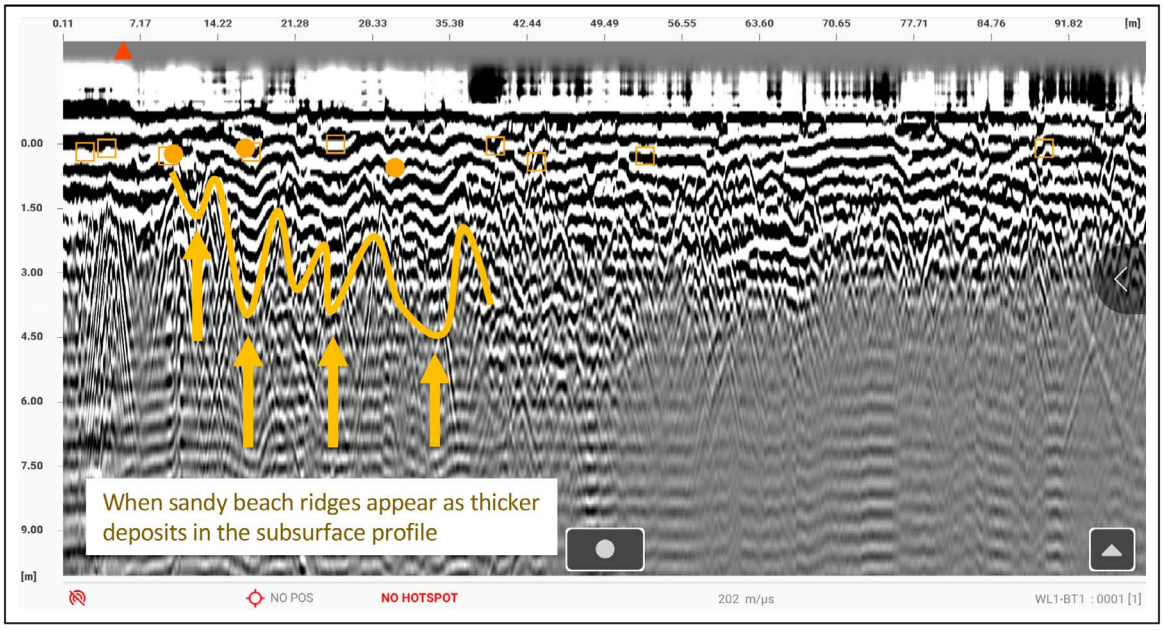

Fig. 6.9. Raw GPR data from one transect taken at raised beaches site WL1 (for location see Fig. 6.2A). Annotated are the locations of the beach ridges and their increased thickness of reflections through the profile.

Sampling for OSL dating – Burial dating by OSL uses the fact that isotopes within quartz sand grains are stimulated by light, which causes lattice charge defects that can store electrons. Once buried/not exposed to light, production of additional defects stops, and the reactive decay of ^{235}U, ^{238}U, ^{232}Th, ^{40}K, and ^{85}Rb from surrounding sediment grains produces electrons within the defects. Re-exposure to sunlight will however reset, or “zero”, electron production within 1 to 100 seconds. Thus, the population of electrons within these defects can be used to date the time of burial (this does assume that the sediment hasn’t been re-exposed since the formation of the geomorphic feature).

OSL samples were taken from sand intervals that were the result of coastal processes (rather than eolian). Sampling was conducted by hammering a PVC pipe into the pit’s side until consumed by the sand (Fig. 6.10A-C). The PVC tubes were 20 cm long and either 4 or 6 cm in diameter. Before removing the sample tube, we took a dosage sample to correct the electron excitement rate within the sample. The sediment around the sample was excavated by hand into a plastic zip lock bag for storage. The pipe could then be removed, attempting to ensure sediment is tightly packed along its length. When not tightly packed, aluminium foil

was added to the unpacked ends to ensure the sediment remained undisturbed/mixed. Each end of the tube was then taped to seal. The PCV should ensure that no light has access to the grains at the centre of the sample. The pits from the sampling locations had a relatively consistent structure of beds. The surface consisted of clast-supported sandy gravels, followed by a deposit of sand.

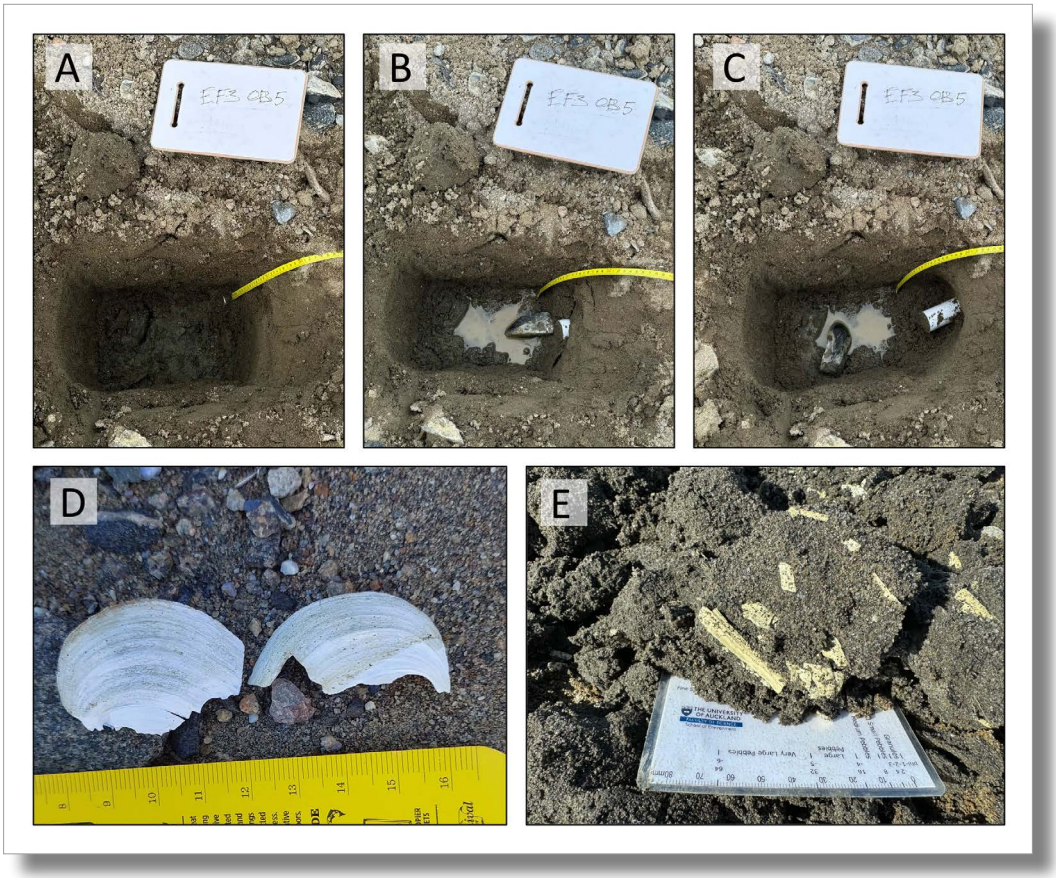

Fig. 6.10. Excavated OSL pit from raised beaches at site EF3 (for location see Fig. 6.2A), showing (A) fresh pit, (B) pit with the tube hammered into the side and (C) further excavated hole for dosage sample exposing tube. Tubes were then taped and stuffed (if necessary). (D) Example of the shell material from EF3 (EF3-Shell1), relatively intact and exposed at the surface, and (E) more fragmented shell pieces occurring within the sands below the surface gravels.

OSL samples could not be taken from site EF1 on the island within Ellis Fjord (Fig. 6.2A). Despite clear ridges, the sediments consisted of clast-supported gravels exclusively, which cannot be used for reliable OSL dating. The data from EF1, therefore, are restricted to GPR and LiDAR data.

Sampling for ^{14}C dating – In the case of site EF3 at the eastern shore of the lagoon (Fig. 6.2A), there was an abundance of shell material within the buried sand deposits in the beach profile (Fig. 6.10E). This ended up the reason for sampling this beach, despite poorly defined ridges. Shell material was sampled from the lower five pits, with the top pit containing no shell. We also sampled some shells exposed at the surface (Fig. 6.10D), as they were in better condition than the ones at depth, which may aid species ID. The shell material shall be used for ^{14}C dating, complementing the OSL dating.

Geodetic measurements

The geological field work at Vestfold Hills was supported by geodetic measurements to gain a georeferencing of sampling sites and Lidar data acquisition as well as to measure the height of lake and sea levels and marine terraces (which can be summarized as ground control points, GCPs).

A temporary GNSS (Global Navigation Satellite Systems) reference station was installed near Watts Hut at the shoreline of Ellis Fjord (Fig. 6.11A to D). At this station, GPS and GLONASS data was collected between 18 December 2023 at 10:52 UTC and 4 January 2024 at 02:17 UTC. A Leica ATX1203+GNSS antenna (#09240102) was mounted at a height of 95 cm above ground on a tripod embedded in rocks. Data collection was done by a Leica GRX1200+GNSS receiver. Preliminary, approximate coordinates of this reference station were determined to be 68°35'53.266'' S / 78°13'16.238'' E.

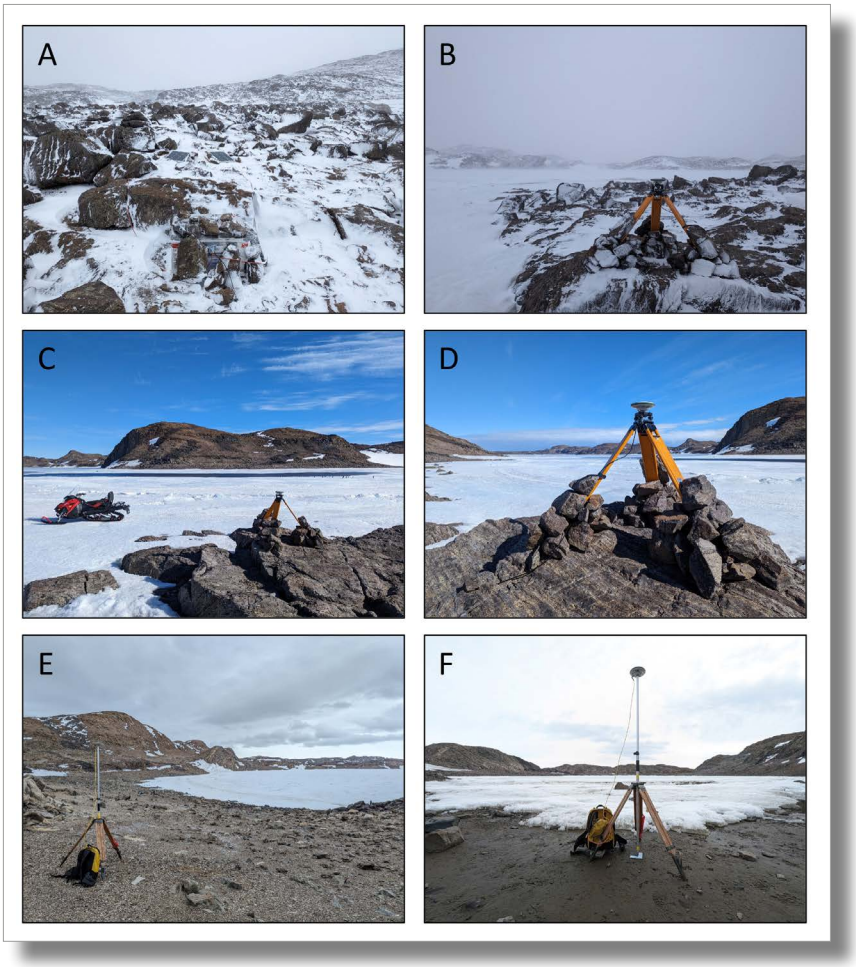

Fig. 6.11. GNSS Reference station near Watts Hut with (A) Zarges box with GNSS receiver, battery and solar charge controller in the front, solar panels in the back, and (B) to (D) Leica antenna mounted on a tripod. (E) and (F) show rover setup for point measurements (backpack with GNSS receiver and battery).

Kinematic and point measurements were performed using a second GNSS setup consisting of a Leica ATX1203+GNSS antenna (#09110050) and a Leica GR25 receiver. The antenna was mounted at a height of 2.10 m on a measuring pole. For point measurements the pole was fixed with a tripod (Fig. 6.11E and F). Table 6.4 gives an overview of the kinematic and point measurements accomplished at Vestfold Hills. The majority of point measurements was done to provide high precision position data to facilitate the georeferencing of Lidar point clouds collected (see description of raised beach analyses above).

Tab. 6.4: Overview of kinematic and point measurements conducted at Vestfold Hills between 19 December 2023 and 1 January 2024.

ID	Location	Latitude [S]	Longitude [E]	Date/Time [UTC]	Remarks
EF-Co1420	Ellis Fjord-Watts Hut-Watts Lake	68°36'00.36''	78°13'24.25''	19 December 2023/03:20-04:12	kinematic profile
WL1	Watts Lake (West)	68°36'17.45''	78°11'10.79''	19 December 2023/06:20-08:00	points (GCPs for Lidar, sed. sampling sites)
WH, WL	Watts Hut, Watts Lake	68°36'00.36''	78°13'23.83''	20 December 2023/07:00-12:12	points (hut and lake level)
EF1	Island in Ellis Fjord	68°35'46.28`'	78°10'01.41''	24 December 2023/09:40-11:30	points (GCPs for Lidar, sed. sampling sites)
EF2	Terraces (East)	68°35'34.25''	78°09'43.71''	28 December 2023/04:10-09:44	points (GCPs for Lidar, sed. sampling sites)
WL-1	Watts Lake shore	68°36'04.08''	78°13'18.09''	31 December 2023/10:40-11:40	point (GCP for sediment samples)
EF3	Terraces (West)	68°35'29.93''	78°09'29.06''	1 January 2024/ 10:55-12:39	points (GCPs for Lidar, sed. sampling sites)

Sampling of soil crusts

Biological soil crusts and their biodiversity so far are poorly investigated in terrestrial areas of Princess Elizabeth Land. In Vestfold Hills, the surfaces of several sites, where the ground was free of snow cover and consisted of lose sediment, were colonized by soil crusts and mosses. We collected biological soil crusts at three sites some 100-200 m to the southeast of Watts Hut (Figs. 6.2A and 6.12, Tab. 6.5). The samples shall be used for biodiversity studies in collaboration with Ulf Karsten (Rostock University), in order to characterize the microbial net-works and functionality in these unique ecosystems. The results will provide a baseline for the current state of microbial diversity, which is needed to document environmental changes on the microbial level.

Fig. 6.12. Photographs showing the sampling of biological soil crusts with petri dishes at 3 sites (VS-1, VS-2 and VS-3) to the southwest of Watts Hut.

The sites sampled most likely were not influenced by anthropogenic activities (such as walking), particularly high nutrient input (for instance from birds) or stagnant or flowing waters. The soil crusts were sampled with petri dishes. At each site four replicates were collected to provide material that is representative for each site. The samples were dried at 30°C for three days in a drying cabinet onboard *Polarstern*, before being closed by tape.

Tab. 6.5: Biological soil crusts sampled to the southeast of Watts Hut, with sampling times, coordinates and grain sizes of populated grounds.

Site ID	Date	Local time	Latitude [S]	Longitude [E]	Ground
VS-1	03.01.2024	8:30 am	68°36´04´´	78°13´39´´	sandy gravel
VS-2	03.01.2024	9:10 am	68°36´00´´	78°13´41´´	gravel
VS-3	03.01.2024	9:30 am	68°36´00´´	78°13´34´´	sandy gravel

6.2 Additional field work on land sites

Setup and maintenance of geodetic and geophysical stations

The measurement of bedrock displacement in East Antarctica is one main goal of the geodesy program within the EASI project. The glacial history of the Antarctic Ice Sheet – from the LGM up to present day – directly affects the deformation of the Earth. The response of the Earth is, on the other hand, governed by its rheological properties (especially effective elastic thickness of the lithosphere, viscosity of the upper and lower mantle). Both quantities – ice-load history and Earth's rheology – lead to the process of glacial-isostatic adjustment (GIA), which is currently being modelled (e.g., Whitehouse et al., 2019; King et al., 2022). The GIA modelling can be constrained by geodetic GNSS (Global Navigation Satellite Systems) observations of the displacement of the Earth's crust. Within the EASI project, we collaborate with the group of Matt King, University of Tasmania (UTAS).

Besides setup and maintenance of GNSS stations it was initially planned to deploy a number of magnetotelluric (MT) stations on EASI-2 (PS140), which were to be recovered by EASI-3 (PS141), and replace a seismometer (Tab. 6.6). However, the two pallets with MT instruments failed to reach Cape Town in time despite being sent 90 days before departure from Cape Town. There is an attempt now to get the MT gear to Hobart in time for a deployment on the following cruise PS141 (EASI-3). Moreover, the GNSS reconnaissance at RANU, Ravich Nunatak in the Princess Elizabeth Land, and the maintenance of the GNSS station and the seismometer replacement at CAD1, Carey Nunatak on the West Ice Shelf, were unfortunately cancelled due to bad flying and sea-ice conditions, making the site out of range for the helicopters onboard *Polarstern*.

Tab. 6.6: Geodetic and geophysical station work initially planned to be conducted on PS140 at four sites to the east of Vestfold Hills (MT = magnetotelluric deployment, GNSS = Global Navigation Satellite Systems), and work actually accomplished.

Site ID	Location	Latitude [S]	Longitude [E]	Method / Remarks
RANU (not visited)	Ravich Nunatak	67°16´01´´	84°04´08´´	MT (not deployed) GNSS reconnaissance
CAD1 (not visited)	Carey Nunatak	67°07´50´´	85°50´11´´	MT (not deployed) GNSS maintenance, seismometer replacement
GAUS	Gaussberg	66°48´15´´	89°10´30´´	MT (not deployed) GNSS set up new site reconnaissance EASI-3
CAD3	Gillies Is.	66°31´10´´	96°21´58´´	MT (not deployed)

GNSS maintenance

At Gaussberg, GAUS, a campaign GNSS station, consisting of a Leica AR10 antenna (#17280009) and a Leica GR25 receiver, was successfully installed (Fig. 6.13). This station will serve as a reference station for the subsequent surveying at Gaussberg planned within cruise PS141 (EASI-3). The recording of observational data for several weeks will allow to infer 3D coordinates with an accuracy of a few centimetres once the land team of PS141 will have arrived at Gaussberg. After some initial problems finding a suitable site, the antenna was mounted securely with a bolt glued in at a height of 15 cm above ground (Fig. 6.13A). The rocks were very weathered, making the installation challenging with several rocks cracking when trying to secure the bolt in the drilled hole. The cable from the antenna was held down by rocks at some points. The solar panel was mounted on a frame horizontally on the instrument box. Once up and running, the environmental conditions for the field camp and additional geodetic instrumentation to be set up at Gaussberg at EASI-3 were checked and documented.

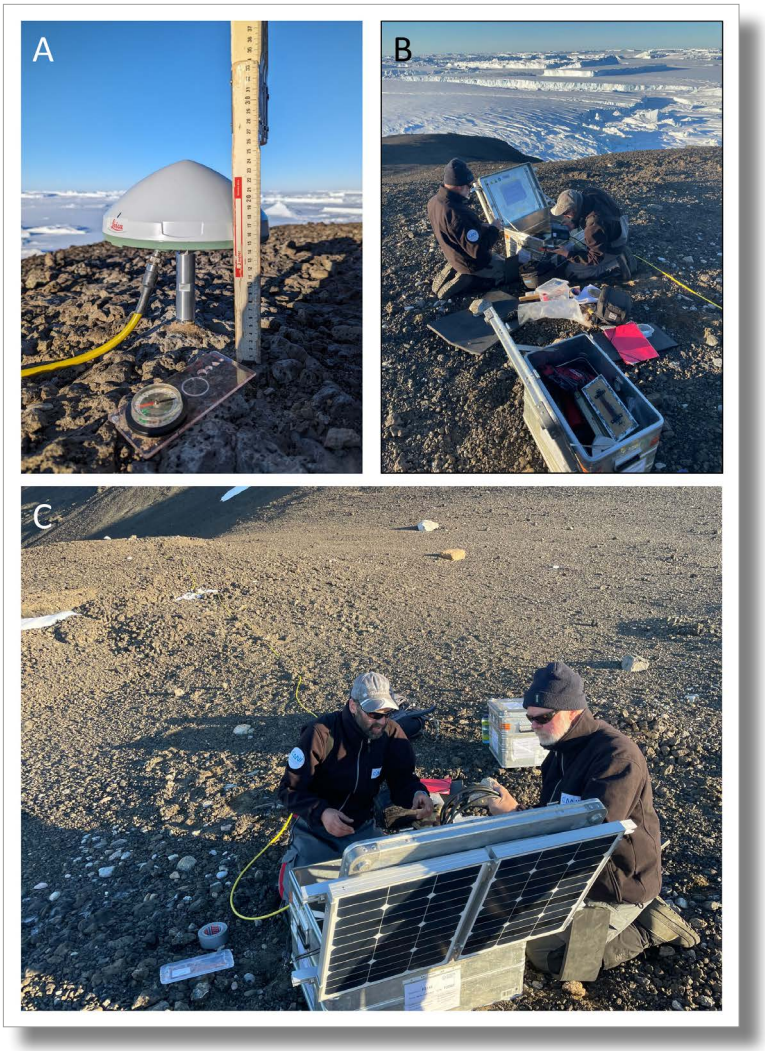

Fig. 6.13. Campaign GNSS station at Gaussberg, with (A) Leica antenna, (B) setup of Zarges receiver box and (C) receiver box connected with the Antenna at the rim in the back.

The maintenance of the GNSS station at CAD3, Gillies Island in Queen Marie Land (Fig. 6.14), took about 3.5 hours altogether. The initial visual check of the station showed no wear and tear or damage of the frame, solar panel, GNSS antenna and the cables. Replacing the GNSS logger and the batteries, and installing a new Iridium antenna, went without problems.

Fig. 6.14. GNSS maintenance at Gillies Island (CAD3).

Sampling of glacial erratics

On 7 January 2024 a helicopter trip of a few hours offered the opportunity to sample first erratics for exposure dating on Gaussberg (Tab. 6.7, Fig. 6.15). The 370 m high volcanic cone Gaussberg is located west of Posadowsky Glacier and on the Davis Sea margin (Fig. 6.1). Gaussberg formed around 56,000 years ago (Tingey et al., 1983). Because of its elevation and age, it provides an excellent site for assessing the rate of ice sheet retreat, both in area and altitude, using exposure dating techniques like in situ cosmogenic nuclide production (e.g., ^{10}Be, ^{14}C, or ^{26}Al) in glacial erratics. The aim was to collect rock samples from the summit to sea level, however, the scree type terrain made this difficult given the timeframe permitted. We ended up with three sample sites and 9 samples spanning elevations of 65 (four samples), 86 (two samples), and 120 (three samples) metres above sea level.

Tab. 6.7: Location data for the erratics taken from Gaussberg using a Garmin InReach handheld GPS.

Sample ID	Latitude [S]	Longitude [E]	Elevation [m]
GA24-01A	66°48´10.07´´	89°10´52.89´´	121±2
GA24-01B	66°48´09.90´´	89°10´52.76´´	118±1
GA24-01C	66°48´09.51´´	89°10´53.57´´	117±2
GA24-02A	66°48´04.53´´	89°10´35.38´´	66±1
GA24-02B	66°48´04.53´´	89°10´35.38´´	66±1
GA24-02C	66°48´04.53´´	89°10´35.38´´	66±1
GA24-02D	66°48´04.53´´	89°10´35.38´´	66±1
GA24-03A	66°48´06.91´´	89°10´42.06´´	86±3
GA24-03B	66°48´06.91´´	89°10´42.06´´	86±3

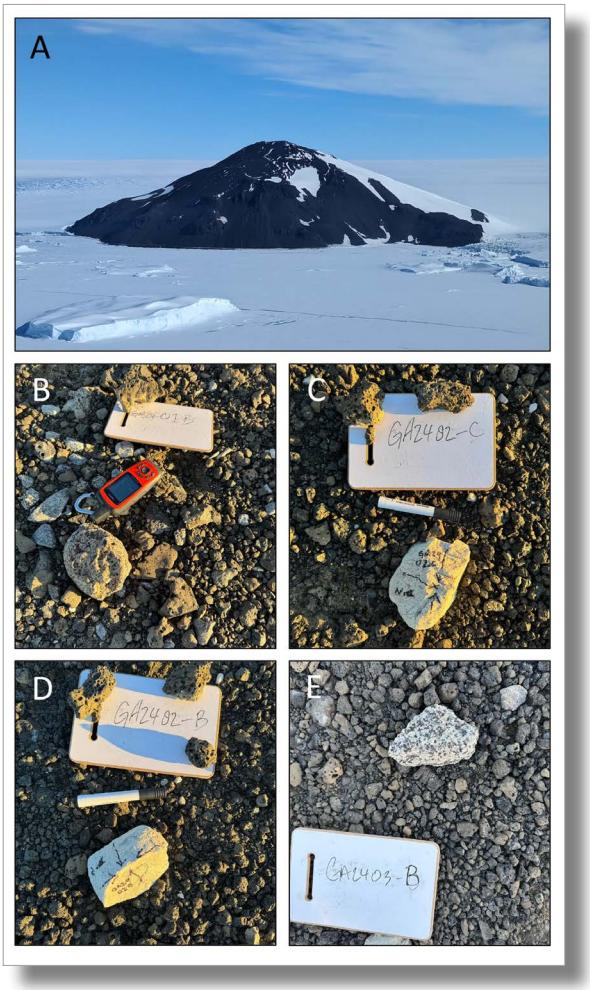

Fig. 6.15. (A) Areal photograph of Gaussberg, view from the north, (B) to (E) examples of cosmogenic samples taken at Gaussberg.

Glacial erratics were abundant up the slope but there was evidence of human disturbance near the helicopter landing site, which was previously used as a camp site, and towards the north-western cliff, where a boulder cairn was present. We avoided sampling too close to the helipad and cairn. All samples collected were light-coloured rocks that appeared to bear quartz and ranged from 8 to 14 cm on the b-axis. Only erratics were sampled, as the bedrock consists of leucitites, mafic volcanic rocks with little quartz content (Sheraton and Cundari 1980).

Location and shielding data were taken in the field. The latitude, longitude, and elevation data were taken via Garmin InReach handheld GPS on the location setting (Tab. 6.7). These data reflected the elevations on the corresponding contour map well. Shielding data (Tab. 6.8) was collected using a traditional mirror compass with a clinometer and declination corrector. The angle to the horizon line was collected every 30 degrees from 0 to 330. Magnetic north was corrected by adjusting the compass to point 88 degrees West and, therefore, 0 degrees represents true north. At the first site (GA24-01), shielding was collected for each sample as the spacing between samples exceeded ~10 m. A single set of shielding data was collected at each of the other two sites (GA24-02 and 03) as the spacing between the samples was <5 m and with no dramatic change in relief. Shielding primarily occurred to the south/south-east towards the summit of Gaussberg (up to ~30 degrees), and there was no, or limited, shielding along the northern 180 degrees.

Tab. 6.8: Shielding data for the samples from Gaussberg. Units in degrees. Gaussberg provided most of the shielding with between east and south of the sampling sites.

ID	0 (N)	30	60	90 (E)	120	150	180 (S)	210	240	270 (W)	300	330
GA24-01A	0	0	0	10	30	25	5	2	0	0	0	0
GA24-01B	0	0	0	12	24	26	8	0	0	0	0	0
GA24-01C	0	0	0	14	28	30	10	0	0	0	0	0
GA24-02A	0	0	0	5	12	22	8	0	0	0	0	0
GA24-02B	0	0	0	5	12	22	8	0	0	0	0	0
GA24-02C	0	0	0	5	12	22	8	0	0	0	0	0
GA24-02D	0	0	0	5	12	22	8	0	0	0	0	0
GA24-03A	0	0	0	12	22	18	14	5	0	0	0	0
GA24-03B	0	0	0	12	22	18	14	5	0	0	0	0

Sampling of dirty ice

Objectives

Basal continental ice may contain sediment particles that host paleoenvironmental information, when analyzed for cosmogenic nuclides, organic remains and detrital neodymium and lead isotopes. The cosmogenic ^{10}Be concentrations may provide information whether the sediment originates from erosion of bedrock in the source area (low 10Be) or from preglacial sediments (high ^{10}Be), which became formed in the currently ice-covered regions during times of ice retreats beyond the modern ice edge. A formerly larger ice-free area could also be documented by organic remains (calcareous fossils or dispersed organic carbon) in the sediments, which can potentially be dated by radiocarbon analyses. The neodymium and lead isotopes in the sediment reflect provenances and may contain vital information towards its physico-chemical weathering behaviour. Comparison of the continental source signatures with corresponding sediments on the East Antarctic shelf and offshore thus will help to better understand the transport of radiogenic isotopes into the Southern Ocean and support the interpretation of respective analyses on marine sediment cores to be recovered on PS140 and PS141. It will further provide information towards continental crustal age and geological boundary conditions in the study areas.

Testing drilling technique in the Vestfold Hills

We brought two electric auger heads that were fabricated at the University of Canberra. Both were made of steel with tungsten-carbide teeth. Auger 1 had an internal diameter of 8.3 cm and a length of 65 cm, while Auger 2 had an internal diameter of 9.5 cm and a length of 56 cm. These were both compatible with an Einhell 18V electric auger motor.

On 21 December 2023, we tested both heads with the supplied electric motor on the surface ice of Watts Lake, Vestfold Hills. Two locations were selected from along a 30 m GPR transect that is denoted as WL3 (Fig. 6.2A). For the small difference in diameter, there was a substantial difference in performance. Auger 1 primarily returned chunks of ice rather than consolidated discs. In contrast, Auger 2 generally returned consolidated ice discs of around 5 cm (but up to 20 cm) thickness, better retaining the ice structure. Upon reversing the rotation direction when the bit was stuck, however, Auger 2 tended to warp away from its regular shape. This didn't appear to greatly affect performance but will likely affect the longevity of the tool and there may be some risk of getting stuck in a deeper hole.

The two test holes (Site VH_23-24 WL3; Fig. 6.2A; Tab. 6.9) were 1.21 to 1.43 m deep and took 1.5 to 2.5 hours when including ice description (Fig. 6.16). This is not a time-efficient process and becomes slower as the hole gets deeper. For this to be a viable technique on the ice sheet, several days would likely be required. However, shallow sampling of exposed dirty ice would be appropriate.

Tab. 6.9: Locations where the electric ice auger was employed to drill lake ice and dirty continental ice.

Site ID	Latitude [S]	Longitude [E]	Remarks
VH_23-24_WL3-LT1-D1	68°36´14.04´´	78°13´14.06´´	Watts Lake test hole no. 1. Handy GPS app on Samsung Galaxy A73.
VH_23-24_WL3-LT1-D2	68°36´13.91´´	78°13´12.95´´	Watts Lake test hole no. 2. Handy GPS app on Samsung Galaxy A73.
VH_23-24_IS1-D1	68°33´36.30´´	78°33´36.46´´	No samples taken. Sampling depth not met. Coordinates were supplied by D. White. Approx. 120 m elevation.
VH_23-24_IS2-D1 (MG-ANT4)	68°37´05.14´´	78°30´51.38´´	Coordinates taken with Avenza Maps on Samsung Galaxy A73. 10-15 kg of ice taken. Sampled exposed dirty ice in ice cliff.
BH24_IS1_D1 (MG-ANT5)	66°13´55.11´´	101°06´41.58´´	Coordinates taken with Avenza Maps on Samsung Galaxy A73. Banded dirty ice dig site.

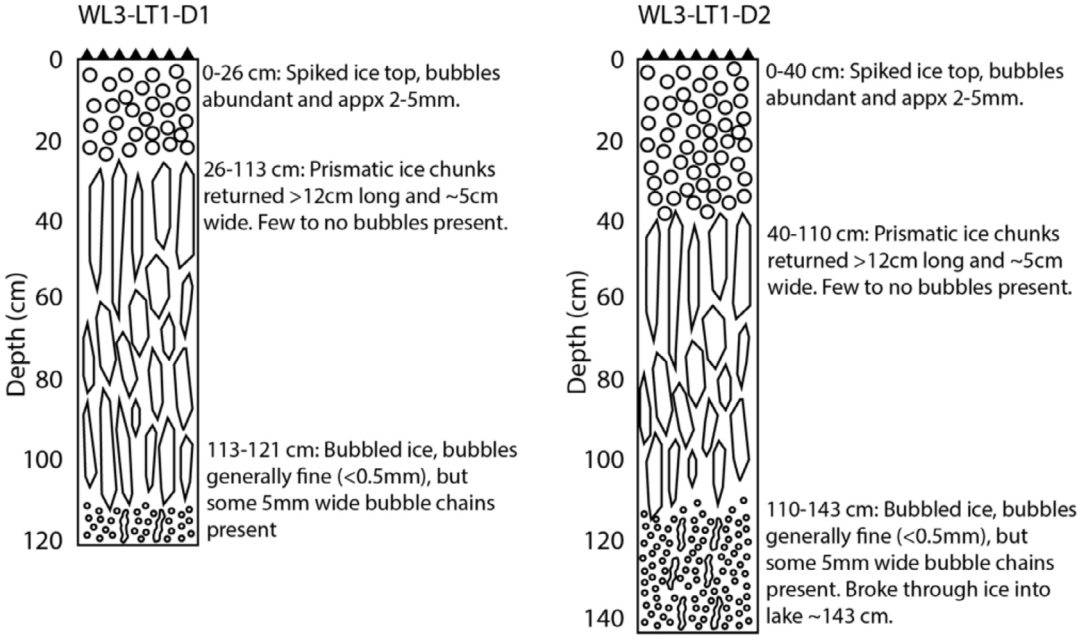

Fig. 6.16: Ice descriptions from the test holes in the Watts Lake ice cover at site WL3 (for location see Fig. 6.2A).

Continental ice sampling during EASI-2

Three sampling trips were carried out in order to collect continental ice with inherited sediment in the area south of the Amery Ice Shelf edge (Fig. 6.1; Tab. 6.10). Additional sampling campaigns took place in the Vestfold Hills area and near Bunger Hills. While the first two trips could sample rock debris for provenance analyses, only stations MG-ANT3 to MG-ANT5 provided strictly enclosed sediment within continental ice that has not been in contact with the atmosphere. Samples from these sites are of adequate purity for assessing the Pb-specific incongruent weathering behavior (Dausmann et al., 2019, Süfke et al., 2019).

Tab. 6.10: Dirty continental ice sampling locations.

Site ID	Latitude [S]	Longitude [E]	Date
MG-ANT1	70°11´56.4´´	72°34´55.2´´	01.01.2024
MG-ANT2	69°59´52.8´´	73°00´18.0´´	01.01.2024
MG-ANT3	69°50´45.6´´	75°00´50.4´´	02.01.2024
MG-ANT4	68°37´26.4´´	78°35´31.2´´	03.01.2024
MG-ANT5	66°07´44.4´´	101°18´46.8´´	10.01.2024

In Vestfold Hills, dirty ice sampling took place on 3 January 2024, during short stays of less than 2 hours at two sites at the ice sheet margin (VH_23-24 IS1 and IS2, Fig. 6.2B). Transport to and from these sites was by helicopter.

At site IS1 we attempted drilling through clean ice sheet ice to sample unexposed shear moraine. We first took a GPR transect to assess a sample location. There was certainly a clear transition from clear ice to shear moraine at depth (Fig. 6.17). We utilised a petrol ice auger (Eskimo, USA) to drill approximately 1.5 m into the ice before, when attempting to sample, continuing with Auger 2. We aborted this site due to the slow sampling speed, and the fact that sampling depth was not met. While this is still possible, at least a day on site is likely required.

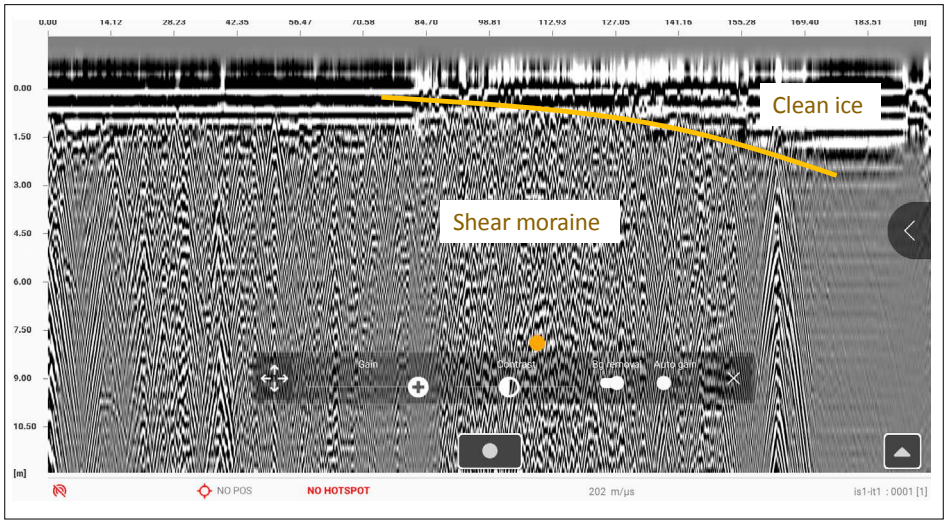

Fig. 6.17. Raw GPR data from a transect on the margin of the ice sheet to the east of Vestfold Hills (site IS1) showing the clear interface (yellow) between clean ice and shear moraine. Unfortunately, direct sampling of the shear moraine was not achieved (for location see Fig. 6.2B).

Pivoting, we decided to assess a north-facing ice cliff that incised the ice sheet and entrained shear moraine sediments to the south (Site VH_23-24 IS2, Figs 6.18B and 6.2B), i.e. we were able to directly sample dirty ice sediments using Auger 2. Two sections of cliff were sampled within 10 m of each other. The Auger was oriented in an approximately horizontal position and driven repeatedly into the ice cliff (Fig. 6.18A). We secured around 30 discs of dirty ice totaling an estimated 10-15 kg (Fig. 6.18C and D).

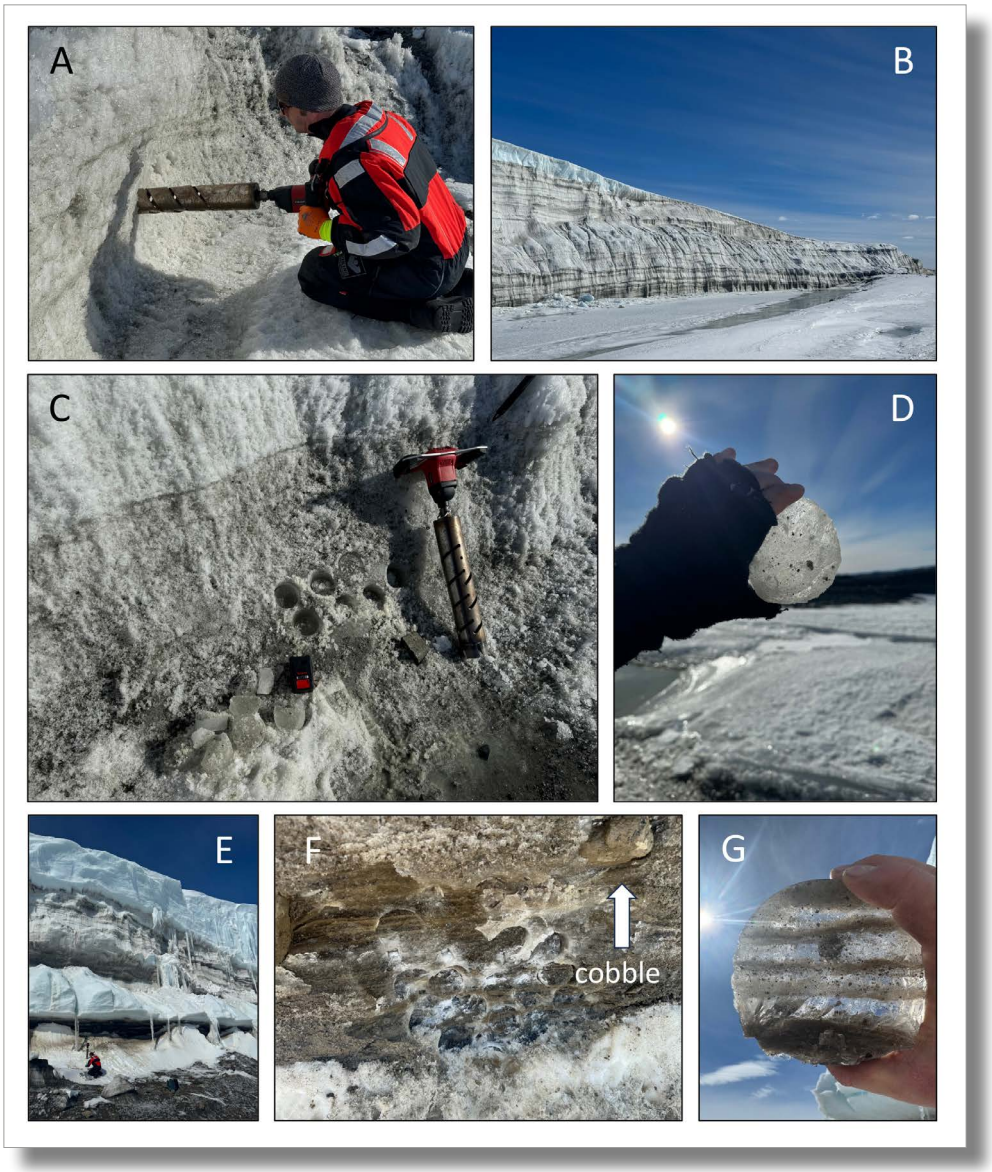

Fig. 6.18. Sampling of dirty ice from the East Antarctic Ice Sheet. (A) Ice drilling, (B) exposed shear moraine at ice cliff, (C) one of the dirty layers sampled and (D) example of dirty ice disc containing bubbles on site IS2 at Vestfold Hills (for location see Fig. 6.2B). (E) Exposed shear moraine at ice cliff, (F) sampled dirty ice layers underneath exposed cobble and (G) drilled ice disc with sediment layers at the ice sheet margin to the east of Bunger Hills.

The ice at VH_23-24 IS2 (MG-ANT4) contained bubbles and the sedimentary component made up <1% of the sample. At the metre/cliff scale, horizontal structure parallel to the surface of the ice sheet was observed in the ice, but at the centimetre scale, within the ice samples, there was no clear structure.

In Bunger Hills, dirty ice sampling was carried out on 10 January 2024. Based of the findings from the Vestfold Hills, we aimed to locate a north-facing ice gully that incised a shear moraine. From satellite imagery, these appeared abundant along the ice sheet front from Leonova Bay to Lake Dalekoje. We decided on a safe site (BH24_IS1, MG-ANT5) while flying along the margin from north to south.

The cliff was approximately 30 m high and consisted of repeating, metre-scale bands (Fig. 6.18E) that extended towards the shear moraine exposed at the surface to the west. Within these bands, the observed sediment grain size ranged from mud to cobble (Fig. 6.18F). We selected an accessible dirty layer within the cliff and employed the same horizontal drilling technique with Auger 2 as used in the Vestfold Hills, this time also using a hammer and chisel in support. The addition of the hammer and chisel was a good one, as the discs often wouldn't come free with the auger alone. Keeping a tight sampling interval also aided in sample recovery. Discs were generally 5 cm thick.

Ice samples contained clear banding structures on the centimetre scale (Fig. 6.18G). While the range in grain size was large, most of the sediment contained within the ice was mud sized. Sediment density was far higher within the ice, perhaps 5%. Fine bubbles, generally <1 mm, were present, but less abundant than in the Vestfold Hills samples.

Sample and data management

Environmental data will be archived, published and disseminated according to international standards by the World Data Center PANGAEA Data Publisher for Earth & Environmental Science (https://www.pangaea.de) within two years after the end of the expedition at the latest. By default, the CC-BY license will be applied.

The geodetic GPS data will be stored within the frame of the SCAR GPS Database which is maintained at TU Dresden. The long-term preservation of the data will be maintained also through the close cooperation within the SCAR Scientific Program INSTANT (Instabilities and Thresholds of Antarctica). A common structure of the data holdings is ensured through the application of the same scientific software package utilised to analyse geodetic GNSS measurements at TU Dresden (i.e., the Bernese GPS Software). Further products and resulting models will be archived in the PANGAEA database at AWI.

This work was supported by the Deutsche Forschungsgemeinschaft (DFG) in the framework of the priority program SPP 1158 "Antarctic Research with comparative investigations in Arctic ice areas" by the grant ME 1169/32-1 and contributes to the Helmholtz Research Programme "Changing Earth – Sustaining our Future" Topic 2, Subtopics 2.1, 2.2, 2.3, and 2.4.

In all publications based on this expedition, the **Grant No. AWI_PS140_04** will be quoted and the following publication will be cited:

Alfred-Wegener-Institut Helmholtz-Zentrum für Polar- und Meeresforschung (2017) Polar Research and Supply Vessel POLARSTERN Operated by the Alfred-Wegener-Institute. Journal of large-scale research facilities, 3, A119. http://dx.doi.org/10.17815/jlsrf-3-163.

Acknowledgements

We would like to thank the German Research Foundation (DFG) for funding of the geological investigationsa on land within the scope of the DFG priority program 1158 "Antarctic Research" (Grant No. ME 1169/32-1). Oliver Esper and Vivian Marissa Sinnen (AWI) are acknowledged for their help in preparing and evaluating the smear slides from the core catchers of the piston cores from Vestfold Hills. We are grateful also to Yvonne Schulze Tenberge (AW) for the production of Figure 6.1. Special thanks go to the Australian Antarctic Division (AAD), in

particular the station leader (Brett Barlee) and crew of the *Davis Station*, for the logistic support and great hospitality.

References

Adamson DA, Pickard J (1983) Late Quaternary ice movement across the Vestfold Hills, East Antarctica. In: Oliver, R.L., James, P.R., Jago, J.B. (Eds.), Antarctic Earth Science. Aust. Acad. Sci, Canberra ACT, pp. 465–469.

Australian Antarctic Data Centre (2021a) Vestfold Hills, Map 4 of 5. Edition 8, Map Catalogue Number: 15490. https://data.aad.gov.au/map-catalogue/map/15782

Australian Antarctic Data Centre (2021b) Vestfold Hills, Map 5 of 5. Edition 9. Map Catalogue Number: 15491. https://data.aad.gov.au/map-catalogue/map/15783

Berg S, White DA, Bennike O et al. (2016) Unglaciated areas in East Antarctica during the last glacial (Marine isotope stage 3) - new evidence from Rauer Group. Quatern. Sci. Rev. 153:1–10. https://doi.org/10.1016/j.quascirev.2016.08.021

Bird MI, Chivas AR, Radnell CJ., Burton HR (1991) Sedimentological and stable-isotope evolution of lakes in the Vestfold Hills, Antarctica. Palaeogeogr., Palaeoclim., Palaeoecol. 84:109–130. https://doi.org/10.1016/0031-0182(91)90039-T

Boere AC, Abbas B, Rijbstra WIC, Versteegh GJM, Volkman JK, Sinninghe Damste JS, Coolen MJL (2009) Late-Holocene succession of dinoflagellates in an Antarctic fjord using a multi-proxy approach: paleoenvironmental genomics, lipid biomarkers and palynomorphs. Geobiology 7:265–281. https://doi.org/10.1111/j.1472-4669.2009.00202.x

Cremer H, Gore D, Melles M, Roberts D (2003) Palaeoclimatic significance of late Quarternary diatom assemblages from southern Windmill Islands, East Antarctica. Palaeogeogr., Palaeoclimatol., Palaeoecol. 195:261–280. https://doi.org/10.1016/S0031-0182(03)00361-4

Damsté JSS, Rijpstra WIC, Coolen MJL, Schouten S, Volkman JK (2007) Rapid sulfurisation of highly branched isoprenoid (HBI) alkenes in sulfidic Holocene sediments from Ellis Fjord, Antarctica. Org. Geochem. 38:128–139. https://doi.org/10.1016/j.orggeochem.2006.08.003

Dausmann V, Gutjahr M, Frank M, Kouzmanov K, Schaltegger U (2019) Experimental evidence for mineral-controlled release of radiogenic Nd, Hf and Pb isotopes from granitic rocks during progressive chemical weathering. Chemical Geology 507:64–84. https://doi.org/10.1016/j.chemgeo.2018.12.024

Domack E, O'Brien P, Harris P et al. (1998) Late Quaternary sediment facies in Prydz Bay, East Antarctica and their relationship to glacial advance onto the continental shelf. Ant. Sci. 10:236–246. https://doi.org/10.1017/S0954102098000339

Fricker HA, Warner RC, Allison I (2000) Mass balance of the Lambert Glacier-Amery Ice Shelf system, East Antarctica: a comparison of computed balance fluxes and measured fluxes. J. Glaciol. 46:561–570. https://doi.org/10.3189/172756500781832765

Gallagher JB, Burton HR (1988) Seasonal Mixing of Ellis Fjord, Vestfold Hills, East Antarctica. Estuarine. Coastal Shelf Sci. 27:363–380. https://doi.org/10.1016/0272-7714(88)90094-7

Gibson JAE (1999) The role of ice in determining mixing intensity in Ellis Fjord Vestfold Hills, East Antarctica. Ant. Sci. 7:479–426. https://doi.org/10.1017/S095410209900053X

Gibson JAE, Dartnall HJG, Swadling KM (1998) On the occurrence of males and production of ephippial eggs in populations of *Daphniopsis studeri* (Cladocera) in lakes of the Vestfold and Larsemann Hills, East Antarctica. Polar Biol. 19:148–150. https://doi.org/10.1007/s003000050227

Gibson JAE, Paterson KS, White CA, Swadling KM (2009) Evidence for the continued existence of Abraxas Lake, Vestfold Hills, East Antarctica during the Last Glacial Maximum. Ant. Sci. 21:269–278. https://doi.org/10.1017/S0954102009001801

Golledge NR, Fogwill CJ, Mackintosh AN, Buckley KM (2012) Dynamics of the Last Glacial Maximum Antarctic ice-sheet and its response to ocean forcing. Proc. Natl. Acad. Sci. Unit. States Am. 109:16052–16056. https://doi.org/10.1073/pnas.1205385109

Gomez-Fell R, Rack W, Purdie H, Marsh O (2022) Parker Ice Tongue collapse, Antarctica, triggered by loss of stabilizing land-fast sea ice. Geoph. Res. Lett. 49:e2021GL096156. https://doi.org/10.1029/2021GL096156

Goodwin ID (1996) A mid to late Holocene readvance of the Law Dome ice margin, Budd Coast, East Antarctica. Ant. Sci. 8:395–406. https://doi.org/10.1017/S0954102096000570

Guitard ME, Shevenell AE, Lavoie C, Domack EW (2016) Mega-scale glacial lineations and grounding-zone wedges in Prydz Channel, East Antarctica. Geol. Soc. London Mem. 46:185–186. https://doi.org/10.1144/M46.110

Harrison JJ, Saunders KM, Chikld DP, Hotchkis MAC (2021) A record of fallout ^{239}Pu and ^{240}Pu at World Heritage Bathurst Harbour, Tasmania, Australia. J. Environm. Radioact. 237:106679. https://doi.org/10.1016/j.jenvrad.2021.106679

Hodgson DA, Whitehouse PL, De Cort G et al. (2016) Rapid early Holocene sea-level rise in Prydz Bay, East Antarctica. Global Planet. Change 139:128–14. https://doi.org/10.1016/j.gloplacha.2015.12.020

Kiernan K, McConnell A, Lawson E (2002) Radiocarbon dating of mumiyo from the Vestfold Hills, East Antarctica*. Papers Proc. Royal Soc. Tasmania* 136:141–144.https://doi.org/10.26749/rstpp.136.141

King MA, Watson CS, White D (2022) GPS rates of vertical bedrock motion suggest late Holocene ice-sheet readvance in a critical sector of East Antarctica. Geophys. Res. Lett. 49:e2021GL097232. https://doi.org/10.1029/2021GL097232

Kirkwood JM, Burton HR (1988) Macrobenthic species assemblages in Ellis Fjord, Vestfold Hills, Antarctica. Mar. Biol. 97:445–457. https://doi.org/10.1007/BF00397776

Mackintosh AN, Verleyen E, O'Brien PE et al. (2014) Retreat history of the East Antarctic Ice Sheet since the Last Glacial Maximum. Quat. Sci. Rev. 100:10–30. https://doi.org/10.1016/j.quascirev.2013.07.024

Marchant HJ, van den Hoff J, Burton HR (1987) Loricate choanoflagellates from Ellis Fjord, Antarctica, including the description of *Acanthocorbis Tintinnabulum* sp. nov. Proc. NIPR Symp. Polar Biol. 1:10–22.

McLennan SM, Haiblen AM, Smith J (2020) Surficial geology of the Vestfold Hills, East Antarctica (1st edition). Scale 1:65 000, Geoscience Australia. http://pid.geoscience.gov.au/dataset/ga/145535

McMinn A (1996) Preliminary investigation of the contribution of fast-ice algae to the spring phytoplankton bloom in Ellis Fjord, eastern Antarctica. Polar Biol. 16:301–307. https://doi.org/10.1007/s003000050057

McMinn A, Hodgson D. (1993) Summer phytoplankton succession in Ellis Fjord, eastern Antarctica*. J. Plankton Res.* 15:925–938. https://doi.org/10.1093/plankt/15.8.925

McMinn A, Gibson J, Hodgson D, Aschman J. (1995) Nutrient limitation in Ellis Fjord, eastern Antarctica. Polar Biol. 15:269 276. https://doi.org/10.1007/BF00239847

McMinn A, Bloxham JJ, Whitehead J (1998) Modern surface sediments and non-deposition in Ellis Fjord, eastern Antarctica. Austr. J. Earth Sci. 45:645–652. https://doi.org/10.1080/08120099808728419

McMinn A, Heijnis H, Harle K, McOrist G (2001) Late-Holocene climatic change recorded in sediment cores from Ellis Fjord, eastern Antarctica. The Holocene 11:291–300. https://doi.org/10.1191/095968301671577682

Miura H, Maemoku H, Seto K, Moriwaki K (1998) Late Quaternary East Antarctic melting event in the Soya Cast region based on stratigraphy and oxygen isotope ratio of fossil mollusks. Polar Geosci. 11:260–274.

O´Brien PE, Smith J, Stark JS et al. (2015) Submarine geomorphology and sea floor processes along the coast of Vestfold Hills, East Antarctica, from multibeam bathymetry and video data. Ant. Sci. 27:566–586. https://doi.org/10.1017/S0954102015000371

Pickard J., Adamson DA, Heath CW (1986) The evolution of Watts Lake, Vestfold Hills, East Antarctica, from marine inlet to freshwater lake. Palaeogeogr., Palaeoclimatol., Palaeoecol. 53:271–288. https://doi.org/10.1016/0031-0182(86)90063-5

Pollard D, DeConto RM (2009) Modelling West Antarctic ice sheet growth and collapse through the past five million years. Nature 458:329–332. https://doi.org/10.1038/nature07809

Pritchard H, Ligtenberg SRM, Fricker HA et al. (2012) Antarctic ice- sheet loss driven by basal melting of ice shelves. Nature 484:502–505. https://doi.org/10.1038/nature10968

Roberts D, McMinn A (1998) A weighted averaging regression and calibration model for inferring lakewater salinity from fossil diatom assemblages in saline lakes of the Vestfold Hills: a new tool for interpreting Holocene lake histories in Antarctica. J. Paleolimnol. 19:99–113. https://doi.org/10.1023/A:1007947402927

Sheraton JW, Cundari A. (1980) Leucitites from Gaussberg, Antarctica. Contrib. Mineral. Petrol. 71:417–427. https://doi.org/10.1007/BF00374713

Süfke F, Gutjahr M, Gilli A, Anselmetti FS, Glur L, Eisenhauer A. (2019) Early stage weathering systematics of Pb and Nd isotopes derived from a high-Alpine Holocene lake sediment record. Chemical Geol, 507: 42–53. https://doi.org/10.1016/j.chemgeo.2018.12.026

Tingey RJ, McDougall I, Gleadow AJW (1983): The age and mode of formation of Gaussberg, Antarctica. J. Geol. Soc. Ausralia 30:241–246. https://doi.org/10.1080/00167618308729251

White DA, Fink D, Gore DB (2011) Cosmogenic nuclide evidence for enhanced sensitivity of an East Antarctic ice stream to change during the last deglaciation. Geology 39:23–26. https://doi.org/10.1130/G31591.1

White DA, Fink D, Lilly K et al. (2022) Rapid ice sheet response to deglacial and Holocene paleoenvironmental changes in eastern Prydz Bay, East Antarctica. Quatern. Sci. Rev. 280:107401. https://doi.org/10.1016/j.quascirev.2022.107401

Whitehouse PL, Bentley MJ, Milne GA, King MA, Thomes ID (2012) A new glacial isostatic adjustment model for Antarctica: calibrated and tested using observations of relative sea-level and present-day uplift rates. Geophys. J. Int. 190:1464–1482. https://doi.org/10.1111/j.1365-246X.2012.05557.x

Whitehouse PL, Gomez N, King MA, Wiens DA (2019) Solid Earth change and the evolution of the Antarctic Ice Sheet. Nature Comm. 10:503. https://doi.org/10.1038/s41467-018-08068-y

Zwartz D, Bird M, Stone J, Lambeck K (1998) Holocene sea-level change and icesheet history in the Vestfold Hills, East Antarctica. Earth Planet Sci. Lett. 155:131–145. https://doi.org/10.1016/S0012-821X(97)00204-5

7. IMPACT OF IRON/MANGANESE/B_{12} (CO-) LIMITATION AND LIGHT AVAILABILITY ON PRIMARY PRODUCTION AND COMMUNITY COMPOSITION OF EAST ANTARCTIC PHYTOPLANKTON

Jasmin Stimpfle[1], Robin van Dijk[2], Marrit Jacob[1], Florine Kooij[2,4], Rob Middag[2,4] not on board: Scarlett Trimborn[1], Florian Koch[1], Willem Willem van de Poll[4]

[1] DE.AWI
[2] NL.NIOZ
[3] DE.UNI-BREMEN
[4] NL.UNI-GRONINGEN

Grant-No. AWI_PS140_02

Outline and objectives

The production of oceanic phytoplankton that form the base of the marine food web depends on the availability of sunlight and nutrients, typically nitrogen and phosphorus (and silicate for diatoms). The Southern Ocean, however, is an important high nutrient low chlorophyll (HNLC) area (Bruland et al., 2014; Moore et al., 2013), where iron (Fe) affects the amount of atmospheric CO_2 sequestered in deep ocean waters and ocean sediments via the biological pump (De La Rocha and Passow, 2014), with far reaching implications for the global climate and the local ecosystem (Arrigo et al., 2008; Boyd and Ellwood, 2010; Tagliabue et al., 2017). Yet, it is becoming increasingly clear that the situation is more complex, and controlled by factors beyond just the scarcity of Fe. New insights highlight the importance of other trace-metals (Morel et al., 2014), co-limitation by two or more nutrients (Arrigo, 2005; Middag et al., 2013; Saito and Goepfert, 2008; Saito et al., 2008) and variability in nutrient requirements between species and environmental conditions (Arrigo and van Dijken, 2003; Klunder et al., 2014; Moore et al., 2013). Specifically, manganese (Mn) and the cobalt containing cobalamine have also been found to (co-)limit primary productivity (Balaguer et al., 2022; Bertrand et al., 2007; Browning et al., 2021; Wu et al., 2019) and to drive carbon export fluxes (Balaguer et al. 2023) in the Southern Ocean.

Notably for Fe, its solubility and probably also its bioavailability depends strongly on the Fe-binding dissolved organic ligands (Ardiningsih et al., 2021; Gledhill and Buck, 2012). Microbial community composition as well as microbial interactions impact the production and cycling of metals and metal-binding ligands (Fourquez et al., 2023; Fourquez et al., 2022). Antarctic waters undergo rapid changes in physiochemical variables due to global climate change, including warming, changing light conditions and altered trace metal input (Jabre et al., 2021; Joy-Warren et al., 2022; McCain et al., 2021). Additionally, these changes may affect the metal requirements and their availability to phytoplankton. This will be reflect in a changing phytoplankton community, as not all phytoplankton species are equally sensitive to changing environmental conditions.

Our aims were:

- Identifying and comparing Fe-Mn-B_{12} (co-)limitation of natural phytoplankton assemblages across the cruise transect (coastal and offshore)
- Assessing how different light and trace metal availabilities affect phytoplankton species composition and carbon fixation

- Determining the photophysiological state of phytoplankton communities and estimating the production of reactive oxygen species in response to Fe-Mn-B_{12} and light amendments
- Quantifying vitamin B_{12} concentrations in surface water and along a depth gradient at up to 5 stations
- Assessing compositional changes of phytoplankton-associated bacterial communities under Fe-Mn-B_{12} (co-)limitation

Work at sea

Following GEOTRACES protocols (www.geotraces.org) and using the Titan trace metal clean seawater sampling system (De Baar et al., 2008, see section 4) water was collected to perform phytoplankton nutrient enrichment experiments and to measure vitamin B_{12} concentrations:

Large volume bioassays

At stations PS140_9, PS140_125 and PS140_126 (Appendix Table 4.2), trace metal clean 2.7L polycarbonate bottles were filled with water from 25m depth and amended in triplicates with 0.5nM $FeCl_3$ or a combination of 0.5nM $FeCl_3$ and 1nM $MnCl_2$. Each trace metal amendment was then combined with two light levels: 30 µmol photons m^{-2} s^{-1} (ambient light) and 80µmol photons m^{-2} s^{-1} (high light) at a light:dark cycle of 18:6 hours. Incubations were grown in a temperature-controlled room at 2°C for 7 to 11 days. During the experiment, nitrate drawdown was monitored using a photometric rapid test (HANNA Instruments). Furthermore, photosynthetic efficiency of the cells (F_v/F_m) was determined via fast repetition rate fluorometry (FRRf, Chelseax) to monitor responses to trace metal additions. At the beginning and end of the experiment, a set of samples was taken to determine species shifts, growth rates and the physiological state of the cells:

- For taxonomic analysis (light microscopy), 100ml unfiltered seawater from each bottle was preserved in Lugol's solution (1% final concentration). To estimate bacterial and picoplankton abundance, unfiltered seawater was preserved in formalin (1% final concentration) and frozen at -80°C until analysis via flow cytometry at AWI.
- To map the distribution of trace metals within single phytoplankton cells, seawater was preserved with formalin (5% final concentration) and will be analyzed at the Australian Synchrotron facility.
- Photophysiological performance of the cells was determined using fast repetition rate fluometry (FRRf) after dark acclimation for 40 minutes and exposure to increasing irradiance (fluorescence light curve, up to 600 µmol photons m^{-2} s^{-1}).
- Seawater pH was measured onboard using a calibrated pH/ion meter (Methrom, three-point calibration).
- Samples for particulate organic carbon (POC) were filtered on precombusted (500° C; 12 h) GFF filters (Whatman) and stored in precombusted petri dishes at -20°C.
- Samples for photosynthetic pigments were filtered on GFF (Whatman) filters and immediately frozen at -80°C.
- Macronutrient concentrations (nitrate, phosphate, silicate and ammonium) in 0.2µm filtered seawater (frozen at -20°C) will be measured at AWI.
- Intracellular concentrations of reactive oxygen species (ROS) were determined after concentrating the cells (10x concentration) via gravity filtration and a subsequent

incubation with a fluorescent dye (H_2DCFDA, carboxy derivative of fluorescein) at a final concentration of 10µM. Raw fluorescence was measured on a Turner Trilogy in combination with a fluorescein module and will be normalized to POC.

- To estimate primary production, cells were spiked with ^{13}C and incubated for 24h. Assuming an in-situ concentration of dissolved inorganic carbon of 2200 µM, 8% ^{13}C was added.
- For the control and $FeCl_3$ treatment under ambient light, 250ml of culture were filtered in series on a 3µm and 0.2µm polycarbonate filter for 16s analysis to determine the composition of phytoplankton-associated bacterial communities. Filters were treated with SL1 buffer for preservation of DNA, flash frozen, and kept at -80°C.

Small volume bioassays

In addition, shorter (72h) small volume bioassays were conducted at 33 stations (see Tab. 7.1) by the addition of 1 nM inorganic Fe, 1 M Mn, and combinations of Fe with 1 nM Mn and 1 nM Mn + 100 pM vitamin B_{12}. The 250 mL incubation bottles (polycarbonate) used were acid cleaned before the expedition using 0.1 M HCl and thoroughly rinsed before drying and packing under clean room conditions at NIOZ. During the expedition, cleaned 1L LDPE bottles were rinsed 5 times with sample seawater, one bottle for each treatment. The micronutrient were added to these bottles. Subsequently the clean incubation bottles were filled and incubated under constant irradiance (30 µmol photons m^{-2} s^{-1}) for ~72 h in a temperature-controlled room at 2°C. Triplicate samples were taken for every treatment. These experiments will use changes in photophysiology (fast repetition rate fluorometry, FRRf, Chelsea), chlorophyll a (measured by fluorometry after extraction from 25 mm GF/F filters), and macronutrient drawdown (phosphate, nitrite and nitrate, sample using the same protocol as the regular nutrient sampling from the clean CTD, see Chapter 4) after ~72 h as proxies to identify responses to the micronutrient additions in comparison to the control treatment. At stations where a small-volume bioassay was started, an HPLC and a chlorophyll-a -sample were taken from the same depth by filtering water over 47mm and 25mm GF/F filters, respectively. After shore-based analysis, the outcome of these experiments can be compared with the chemical (nutrient and trace metal concentrations) and biological (phytoplankton biomass and taxonomic composition assessed from HPLC derived pigments) context of the sample, mapping limitation by Fe, Mn and or B_{12} limitation along the transect of PS140.

Vitamin B_{12} concentrations

At all stations where small volume bioassays were started (Tab. 7.1), 2L of 0.2µm filtered seawater from the same depth were concentrated on a prepacked SPE column. Vitamin B12 concentrations will be determined by solid phase extraction at AWI.

Additionally, depth profiles of vitamin B_{12} concentrations were taken at 3 stations (Tab. 7.2)

Preliminary (expected) results

The expected data set will characterize vitamin B_{12} distribution in open water as well as coastal areas of East Antarctica and provide concentrations in surface and deep water. Further, incubation experiments in which natural phytoplankton communities are enriched with trace metals (Fe and Mn) and vitamin B_{12} will reveal (co-) limitation of these nutrients in different regions of Prydz Bay. The exposure of these incubations to ambient and elevated light intensities will additionally elucidate physiological responses in relation to these two environmental drivers (trace metal and light availability) that are suspected to change in the future.

Large volume bioassays

Preliminiary results from fast repetition rate fluometry hint towards iron limitation of the phytoplankton community at station 9 and 125 and potentially iron and manganese co-limitation at station 126, as photosynthetic efficiency increased in response to the respective trace metal additions. These results, however, need to be interpreted within the context of all the other parameters that were taken and that will be measured at AWI to validate iron and manganese (co-) limitation and potential effects on cell physiology.

Tab. 7.1: List and sampling depth of all CTD stations from PS140 that have been sampled for small bioassay experiments.

Station	Depth (m)
PS140_2-2	30
PS140_3-2	30
PS140_9-1	35
PS140_11-6	35
PS140_12-2	35
PS140_13-6	35
PS140_14-2	15
PS140_15-2	30
PS140_17-2	15
PS140_19-3	20
PS140_25-2	25
PS140_32-2	30
PS140_36-2	20
PS140_43-2	25
PS140_51-2	30
PS140_57-2	20
PS140_73-2	20
PS140_74-2	20
PS140_82-2	35
PS140_90-2	25
PS140_107-2	20
PS140_116-2	20
PS140_123-2	20
PS140_124-6	20
PS140_125-5	20
PS140_126-2	20
PS140_128-2	20
PS140_129-2	20
PS140_130-2	20
PS140_131-2	20
PS140_132-2	20
PS140_134-4	20
PS140_135-2	20

Small volume bioassays

The analysis of the GF/F filters will be conducted at the University of Groningen, the Netherlands, by high performance liquid chromatography (HPLC). An example of the data collected on board by measuring photosynthetic efficiency (Fv/Fm) and chlorophyll-a-concentration using the FRRf (as described in chapter 4 is shown in Figure 7.1. Measured F_v/F_m can be an indication of Fe limitation as Fe is an essential nutrient for photosystem II in phytoplankton.

Vitamin B12 concentrations
To be analyzed at AWI

Tab. 7.2: Sampling depths for vertical profiles to determine vitamin B_{12} concentrations.

Station	Depth (m)
PS140_11-6	12
	28
	63
	989
	2233
PS140_16-2	8
	52
	134
	580
	758
PS140_51-2	11
	30
	47
	98
	318
	681

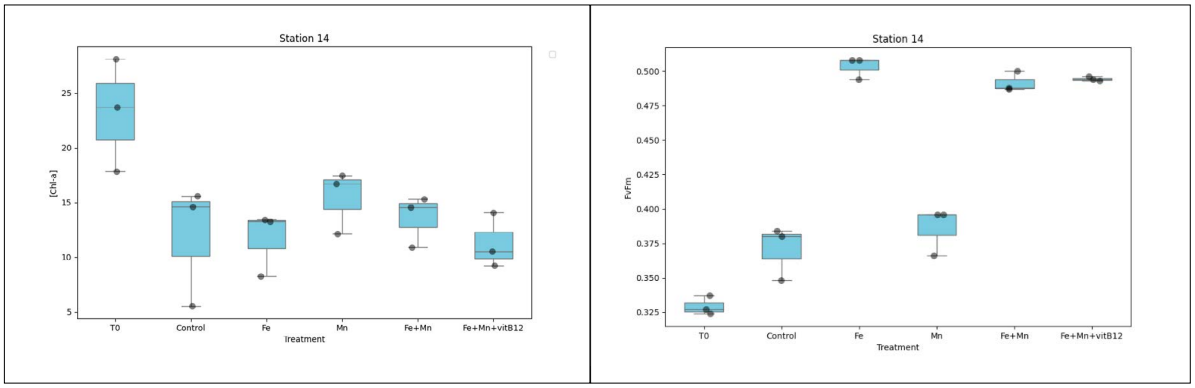

(a) (b)

Fig. 7.1: Preliminary results of (a) chlorophyll a measured, and (b) photosynthetic efficiency (Fv/Fm) after 72 h of incubation of surface water at station 14 at different treatment levels

Data management

Environmental data will be archived, published and disseminated according to international standards by the World Data Center PANGAEA Data Publisher for Earth & Environmental Science (https://www.pangaea.de) within two years after the end of the expedition at the latest. By default, the CC-BY license will be applied.

Molecular data (DNA and RNA data) will be archived, published and disseminated within one of the repositories of the International Nucleotide Sequence Data Collaboration (INSDC, www.insdc.org) comprising of EMBL-EBI/ENA, GenBank and DDBJ).

Any other data will be submitted to an appropriate long-term archive that provides unique and stable identifiers for the datasets and allows open online access to the data.

This work contributes to the Helmholtz Research Programme “Changing Earth – Sustaining our Future” Topic 6, Subtopic 6.1 and 6.2. It further contributes to Topic 2, Subtopics 2.1, 2.2, and 2.4.

References

Ardiningsih I, Seyitmuhammedov K, Sander SG, Stirling CH, Reichart GJ, Arrigo KR, Gerringa LJA, Middag R (2021) Fe-binding organic ligands in coastal and frontal regions of the western Antarctic Peninsula. Biogeosciences 18:4587–4601. https://doi.org/10.5194/bg-18-4587-2021

Arrigo KR (2005) Marine microorganisms and global nutrient cycles. Nature 437:349–355. https://doi.org/10.1038/nature04159

Arrigo KR, van Dijken G, Long M (2008) Coastal Southern Ocean: A strong anthropogenic CO_2 sink. Geophys Res Lett 35. https://doi.org/10.1029/2008GL035624

Arrigo KR, van Dijken GL (2003) Phytoplankton dynamics within 37 Antarctic coastal polynya systems. J Geophys Res Oceans 108. https://doi.org/10.1029/2002JC001739

Balaguer J, Koch F, Hassler C, Trimborn S (2022) Iron and manganese co-limit the growth of two phytoplankton groups dominant at two locations of the Drake Passage. Commun Biol 5:207. https://doi.org/10.1038/s42003-022-03148-8

Balaguer J, Koch F, Flintrop C, Völkner C, Iversen M, Trimborn S (2023) Iron and manganese availability drive primary production and carbon export in the Weddell Sea. Curr Biol, https://doi.org/doi.org/10.2139/ssrn.4342993

Bertrand EM, Saito MA, Rose JM, Riesselman CR, Lohan MC, Noble AE, Lee PA, DiTullio GR (2007) Vitamin B-12 and iron colimitation of phytoplankton growth in the Ross Sea. Limnol Oceanogr 52:1079–1093. https://doi.org/10.4319/lo.2007.52.3.1079

Boyd PW, Ellwood MJ (2010) The biogeochemical cycle of iron in the ocean. Nat Geosci 3: 675–682. https://doi.org/10.1038/ngeo964

Browning TJ, Achterberg EP, Engel A, Mawji E (2021) Manganese co-limitation of phytoplankton growth and major nutrient drawdown in the Southern Ocean. Nat Commun 12:884. https://doi.org/10.1038/s41467-021-21122-6

Bruland KW, Middag R, Lohan MC (2014) 8.2 - Controls of Trace Metals in Seawater, in: Holland, H.D., Turekian, K.K. (Eds.), Treatise on Geochemistry (Second Edition). Elsevier, Oxford, pp. 19–51. https://doi.org/10.1016/B978-0-08-095975-7.00602-1

De Baar HJW, Timmermans KR, Laan P, De Porto HH, Ober S, Blom JJ, Bakker MC, SchillingJ, Sarthou G, Smit MG, Klunder M (2008) Titan: A new facility for ultraclean sampling of trace elements and isotopes in the deep oceans in the international Geotraces program. Mar Chem 111:4–21. https://doi.org/10.1016/j.marchem.2007.07.009

De La Rocha CL, Passow U (2014) 8.4 - The Biological Pump, in: Turekian, H.D.H.K. (Ed.), Treatise on Geochemistry (Second Edition). Elsevier, Oxford, pp. 93–122. https://doi.org/10.1016/B978-0-08-095975-7.00604-5

Fourquez M, Janssen DJ, Conway TM, Cabanes D, Ellwood MJ, Sieber M, Trimborn S, Hassler C (2023) Chasing iron bioavailability in the Southern Ocean: Insights from Phaeocystis antarctica and iron speciation. Sci Adv 9:eadf9696. https://doi.org/10.1126/sciadv.adf9696

Fourquez M, Strzepek RF, Ellwood MJ, Hassler C, Cabanes D, Eggins S, Pearce I, Deppeler S, Trull TW, Boyd PW, Bressac M (2022) Phytoplankton Responses to Bacterially Regenerated Iron in a Southern Ocean Eddy. Microorganisms 10:1655. https://doi.org/10.3390/microorganisms10081655

Gledhill M, Buck KN (2012) The organic complexation of iron in the marine environment: a review. Front in Microbiol 3. https://doi.org/10.3389/fmicb.2012.00069

Jabre LJ, Allen AE, McCain JSP, McCrow JP, Tenenbaum N, Spackeen JL, Sipler RE, Green BR, Bronk DA, Hutchins DA, Bertrand EM (2021) Molecular underpinnings and biogeochemical consequences of enhanced diatom growth in a warming Southern Ocean. Proc Natl Acad Sci 118:e2107238118. https://doi.org/10.1073/pnas.2107238118

Joy-Warren HL, Alderkamp A-C, van Dijken GL, J Jabre L, Bertrand EM, Baldonado EN, Glickman MW, Lewis KM, Middag R, Seyitmuhammedov K, Lowry KE, van de Poll W, Arrigo KR (2022) Springtime phytoplankton responses to light and iron availability along the western Antarctic Peninsula. Limnol Oceanogr 67:800–815. https://doi.org/10.1002/lno.12035

Klunder MB, Laan P, De Baar HJW, Middag R, Neven I, Van Ooijen J (2014) Dissolved Fe across the Weddell Sea and Drake Passage: impact of DFe on nutrient uptake. Biogeosciences 11: 651–669. https://doi.org/10.5194/bg-11-651-2014

McCain JSP, Tagliabue A, Susko E, Achterberg EP, Allen AE, Bertrand EM (2021) Cellular costs underpin micronutrient limitation in phytoplankton. Sci Adv 7:eabg6501. https://doi.org/10.1126/sciadv.abg6501

Middag R, de Baar HJW, Klunder MB, Laan P (2013) Fluxes of dissolved aluminum and manganese to the Weddell Sea and indications for manganese co-limitation. Limnol Oceanogr 58:287–300. https://doi.org/10.4319/lo.2013.58.1.0287

Moore CM, Mills MM, Arrigo KR, Berman-Frank I, Bopp L, Boyd PW, Galbraith ED, Geider RJ, Guieu C, Jaccard SL, Jickells TD, La Roche J, Lenton TM, Mahowald NM, Maranon E, Marinov I, Moore JK, Nakatsuka T, Oschlies A, Saito MA, Thingstad TF, Tsuda A, Ulloa O (2013) Processes and patterns of oceanic nutrient limitation. Nat Geosci 6:701–710. https://doi.org/10.1038/ngeo1765

Morel FMM, Milligan AJ, Saito MA (2014). 8.5 - Marine Bioinorganic Chemistry: The Role of Trace Metals in the Oceanic Cycles of Major Nutrients, in: Holland, H.D., Turekian, K.K. (Eds.), Treatise on Geochemistry (Second Edition). Elsevier, Oxford, pp. 123–150.

Saito MA, Goepfert TJ (2008) Zinc-cobalt colimitation of Phaeocystis antarctica. Limnol Oceanogr 53:266–275. https://doi.org/10.2307/40006167

Saito MA, Goepfert TJ, Ritt JT (2008) Some thoughts on the concept of colimitation: Three definitions and the importance of bioavailability. Limnol Oceanogr 53:276–290. https://doi.org/10.4319/lo.2008.53.1.0276

Tagliabue A, Bowie AR, Boyd PW, Buck KN, Johnson KS, Saito MA (2017) The integral role of iron in ocean biogeochemistry. Nature 543:51–59. https://doi.org/10.1038/nature21058

Wu M, McCain JSP, Rowland E, Middag R, Sandgren M, Allen AE, Bertrand EM (2019) Manganese and iron deficiency in Southern Ocean Phaeocystis antarctica populations revealed through taxon-specific protein indicators. Nat Commun 10:3582. https://doi.org/10.1038/s41467-019-11426-z

8. RESPONSE OF ANTARCTIC PHYTOPLANKTON TO EPIBIOTIC MICROBIAL COLONIZATION

Marrit Jacob[1,2], Jasmin Stimpfle[2], Florine Kooij[3,4], Robin van Dijk[4], Rob Middag[3,4]

not on board: Tilmann Harder[1], Jan Tebben[2]

[1]DE.UNI-BREMEN
[2]DE.AWI
[3]NL.NIOZ
[4]NL.UNI-GRONINGEN

Grant-No. AWI_PS140_02

Outline

Diatoms are essential players in the global carbon cycle and the oceans' food webs (Field et al., 1998). Their productivity is substantially influenced by their microbiome, a community of bacterial epibionts colonizing the microenvironment ("phycosphere") immediately surrounding the host (Amin et al., 2012; Jackrel et al., 2021; Seymour et al., 2017). The taxonomic composition of microbiomes benefitting host growth varies between host taxa and is rather stable across time and different environments (Behringer et al., 2018; Mönnich et al., 2020). Phytoplankton hosts must therefore recognize and select their preferred epibionts from the surrounding water through processes yet uncovered. The dynamics of microbiome assembly in the phycosphere of important Southern Ocean diatoms and the effect of the microbiome on host productivity and fitness are largely unknown.

Pre-experiments revealed an algicidal effect of a *Croceibacter atlanticus* (*Flavobacteriales*) isolate obtained in the Weddell Sea to a co-occuring *Fragilariopsis kerguelensis* strain. After one week of co-culture, the diatom chlorophyll fluorescence was significantly reduced in the presence of *C. atlanticus* (Jacob et al., unpublished). These findings are in accordance with recent observations by Bartolek et al. (2022) and Van Tol et al. (2017), yet their studies assessed co-cultures of algae and bacteria from geographically unrelated environments. Long-term culturing revealed a delayed but similarly detrimental effect when *C. atlanticus* was inoculated to *F. kerguelensis* in conjunction with 36 other bacterial strains, as well as in the presence of an intact microbiome of a xenic *F. kerguelensis* culture. The difference in timing in the onset of the algicidal effect of *C. atlanticus* on *Fragilariopsis* suggests a potential protective or buffering effect of co-occuring bacteria and the established *F. kerguelensis* microbiome.

Objectives

We aimed to

- examine the effects of natural Southern Ocean bacterial assemblages on Southern Ocean diatom growth (fitness/productivity effects of bacterial epibionts)
- examine the effects of natural Southern Ocean bacterial assemblages on a Southern Ocean diatom transcriptome at different timepoints (host recognition, signalling, and response to bacterial epibionts)
- assess the role of microbiome composition in mediating the vulnerability to the algicidal bacterium *C. atlanticus* (protective effect of different consolidated microbiomes)

The growth of the Southern Ocean diatom *Thalassiosira antarctica* measured on the cruise will be correlated with the relative abundances of different bacterial taxa in the source communities to characterize the influence of different bacterial communities on diatom growth. The host transcriptome will be analysed to assess the accompanying processes of recognition, signal transduction, and host response. After establishment of newly consolidated microbiomes in the co-cultures, exposure to *C. atlanticus* has been used to assess the role of the newly established microbiomes in facilitating the host's resilience towards algicidal bacteria. The project seeks to improve the understanding of diatom-bacteria community dynamics in a host species with great importance for Southern Ocean ecosystems, and to foster a mechanistic understanding of general processes in the assembly and consolidation of diatom microbiomes and their implications for diatom productivity under ongoing global change.

Work at sea

Water sampling

Using the Titan trace metal clean seawater sampling system (De Baar *et al.*, 2008; see Chapter 4/sea water sampling from the clean CTD), 10-20L of sea water from the chlorophyll maximum at 14-31m depth was collected at oceanographically diverse stations (see Tab. 8.1) to harvest natural bacterial and phytoplankton communities. For the Microbiome Assembly Experiment (MAE, see Fig. 8.1), stations were chosen by location, suspected nutrient availability, and by roughly microscopically assessed phytoplankton composition and bloom stage (stations 14 and 32: relatively diverse diatom communities, station 51: mostly *Phaeocystis sp.,* few diatoms). The sampled seawater was sequentially filtered over 3µm and 1µm and the filtrate was concentrated over a 0.2µm pore-size tangential flow filtration system (Vivaflow® 200 TFF system, Sartorius, Göttingen/Germany) by a concentration factor of 200-1000x to harvest and concentrate the bacterioplankton. Samples for phytoplankton and bacterial community composition (Lugol- and Formalin-fixed) as well as for macronutrients and iron (see chapter 4/ sea water sampling from the clean CTD) were additionally taken at each of the four stations to characterize the abiotic and biotic source conditions. At station PS140_14, 9L of seawater containing a natural phytoplankton community was retrieved for use in the Field Phytoplankton/ Lab Bacteria Experiment (FiPLaB, see below). To assess phytoplankton community composition and the functional range of associated bacteria, an additional 1L of seawater was taken at 6 stations (stations PS140_9, PS140_14, PS140_57, PS140_124, PS140_126, PS140_129, PS140_131) for assessment of phytoplankton taxonomic composition (18S rRNA DNA metabarcoding) and analysis of bacterial metagenomics (MG experiment). The samples were taken from the water depth with maximum chlorophyll ("bioassays", see supplementary table 4.2) and 500-900ml were filtered in series over a 3µm polycarbonate filter (18S analysis) and then a 0.2µm filter (bacterial metagenomics). Filters were treated with SL1 buffer for preservation of DNA, flash frozen, and kept at -80°C.

An attempted isolation of single strains of diatoms (*Navicula sp.* and *Fragilariopsis sp*.) failed (no growth after two weeks in Keller growth medium with silicate addition), so a complex natural phytoplankton community incubated in sterile filtered sea water and Keller medium with silicate addition from stations PS140_9, PS140_14, PS140_125, PS140_126, and PS131 will be brought back to Bremerhaven for subsequent isolation of single diatom strains.

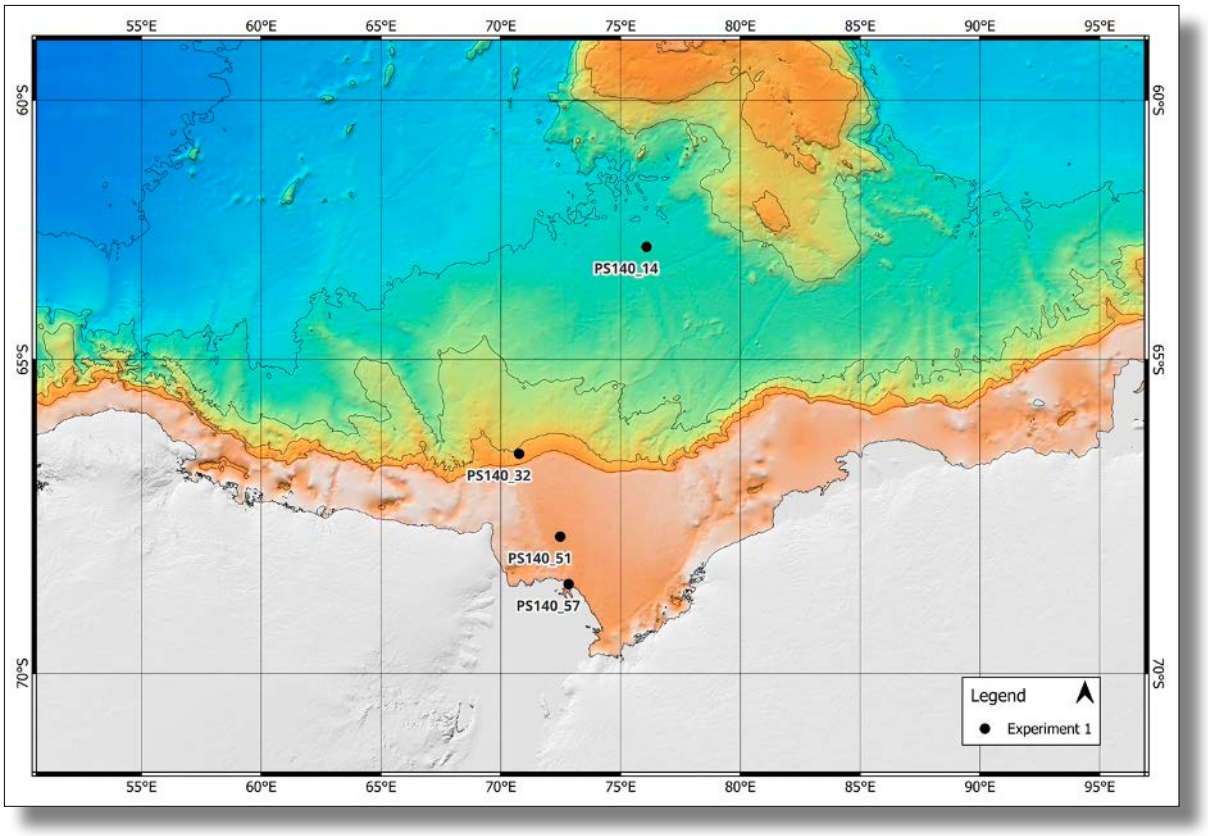

Fig. 8.1: Locations of sampling sites for the Microbiome Assembly Experiment (MAE, all depicted stations, black dots) and Field Phytoplankton/Lab Bacteria Experiment (FiPLaB, station PS140_14, red circle)

Tab. 8.1: Station metadata for sampled seawater stations

Station	Location	Station depth	Sampling depth	Chlorophyll a (CTD sensor)	Latitude	Longitude	Date	Experiment
PS140_9	open ocean	4740 m	20.5 m		-53.2580	57.1734	09.12.2023	MG
PS140_14	open ocean	3824 m	30.5 m	3.65 mg/m3	-62.9286	76.08094	14.12.2023	MAE/FiPLaB
PS140_32	Antarctic shelf edge	1800 m	31 m	6.06 mg/m3	-66.614	70.76462	23.12.2023	MAE
PS140_51	on Antarctic shelf	693 m	30.5 m	26.37 mg/m3	-67.9501	72.48076	27.12.2023	MAE
PS140_57	ice shelf edge	697 m	21.2 m	8.84 mg/m3	-68.6821	72.82998	29.12.2023	MAE/MG
PS140_124	open ocean	4490 m	14 m		-60.9016	100.9442	12.01.2024	MG
PS140_126	open ocean	4231 m	26.5 m		-57.4321	101.4168	14.01.2024	MG
PS140_129	open ocean	3719 m	23.5 m		-53.4220	103.9230	16.01.2024	MG
PS140_131	open ocean	3274 m	18 m		-50.2236	104.5105	19.01.2024	MG

Ice sampling

Ice samples were taken at four stations from a zodiac (5-20L per station). Samples were stored in trace-metal clean plastic bags which were labelled according to Table 8.2. Position data was recorded with a portable GPS. A rubber hammer and latex gloves were used to keep the samples as trace metal clean as possible. Ice containing visible amounts of ice algae was gently thawed at 2°C and kept in 0.45µm filtered sea water for cultivation. Samples are cultivated at 4°C and approximately 3 µE light intensity with a 4:20 day/night cycle for the transfer back to Bremerhaven for subsequent isolation of single strains of ice algae.

Tab. 8.2: Metadata of ice sampling

Sample #	Latitude	Longitude	
1	68° 35.000’ S	77° 50.000’ E	17.12.2023
2	68° 35.000’ S	77° 50.000’ E	17.12.2023
3	68° 35.000’ S	77° 50.000’ E	17.12.2023
4	68° 35.000’ S	77° 50.000’ E	17.12.2023
5	68° 35.000’ S	77° 50.000’ E	17.12.2023
6	68° 35.000’ S	77° 50.000’ E	17.12.2023
7	68° 38.306’ S	77° 45.421’ E	04.01.2024
8	68° 37.906’ S	77° 45.049’ E	04.01.2024
9	68° 32.992’ S	77° 52.463’ E	18.01.2024
10	68° 38.327’ S	77° 45.847’ E	04.01.2024
11	68° 38.114’ S	77° 45.665’ E	04.01.2024
12	68° 33.209’ S	77° 52.290’ E	18.01.2024
13	68° 38.302’ S	77° 45.941’ E	04.01.2024
14	69° 18.994’ S	75° 06.768’ E	30.12.2024
16	68° 33.068’ S	77° 52.995’ E	18.01.2024
17	68° 33.005’ S	77° 53.210’ E	18.01.2024

Incubation experiments

An axenic (bacteria-free) and a xenic (bacteria-containing) laboratory *Fragilariopsis kerguelensis* culture were brought on board in Bremerhaven before the transit. They were kept at 0°C and 30µE light intensity with a 16:8 day/night cycle and were refreshed with sterile culture media once during the transit. The axenic and xenic stock cultures kept at the laboratory at the University of Bremen, which the cultures on board originated from, seized growth completely around that time and the original stock culture from the culture archive CCAC in Cologne, Germany, was also not viable anymore, which is why it was suspected that also the culture on board was not viable. Therefore, a back-up culture of the Southern Ocean diatom species *Thalassiosira antarctica* was retrieved from CCAC and brought along to the cruise by plane in cooled containers (300ml total culture volume). *T. antarctica* was then cultivated on board at 2°C and 35µE at a 18:6 day/night cycle to large volumes and rendered axenic through a combination of mechanical and chemical removal of the associated bacteria using filtration, a detergent treatment, and an antibiotics mix. After having reached sufficient biomass of the culture, axenic *T. antarctica* was inoculated with bacterial communities obtained at the 4 stations mentioned above with axenic and xenic control treatments running alongside. All treatments were run in triplicates and incubated for 12 days to allow for establishment of a stable diatom microbiome (Microbiome Assembly Experiment, MAE). Samples of diatom RNA (40-50 ml) were taken from the co-cultures in fixed time intervals (2 hours, 2 days, and 12 days after inoculation with the bacterial communities) to track the transcriptomic response

of the diatom to the presence of bacterioplankton from different sources. RNA sampling was supplemented by sampling for 16S metabarcoding (40ml of culture on 3µm/0.2µm filters) on day 2 and 12 to track dynamics of bacterial community composition during the establishment of diatom microbiomes. Filters for RNA and DNA were treated with buffer, flash frozen, and kept at -80°C. Growth of the diatom was tracked by *in vivo* chlorophyll-a-fluorescence (Turner Trilogy fluorometer, Turner Designs, USA) over time and by sampling for bacterial and algal abundance on 3 timepoints during the experiment as well as biomass/particulate organic carbon and dissolved silicate/nitrate/phosphate at the final sampling. Measurement of F_v/F_m (indicative of the quantum yield of photosystem II) via fast repetition rate fluometry (FRRf, Chelsea, USA) gave an indication of potentially accompanying photophysiological changes. After 12 days, 1 solidly growing replicate of each of the diatom-bacteria co-cultures was selected (replicates 14A, 32A, 51B, 57B), diluted to matching abundances of 8000 cells/ml, and exposed to the algicidal bacterium *Croceibacter atlanticus* in triplicates, using a non-exposed culture as control (*Croceibacter* response experiment, CRE). Again, diatom growth as well as shifts in bacterial community composition (16S metabarcoding) were tracked over time. Due to the necessity of re-establishing and cultivating an axenic back-up culture during the course of the cruise, there were considerable time constraints for CRE. As a result, sampling for RNA as well as bacterial and algal abundance was only conducted on day 5 of the CRE and the experiment was terminated on day 6.

During establishment of the axenic back-up culture, one smaller experiment (Field phytoplankton/ lab bacteria experiment, FiPLaB) was run using a natural phytoplankton community (PS140_14), which was inoculated with either *Croceibacter atlanticus* (with presumed algicidal effect on diatoms) or *Pseudomonas sp.* (with presumed beneficial/neutral effect on diatoms), run alongside a non-inoculated control. The objective of this experiment was to assess transcriptomic and compositional dynamics of a natural phytoplankton community under a simulated invasion of bacteria. Growth was tracked as *in vivo* chlorophyll a fluorescence. RNA samples (200ml) were taken 2 hours, 2 days and 7 days after inoculation and were supplemented with samples for 16S metabarcoding (bacterial community composition) as well as samples for bacterial and algal abundance, biomass/particulate organic carbon, and dissolved silicate/nitrate/phosphate.

Sample processing and sequencing for all experiments will commence on land.

Preliminary results

During MAE, axenic and xenic controls showed more consistent (less variable) *in vivo* chlorophyll-a-values, whereas the treatments using field bacteria showed strong variability in *in vivo* chlorophyll-a-responses between replicates over time (see Figure 8.2). Median *in vivo* chlorophyll-a-values on day 12 were lowest for the axenic control and highest for the xenic control, whereas the bacterial community treatments all had intermediate *in vivo* chlorophyll-a -responses (Fig. 8.3). This suggests a potential positive and possibly differential effect of the presence of field bacteria on diatom growth during the establishment of a new diatom microbiome. All samples apart from *in vivo* chlorophyll fluorescence and F_v/F_m measurements will be processed on land.

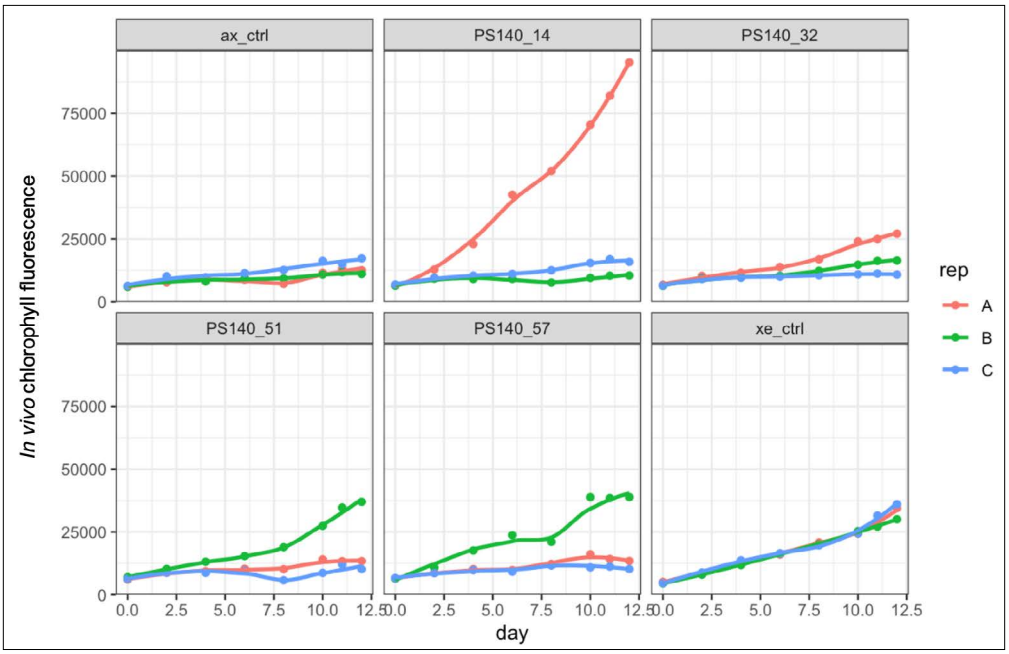

Fig. 8.2: Microbiome Assembly Experiment MAE. Time series of in vivo chlorophyll fluorescence by treatment. ax_ctrl: axenic control. xe_ctrl: xenic control

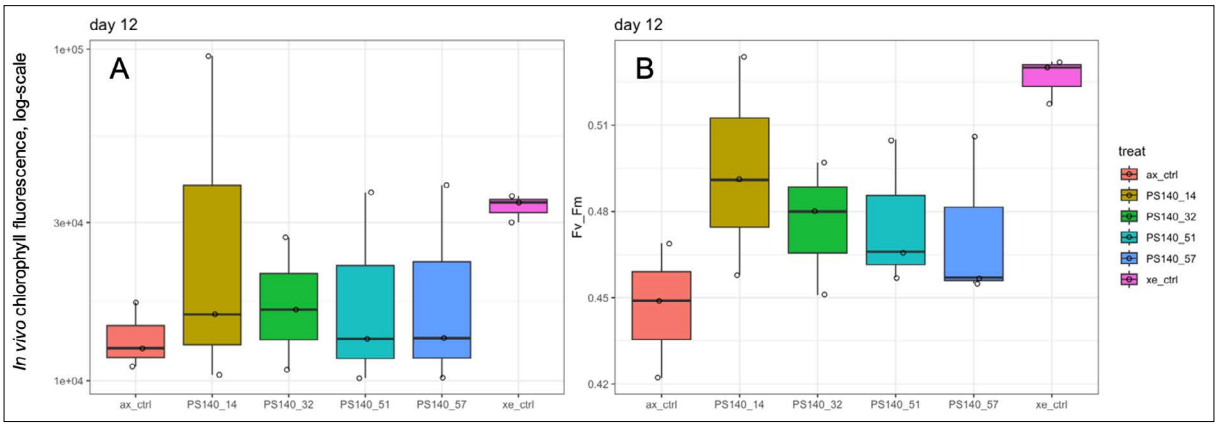

Fig. 8.3: Microbiome Assembly Experiment MAE, day 12. A: concentration-corrected relative fluorescence units (RFU) for in vivo chlorophyll fluorescence, log-scale. B: F_v/F_m values

Data management

Environmental data will be archived, published and disseminated according to international standards by the World Data Center PANGAEA Data Publisher for Earth & Environmental Science (https://www.pangaea.de) within two years after the end of the cruise at the latest. By default, the CC-BY license will be applied.

Any other data will be submitted to an appropriate long-term archive that provides unique and stable identifiers for the datasets and allows open online access to the data.

In all publications, based on this cruise, the Grant No. AWI_PS140_02 will be quoted and the following *Polarstern* article will be cited:

Alfred-Wegener-Institut Helmholtz-Zentrum für Polar- und Meeresforschung (2017) Polar Research and Supply Vessel POLARSTERN Operated by the Alfred-Wegener-Institute. Journal of large-scale research facilities, 3, A119. http://dx.doi.org/10.17815/jlsrf-3-163.

This work contributes to the Helmholtz Research Programme “Changing Earth – Sustaining our Future” Topic 6, Subtopic 6.1 and 6.2. It further contributes to Topic 2, Subtopics 2.1, 2.2, and 2.4.

References

Amin SA, Parker MS, Armbrust EV (2012) Interactions between diatoms and bacteria. Microbiol Mol Biol Rev 76(3): 667–684. https://doi.org/10.1128/mmbr.00007-12

Bartolek Z, Creveld SG, van Coesel S, Cain KR, Schatz M, Morales R, Armbrust EV (2022) Flavobacterial exudates disrupt cell cycle progression and metabolism of the diatom Thalassiosira pseudonana. ISME J 16(12):2741–2751. https://doi.org/10.1038/s41396-022-01313-9

Behringer G, Ochsenkühn MA, Fei C, Fanning J, Koester JA, Amin SA (2018) Bacterial communities of diatoms display strong conservation across strains and time. Front Microbiol 9:659. https://doi.org/10.3389/fmicb.2018.00659

De Baar HJW, Timmermans KR, Laan P, De Porto HH, Ober S, Blom JJ, Bakker MC, Schilling J, Sarthou G, Smit MG, Klunder M (2008) Titan: A new facility for ultraclean sampling of trace elements and isotopes in the deep oceans in the international Geotraces program. Mar Chem 111(1–2):4–21. https://doi.org/10.1016/j.marchem.2007.07.009

Field CB, Behrenfeld MJ, Randerson JT, Falkowski P (1998) Primary production of the biosphere: Integrating terrestrial and oceanic components. Science 281(5374):237–240. https://doi.org/10.1126/science.281.5374.237

Jackrel SL, Yang JW, Schmidt KC, Denef VJ (2021) Host specificity of microbiome assembly and its fitness effects in phytoplankton. ISME J 15(3):774–788. https://doi.org/10.1038/s41396-020-00812-x

Mönnich J, Tebben J, Bergemann J, Case R, Wohlrab S, Harder T (2020) Niche-based assembly of bacterial consortia on the diatom Thalassiosira rotula is stable and reproducible. ISME J 14(6) 1614–1625. https://doi.org/10.1038/s41396-020-0631-5

Pinkernell S, Beszteri B (2014) Potential effects of climate change on the distribution range of the main silicate sinker of the Southern Ocean. Ecol Evol 4(16):3147–3161. https://doi.org/10.1002/ece3.1138

Seymour JR, Amin SA, Raina J-B, Stocker R (2017) Zooming in on the phycosphere: The ecological interface for phytoplankton–bacteria relationships. Nat Microbiol 2(7), 1–12. https://doi.org/10.1038/nmicrobiol.2017.65

Van Tol HM, Amin SA, Armbrust EV (2017) Ubiquitous marine bacterium inhibits diatom cell division. ISME J 11(1):31–42. https://doi.org/10.1038/ismej.2016.112

9. ISOMETHANE: ONBOARD *IN-SITU* ANALYSES OF METHANE CONCENTRATION AND ITS STABLE CARBON ISOTOPIC SIGNATURE ($\delta^{13}C\text{-}CH_4$) IN THE LOWER TROPOSPHERE ABOVE THE SOUTHERN OCEAN

Samuel Sellmaier[1] [1]DE.AWI
not on board: Ellen Damm[1], Markus Rex[1]

Grant-No. AWI_PS140_11

Objectives

The objective is to record a time series of methane concentration and its stable carbon isotopic signature in the lower troposphere above the Southern Ocean during the cruise from Cape Town to Hobart. Methane (CH_4) is the second most important human-influenced greenhouse gas in terms of climate forcing. For methane, both bottom-up and top-down approaches are subject to large uncertainties, leading to a significant mismatch in modelling. The time series will contribute to quantify methane sources and sinks in the Southern Ocean and East Antarctica needed for the improvement of model parameterizations.

Work at sea

The continuous ship-borne measurements of CH_4 concentration and $\delta^{13}C\text{-}CH_4$ were carried out by Cavity Ring-Down Spectroscopy (CRDS) using a Picarro G2132-i isotope analyser (Picarro, Inc., Santa Clara, USA). CRDS is a highly sensitive gas analysis technique that measures the near-infrared absorption spectra of small gas-phase molecules within a high-reflectivity cavity using a laser diode. Air was sucked from the starboard side of the Peildeck at about 21 m above sea-ice/water surface using a Teflon tube. A constant flow was generated with a 3KQ Diaphragma pump (Boxer, Ottobeuren, Germany). The Picarro G2132 was maintained during the cruise to ensure high data quality. The recorded raw data was processed with a spike detection code to distinguish the background signal from contamination by local pollution (like pollution from the ship stack).

Preliminary (expected) results

Variations in CH_4 concentration and $\delta^{13}C\text{-}CH_4$ ratios over time will help to understand and validate source and sink capacities in the Southern Ocean. The data evaluation will focus on using backwards airmass trajectories to monitor air masses and to distinguish locally induced signals from signals transported from remote areas. Combined with the time series recorded during MOSAiC (Multidisciplinary drifting Observatory for the Study of Arctic Climate 2019-2020) the project aims to study differences in the source-sink balance along a global North-South transect. Exemplary for the recordings in Prydz Bay, Figure 9.1 shows the course of the processed CH_4 concentration and $\delta^{13}C\text{-}CH_4$ data from the 21.12. to the 28.12.2023. During this time the CH_4 concentration varied between 1.836 and 1.845 ppm, while the $\delta^{13}C\text{-}CH_4$ values between -47.5 and -50 ‰ show a slight depletion in ^{13}C compared with the background values.

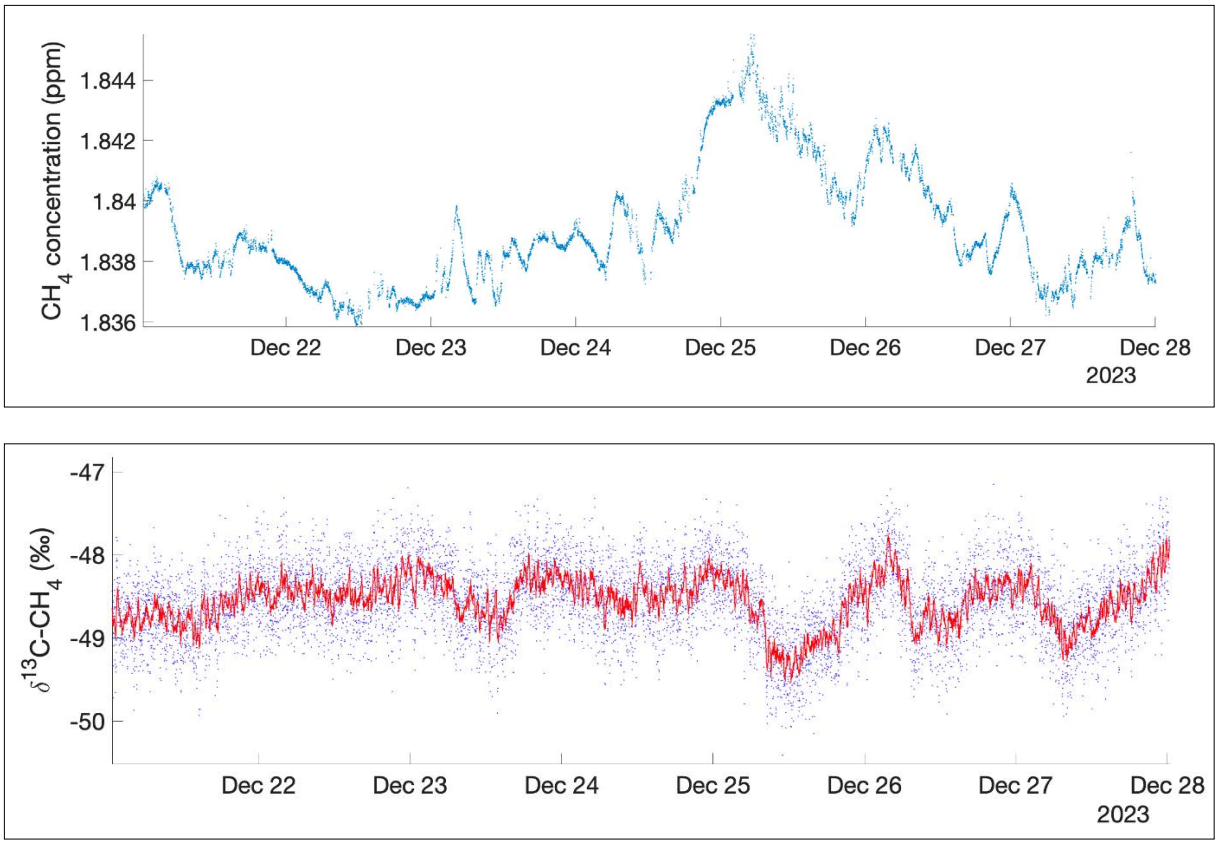

Fig. 9.1: Processed time series of atmospheric CH_4 concentration and $\delta^{13}C$-CH4 recorded close to the Shelf-ice edge in Prydz Bay

Data management

The atmospheric data will be archived, published and disseminated according to international standards by the World Data Center PANGAEA Data Publisher for Earth & Environmental Science (https://www.pangaea.de) within two years after the end of the expedition at the latest. By default, the CC-BY license will be applied.

This work contributes to the Helmholtz Research Programme “Changing Earth – Sustaining our Future” Topic 6, Subtopic 6.1 and 6.2. It further contributes to Topic 2, Subtopics 2.1, 2.2, and 2.4.

In all publications based on this expedition, the **Grant No. AWI_PS140_11** will be quoted and the following publication will be cited:

Alfred-Wegener-Institut Helmholtz-Zentrum für Polar- und Meeresforschung (2017) Polar Research and Supply Vessel POLARSTERN Operated by the Alfred-Wegener-Institute. Journal of large-scale research facilities, 3, A119. http://dx.doi.org/10.17815/jlsrf-3-163.

References

Matthew Shupe, Markus Rex,..., Ellen Damm, et al., Overview of the MOSAiC expedition: Atmosphere, Elementa: Science of the Anthropocene (2022) 10(1):00060. https://doi.org/10.1525/elementa.2021.00060.

Lannuzel D, Tedesco L, ...Damm E, van Leeuwe M *et al.* The future of Arctic sea-ice biogeochemistry and ice-associated ecosystems. *Nat. Clim. Chang.* 10:983–992 (2020). https://doi.org/10.1038/s41558-020-00940-4

Damm E, Rudels B, Schauer U et al. Methane excess in Arctic surface water- triggered by sea ice formation and melting. Sci Rep 5:16179 (2015). https://doi.org/10.1038/srep16179

Damm E, Bauch D, Krumpen T et al. The Transpolar Drift conveys methane from the Siberian Shelf to the central Arctic Ocean. Sci Rep 8:4515 (2018). https://doi.org/10.1038/s41598-018-22801-z

Astrid Lampert, Falk Pätzold, ... and Ellen Damm, Studying boundary layer methane isotopy and vertical mixing processes at a rewetted peatland site using an unmanned aircraft system, Atmospheric Measurement Techniques, 1:1937– 1952, 2020, https://doi.org/10.5194/amt-13-1937-2020

APPENDIX

A.1 TEILNEHMENDE INSTITUTE / PARTICIPATING INSTITUTES

Affiliation	Address
AU.UNI-ADELAIDE	The University of Adelaide 5005 Adelaide SA Australia
AU.UNI-CANBERRA	University of Canberra 11 Kirinari St 2617 Bruce ACT Australia
AU.IMAS	Institute for Marine and Antarctic Studies, University of Tasmania 20 Castray Esplanade 7004 Battery Point, Tasmania Australia
AU.ANSTO Sydney	Australia's Nuclear Science and Technology Organisation New Illawarra Rd 2234 Lucas Heights NSW Australia
AU.CSIRO-ENVIRONMENT	Commonwealth Scientific and Industrial Research Organization Oceans and Atmosphere and Centre for Southern Hemisphere Oceans Research Hobart,Tasmania Australia
CA.UNI-WATERLOO	Department of Anthropology Department of Sociology & Legal Studies University of Waterloo PAS 2041 200 University Avenue West Waterloo, ON N2L 3G1 Canada
CH.UNI-LAUSANNE	Institute of Earth Sciences (ISTE) University of Lausanne Bâtiment Géopolis Quartier Mouline 1015 Lausanne Switzerland
CN.SUN-YAT-SEN-ZHUHAI	Sun Yat-sen University Hailin Rd 519082 Zhuhai China

Affiliation	**Address**
DE.AWI	Alfred-Wegener-Institut Helmholtz-Zentrum für Polar- und Meeresforschung Postfach 120161 27515 Bremerhaven Germany
DE.DWD	Deutscher Wetterdienst Seewetteramt Bernhard Nocht Str. 76 20359 Hamburg Germany
DE.GEOMAR	GEOMAR Helmholtz-Zentrum für Ozeanforschung Kiel Wischhofstraße 1-3 24148 Kiel Germany
DE.MEDIA-UNI	Stuttgart Media University (Hochschule der Medien) Nobelstraße 10 70569 Stuttgart Germany
DE.UNI-KIEL	University of Kiel Christian-Albrechts-Platz 4 24118 Kiel Germany
DE.TUD	Technische Universität Dresden Helmholtzstr. 10 01069 Dresden Germany
DE.TUM	Technische Universität München Arcisstraße 21 80333 München Germany
DE.UNI-BREMEN	Universität Bremen Bibliothekstraße 1 28359 Bremen Germany
DE.UNI-Köln	Universität Köln Albertus-Magnus-Platz 50923 Köln Germany
DE.UNI-HEIDELBERG	Universität Heidelberg Im Neuenheimer Feld 69120 Heidelberg Germany

Affiliation	Address
NL.NIOZ	NIOZ Koninklijk Nederlands Instituut voor Onderzoek der Zee Landsdiep 4 1797 SZ ‘t Horntje, Texel Netherlands
NL.UNI-GRONINGEN	University of Groningen Broerstraat 5 9712 CP Groningen Netherlands
NL.UNI-RADBOUD	Radboud University Nijmegen Houtlaan 4 6525 XZ Nijmegen Netherlands

A.2 FAHRTTEILNEHMER:INNEN / CRUISE PARTICIPANTS

Name/ Last name	Vorname/ First name	Institut/ Institute	Beruf/ Profession	Fachrichtung/ Discipline
Anagnostou	Eleni	DE.GEOMAR	Scientist	Oceanography
Andreas	Pascal Horst	DE.UNI-BREMEN	Student (Master)	Glaciology
Arevalo Gonzalez	Marcelo	Servicio de Apoyo a Expediciones Científicas y Exploración	Engineer	Geology
Asadi	Nazanin	DE.UNI-BREMEN	Student (Master)	Earth Sciences
Boren	Goran Ingemar	AU.UNI-ADELAIDE	Scientist	Geophysics
Bozkuyu	Tarik	DE.UNI-BREMEN	Student (Master)	Earth Sciences
Brehmer-Moltmann	Johanna Karen	DE.UNI-BREMEN	Student (Master)	Geophysics
Colias Blanco	Manuel	Northern HeliCopter GmbH	Technician	Helicopter Service
Creac'h	Layla	DE.UNI-HEIDELBERG	Scientist	Chemistry
Deprie	Patrick	DE.GEOMAR	Student (Bachelor)	Biology
Ederer	Katrin	DE.AWI	Engineer	Engineering
Ehnis	Manuel	DE.UNI-HEIDELBERG	Student (Master)	Earth Sciences
Esper	Oliver	DE.AWI	Scientist	Geology
Feller	Jacob Ryan	DE.UNI-KÖLN	Technician	Geology
Gischler	Michael	Northern HeliCopter GmbH	Pilot	Helicopter Service
Groß	Kathrin	DE.GEOMAR	Student (Master)	Earth Sciences
Gutjahr	Marcus	DE.GEOMAR	Scientist	Earth Sciences
Hoeppe	Götz	CA.UNI-WATERLOO	Scientist	Earth Sciences
Huang	Huang	CN.SUN-YAT-SEN-ZHUHAI	Scientist	Chemistry
Ivanova	Alina	DE.UNI-BREMEN	Student (Master)	Geology
Jacob	Marrit	DE.UNI-BREMEN	PhD Student	Biology
Jeromson	Matthew	AU.UNI-CANBERRA	Scientist	Geology
Kooij	Florine	NL.NIOZ	PhD Student	Oceanography
Leicher	Niklas	DE.UNI-KÖLN	Scientist	Geology
Lembke-Jene	Lester	DE.AWI	Scientist	Geology

Name/ Last name	Vorname/ First name	Institut/ Institute	Beruf/ Profession	Fachrichtung/ Discipline
Lemire	Annie Catherine Juliette	DE.TUM	Student (Master)	Geophysics
Lensch	Norbert	DE.AWI	Technician	Geology
Lenstra	Wytze	NL.UNI-RADBOUD	Scientist	Oceanography
Melles	Martin	DE.UNI-KÖLN	Scientist	Geology
Menzel	David Milan Joshua	DE.GEOMAR	Student (Master)	Oceanography
Middag	Rob	NL.NIOZ	Scientist	Chemistry
Oetjens	Annika	AU.UNI-TASMANIA	PhD Student	Oceanography
Otte	Frank	DE.DWD	Scientist	Meteorology
Otto	Denise	DE.UNI-BREMEN	Student (Master)	Geology
Reinisch	Ines	Ines Reinisch – Design & Film	Other	Science outreach
Rieke	Ole	AU.UNI-TASMANIA	PhD Student	Oceanography
Rode	Jörg	DRF Luftrettung gAG	Engineer	Engineering
Ruben	Manuel	DE.AWI	PhD Student	Earth Sciences
Schaubensteiner	Stefan	Northern HeliCopter GmbH	Pilot	Helicopter Service
Schneider	Fabian Wieland Patrick	DE.UNI-HEIDELBERG	Student (Master)	Physics
Schröter	Benjamin	DE.TUD	PhD Student	Earth Sciences
Schulze Tenberge	Yvonne	DE.AWI	Scientist	Geophysics
Schumacher	Valea	DE.AWI	Technician	Geology
Sellmaier	Samuel	DE.UNI-POTSDAM	Student (Master)	Earth Sciences
Sinnen	Vivian Marissa	DE.AWI	PhD Student	Geology
Stimpfle	Jasmin	DE.AWI	PhD Student	Biology
Stöckle	Sonja	DE.DWD	Other	Meteorology
Thielen	Bianca	DE.MEDIA-UNI	Student (Master)	Science outreach
van Dijk	Robin	NL.UNI-GRONINGEN	Student (Master)	Biology

A.3 SCHIFFSBESATZUNG / SHIP‘S CREW

No.	Name/ Last name	Vorname/ First name	Position/ Rank
1	Lauber	Felix	Master
2	Kentges	Felix	Chief Mate (P)
3	Eckenfels	Hannes	2nd Mate (P)
4	Peine	Lutz	2nd Mate (P)
5	Weiß	Daniel	2nd Mate (P)
6	Rusch	Torben	Chief Engineer (P)
7	Ehrke	Tom	2nd Engineer (P)
8	Krinfeld	Oleksandr	2nd Engineer (P)
9	Farysch	Tim	3rd Engineer (P)
10	Mueller	Andreas	Electrical Engineer - Communication (P)
11	Krueger	Lars	Electrical Engineer
12	Schwedka	Thorsten	Electrical Engineer
13	Zivanov	Stefan	Electrical Engineer
14	Frank	Gerhard	Electrical Engineer (P)
15	Winter	Andreas	Electrical Engineer (P)
16	Brueck	Sebastian	Bosun
17	Decker	Jens	Bosun
18	Buchholz	Joscha	MPR
19	Jassmann	Marvin	MPR
20	Mahlmann	Oliver Karl - Heinz	MPR
21	Moeller	Falko	MPR
22	Probst	Lorenz	MPR
23	Schade	Tom	MPR
24	Wieckhorst	André	MPR
25	Keller	Juergen	Carp.
26	Niebuhr	Tim	AB
27	Plehn	Marco Markus	Fitter/E
28	Deutschbein	Felix Maximilian	MPR Tr.

No.	Name/ Last name	Vorname/ First name	Position/ Rank
29	Schroeder	Paul	MPR Tr.
30	Skrzipale	Mitja	Cook
31	Fehrenbach	Martina	2./Cook
32	Witusch	Petra Gertrud Ramona	C/Stew.
33	Ilk	Romy	Stew./Nurse
34	Chen	Jirong	2./Stew.
35	Chen	Quanlun	2./Stew.
36	Golla	Gerald	2./Stew.
37	Probst	Sabine	2./Stew.
38	Prummer	Leon	2./Stew.
39	Shi	Wubo	2./Stew.
40	Guba	Klaus	Ships doc

A.4 STATIONSLISTE / STATION LIST PS140

Station list of expedition PS140 from Cape Town – Hobart;
the list details the action log for all stations along the cruise track.

See https://www.pangaea.de/expeditions/events/PS140 to display the station (event) list for expedition PS140.
This version contains Uniform Resource Identifiers for all sensors listed under https://sensor.awi.de. See https://www.awi.de/en/about-us/service/computing-centre/data-flow-framework.html for further information about AWI's data flow framework from sensor observations to

Event label	Optional label	Date/Time	Latitude	Longitude	Depth [m]	Gear	Action	Comment
PS140-track		2023-11-28T00:00:00	-33.90680	18.43370		CT	Station start	Cape Town –
PS140-track		2024-01-29T00:00:00	-42.89320	147.34110		CT	Station end	Cape Town – Hobart
PS140_0_Underway-51		2023-11-28T18:00:00	-33.91539	18.43344	3	SWEAS	Station start	
PS140_0_Underway-51		2024-01-29T23:53:15	-42.84469	147.33058	9	SWEAS	Station end	
PS140_0_Underway-3		2023-11-29T07:31:29	-35.51816	20.42499	122	ADCP	Station start	
PS140_0_Underway-3		2024-01-28T06:33:51	-45.74560	138.69129	4040	ADCP	Station end	
PS140_0_Underway-13		2023-11-29T07:32:14	-35.51967	20.42803	121	FBOX	Station start	
PS140_0_Underway-13		2024-01-28T06:34:46	-45.74483	138.69481	4043	FBOX	Station end	
PS140_0_Underway-44		2023-11-29T07:33:11	-35.52154	20.43194	120	TSG	Station start	
PS140_0_Underway-44		2024-01-28T06:36:41	-45.74332	138.70203	4036	TSG	Station end	
PS140_0_Underway-43		2023-11-29T07:34:26	-35.52396	20.43705	118	TSG	Station start	
PS140_0_Underway-43		2024-01-28T06:35:47	-45.74404	138.69865	4037	TSG	Station end	
PS140_0_Underway-34		2023-11-29T07:35:42	-35.52652	20.44215	120	pCO2	Station start	
PS140_0_Underway-34		2024-01-28T06:32:50	-45.74652	138.68741	4032	pCO2	Station end	
PS140_0_Underway-23		2023-11-29T13:00:00	-36.18650	21.77200	199	MAG	Station start	
PS140_0_Underway-23		2024-01-29T02:07:57	-44.74011	142.98261	3945	MAG	Station end	
PS140_0_Underway-28		2023-11-30T00:05:43	-37.56133	24.57829	4271	DS3	Station start	

** Comments are limited to 130 characters. See https://www.pangaea.de/expeditions/events/PS140 to show full comments in conjunction with the station (event) list for expedition PS140*

Event label	Optional label	Date/Time	Latitude	Longitude	Depth [m]	Gear	Action	Comment
PS140_0_Underway-28		2024-01-28T20:39:11	-45.03784	141.81340	5064	DS3	Station end	
PS140_0_Underway-39		2023-11-30T00:17:34	-37.58584	24.62771	3657	P70	Station start	Event shows start point (date/time & coordinates) of first/last data record using Atlas Parasound P70 echosounder during cruise PS140
PS140_0_Underway-39		2024-01-28T20:42:46	-45.03487	141.82527	5156	P70	Station end	Event shows start point (date/time & coordinates) of first/last data record using Atlas Parasound P70 echosounder during cruise PS140
PS140_1-1		2023-11-30T15:21:20	-39.05010	28.24530	4270	MSN	Station start	
PS140_1-1		2023-11-30T16:58:06	-39.06461	28.24644	4269	MSN	Station end	
PS140_1-2		2023-11-30T18:49:38	-39.06603	28.24846	4270	CTD-RO	max depth	
PS140_1-3		2023-11-30T23:02:47	-39.07815	28.24625	4279	CTD-RO	max depth	
PS140_1-4		2023-12-01T02:53:17	-39.04894	28.24520	4282	MUC	max depth	
PS140_2-1		2023-12-02T02:46:34	-41.71158	31.64090	4465	CTD-RO	max depth	
PS140_2-2		2023-12-02T06:28:49	-41.71068	31.64072	4466	CTD-RO	max depth	
PS140_2-3		2023-12-02T08:03:41	-41.71010	31.64076	4457	MSN	Station start	
PS140_2-3		2023-12-02T09:31:20	-41.71020	31.64042	4456	MSN	Station end	
PS140_2-4		2023-12-02T11:03:27	-41.71056	31.64033	4454	MUC	max depth	
PS140_2-5		2023-12-02T14:59:02	-41.71040	31.63999	4458	PC	max depth	
PS140_3-1		2023-12-03T18:33:52	-43.00574	38.15384	2992	CTD-RO	max depth	
PS140_3-2		2023-12-03T21:08:38	-43.02129	38.15897	2983	CTD-RO	max depth	

Event label	Optional label	Date/Time	Latitude	Longitude	Depth [m]	Gear	Action	Comment
PS140_3-3		2023-12-03T23:55:24	-42.99935	38.15313	2980	MUC	max depth	
PS140_3-4		2023-12-04T02:04:48	-42.99986	38.15160	2983	GC	max depth	
PS140_3-5		2023-12-04T03:07:49	-43.00137	38.15184	2981	MSN	Station start	
PS140_3-5		2023-12-04T04:40:13	-43.00187	38.15455	2979	MSN	Station end	
PS140_3-6		2023-12-04T04:44:03	-43.00217	38.15432	2979	APN	Station start	aborted
PS140_3-6		2023-12-04T05:03:54	-43.00126	38.15494	2983	APN	Station end	aborted
PS140_3-7		2023-12-04T07:40:00	-42.97839	38.21087	2956	MAG	Station start	
PS140_3-7		2023-12-04T08:33:30	-42.97841	38.19828	2961	MAG	Station end	
PS140_4-1		2023-12-05T12:35:15	-46.99511	42.98588	3535	ARGOFL	Station start	
PS140_4-1		2023-12-05T12:37:21	-46.99665	42.98993	3533	ARGOFL	Station end	
PS140_5-1		2023-12-06T03:20:27	-48.99619	45.99384	4354	ARGOFL	Station start	
PS140_5-1		2023-12-06T03:22:46	-48.99874	45.99842	4347	ARGOFL	Station end	
PS140_6-1		2023-12-07T06:50:38	-50.54040	51.16154	4457	CTD-RO	max depth	
PS140_6-2		2023-12-07T10:13:03	-50.54104	51.16127	4457	MUC	max depth	
PS140_6-3		2023-12-07T11:44:08	-50.52614	51.16108	4517	ARGOFL	Station start	
PS140_6-3		2023-12-07T11:46:33	-50.52298	51.15873	4458	ARGOFL	Station end	
PS140_7-1		2023-12-07T21:49:40	-51.97831	53.95549	4257	ARGOFL	Station start	
PS140_7-1		2023-12-07T21:54:16	-51.98439	53.96776	4181	ARGOFL	Station end	
PS140_8-1		2023-12-08T09:33:07	-52.75464	55.73073	4475	CTD-RO	max depth	
PS140_8-2		2023-12-08T13:37:37	-52.75436	55.73108	4468	CTD-RO	max depth	
PS140_8-3		2023-12-08T15:25:15	-52.75332	55.73071	4465	MSN	Station start	
PS140_8-3		2023-12-08T17:00:07	-52.75448	55.73031	4464	MSN	Station end	
PS140_8-4		2023-12-08T17:01:28	-52.75460	55.73023	4472	WP2	Station start	
PS140_8-4		2023-12-08T17:28:19	-52.75427	55.73104	4471	WP2	Station end	
PS140_8-5		2023-12-08T18:53:42	-52.75432	55.73140	4468	MUC	max depth	
PS140_8-6		2023-12-08T23:22:03	-52.75439	55.73037	4470	PC	max depth	
PS140_9-1		2023-12-09T08:28:56	-53.25794	57.17359	4542	CTD-RO	max depth	

Event label	Optional label	Date/Time	Latitude	Longitude	Depth [m]	Gear	Action	Comment
PS140_10-1		2023-12-09T13:25:18	-53.45032	57.57886	4330	MSN	Station start	
PS140_10-1		2023-12-09T14:56:08	-53.45141	57.57754	4324	MSN	Station end	
PS140_10-2		2023-12-09T15:03:36	-53.45112	57.57826	4328	WP2	Station start	
PS140_10-2		2023-12-09T15:18:35	-53.45189	57.57734	4325	WP2	Station end	
PS140_10-3		2023-12-09T17:01:19	-53.45155	57.57784	4326	CTD-RO	max depth	
PS140_10-4		2023-12-09T20:28:33	-53.45154	57.57751	4324	CTD-RO	max depth	
PS140_10-5		2023-12-09T23:20:07	-53.45142	57.57786	4325	MUC	max depth	
PS140_10-6		2023-12-10T03:05:50	-53.45183	57.57759	4327	PC	max depth	
PS140_11-1		2023-12-11T08:10:22	-55.61283	65.64046	2295	MSN	Station start	
PS140_11-1		2023-12-11T09:14:53	-55.61321	65.63975	2296	MSN	Station end	
PS140_11-2		2023-12-11T09:17:52	-55.61325	65.63978	2292	WP2	Station start	
PS140_11-2		2023-12-11T09:29:51	-55.61341	65.63969	2296	WP2	Station end	
PS140_11-3		2023-12-11T10:27:06	-55.61368	65.64098	2296	MUC	max depth	
PS140_11-4		2023-12-11T13:10:46	-55.61340	65.63788	2296	PC	max depth	
PS140_11-5		2023-12-11T16:07:09	-55.60797	65.60847	2309	CTD-RO	max depth	
PS140_11-6		2023-12-11T18:18:26	-55.60705	65.61236	2306	CTD-RO	max depth	
PS140_12-1		2023-12-12T16:39:29	-58.16432	72.11434	4449	CTD-RO	max depth	
PS140_12-2		2023-12-12T20:14:23	-58.16510	72.11471	4450	CTD-RO	max depth	
PS140_12-3		2023-12-12T23:13:16	-58.16483	72.11488	4448	MUC	max depth	
PS140_13-1		2023-12-13T11:32:47	-59.15927	76.01519	1184	MUC	max depth	
PS140_13-2		2023-12-13T12:50:23	-59.15939	76.01313	1184	GC	max depth	
PS140_13-3		2023-12-13T13:36:48	-59.15435	75.97665	1195	MSN	Station start	
PS140_13-3		2023-12-13T15:00:46	-59.15306	75.97748	1194	MSN	Station end	
PS140_13-4		2023-12-13T15:04:54	-59.15321	75.97730	1194	WP2	Station start	
PS140_13-4		2023-12-13T15:19:55	-59.15305	75.97703	1194	WP2	Station end	
PS140_13-5		2023-12-13T16:13:06	-59.15286	75.97563	1195	CTD-RO	max depth	
PS140_13-6		2023-12-13T17:52:13	-59.15318	75.97565	1195	CTD-RO	max depth	
PS140_14-1		2023-12-14T12:30:27	-62.92854	76.08016	3872	CTD-RO	max depth	

Event label	Optional label	Date/Time	Latitude	Longitude	Depth [m]	Gear	Action	Comment
PS140_14-2		2023-12-14T15:42:41	-62.92858	76.08094	3836	CTD-RO	max depth	
PS140_14-3		2023-12-14T17:11:42	-62.92878	76.08128	3836	MSN	Station start	
PS140_14-3		2023-12-14T18:16:01	-62.92871	76.08051	3836	MSN	Station end	
PS140_14-4		2023-12-14T19:31:01	-62.92869	76.08036	3837	MUC	max depth	
PS140_14-5		2023-12-14T22:54:22	-62.92824	76.08122	3836	PC	max depth	
PS140_15-1		2023-12-16T00:29:16	-66.37405	77.05765	2865	CTD-RO	max depth	
PS140_15-2		2023-12-16T03:09:05	-66.37471	77.06441	2835	CTD-RO	max depth	
PS140_15-3		2023-12-16T04:17:40	-66.37623	77.06458	2833	MSN	Station start	
PS140_15-3		2023-12-16T05:56:18	-66.38027	77.06465	2827	MSN	Station end	
PS140_15-4		2023-12-16T05:56:44	-66.38025	77.06462	2828	WP2	Station start	
PS140_15-4		2023-12-16T06:11:55	-66.38055	77.06416	2828	WP2	Station end	
PS140_15-5		2023-12-16T07:07:56	-66.37949	77.06338	2830	MUC	max depth	
PS140_15-6		2023-12-16T08:15:20	-66.37808	77.06314	2830	GC	max depth	
PS140_16-1		2023-12-18T19:42:24	-68.68495	76.74402	842	CTD-RO	max depth	
PS140_16-2		2023-12-18T20:44:23	-68.68511	76.74401	817	CTD-RO	max depth	
PS140_16-3		2023-12-18T21:47:48	-68.68505	76.74347	817	MUC	max depth	
PS140_16-4		2023-12-18T22:42:43	-68.68505	76.74493	817	MUC	max depth	
PS140_16-5		2023-12-19T00:21:19	-68.68484	76.74545	817	PC	max depth	
PS140_16-6		2023-12-19T02:01:44	-68.67573	76.80371	811	MSN	Station start	
PS140_16-6		2023-12-19T03:17:09	-68.67584	76.80244	811	MSN	Station end	
PS140_16-7		2023-12-19T03:17:34	-68.67585	76.80248	811	WP2	Station start	
PS140_16-7		2023-12-19T03:35:34	-68.67626	76.80220	811	WP2	Station end	
PS140_17-1		2023-12-19T11:44:40	-68.93099	77.31195	1437	CTD-RO	max depth	
PS140_17-2		2023-12-19T13:09:58	-68.93149	77.30962	1418	CTD-RO	max depth	
PS140_17-3		2023-12-19T14:28:49	-68.93120	77.31012	1416	MUC	Station start	
PS140_17-3		2023-12-19T14:35:10	-68.93133	77.31006	1417	MUC	Station end	
PS140_17-4		2023-12-19T16:29:52	-68.93105	77.30980	1416	PC	max depth	
PS140_17-5		2023-12-19T17:58:34	-68.92022	77.33200	2240	MSN	Station start	

Event label	Optional label	Date/Time	Latitude	Longitude	Depth [m]	Gear	Action	Comment
PS140_17-5		2023-12-19T19:15:26	-68.92626	77.33045	904	MSN	Station end	
PS140_17-6		2023-12-19T19:17:09	-68.92649	77.33037	906	WP2	Station start	
PS140_17-6		2023-12-19T19:32:36	-68.92836	77.33039	959	WP2	Station end	
PS140_17-7		2023-12-19T19:36:44	-68.92883	77.33043	963	ARGOFL	Station start	
PS140_17-7		2023-12-19T19:50:30	-68.92349	77.30843	948	ARGOFL	Station end	
PS140_18-1		2023-12-20T08:56:21	-68.23797	74.47679	601	GKG	Station start	
PS140_18-1		2023-12-20T08:59:32	-68.23799	74.47719	601	GKG	Station end	
PS140_18-2		2023-12-20T09:32:18	-68.23804	74.47700	601	GKG	Station start	
PS140_18-2		2023-12-20T09:35:26	-68.23795	74.47671	601	GKG	Station end	
PS140_18-3		2023-12-20T10:52:41	-68.23822	74.47608	602	GC	max depth	
PS140_19-1		2023-12-20T14:05:44	-68.14801	75.69518	493	B_LANDER	Station start	
PS140_19-1		2023-12-20T14:36:48	-68.14630	75.69422	506	B_LANDER	Station end	
PS140_19-2		2023-12-20T15:08:15	-68.14081	75.67916	519	CTD-RO	max depth	
PS140_19-3		2023-12-20T16:00:36	-68.14073	75.67856	503	CTD-RO	max depth	
PS140_19-4		2023-12-20T17:17:24	-68.14084	75.67891	502	GC	max depth	
PS140_19-5		2023-12-20T18:44:54	-68.13970	75.65717	503	TVMUC	max depth	
PS140_19-6		2023-12-20T19:45:19	-68.13960	75.65733	503	MUC	max depth	
PS140_19-7		2023-12-20T20:07:23	-68.13958	75.65710	503	MSN	Station start	
PS140_19-7		2023-12-20T21:08:33	-68.13959	75.65729	503	MSN	Station end	
PS140_19-8		2023-12-20T21:14:07	-68.13964	75.65653	503	WP2	Station start	
PS140_19-8		2023-12-20T21:31:17	-68.13930	75.65560	502	WP2	Station end	
PS140_19-9		2023-12-20T21:34:29	-68.13901	75.65627	503	B_LANDER	Station start	
PS140_19-9		2023-12-20T22:18:35	-68.13766	75.65875	502	B_LANDER	Station end	
PS140_20-1		2023-12-21T01:24:19	-67.70187	75.37745	467	CTD-RO	max depth	
PS140_21-1		2023-12-21T04:44:18	-67.24981	75.04959	430	CTD-RO	max depth	
PS140_21-2		2023-12-21T05:44:12	-67.24995	75.04977	416	CTD-RO	max depth	
PS140_22-1		2023-12-21T07:38:18	-67.11435	75.03946	399	CTD-RO	max depth	

Event label	Optional label	Date/Time	Latitude	Longitude	Depth [m]	Gear	Action	Comment
PS140_23-1		2023-12-21T09:14:32	-66.98002	75.03253	383	CTD-RO	max depth	
PS140_24-1		2023-12-21T10:40:24	-66.90038	75.01675	1024	CTD-RO	max depth	
PS140_25-1		2023-12-21T13:04:48	-66.72013	74.99950	1991	CTD-RO	max depth	
PS140_25-2		2023-12-21T14:56:20	-66.71989	75.00068	1996	CTD-RO	max depth	
PS140_25-3		2023-12-21T15:53:41	-66.71999	75.00003	1993	MSN	Station start	
PS140_25-3		2023-12-21T17:14:24	-66.71992	75.00016	1994	MSN	Station end	
PS140_26-1		2023-12-22T07:50:01	-67.23235	73.15915	556	CTD-RO	max depth	
PS140_26-2		2023-12-22T08:41:33	-67.23256	73.15541	556	CTD-RO	max depth	
PS140_26-3		2023-12-22T10:23:36	-67.23251	73.15556	556	TVMUC	max depth	
PS140_26-4		2023-12-22T11:06:36	-67.23210	73.15511	555	GC	max depth	
PS140_26-5		2023-12-22T11:53:29	-67.23202	73.15555	555	TVMUC	max depth	
PS140_26-6		2023-12-22T12:43:55	-67.23194	73.15579	555	MSN	Station start	
PS140_26-6		2023-12-22T13:49:17	-67.23247	73.15792	555	MSN	Station end	
PS140_27-1		2023-12-22T16:35:42	-67.01673	72.33312	530	CTD-RO	max depth	
PS140_28-1		2023-12-22T18:44:18	-66.99960	71.65995	541	CTD-RO	max depth	
PS140_29-1		2023-12-22T20:35:28	-66.99959	71.00002	477	CTD-RO	max depth	
PS140_29-2		2023-12-22T21:25:27	-66.99973	71.00024	477	CTD-RO	max depth	
PS140_30-1		2023-12-22T23:16:29	-66.81664	70.86728	518	CTD-RO	max depth	
PS140_31-1		2023-12-23T00:27:08	-66.77519	70.86310	991	CTD-RO	max depth	
PS140_32-1		2023-12-23T02:45:06	-66.61387	70.76425	1833	CTD-RO	max depth	
PS140_32-2		2023-12-23T04:46:26	-66.61397	70.76462	1833	CTD-RO	max depth	
PS140_33-1		2023-12-23T09:27:56	-66.63704	70.78778	1742	GC	max depth	
PS140_34-1		2023-12-23T13:00:50	-66.94145	70.92934	501	TVMUC	max depth	
PS140_34-2		2023-12-23T13:47:02	-66.94146	70.93005	500	GC	max depth	
PS140_35-1		2023-12-23T15:20:04	-66.99408	71.12452	518	GC	max depth	
PS140_35-2		2023-12-23T16:03:42	-66.99254	71.12705	505	GC	max depth	
PS140_36-1		2023-12-23T19:59:59	-67.49693	71.14938	422	CTD-RO	max depth	

Event label	Optional label	Date/Time	Latitude	Longitude	Depth [m]	Gear	Action	Comment
PS140_36-2		2023-12-23T20:50:33	-67.49689	71.14887	423	CTD-RO	max depth	
PS140_37-1		2023-12-24T01:16:48	-67.99939	70.94148	501	CTD-RO	max depth	
PS140_37-2		2023-12-24T02:10:49	-67.99971	70.93868	502	CTD-RO	max depth	
PS140_37-3		2023-12-24T02:44:19	-68.00010	70.93883	501	ARGOFL	Station start	
PS140_37-3		2023-12-24T02:46:32	-67.99968	70.93544	483	ARGOFL	Station end	
PS140_38-1		2023-12-24T04:19:06	-68.08784	70.38797	359	CTD-RO	max depth	
PS140_39-1		2023-12-24T06:20:43	-68.18498	69.88844	225	CTD-RO	max depth	
PS140_40-1		2023-12-24T07:31:49	-68.29542	69.86985	214	CTD-RO	max depth	
PS140_41-1		2023-12-25T22:50:13	-68.46827	70.12030	689	CTD-RO	max depth	
PS140_42-1		2023-12-26T01:36:40	-68.66432	70.46836	409	CTD-RO	max depth	
PS140_43-1		2023-12-26T03:40:01	-68.51590	70.28168	1235	CTD-RO	max depth	
PS140_43-2		2023-12-26T05:00:20	-68.51603	70.28187	1235	CTD-RO	max depth	
PS140_43-3		2023-12-26T05:43:09	-68.51595	70.28164	1235	MSN	Station start	
PS140_43-3		2023-12-26T07:14:46	-68.51565	70.28237	1236	MSN	Station end	
PS140_43-4		2023-12-26T07:15:59	-68.51560	70.28246	1236	WP2	Station start	
PS140_43-4		2023-12-26T07:34:40	-68.51581	70.28175	1236	WP2	Station end	
PS140_43-5		2023-12-26T08:31:09	-68.51589	70.28186	1235	TVMUC	max depth	
PS140_43-6		2023-12-26T09:54:22	-68.51525	70.28134	1239	GC	max depth	
PS140_43-7		2023-12-26T10:45:20	-68.51678	70.28197	1236	TVMUC	max depth	
PS140_44-1		2023-12-26T13:28:34	-68.56878	70.83444	700	CTD-RO	max depth	
PS140_45-1		2023-12-26T15:16:59	-68.56792	71.29068	561	CTD-RO	max depth	
PS140_45-2		2023-12-26T16:20:31	-68.56806	71.29072	561	CTD-RO	max depth	
PS140_46-1		2023-12-26T18:13:05	-68.54551	71.58802	410	CTD-RO	max depth	
PS140_47-1		2023-12-26T20:07:15	-68.50049	72.03884	501	CTD-RO	max depth	
PS140_48-1		2023-12-26T22:09:39	-68.56513	72.51357	567	CTD-RO	max depth	
PS140_48-2		2023-12-26T23:03:36	-68.56307	72.51267	568	CTD-RO	max depth	
PS140_49-1		2023-12-27T04:02:22	-68.24978	72.72984	743	MSN	Station start	

Event label	Optional label	Date/Time	Latitude	Longitude	Depth [m]	Gear	Action	Comment
PS140_49-1		2023-12-27T05:22:30	-68.25072	72.73089	771	MSN	Station end	
PS140_49-2		2023-12-27T05:22:52	-68.25072	72.73089	771	WP2	Station start	
PS140_49-2		2023-12-27T05:40:21	-68.25038	72.73115	771	WP2	Station end	
PS140_49-3		2023-12-27T06:13:16	-68.25055	72.73061	771	MUC	max depth	
PS140_49-4		2023-12-27T07:50:48	-68.25052	72.73064	771	GC	max depth	
PS140_49-5		2023-12-27T09:06:16	-68.25048	72.73071	771	BC	max depth	
PS140_50-1		2023-12-27T12:54:31	-67.96830	71.78533	660	CTD-RO	max depth	
PS140_51-1		2023-12-27T15:30:45	-67.95004	72.48072	711	CTD-RO	max depth	
PS140_51-2		2023-12-27T16:29:08	-67.95005	72.48076	711	CTD-RO	max depth	
PS140_52-1		2023-12-28T04:22:34	-67.42443	73.11732	605	MSN	Station start	
PS140_52-1		2023-12-28T05:35:29	-67.42409	73.11688	592	MSN	Station end	
PS140_52-2		2023-12-28T05:35:52	-67.42412	73.11690	592	WP2	Station start	
PS140_52-2		2023-12-28T05:50:48	-67.42392	73.11671	593	WP2	Station end	
PS140_52-3		2023-12-28T06:41:05	-67.42421	73.11647	592	MUC	max depth	
PS140_52-4		2023-12-28T07:33:51	-67.42428	73.11696	593	GC	max depth	
PS140_53-1		2023-12-28T22:58:54	-68.16262	72.94476	732	CTD-RO	max depth	
PS140_53-2		2023-12-28T23:56:32	-68.16013	72.94387	731	CTD-RO	max depth	
PS140_53-3		2023-12-29T01:02:31	-68.16037	72.94629	731	MUC	max depth	
PS140_53-4		2023-12-29T02:00:00	-68.16042	72.94592	731	GC	max depth	
PS140_54-1		2023-12-29T03:01:43	-68.16113	72.98962	696	GC	max depth	
PS140_55-1		2023-12-29T03:48:58	-68.16114	73.00415	669	GC	max depth	
PS140_56-1		2023-12-29T04:42:18	-68.16138	73.04849	684	GC	max depth	
PS140_57-1		2023-12-29T08:48:02	-68.68158	72.83078	710	CTD-RO	max depth	
PS140_57-2		2023-12-29T09:42:50	-68.68211	72.82998	708	CTD-RO	max depth	
PS140_58-1		2023-12-29T12:10:27	-68.57769	73.17825	748	CTD-RO	max depth	
PS140_58-2		2023-12-29T12:30:14	-68.57803	73.18022	749	ARGOFL	Station start	
PS140_58-2		2023-12-29T12:33:25	-68.57864	73.18059	750	ARGOFL	Station end	

Event label	Optional label	Date/Time	Latitude	Longitude	Depth [m]	Gear	Action	Comment
PS140_59-1		2023-12-29T14:24:50	-68.60608	73.61693	761	CTD-RO	max depth	
PS140_60-1		2023-12-29T17:23:21	-68.74516	73.92171	768	CTD-RO	max depth	
PS140_60-2		2023-12-29T18:14:55	-68.74514	73.92169	767	CTD-RO	max depth	
PS140_61-1		2023-12-29T20:55:40	-68.86933	74.21191	696	CTD-RO	max depth	
PS140_62-1		2023-12-29T22:51:37	-69.00562	74.31404	762	CTD-RO	max depth	
PS140_63-1		2023-12-30T01:15:57	-69.14082	74.56984	829	CTD-RO	max depth	
PS140_63-2		2023-12-30T02:12:38	-69.14086	74.56980	828	CTD-RO	max depth	
PS140_64-1		2023-12-30T06:10:04	-69.27264	74.77714	837	CTD-RO	max depth	
PS140_65-1		2023-12-30T12:00:30	-69.31955	75.11122	657	ICE	Station start	
PS140_65-1		2023-12-30T12:26:00	-69.31658	75.11280	653	ICE	Station end	
PS140_65-2		2023-12-30T13:39:12	-69.31676	75.11260	675	GC	max depth	
PS140_66-1		2024-01-01T11:32:45	-69.32354	74.18927	715	CTD-RO	max depth	
PS140_66-2		2024-01-01T12:31:45	-69.32357	74.18941	714	CTD-RO	max depth	
PS140_66-3		2024-01-01T13:20:53	-69.32357	74.18930	714	MUC	max depth	
PS140_66-4		2024-01-01T14:05:19	-69.32358	74.18930	714	MUC	max depth	
PS140_66-5		2024-01-01T14:56:50	-69.32357	74.18928	714	GC	max depth	
PS140_67-1		2024-01-01T17:47:28	-69.33722	74.41819	793	CTD-RO	max depth	
PS140_68-1		2024-01-01T19:57:06	-69.34738	74.62227	771	CTD-RO	max depth	
PS140_69-1		2024-01-01T21:14:05	-69.36744	74.79778	694	CTD-RO	max depth	
PS140_70-1		2024-01-01T23:58:19	-69.31738	75.11279	676	CTD-RO	max depth	
PS140_70-2		2024-01-02T00:52:03	-69.31747	75.11268	676	MUC	max depth	
PS140_70-3		2024-01-02T01:49:46	-69.31746	75.11275	676	GC	max depth	
PS140_71-1		2024-01-02T03:08:27	-69.30519	75.07197	705	GC	max depth	
PS140_72-1		2024-01-02T04:23:52	-69.30432	75.01540	773	GC	max depth	
PS140_73-1		2024-01-02T11:53:58	-68.85674	75.59922	725	CTD-RO	max depth	
PS140_73-2		2024-01-02T12:48:25	-68.85699	75.60168	725	CTD-RO	max depth	
PS140_73-3		2024-01-02T13:32:22	-68.85784	75.60531	724	MSN	Station start	

Event label	Optional label	Date/Time	Latitude	Longitude	Depth [m]	Gear	Action	Comment
PS140_73-3		2024-01-02T14:41:43	-68.85777	75.59936	725	MSN	Station end	
PS140_74-1		2024-01-02T20:45:24	-69.24731	76.51600	1207	CTD-RO	max depth	
PS140_74-2		2024-01-02T21:22:52	-69.24746	76.51194	1194	CTD-RO	max depth	
PS140_74-3		2024-01-02T23:09:26	-69.24641	76.51997	1236	MUC	max depth	
PS140_74-4		2024-01-03T01:42:05	-69.24702	76.52261	1235	PC	max depth	
PS140_74-5		2024-01-03T03:30:37	-69.24715	76.52260	1210	MUC	max depth	
PS140_75-1		2024-01-03T10:38:42	-68.72093	76.68041	843	PC	max depth	
PS140_76-1		2024-01-03T15:35:00	-68.94267	77.33211	1404	PC	max depth	
PS140_77-1		2024-01-04T04:53:17	-68.72638	77.70295	1019	CTD-RO	max depth	
PS140_77-2		2024-01-04T06:30:40	-68.72617	77.70392	1017	GC	max depth	
PS140_78-1		2024-01-04T15:49:41	-68.72627	77.70403	1018	MUC	max depth	
PS140_79-1		2024-01-04T19:36:54	-68.17644	77.70478	519	XBT	Station start	
PS140_79-1		2024-01-04T19:46:09	-68.16057	77.72872	497	XBT	Station end	
PS140_80-1		2024-01-04T22:07:41	-67.82276	78.24636	734	CTD-RO	max depth	
PS140_80-2		2024-01-04T22:58:05	-67.82410	78.24537	760	CTD-RO	max depth	
PS140_80-3		2024-01-04T23:58:02	-67.81845	78.24520	754	MUC	max depth	
PS140_81-1		2024-01-05T03:23:02	-67.60553	79.26904	601	XBT	Station start	
PS140_81-1		2024-01-05T03:28:32	-67.59459	79.30954	607	XBT	Station end	
PS140_82-1		2024-01-05T08:24:57	-67.22813	80.53590	1614	CTD-RO	max depth	
PS140_82-2		2024-01-05T09:49:16	-67.22796	80.53691	1612	CTD-RO	max depth	
PS140_82-3		2024-01-05T11:31:41	-67.22830	80.53832	1620	TVMUC	max depth	
PS140_82-4		2024-01-05T13:20:46	-67.22804	80.53667	1613	GC	max depth	
PS140_82-5		2024-01-05T14:00:07	-67.22841	80.53964	1623	ARGOFL	Station start	
PS140_82-5		2024-01-05T14:03:40	-67.22795	80.54628	1586	ARGOFL	Station end	
PS140_83-1		2024-01-05T19:11:49	-66.15140	80.21324	421	XBT	Station start	
PS140_83-1		2024-01-05T19:15:26	-66.13649	80.21182	444	XBT	Station end	
PS140_83-2		2024-01-05T19:16:28	-66.13216	80.21148	456	XBT	Station start	

Event label	Optional label	Date/Time	Latitude	Longitude	Depth [m]	Gear	Action	Comment
PS140_83-2		2024-01-05T19:23:38	-66.10257	80.21485	500	XBT	Station end	
PS140_84-1		2024-01-05T19:35:20	-66.07227	80.21924	371	XBT	Station start	
PS140_84-1		2024-01-05T19:42:13	-66.05692	80.21797	577	XBT	Station end	
PS140_85-1		2024-01-05T19:53:28	-66.02669	80.22044	758	XBT	Station start	
PS140_85-1		2024-01-05T20:00:26	-66.00824	80.22187	877	XBT	Station end	
PS140_86-1		2024-01-05T20:12:25	-65.97982	80.22119	1086	XBT	Station start	
PS140_86-1		2024-01-05T20:19:24	-65.96118	80.21403	1400	XBT	Station end	
PS140_87-1		2024-01-05T20:27:07	-65.94074	80.20578	1314	XBT	Station start	
PS140_87-1		2024-01-05T20:33:14	-65.92419	80.20212	1383	XBT	Station end	
PS140_88-1		2024-01-08T05:18:58	-66.05403	95.46389	719	CTD-RO	max depth	
PS140_89-1		2024-01-08T06:26:14	-65.93406	95.43325	572	XBT	Station start	
PS140_89-1		2024-01-08T06:33:27	-65.91404	95.42776	505	XBT	Station end	
PS140_90-1		2024-01-08T07:53:40	-65.80622	95.40256	1031	CTD-RO	max depth	
PS140_90-2		2024-01-08T09:01:26	-65.80628	95.40277	1029	CTD-RO	max depth	
PS140_90-3		2024-01-08T10:11:00	-65.80528	95.40066	1026	MUC	max depth	
PS140_91-1		2024-01-08T11:28:31	-65.69537	95.31389	550	XBT	Station start	
PS140_91-1		2024-01-08T11:36:21	-65.67570	95.29432	519	XBT	Station end	
PS140_92-1		2024-01-08T12:39:53	-65.56915	95.21385	540	CTD-RO	max depth	
PS140_93-1		2024-01-08T14:36:14	-65.41100	95.31242	376	XBT	Station start	
PS140_93-1		2024-01-08T14:41:42	-65.39227	95.32452	383	XBT	Station end	
PS140_94-1		2024-01-08T15:23:00	-65.25070	95.41187	531	XBT	Station start	
PS140_94-1		2024-01-08T15:27:41	-65.23464	95.42195	545	XBT	Station end	
PS140_95-1		2024-01-08T16:11:42	-65.08367	95.51388	499	XBT	Station start	
PS140_95-1		2024-01-08T16:15:51	-65.06962	95.52420	474	XBT	Station end	
PS140_96-1		2024-01-08T16:56:52	-64.92314	95.60571	169	XBT	Station start	
PS140_96-1		2024-01-08T17:04:29	-64.89548	95.63022	154	XBT	Station end	
PS140_97-1		2024-01-08T17:53:07	-64.78826	95.82841	164	XBT	Station start	

Event label	Optional label	Date/Time	Latitude	Longitude	Depth [m]	Gear	Action	Comment
PS140_97-1		2024-01-08T18:00:33	-64.77075	95.87943	196	XBT	Station end	
PS140_98-1		2024-01-08T18:43:34	-64.68280	96.15208	187	XBT	Station start	
PS140_98-1		2024-01-08T18:47:19	-64.67178	96.17555	198	XBT	Station end	
PS140_99-1		2024-01-08T20:43:10	-64.56977	96.41881	233	CTD-RO	max depth	
PS140_100-1		2024-01-08T22:27:17	-64.46820	96.68197	240	XBT	Station start	
PS140_100-1		2024-01-08T22:43:13	-64.45892	96.70269	248	XBT	Station end	
PS140_101-1		2024-01-09T00:20:59	-64.29026	97.10803	538	XBT	Station start	
PS140_101-1		2024-01-09T00:34:54	-64.27121	97.15099	913	XBT	Station end	
PS140_102-1		2024-01-09T01:52:55	-64.13746	97.41784	1970	XBT	Station start	
PS140_102-1		2024-01-09T02:02:07	-64.11522	97.42730	1956	XBT	Station end	
PS140_103-1		2024-01-09T04:51:31	-64.13173	98.17412	1467	XBT	Station start	
PS140_103-1		2024-01-09T04:57:04	-64.13576	98.20522	1386	XBT	Station end	
PS140_104-1		2024-01-09T06:24:16	-64.14193	98.54708	970	XBT	Station start	
PS140_104-1		2024-01-09T06:31:37	-64.14662	98.57306	914	XBT	Station end	
PS140_105-1		2024-01-09T08:05:38	-64.21798	98.85904	394	XBT	Station start	
PS140_105-1		2024-01-09T08:09:47	-64.22130	98.87685	398	XBT	Station end	
PS140_106-1		2024-01-09T09:11:45	-64.29018	99.16049	459	XBT	Station start	
PS140_106-1		2024-01-09T09:22:32	-64.28859	99.18448	464	XBT	Station end	
PS140_107-1		2024-01-09T11:08:22	-64.37138	99.55601	539	CTD-RO	max depth	
PS140_107-2		2024-01-09T11:55:55	-64.37209	99.55747	544	CTD-RO	max depth	
PS140_107-3		2024-01-09T12:49:45	-64.37475	99.55623	546	MUC	max depth	
PS140_108-1		2024-01-09T14:26:34	-64.50740	99.79435	569	XBT	Station start	device broken; end XBT
PS140_108-1		2024-01-09T14:37:46	-64.52172	99.84607	571	XBT	Station end	device broken; end XBT
PS140_109-1		2024-01-09T15:45:04	-64.57097	100.15022	543	XBT	Station start	
PS140_109-1		2024-01-09T15:56:23	-64.59088	100.15091	542	XBT	Station end	
PS140_110-1		2024-01-09T17:16:25	-64.72946	100.27377	493	CTD-RO	max depth	

Event label	Optional label	Date/Time	Latitude	Longitude	Depth [m]	Gear	Action	Comment
PS140_111-1		2024-01-09T18:27:34	-64.87472	100.27715	443	XBT	Station start	
PS140_111-1		2024-01-09T18:33:43	-64.89014	100.26986	435	XBT	Station end	
PS140_112-1		2024-01-09T19:58:33	-65.00061	100.00487	520	CTD-RO	max depth	
PS140_112-2		2024-01-09T20:43:00	-65.00001	100.01256	521	CTD-RO	max depth	
PS140_113-1		2024-01-09T22:09:32	-65.15398	100.03259	461	XBT	Station start	
PS140_113-1		2024-01-09T22:23:32	-65.17054	100.00070	465	XBT	Station end	
PS140_114-1		2024-01-09T23:29:44	-65.33241	99.96065	412	CTD-RO	max depth	
PS140_115-1		2024-01-10T00:19:20	-65.45319	99.98461	490	XBT	Station start	
PS140_115-1		2024-01-10T00:25:04	-65.47026	99.97285	494	XBT	Station end	
PS140_116-1		2024-01-10T01:22:00	-65.59346	99.85320	542	CTD-RO	max depth	
PS140_116-2		2024-01-10T02:05:46	-65.59341	99.85290	542	CTD-RO	max depth	
PS140_116-3		2024-01-10T02:55:10	-65.59291	99.85270	542	MUC	max depth	
PS140_117-1		2024-01-10T04:08:13	-65.71716	99.74900	350	CTD-RO	max depth	
PS140_118-1		2024-01-10T06:30:30	-65.87198	99.67948	604	CTD-RO	max depth	
PS140_118-2		2024-01-10T07:17:51	-65.87193	99.67903	606	CTD-RO	max depth	
PS140_119-1		2024-01-10T17:13:34	-64.33615	100.54580	455	XBT	Station start	
PS140_119-1		2024-01-10T17:18:48	-64.32168	100.54788	446	XBT	Station end	
PS140_120-1		2024-01-10T17:34:45	-64.27852	100.55516	451	XBT	Station start	
PS140_120-1		2024-01-10T17:42:27	-64.25732	100.54934	453	XBT	Station end	
PS140_121-1		2024-01-10T18:11:27	-64.18668	100.52495	794	XBT	Station start	
PS140_121-1		2024-01-10T18:15:56	-64.18573	100.52231	802	XBT	Station end	
PS140_122-1		2024-01-10T18:51:14	-64.11627	100.51708	1218	XBT	Station start	
PS140_122-1		2024-01-10T18:54:11	-64.11303	100.51752	1230	XBT	Station end	
PS140_123-1		2024-01-10T23:54:10	-63.68897	100.77434	1399	CTD-RO	max depth	
PS140_123-2		2024-01-11T01:13:54	-63.68870	100.77304	1398	CTD-RO	max depth	
PS140_123-3		2024-01-11T01:59:18	-63.68877	100.77268	1398	MSN	Station start	
PS140_123-3		2024-01-11T03:30:29	-63.68861	100.77332	1398	MSN	Station end	

Event label	Optional label	Date/Time	Latitude	Longitude	Depth [m]	Gear	Action	Comment
PS140_123-4		2024-01-11T04:06:50	-63.68865	100.77328	1399	MUC	max depth	
PS140_123-5		2024-01-11T06:30:41	-63.68891	100.77379	1400	PC	max depth	
PS140_124-1		2024-01-12T03:13:06	-60.89650	100.97448	4515	PC	max depth	
PS140_124-2		2024-01-12T08:44:33	-60.89616	100.97384	4515	MUC	max depth	
PS140_124-3		2024-01-12T10:21:51	-60.90071	100.94148	4515	MSN	Station start	
PS140_124-3		2024-01-12T11:30:37	-60.90060	100.94373	4515	MSN	Station end	
PS140_124-4		2024-01-12T10:35:59	-60.90075	100.94256	4514	WS	max depth	
PS140_124-5		2024-01-12T13:13:31	-60.90135	100.94389	4515	CTD-RO	max depth	
PS140_124-6		2024-01-12T16:30:48	-60.90147	100.94399	4515	CTD-RO	max depth	
PS140_125-1		2024-01-13T04:03:32	-59.56981	101.12408	4167	CTD-RO	max depth	
PS140_125-2		2024-01-13T04:31:32	-59.56882	101.12450	4168	MSN	Station start	
PS140_125-2		2024-01-13T05:52:00	-59.56917	101.12415	4167	MSN	Station end	
PS140_125-3		2024-01-13T07:19:03	-59.56876	101.12370	4166	MUC	max depth	
PS140_125-4		2024-01-13T10:36:47	-59.54626	101.12496	4159	CTD-RO	max depth	
PS140_125-5		2024-01-13T13:40:40	-59.54647	101.12560	4158	CTD-RO	max depth	
PS140_125-6		2024-01-13T18:31:29	-59.56899	101.12389	4166	PC	max depth	
PS140_126-1		2024-01-14T11:27:43	-57.44336	101.45036	4225	PC	max depth	
PS140_126-2		2024-01-14T15:44:40	-57.44329	101.45095	4228	MUC	max depth	
PS140_126-3		2024-01-14T19:09:30	-57.43094	101.41667	4235	CTD-RO	max depth	
PS140_126-4		2024-01-14T22:22:07	-57.43212	101.41682	4237	CTD-RO	max depth	
PS140_126-5		2024-01-14T23:50:13	-57.43131	101.41641	4235	MSN	Station start	
PS140_126-5		2024-01-15T01:03:28	-57.43185	101.41835	4233	MSN	Station end	
PS140_127-1		2024-01-15T08:10:20	-56.42144	101.77976	3884	PC	max depth	
PS140_127-2		2024-01-15T12:25:06	-56.42099	101.77987	3880	MUC	max depth	
PS140_128-1		2024-01-15T18:02:57	-55.87152	102.47033	3809	CTD-RO	max depth	
PS140_128-2		2024-01-15T21:18:05	-55.87288	102.46783	3801	CTD-RO	max depth	
PS140_128-3		2024-01-16T00:04:19	-55.87332	102.46788	3797	MUC	max depth	

Event label	Optional label	Date/Time	Latitude	Longitude	Depth [m]	Gear	Action	Comment
PS140_128-4		2024-01-16T02:40:46	-55.87300	102.46837	3799	GC	max depth	
PS140_129-1		2024-01-16T18:16:25	-53.42189	103.92224	3712	CTD-RO	max depth	
PS140_129-2		2024-01-16T21:15:42	-53.42202	103.92303	3709	CTD-RO	max depth	
PS140_129-3		2024-01-16T22:36:15	-53.42145	103.92181	3711	MSN	Station start	
PS140_129-3		2024-01-16T23:45:31	-53.42166	103.92218	3714	MSN	Station end	
PS140_129-4		2024-01-17T01:43:58	-53.44192	103.90915	3905	MUC	max depth	
PS140_129-5		2024-01-17T04:16:04	-53.44194	103.90845	3914	GC	max depth	
PS140_130-1		2024-01-17T20:07:00	-51.65306	103.88193	3159	CTD-RO	max depth	
PS140_130-2		2024-01-17T22:42:55	-51.65296	103.88223	3157	CTD-RO	max depth	
PS140_130-3		2024-01-17T23:52:02	-51.65264	103.88220	3167	MSN	Station start	
PS140_130-3		2024-01-18T01:05:47	-51.65281	103.88233	3164	MSN	Station end	
PS140_130-4		2024-01-18T02:10:20	-51.65275	103.88237	3168	MUC	max depth	
PS140_130-5		2024-01-18T05:34:41	-51.65287	103.88175	3167	PC	max depth	
PS140_131-1		2024-01-18T17:42:54	-50.20458	104.52256	3112	PC	max depth	
PS140_131-2		2024-01-18T21:22:31	-50.20486	104.52306	3111	MUC	max depth	
PS140_131-3		2024-01-19T00:02:48	-50.22370	104.51108	3291	CTD-RO	max depth	
PS140_131-4		2024-01-19T02:36:08	-50.22357	104.51049	3289	CTD-RO	max depth	
PS140_131-5		2024-01-19T03:50:11	-50.22308	104.51274	3271	MSN	Station start	
PS140_131-5		2024-01-19T04:57:47	-50.22400	104.50956	3313	MSN	Station end	
PS140_132-1		2024-01-19T15:56:29	-48.82245	104.61488	3126	CTD-RO	max depth	
PS140_132-2		2024-01-19T18:31:49	-48.82203	104.61482	3129	CTD-RO	max depth	
PS140_132-3		2024-01-19T20:50:39	-48.82208	104.61556	3127	MUC	max depth	
PS140_132-4		2024-01-20T00:27:42	-48.82250	104.61524	3129	PC	max depth	
PS140_133-1		2024-01-20T02:45:04	-48.82616	104.62620	3135	MSN	Station start	
PS140_133-1		2024-01-20T03:56:18	-48.81586	104.63866	3341	MSN	Station end	
PS140_134-1		2024-01-20T16:22:23	-46.96816	104.19826	3327	PC	max depth	
PS140_134-2		2024-01-20T20:11:00	-46.96821	104.19918	3328	MUC	max depth	

Event label	Optional label	Date/Time	Latitude	Longitude	Depth [m]	Gear	Action	Comment
PS140_134-3		2024-01-20T22:59:42	-46.97391	104.22499	3395	CTD-RO	max depth	
PS140_134-4		2024-01-21T01:39:47	-46.97385	104.22447	3404	CTD-RO	max depth	
PS140_134-5		2024-01-21T02:54:43	-46.97405	104.22406	3401	MSN	Station start	
PS140_134-5		2024-01-21T04:08:53	-46.97533	104.22920	3413	MSN	Station end	
PS140_135-1		2024-01-21T16:20:40	-45.07362	103.99427	3632	CTD-RO	max depth	
PS140_135-2		2024-01-21T19:06:30	-45.07278	103.99320	3638	CTD-RO	max depth	
PS140_135-3		2024-01-21T21:47:16	-45.07388	103.99387	3643	MUC	max depth	
PS140_135-4		2024-01-22T01:04:46	-45.07356	103.99438	3640	PC	max depth	
PS140_135-5		2024-01-22T02:53:27	-45.07822	103.97090	3645	MSN	Station start	
PS140_135-5		2024-01-22T04:05:55	-45.08130	103.96751	3673	MSN	Station end	
PS140_136-1		2024-01-22T18:00:17	-46.85431	107.10216	3365	PC	max depth	
PS140_137-1		2024-01-23T14:26:22	-48.62585	111.74569	3568	CTD-RO	max depth	
PS140_137-2		2024-01-23T16:27:04	-48.62709	111.74677	3555	RN	max depth	
PS140_137-3		2024-01-23T18:40:26	-48.62583	111.74580	3567	PC	max depth	
PS140_137-4		2024-01-23T21:44:55	-48.62600	111.74583	3550	MUC	max depth	
PS140_138-1		2024-01-25T05:34:37	-50.03995	120.75202	3445	MUC	max depth	
PS140_139-1		2024-01-25T22:09:44	-49.86102	124.47132	3380	MUC	max depth	
PS140_139-2		2024-01-26T01:07:54	-49.85775	124.44246	3463	CTD-RO	max depth	
PS140_140-1		2024-01-26T02:40:50	-49.84889	124.42523	3641	MAG	Station start	
PS140_140-1		2024-01-26T03:28:22	-49.84689	124.42525	3625	MAG	Station end	

** Comments are limited to 130 characters. See https://www.pangaea.de/expeditions/events/PS140 to show full comments in conjunction with the station (event) list for expedition PS140*

Abbreviation	Method/Device
ADCP	Acoustic Doppler Current Profiler
APN	Apstein plankton net
ARGOFL	Argo float
BC	Box corer
B_LANDER	Bottom lander
CT	Underway cruise track measurements
CTD-RO	CTD/Rosette
DS3	Swath-mapping system Atlas Hydrosweep DS-3
FBOX	FerryBox
GC	Gravity corer
GKG	Giant box corer
ICE	Ice station
MAG	Magnetometer
MSN	Multiple opening/closing net
MUC	MultiCorer
P70	ATLAS Parasound P70 Deep-Sea Parametric Sub-Bottom Profiler
PC	Piston corer
RN	Ring net
SWEAS	Ship Weather Station
TSG	Thermosalinograph
TVMUC	Multicorer with television
WP2	WP-2 towed closing plankton net
WS	Water sample
XBT	Expendable bathythermograph
pCO2	pCO2 sensor

A.5 SUPPLEMENTARY MATERIALS

This part of the appendix contains the following Appendix tables:

- Appendix Tables 4.1 to 4.8
- Appendix Tables 5.1 and 5.2

Appendix A.5 is available in a separate file.

Die **Berichte zur Polar- und Meeresforschung** (ISSN 1866-3192) werden beginnend mit dem Band 569 (2008) als Open-Access-Publikation herausgegeben. Ein Verzeichnis aller Bände einschließlich der Druckausgaben (ISSN 1618-3193, Band 377-568, von 2000 bis 2008) sowie der früheren **Berichte zur Polarforschung** (ISSN 0176-5027, Band 1–376, von 1981 bis 2000) befindet sich im electronic Publication Information Center **(ePIC)** des Alfred-Wegener-Instituts, Helmholtz-Zentrum für Polar- und Meeresforschung (AWI); see https://epic.awi.de. Durch Auswahl "Reports on Polar- and Marine Research" (via "browse"/"type") wird eine Liste der Publikationen, sortiert nach Bandnummer, innerhalb der absteigenden chronologischen Reihenfolge der Jahrgänge mit Verweis auf das jeweilige pdf-Symbol zum Herunterladen angezeigt.

The **Reports on Polar and Marine Research** (ISSN 1866-3192) are available as open access publications since 2008. A table of all volumes including the printed issues (ISSN 1618-3193, Vol. 377-568, from 2000 until 2008), as well as the earlier **Reports on Polar Research** (ISSN 0176-5027, Vol. 1–376, from 1981 until 2000) is provided by the electronic Publication Information Center **(ePIC)** of the Alfred Wegener Institute, Helmholtz Centre for Polar and Marine Research (AWI); see URL https://epic.awi.de. To generate a list of all Reports, use the URL http://epic.awi.de and select "browse"/"type" to browse "Reports on Polar and Marine Research". A chronological list in declining order will be presented, and pdf-icons displayed for downloading.

Zuletzt erschienene Ausgaben:

Recently published issues:

790 (2024) The Expedition PS140 of the Research Vessel POLARSTERN to the Cooperation Sea and Davis Sea in 2023 / 2024, edited by Marcus Gutjahr and Oliver Esper with contributions of the participants

789 (2024) The Expedition PS142 of the Research Vessel POLARSTERN to the Atlantic Ocean in 2024, edited by Simon Dreutter with contributions of the participants

788 (2024) The Expedition PS138 of the Research Vessel POLARSTERN to the Arctic Ocean in 2024 edited by Antje Boetius and Christina Bienhold with contributions of the participants

786 (2024) The MOSES Sternfahrt Expeditions of the Research Vessels ALBIS, LITTORINA, LUDWIG PRANDTL and MYA II to the Elbe River, Elbe Estuary and German Bight in 2023 edited by Ingeborg Bussmann, Martin Krauss, Holger Brix, Norbert Kamjunke, Björn Raupers and Tina Sanders with contributions of the participants

785 (2024) The Expeditions PS139 / 1 and PS139 / 2 of the Research Vessel POLARSTERN to the Atlantic Ocean in 2023, edited by Simon Dreutter and Claudia Hanfland with contributions of the participants

784 (2024) Expeditions to Antarctica: ANT-Land 2022/23 NEUMAYER STATION III, Kohnen Station, Flight Operations and Field Campaigns. Edited by Julia Regnery, Thomas Matz, Peter Köhler and Christine Wesche with contributions of the participants

783 (2024) Mit Wilhelm Filchner in das Weddellmeer – Paul Björvigs Tagebuch von der deutschen Antarktischen Expedition 1911 – 1912. Aus dem Norwegischen übersetzt von Volkert Gazert und herausgegeben von Cornelia Lüdecke

782 (2024) Arctic Land Expeditions in Permafrost Research The MOMENT project: Expedition to the Arctic Station, Qeqertarsuaq, Disko Island and Ilulissat, West Greenland in 2022 edited by Julia Boike, Simone M. Stuenzi, Jannika Gottuk, Niko Bornemann, Brian Groenke

781 (2023) The Expedition PS137 of the Research Vessel POLARSTERN to the Arctic Ocean in 2023 edited by Vera Schlindwein with contributions of the participants

ALFRED-WEGENER-INSTITUT
HELMHOLTZ-ZENTRUM FÜR POLAR-
UND MEERESFORSCHUNG

BREMERHAVEN

Am Handelshafen 12
27570 Bremerhaven
Telefon 0471 4831-0
Telefax 0471 4831-1149
www.awi.de

HELMHOLTZ